Solar Photocatalytic Degradation of Antibiotics: Chemical, Ecotoxicological and Biodegradability Assessment

A Dissertation to the UNIVERSITY OF PORTO
for the degree of Doctor in Environmental Engineering by

João Henrique de Oliveira da Silva Pereira

Supervisor: Dr. Rui Alfredo Rocha Boaventura

Co-Supervisors: Dr. Vítor Jorge Pais Vilar

Dr. Maria Teresa Martins Borges [FCUP]

Associated Laboratory LSRE-LCM
Department of Chemical Engineering
Faculty of Engineering
University of Porto
June, 2014

Acknowledgments

My sincere gratitude goes to Dr. Rui Boaventura and Dr. Vítor Vilar, for the opportunity of developing my work with all the required conditions in their research group (LSRE-FEUP). Their scientific supervision, trust and support, ideas and patience, were essential to the concretization of this thesis. Notwithstanding the physical and "scientific" distance, the supervision of Dr. Maria Teresa Borges was greatly appreciated for many, many reasons.

A mention must be made to the following institutions that supported this work: the Foundation for Science and Technology (FCT) (doctoral grant: SFRH/BD/62277/2009); the Laboratory of Separation and Reaction Engineering (LSRE) and Faculty of Engineering of the University of Porto (FEUP), for the technical resources; Coordenação de Aperfeiçoamento de Pessoas de Nível Superior (CAPES) and FCT (CAPES/FCT Proc. 308/11 project) and the University of Porto (AQUAPHOTOBIO - Multidisciplinary project).

I also am very thankful for the collaborative work developed with Dr. Olga Nunes (LEPABE), and for the esteemed contribution of Ana Reis. Cheers to Daniel Birra Queirós for his assistance, partnership and patience. To all other people who also gave a hand, in one way or the other, you have not been forgotten.

I am also very grateful to Prof. Dr. Santiago Esplugas for having accepted me in his AOP Engineering Group (Universitat de Barcelona, Facultat de Quimica). A special salute goes to Dr. Óscar González Alvarez for a most invaluable guidance during such short, but fruitful stay back in 2010. The other members of their research group will always be fondly remembered for the great moments and friendships, and also Anna May, for the Catalan translation. *Fins aviat!* To Jordi Bueso, for the treasurable hospitality, and the rest of the Bueso family: *moltes gràcies a tots!*

An extended greeting goes to my esteemed past and present colleagues from LSRE-FEUP, Portuguese, Brazilian, German, Finnish, French, Argentinian, Mexican, Indian, *et cetera*, for all the good, bad, and overall funny moments spent together, for the coffee break sessions and for all the awkward lunch time conversations and dilemmas. I wish you the best of luck. To the many interesting people I met from all over the world in the scientific meetings I attended: I hope to see you again one day.

A kind word is due towards all the good-willed individuals who shared their cherished time and spirit with me along the trodden Way, during these last four and a half years; particularly, Pedro Cunha, Luís Lomba, Cristiana Barbosa and Lívia Xerez.

Obrigado, André Monteiro, Sérgio Mota and Rita Félix, pela vossa amizade genuína.

Finally, my gratefulness goes to the Source of all things, both finite and infinite.

With love to my parents, brothers, nieces and nephew.

To know that you do not know is highest
to not know but think you know is flawed

Only when one recognizes the fault as a fault
can one be without fault

The sages are without fault
because they recognize the fault as a fault
That is why they are without fault

Chapter 71 of the *Tao Teh King*, by Laozi. Translation by Derek Lin.

Abstract

The extensive use of human and veterinary antibiotics has resulted in a ubiquitous presence of trace amounts in natural aquatic environments all over the world, since conventional wastewater treatments have been shown unable to remove these highly stable and/or non-biodegradable compounds. This has led to increasing concerns with the risks of potential ecotoxicological effects and of antibiotic resistance propagation in bacterial communities. The development of alternative processes to secure water quality and overall environmental health has thus become a topmost scientific priority.

The use of Advanced Oxidation Processes (AOPs) to degrade recalcitrant pollutants such as antibiotics has been showing promising results in recent years. AOPs are characterized by the production of the highly reactive and non-selective hydroxyl radicals ($^{\bullet}OH$), leading to largely satisfactory results in the mineralization of pollutants to CO_2, water and inorganic compounds, or at least in their partial degradation to less harmful and/or more biodegradable compounds. Two of these AOPs, heterogeneous photocatalysis mediated by titanium dioxide (TiO_2/UV) and the photo-Fenton process, are regarded as of great interest. Their ability of using naturally available solar radiation as the source of ultraviolet/visible (UV-Vis) radiation greatly reduces energetic costs, while the required catalysts and reactants are fairly inexpensive. Due to the highly efficient use of both direct and diffuse UV solar radiation, Compound parabolic collectors (CPCs) are commonly used as the photoreactors of choice.

The main aim of this thesis was the study of the detoxification of three selected antibiotics, Oxytetracycline (OTC), Oxolinic acid (OXA) and Amoxicillin (AMX), by means of these two solar-driven photocatalytic processes. Experiments were performed in lab-scale photocatalytic apparatus provided with a sunlight simulator (Suntest device) and in a solar pilot-plant, both equipped with CPCs. The following objectives were pursued: i) attainment of photocatalytic degradation rate constants with pure antibiotic solutions; ii) assessment of required phototreatment times to achieve antibiotic degradation levels below resistance-inducing concentrations and desirable mineralization; iii) evaluation of the role of photocatalytic process variables; iv) assessment of the influence of individual wastewater components and real matrices and v) development of an alternative multistage treatment combining the biological degradation of AMX by means of an enriched culture with a solar photocatalytic system. Results are compared in terms of required accumulated UV energy per liter of solution, Q_{UV} ($kJ_{UV}\ L^{-1}$).

Solar photolysis showed to be insufficient in OTC, OXA and AMX degradation and/or mineralization. In an initial testing of the TiO_2/UV system to treat a pure OTC solution, the optimal parameters were found to be 0.5 g L^{-1} of TiO_2 with no initial pH adjustment (pH_0 ~ 4.4). The same photocatalytic conditions led to an increase of the biodegradability of the solution and a decrease in the bioluminescence inhibition of *Vibrio fischeri*. The same catalyst load used at neutral pH conditions (~7.5) in the pilot plant presented the following pseudo-first order kinetic rate constants in the individual treatment of 20 mg L^{-1} OTC, OXA and AMX solutions: 4.03 ± 0.07 (OTC), 1.9 ± 0.1 (OXA) and 0.80 ± 0.02 L kJ_{UV}^{-1} (AMX). In a mixture of OTC and OXA (C_0 = 20 mg L^{-1} each), rate constants nearly halved due to competition for hydroxyl radicals. Individually treated OTC, OXA and AMX solutions (C_0 = 40 mg L^{-1}) required around 2.0 (OTC) and 4.6 kJ_{UV} L^{-1} (OXA, AMX) to cease growth inhibition of tested bacterial strains. By the end of the respective photo-treatment periods, a high percentage of remaining dissolved organic carbon (DOC) was in the form of easily biodegradable low-molecular-weight carboxylate anions (LMWCA). Original nitrogen content of OTC, OXA and AMX molecules was incompletely released as ammonium, while 100% dessulfurization of AMX by-products was achieved. Phosphates were found to be the most interfering species amongst various inorganic ions tested (Cl^-, SO_4^{2-}, HCO_3^-, PO_4^{3-}, NH_4^+), and the role of $^{\bullet}OH$ radicals was highlighted by means of the presence of some reactive oxygen species scavengers.

The use of the Fe^{3+}/Oxalate or Fe^{3+}/Citrate/H_2O_2/UV-Vis processes to treat OTC solutions was proposed, due to the formation of a Fe (III):OTC complex during the conventional photo-Fenton process at near neutral pH levels. Process efficiency was evaluated for different variables and reaction rates were compared in the presence of different inorganic anions and humic acids, and in two different real wastewater matrixes. Distribution of Fe(III)-oxalate species favoured the Fe^{3+}/Oxalate/H_2O_2/UV-Vis reaction and optimal process parameters were [Fe (III)] = 2 mg L^{-1}, pH_0 = 5.0 and an iron/oxalate molar ratio of 1:3, with a total addition of 90 mg L^{-1} of H_2O_2. Results obtained in the solar pilot plant showed that the antibiotic is quickly removed from solution (Q_{UV} = 0.4 against 2.0 kJ_{UV} L^{-1} in the TiO_2/UV system), with consequent loss of antibacterial activity. The original DOC was decreased by 51%, with a remaining high percentage of LMWCA, and the final pH is within the legal discharge limits.

The Fe^{3+}/Oxalate/H_2O_2/UV-Vis system (same operational conditions) was found to be more efficient than TiO_2/UV ([TiO_2] = 0.2 g L^{-1}, pH_0 = 5.5) in the degradation of the transformation products obtained after the biodegradation of AMX spiked in different matrices enriched with a mixed bacterial culture.

Resumo

A administração generalizada de antibióticos em tratamentos médicos e veterinários tem resultado na presença ubíqua de quantidades residuais destes fármacos em ambientes aquáticos naturais por todo o mundo. Tal deve-se em grande parte à incapacidade dos sistemas convencionais de tratamento de efluentes líquidos em remover totalmente estes compostos altamente estáveis e/ou não-biodegradáveis. Estas circunstâncias têm levado a uma crescente preocupação com o risco de potenciais efeitos ecotoxicológicos e de propagação de resistência bacteriana. Por conseguinte, o desenvolvimento de processos alternativos para assegurar globalmente a qualidade da água e a própria saúde ambiental tornou-se uma das principais prioridades científicas da actualidade.

A aplicação de Processos de Oxidação Avançados (POAs) para degradar contaminantes recalcitrantes, tais como antibióticos, tem vindo a demonstrar resultados promissores nos últimos anos. Os POAs são distinguidos pela produção de radicais hidroxilo ($^{\bullet}OH$), cuja elevada reactividade e não-selectividade tem demonstrado resultados satisfatórios na mineralização de contaminantes a CO_2, água e iões inorgânicos, ou pelo menos à sua conversão parcial em compostos menos prejudiciais e/ou mais biodegradáveis. Dois destes processos são considerados de grande interesse, a fotocatálise heterogénea mediada por dióxido de titânio (TiO_2/UV) e o processo de foto-Fenton. A sua capacidade de utilização da radiação solar como fonte de radiação ultravioleta/visível (UV-Vis) reduz os custos energéticos, enquanto os catalisadores e reagentes necessários são pouco dispendiosos. Os colectores parabólicos compostos (CPCs) são a escolha mais comum de foto-reactores permitindo a utilização de radiação solar directa e difusa.

O objectivo geral desta tese foi o estudo da destoxificação de três antibióticos, Oxitetraciclina (OTC), Ácido Oxolínico (OXA) e Amoxicilina (AMX), através dos dois processos referidos. As experiências foram realizadas à escala laboratorial, num dispositivo fotocatalítico equipado com um simulador de luz solar (Suntest), e em escala piloto, numa instalação solar piloto, ambos equipados com CPCs. Os objetivos específicos foram os seguintes: i) estimativa das constantes cinéticas de degradação usando soluções puras de antibiótico; ii) avaliação do tempo de foto-tratamento necessário para atingir níveis de degradação abaixo das concentrações induzíveis de resistência bacteriana e níveis de mineralização desejáveis; iii) avaliação do papel das variáveis dos processos fotocatalíticos; iv) avaliação da influência de componentes individuais típicos de efluentes líquidos e de matrizes reais e v) desenvolvimento de um tratamento alternativo combinando a degradação biológica de AMX por intermédio de uma cultura enriquecida com um sistema fotocatalítico. Os resultados foram comparados em termos de energia UV acumulada por litro de solução, Q_{UV} ($kJ_{UV}\ L^{-1}$).

A fotólise solar demonstrou-se insuficiente para a degradação e/ou mineralização de OTC, OXA e AMX. Em testes iniciais com o sistema TiO_2/UV para tratar uma solução pura de OTC, os parâmetros óptimos foram 0,5 g L^{-1} de TiO_2, sem ajuste inicial de pH (pH_0 ~ 4,4). Nestas condições, a biodegradabilidade da solução aumentou, enquanto a inibição da bioluminiscência de *Vibrio fischeri* foi reduzida. Utilizando a mesma quantidade de catalisador mas em condições de pH neutro (~7,5) no tratamento de soluções individuais contendo 20 mg L^{-1} de cada antibiótico na instalação piloto, foram obtidas as seguintes constantes cinéticas de pseudo-primeira ordem: 4,03 ± 0,07 (OTC), 1,9 ± 0,1 (OXA) e 0,80 ± 0,02 L kJ_{UV}^{-1} (AMX). Numa mistura de OTC e OXA (C_0 = 20 mg L^{-1} cada), a velocidade de reacção diminuiu para metade devido à competição por $^{\bullet}OH$. Soluções de 40 mg L^{-1} de OTC, OXA e AMX tratadas individualmente necessitaram à volta de 2,0 (OTC) e de 4,6 kJ_{UV} L^{-1} (OXA, AMX) para cessar a inibição do crescimento das estirpes bacterianas testadas. No final dos respectivos períodos de foto-tratamento, uma elevada percentagem do carbono orgânico dissolvido (DOC) estava na forma de aniões carboxilato de baixo peso molecular (LMWCA) facilmente biodegradáveis. O azoto contido nas moléculas originais de OTC, OXA e AMX foi parcialmente convertido em amónio, mas a dessulfurização dos produtos intermediários de AMX foi completa. Os fosfatos foram a espécie mais interferente no processo, entre vários iões inorgânicos testados, e o papel dos $^{\bullet}OH$ foi realçado na presença de sequestradores de espécies de oxigénio reactivas.

A utilização dos processos Fe^{3+}/Oxalato ou Fe^{3+}/Citrato/H_2O_2/UV-Vis foi proposta para tratar soluções de OTC devido à formação de um complexo Ferro (III):OTC durante o processo convencional de foto-Fenton em condições de pH próximas da neutralidade. A eficiência foi avaliada para diferentes variáveis e as constantes cinéticas de reacção foram comparadas na presença de diferentes aniões inorgânicos, de ácidos húmicos, e em duas matrizes de efluentes reais. A distribuição das espécies de Fe (III)-oxalato favoreceu o uso do sistema Fe^{3+}/Oxalato/H_2O_2/UV-Vis, e os parâmetros processuais ótimos foram [Fe (III)] = 2 mg L^{-1}, pH_0 = 5,0 e rácio molar ferro/oxalato de 1:3, com adição total de 90 mg L^{-1} de H_2O_2. Resultados obtidos na instalação solar piloto mostraram que o antibiótico é rapidamente removido da solução, com perda subsequente de actividade antibacteriana (Q_{UV} = 0,4 contra 2,0 kJ_{UV} L^{-1} no sistema TiO_2/UV). O DOC original foi reduzido em 51%, com uma elevada percentagem de LMWCA remanescente, e o pH final ficou dentro dos limites de descarga legais.

Nas mesmas condições operacionais, o sistema Fe^{3+}/Oxalato/H_2O_2/UV-Vis foi mais eficiente do que o Sistema TiO_2/UV ([TiO_2] = 0,2 g L^{-1}, pH_0 = 5,5) na remoção de produtos resultantes da biodegradação de AMX introduzida em diferentes matrizes enriquecidas com uma cultura bacteriana mista.

Resum

L'ús generalitzat d'antibiòtics en els tractaments mèdics i veterinaris, s'ha traduït en la presència ubiqua de quantitats traça d'aquests compostos en entorns aquàtics naturals a tot el món. Això es deu en gran part a la incapacitat dels tractaments convencionals d'aigües residuals per eliminar aquests compostos altament estables i/o no biodegradables. Aquestes circumstàncies han donat lloc a una creixent preocupació pel risc de potencials efectes ecotoxicològics i de propagació de la resistència bacteriana. Així doncs, el desenvolupament de processos alternatius per garantir la qualitat de l'aigua en general i la pròpia salut del medi ambient s'ha convertit en una de les principals prioritats científiques actuals.

L'aplicació dels Processos d'Oxidació Avançada (POA) per degradar contaminants recalcitrants, com els antibiòtics, ha mostrat resultats prometedors en els últims anys. Els POA es caracteritzen per la producció de radicals hidroxils (•OH), altament reactius i no selectius, que condueixen a resultats altament satisfactoris en la mineralització dels contaminants a CO_2 , aigua i compostos inorgànics, o almenys en la seva conversió parcial a compostos menys perjudicials i/o més biodegradables. Dos d'aquests POA, la fotocatàlisi heterogènia mitjançant diòxid de titani (TiO_2/UV) i el procés de foto-Fenton, es consideren de gran interès. La seva capacitat d'utilitzar la radiació solar disponible de forma natural com a font de llum ultraviolada/visible (UV - Vis) redueix en gran mesura els costos energètics, mentre que els catalitzadors i reactius requerits són de baix cost. Els col•lectors parabòlics compostos (CPC) són l'elecció més comuna de foto-reactors, a causa del seu ús altament eficient de la radiació solar UV, tant directa com difusa.

L'objectiu principal d'aquesta tesi va ser estudiar la degradació de tres antibiòtics, l'oxitetraciclina (OTC), l'àcid oxolínic (OXA) i l'amoxicil•lina (AMX), a través d'aquests dos processos fotocatalítics, que requereixen radiació solar. Els experiments es van realitzar a escala de laboratori, en un dispositiu fotocatalític proveït d'un simulador de llum solar (Suntest), i en una planta pilot solar; les dues instal•lacions equipades amb CPC. Es van perseguir els següents objectius: i) l'estimació de les constants de velocitat de degradació fotocatalítica amb solucions pures d'antibiòtics ii) l'avaluació dels temps de foto tractament necessaris per assolir nivells de degradació per sota de les concentracions d'inducció de resistència, i nivells de mineralització desitjables per a la seva possible integració amb sistemes de degradació biològica, iii) l'avaluació de la funció de les variables dels processos fotocatalítics, iv) l'avaluació de la influència dels components individuals presents en les aigües residuals i en les matrius reals i v) el desenvolupament d'un tractament alternatiu de múltiples etapes, combinant la degradació biològica de l'AMX per mitjà d'un cultiu enriquit amb un sistema fotocatalític solar. Els resultats es van comparar en termes d'energia UV acumulada per litre de solució, Q_{UV} ($kJ_{UV}\ L^{-1}$).

La fotòlisi Solar va resultar ser insuficient en la degradació i/o mineralització d'OTC, OXA i AMX. En els experiments preliminars utilitzant el sistema TiO_2/UV per tractar una solució d'OTC pura, es van trobar els paràmetres òptims del procés: 0,5 g L^{-1} de TiO_2, sense ajust de pH inicial (pH_0 ~ 4,4). Amb aquestes condicions es va registrar un augment en la biodegradabilitat de la solució i una disminució en la inhibició de la bioluminescència de Vibrio fischeri. Utilitzant la mateixa càrrega de catalitzador, però sota condicions de pH neutre (~7,5) a la planta pilot, es van obtenir les següents cinètiques de pseudo-primer ordre pel tractament individual de solucions de 20 mg L^{-1} d'OTC, OXA i AMX: 4,03 ± 0,07 (OTC), 1,9 ± 0,1 (OXA) i 0,80 ± 0,02 kJ_{UV} L^{-1} (AMX). En una barreja d'OTC i OXA (C_0 = 20 mg L^{-1} cada un), les constants de velocitat gairebé es van veure reduïdes a la meitat, a causa de la competència pels radicals hidroxil. Les solucions d'OTC, OXA i AMX tractades individualment (C_0 = 40 mg L^{-1}) requereixen al voltant de 2,0 (OTC) i 4,6 kJ_{UV} L^{-1} (OXA, AMX) per aturar la inhibició del creixement de les soques bacterianes analitzades. Al final dels respectius períodes de foto-tractament, un alt percentatge del carboni orgànic dissolt (DOC) es trobava en forma d'anions carboxilat de baix pes molecular (LMWCA) més fàcilment biodegradables. El contingut original de nitrogen en les molècules d'OTC, OXA i AMX, es van convertir parcialment en amoni, mentre que la dessulfuració dels productes intermedis de l'AMX va ser completa. Els fosfats van resultar ser l'espècie que més va interferir en el procés, entre diversos ions inorgànics analitzats (Cl^-, SO_4^{2-}, HCO_3^-, PO_4^{3-}, NH_4^+), i el paper dels radicals $^{\bullet}OH$ va millorar en presència de segrestadors d'espècies reactives amb l'oxigen.

Es va proposar l'ús dels processos de Fe^{3+}/oxalat o Fe^{3+}/citrat/H_2O_2/UV Vis per al tractament de solucions d'OTC, a causa de la formació del complex Fe(III):OTC durant el procés convencional de foto-Fenton a nivells de pH gairebé neutre. L'eficiència del procés va ser avaluada per diferents variables i condicions experimentals, i es van comparar les velocitats de reacció en presència de diferents anions inorgànics i àcids húmics, i en dues matrius d'efluents reals. La distribució de les espècies Fe(III)-oxalat van afavorir la reacció de Fe^{3+}/oxalat/H_2O_2/UV-Vis, i els paràmetres òptims del procés van ser [Fe(III)] = 2 mg L^{-1}, pH_0 = 5,0 i una relació molar de ferro/oxalat de 1:3, amb una addició total de 90 mg L^{-1} de H_2O_2. Els resultats obtinguts a la planta pilot solar mostren que l'antibiòtic s'elimina ràpidament de la solució (Q_{UV} = 0,4 contra 2,0 kJ_{UV} L^{-1} en el sistema de TiO_2/UV), amb la consegüent pèrdua d'activitat antibacteriana. El DOC original es va veure reduït en un 51 %, amb un alt percentatge restant en forma de LMWCA, trobant-se el pH final es trobava dins dels límits de descàrrega legals.

Es va observar que el sistema Fe^{3+}/oxalat/H_2O_2/UV-Vis, en les mateixes condicions de funcionament, era més eficient que el sistema TiO2/UV ([TiO_2] = 0,2 g L^{-1}, pH_0 = 5,5) en la degradació dels productes resultants de la degradació d'AMX inoculada en diferents matrius enriquides amb un cultiu bacterià.

Table of Contents

Table of Figures

List of Tables

Notation

Acronyms

AA	Antibacterial activity
AMX	Amoxicillin
AOP(s)	Advanced oxidation process(es)
BOD_5	Biological oxygen demand (5 days)
CAS	Conventional activated sludge
COD	Chemical oxygen demand
CPC(s)	Compound parabolic pollector
DAD	Diode array detector
DBE	Double bond equivalent
DOC	Dissolved organic carbon
EM	Enrichment medium
ESI	Electrospray ionization
FBR	Fixed-bed reactor
HPLC	High performance liquid chromatography
LC	Liquid chromatography
LMWCA	Low-molecular-weight carboxylate anions
LOD	Limit of detection
LOQ	Limit of quantification
MBR	Membrane bioreactor
MC	Mixed culture
MS	Mass spectrometry
OTC	Oxytetracycline
OXA	Oxolinic acid
PCR	Polymerase chain reaction
PPCPs	Pharmaceuticals and personal care products
rRNA	Ribosomal ribonucleic acid
TiO_2	Titanium dioxide
TP	Transformation products
UV	Ultraviolet
Vis	Visible
YE	Yeast extract
WW	Wastewater matrix
WWTP	Wastewater treatment plant

Variables

A_r	Illuminated area (m^2)
A_{CO}	Collector area per order(m^2 m^{-3}-order)
C	Concentration (mg L^{-1} or mM)
i_0	Initial value of compound/species/acronym i
[i]	Concentration of compound/species i (mg L^{-1} or mM)
I	Irradiance (W m^{-2})
Q_{UV}	Accumulated UV energy per litre of solution (kJ_{UV} L^{-1})
T	Temperature (°C)
t	Time (s, min or h)
$\overline{UV}_G$	Average solar ultraviolet irradiance (W m^{-2})
V	Volume (L)

1 Introduction

This chapter presents the introduction to this thesis. The background and motivation are presented. An overview of the problematic of aquatic contamination by antibiotic residues will be provided, as well as of current and potential decontamination methods. The concepts and operational parameters of the two advanced oxidation processes herein proposed will be presented, complemented with a survey of current literature.

1.1 Motivation and thesis outline

The environmental pressure on fresh water resources resulting from the discharge of wastewaters contaminated with non-biodegradable pollutants all over the world is regarded as a major challenge to be tackled. Scientific research has been increasingly focused on new methods of water purification, allowing for safe wastewater reutilization. In 2000, the European Commission and European Parliament published Directive 2000/60/EC, establishing a framework for Community action in the field of water policy, the European Water Framework Directive (WFD). One of the highlights of the WFD was the requirement for controlling, reducing or phasing out emissions of micropollutants identified as priority substances (such as pesticides), which represent significant risks to aquatic environments. Antibiotics are an important group of pharmaceuticals used in the treatment of human infections, veterinary medicine and fish farms, to name a few examples. In recent years, a significant body of work has identified trace antibiotics in natural aquatic environments, raising the question of the inability of conventional wastewater treatment methods to deter contamination, leading to an ubiquitous persistence of these compounds which increase the risks of ecotoxicological effects on aquatic organisms and the spread of antibiotic resistant genes in bacterial communities.

The establishment of advanced oxidation processes (AOPs) has been emphasized to become the most widely used wastewater treatment technologies for organic pollutants that possess high chemical stability and/or low biodegradability, such as antibiotics. These processes involve generation and subsequent reaction of hydroxyl radicals ($^{\bullet}OH$), which possess a high standard reduction potential ($E^{o}(^{\bullet}OH/H_2O)$ = 2.80 V/SHE) and react non-selectively with most organics. The endpoint would be complete pollutant transformation into CO_2, water and inorganic ions (mineralization), or otherwise conversion of pollutants into non-toxic and more bio-degradable intermediaries. From the many different $^{\bullet}OH$ production possibilities, research is being focused on catalytic AOPs which can be driven by solar radiation, such as heterogeneous catalysis with TiO_2/UV and the photo-Fenton process. Their main advantage is low-reactant costs and the inexpensive source of UV/Vis photons. Compound parabolic collectors (CPCs), a type of low-concentration collectors used in thermal applications, have been considered as a good option for solar photochemical applications due to the highly efficient use of both direct and diffuse UV solar radiation.

For these reasons, the present thesis focuses on the detoxification study of three selected antibiotics, Oxytetracycline (OTC), Oxolinic acid (OXA) and Amoxicillin (AMX), by means of two solar-driven photocatalytic processes, TiO_2/UV and photo-Fenton. OTC and OXA were chosen due to their wide use in veterinary applications and shortage or non-existance of degradation studies using these processes. AMX is widely used in human medicine and, notwithstanding the number of existing photocatalytic removal studies, none so far have applied (CPC) as photoreactors.

The main objectives were:

i. Attainment of photocatalytic degradation rate constants in pure antibiotic solutions;
ii. Assessment of required phototreatment times to achieve antibiotic degradation levels below resistance-inducing concentrations;
iii. Evaluation of the role of photocatalytic process variables;
iv. Assessment of the influence of individual wastewater components and real matrices;
v. Development of an alternative multistage treatment combining the biological degradation of AMX by means of an enriched culture with a solar photocatalytic system.

The thesis is structured in 8 chapters:

Chapter I corresponds to the present introductory section, wherein the problem of environmental contamination by antibiotics, as well as current and potential decontamination methods, are covered. The main concepts and operational parameters of TiO_2/UV photocatalysis and photo-Fenton processes are presented, complemented with a literature survey.

Chapter 2 describes the employed materials and methods and followed experimental procedures

The subsequent five Chapters report the experimental results obtained with both photocatalytic systems tested:

Chapter 3 focuses on the role of variables such as catalyst load and solution pH on the degradation and mineralization of OTC in a pure solution. Biodegradability, ecotoxicity and generated intermediary by-products of a solution tested under optimal conditions were evaluated. Differences in the performance between lab-scale and pilot-plant scale were also assessed.

Chapter 4 compares the photocatalytic degradation and mineralization under fixed catalyst and pH conditions of OTC with OXA, in pure solutions and in a mixture, while Chapter 5

deals exclusively with pure solutions of AMX. In these two Chapters, the antibacterial activity of treated solutions is assessed, as well as the conversion of dissolved organic carbon (DOC) into low-molecular-weight carboxylate anions and the release of inorganic ions. The effect of inorganic ions on the photocatalytic degradation of each individual antibiotic solution was also evaluated and the formation of different reactive oxygen species was probed using selective scavengers.

In Chapter 6, the application at near neutral pH of the photo-Fenton process mediated by ferricarboxylates (oxalate and citrate) is proposed to overcome the problem of ferric iron-OTC complex formation during the conventional photo-Fenton treatment of OTC aqueous solutions. Results mainly cover the influence of process parameters, and reaction rates were compared in the presence of different interferents and in two different real wastewater matrices.

Chapter 7 reports on the feasibility of using a multistage treatment system for AMX-spiked solutions combining: i) a biological treatment process using an enriched culture to metabolize AMX, with ii) a solar photocatalytic system (TiO_2/UV or Fe^{3+}/Oxalate/H_2O_2/UV-Vis) to achieve the removal of the metabolized transformation products (TPs) identified via LC-MS, recalcitrant to further biological degradation.

Finally, Chapter 8 presents a discussion of the most pertinent results and conclusions of this thesis and a list of subsequent suggestions for future work.

1.2 The problem of antibiotic residues in the environment

Human and veterinary pharmaceutical chemicals are widely used for diagnosis, treatment, alteration or prevention of disease and other health conditions, and include a broad class of substances such as analgesics, antibiotics, lipid lowering agents, hormones and other endocrine disrupting compounds. They are distinguished by their functionalities, physico-chemical and biological properties (Kümmerer, 2001), and are designed to perform a certain biological activity on human beings, animals, bacteria or other organisms (Halling-Sørensen et al., 1998).

The contamination of the environment by Pharmaceuticals and Personal Care Products (PPCPs) as a result of metabolic excretion, improper disposal and/or industrial waste has been the subject of special attention over recent years, as reflected by the increasing literature regarding their sources, fate and biological effects, as well as studies on their removal and degradation from different environmental matrices. Such works range from general reviews, approaches to environmental risk assessment, measurement and detection in effluents from wastewater treatment plants (WWTPs) and assorted environmental compartments, development of analytical methods of extraction and identification and, finally, different processes of removal and degradation of PPCPs (Halling-Sørensen et al., 1998; Andreozzi et al., 1999; Adams et al., 2002; Heberer, 2002; Kolpin et al., 2002; Fent et al., 2006; Seifrtová et al., 2009).

Amongst all PPCPs, antibiotics are a diverse group of medical substances whose antibacterial, anti-fungal or anti-parasitical properties play a major role in modern medicine, both human and veterinary. They can be either derived from certain microorganisms or obtained by chemical synthesis.

A general classification is made grouping antibiotics by chemical structure or by mechanism of action (Kümmerer, 2009). For instance, β-lactams inhibit cell wall synthesis, Tetracyclines and Macrolides inhibit protein synthesis, Quinolones interfere with nucleic acid metabolism and Sulfonamides act as competitive inhibitors of growth factors and other metabolites (Son et al., 2009). Depending on the mechanism of action, antibiotics can be bactericidal (they kill bacteria) or bacteriostatic (they inhibit bacterial reproduction or growth).

Antibiotic usage for human and veterinary consumption varies significantly by groups and by country (Mölstad et al., 2002; Sarmah et al., 2006), but information on the values of production and usage is still not widely available. A few international comparisons have been made so far (Cars et al., 2001). Goossens and co-workers (Goossens et al., 2007), under the European Surveillance of Antimicrobial Consumption (ESAC) project, have shown that the outpatient use of Tetracyclines, Macrolides and Quinolones antibiotics in the United States of America is

higher than in any country of Europe, where the β-lactams make up the largest share. Regarding veterinary antibiotics, a review by Sarmah and co-workers (2006) has collected values of use and production on a global scale, showing Ionophores, a veterinary-only class of antibiotics, to represent the largest class by reported use in the United States and New Zealand.

On a global level, human antibiotics are consumed domestically, in clinics or in hospitals, whereas veterinary antibiotics are generally used in livestock therapeutics and fish feeds. As they are only partially metabolized in the organism (Hirsch et al., 1999), they are excreted (together with their metabolites), to receiving WWTPs and, ultimately, to other environmental compartments (Hektoen et al., 1995; Thiele-Bruhn, 2003; Jones et al., 2005b). The degree to which antibiotics are metabolized in human and animal bodies varies substantially, but when the amounts used are multiplied by excretion rates, even those with high metabolization rates can be important (Kümmerer, 2009). On a local level, effluents from drug production facilities are also considered an important source of antibiotics (Larsson et al., 2007; Li et al., 2008a; Li et al., 2008b). Sorption of non-biodegradable antibiotics in the biomass of WWTPs may also become an issue when desorption conditions change during land application of biosolids, increasing antibiotic bioavailability (Kim et al., 2005). Thus, with their release to the environment (Figure 1.1) and with the improvement of detection methods, antibiotics have been measured on different matrices all over the world (Table 1.1).

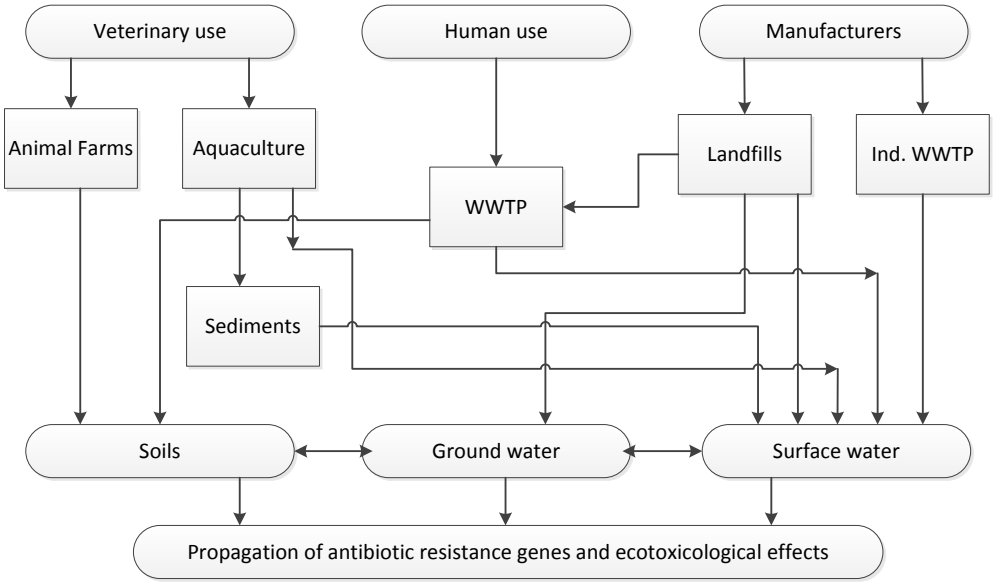

Figure 1.1. Sources and possible routes of exposure of antibiotics in the environment. Adapted from Kemper (2008).

Concentrations found are generally low (Table 1.1) but nevertheless, a continuous introduction can offset antibiotic natural transformation and removal rates (Jones et al., 2005a), raising concerns about more subtle changes. On the one hand, acute environmental impacts of most studied substances may be unlikely (Baguer et al., 2000; Boxall et al., 2003), but on the other hand, several studies have shown the development of resistance in environmental bacteria

(McKeon et al., 1995; Morris and Masterton, 2002; Kümmerer, 2004; Baquero et al., 2008; Dantas et al., 2008; Martinez, 2009), effects on activated sludge bacteria (Halling-Sørensen et al., 2002; Cunningham et al., 2006; Alighardashi et al., 2009) and on algal communities (Halling-Sørensen, 2000; Wilson et al., 2003). Finally, a possible cumulative exposure to human beings in drinking water is especially worrisome (Webb et al., 2003; Collier, 2007; Vaz-Moreira et al., 2011).

The importance of developing practical and effective wastewater treatment processes to avert antibiotic pollution is thus of the utmost importance to assure the quality of aquatic environments.

Table 1.1. Examples of reported levels of some antibiotics in different aquatic media in various countries.

Group	Antibiotic	Concentration ($\mu g\ L^{-1}$)	Compartment	Location	References
β-Lactams	Amoxicillin	0.280[a] 0.030[b]	Domestic WWTP	Australia	Watkinson et al. (2007)
	Penicillin G	0.153[a] 0.002[b]	Production facility WWTP	China	Li et al. (2008b)
Macrolides	Clarithromycin	0.059 – 1.433[a] 0.012 - 0.232[b]	Domestic WWTP	Taiwan	Lin et al. (2009)
	Erythromycin	0.113[a] 0.290[b]	Domestic WWTP	U.K.	Roberts and Thomas (2006)
		0.070	Surface water		
Quinolones	Ciprofloxacin	0.017 – 2.500[a] 0.022 – 0.620[b]	Domestic WWTP	Canada	Guerra et al. (2014)
	Norfloxacin	0.059[a] 0.013[b]	Domestic WWTP	China	Li et al. (2009)
	Oxolinic Acid	10 - 2500	Shrimp pond water	Vietnam	Le and Munekage (2004)
Sulfonamides	Sulfamethoxazole	0.013 - 0.155[a] 0.004 - 0.039[b]	Domestic WWTP	Luxembourg	Pailler et al. (2009)
		0.001 - 0.022	Surface water		
	Sulfamethazine	0.29[a] 0.036[b]	Domestic WWTP	U.S.A.	Karthikeyan and Meyer (2006)
Tetracyclines	Tetracycline	42.2 – 158 23.2 – 29.2[a]	Hospital wastewater Domestic WTTP	Portugal	Pena et al. (2010)
	Oxytetracycline	0.07 – 1.34	Surface water	U.S.A.	Lindsey et al. (2001)
		19.5 – 920 ($\times 10^3$)[b] 235 – 484	OTC production facility WWTP Receiving river	China	Li et al. (2008a)

[a]Influent, [b]Effluent

1.3 Removal of antibiotics by conventional and advanced treatments

In conventional WWTPs, biological degradation is the main process associated to the elimination of micropollutants such as antibiotics. Physical steps such as sorption on sludge or particulate matter, filtration or stripping simply alter the phase in which antibiotics are present

(Larsen et al., 2004; Kim et al., 2005). Still, in accordance to studies that show how many of these substances fail to be readily biodegradable in simulated conditions, it is expected that certain antibiotics persist through conventional wastewater treatment systems conditions (Kümmerer et al., 2000; Ingerslev et al., 2001; Drillia et al., 2005). Several authors also note the importance of studying transformation products (TPs) resulting from biological conversion of parent compounds, which may be more stable in the environment (Lamm et al., 2009; Tambosi et al., 2010; Pérez-Parada et al., 2011).

Le-Minh et al. (2010) dedicated a review to summarize the most important factors affecting the reported varying efficiencies of the removal by conventional and advanced treatments methods of the different classes of antibiotics. For instance, β-lactam antibiotics are highly susceptible to chemical and biochemical hydrolysis of the β-lactam ring during biological treatments while the capacity of activated carbon to adsorb particular compounds depends on the hydrophobic (non-polar) or hydrophilic (polar) nature of the chemical. The removal efficiencies may even vary between antibiotics belonging to the same class, i.e., presenting similar molecular structure and physic-chemical properties, as seen on a work by García Galán et al. (2012) reporting on the removal of several sulfonamide antibiotics upon conventional activated sludge (CAS) and advanced membrane bioreactor (MBR).

Miège and co-workers (2009) published a database on the fate of PPCPs in WWTPs. For the seven most cited antibiotics over 117 papers involving 184 molecules, mean removal efficiencies ranged from 18 % (Trimethoprim) to 80 % (Norfloxacin). In a reported study (Göbel et al., 2007), the elimination of detected antibiotics in the raw wastewater of two WWTPs (two sulfonamides, four macrolides and trimethoprim) was studied through CAS systems coupled with a fixed-bed reactor (FBR) and MBR, respectively. Removal in primary treatment (sand filter) was generally low and considered as not significant for all antibiotics. As to the secondary effluents of CAS systems and FBR, the two sulfonamides inconsistently showed either high positive or negative elimination values, suggesting a possible retransformation between their main metabolites. Trimethoprim showed only a slight elimination of up to 20 %, and varying results, including negative values, were obtained for the studied macrolides (-20 to 20 %). This is in contrast to the results of the CAS system coupled with the MBR, which not only showed no increase in the load of any antibiotic but also a higher tendency of elimination. Despite this, full removal was not obtained for any molecule.

Camacho-Muñoz et al. (2012) compared the effectiveness of conventional suspended wastewater treatments (activated sludge and oxidation ditches) and low-cost treatments (trickling filters, anaerobic lagoons and constructed wetlands) on the removal of several PPCPs, including the antibiotics Sulfamethoxazole and Trimethoprim, detected in influents from 11

urban WWTPs. Reported removal rates of these antibiotics were as high as 99 %, while mean removal rates of other PPCPs were 64 and 55 % for conventional and low-cost techniques, respectively. Nevertheless, most compounds were still detected in effluent wastewater.

Adams et al. (2002) determined the effectiveness of common drinking water treatment processes in the removal of seven common antibiotics. Powdered activated carbon, reverse osmosis and oxidation with chlorine and ozone were shown to be effective in removing over 90% of each compound from both distilled and river water. In contrast, coagulation, flocculation and sedimentation with alum and iron salts, excess lime/soda ash softening, ultraviolet (UV) irradiation at disinfection dosages and ion exchange were not. Moreover, Rizzo and co-workers (2013) remarked that the common UV disinfection process is inappropriate for assorted antibiotic removal, given that not all antibiotics present UV absorption spectra which overlap with the UV lamp emission (peak at 254 nm).

Choi et al. (2008) also evaluated the treatment of seven Tetracycline antibiotics from raw waters by coagulation (poly-aluminum chloride as coagulant) and adsorption (granular activated carbon (GAC) filter). Efficiency of coagulation removal ranged from 43 to 94%, depending on the type of tetracycline, at optimum conditions, from synthetic water, but it slightly decreased (44~67%) in river water due to organic interference, notwithstanding an insignificant difference between removal efficiencies. On the other hand, GAC filtration showed to be more effective, removing more than 68% of incoming tetracyclines, with general removal efficiencies above 90%. A coupling of both techniques was suggested to improve tetracycline removal.

Two wide-ranging studies by Rivera-Utrilla discussed the removal from water of nitroimidazoles (2009) and tetracycline antibiotics (2013a) by adsorption/biosorption on activated carbons and sludge-derived adsorbents. They addressed the role of the chemical properties of the different activated carbons and of the solution pH and also the influence of the presence of electrolytes and bacteria, matrix effects and different regimes on adsorption rates. In 2011, the same authors published an overview on activated carbon modifications to enhance their water treatment applications (Rivera-Utrilla et al., 2011). Regardless of the advantage of not generating toxic nor pharmaceutically active products, the major drawback of activated carbon adsorption is that concerning the transference of the contaminants to a new phase, concentrating them (Daghrir and Drogui, 2013; Rivera-Utrilla et al., 2013b).

Chamberlain and Adams (2006) reported the application of free chlorination and monochloramination for the oxidation of antibiotics (Carbadox and sulfonamides, macrolides) in surface waters in laboratory under conditions similar to drinking water treatment. Chlorination readily removed sulfonamides at near neutral pH levels, whereas for macrolides,

only partial removal was obtained. Little removal of both antibiotic classes was observed with monochloramination at any condition. However, for Carbadox, both processes showed fast reactions and a near complete removal of the parent compound would be expected. However, specific oxidation byproducts were not analyzed. Several authors contend the application of chlorination processes to treat micropollutants, since thorough information regarding the formation and fate of harmful chlorinated byproducts is still lacking (Le-Minh et al., 2010; Oncu and Balcioglu, 2013).

Tambosi et al. (2010) underlined the role of biodegradation in the removal of three antibiotics, amongst other PPCPs, in two different MBR set-ups, compared to sludge sorption or physical retention in the membranes. The antibacterial properties of each compound are suggested to account for differences in antibiotic removal efficiency. Conversely, Radjenovic et al. (2007) and Radjenović et al. (2009) found varying removal rates of PPCPs (including the antibiotics Erythromycin, Sulfamethoxazole, Ofloxacin and Trimethoprim) when comparing CAS system to MBR treatment. As in the abovementioned studies, these authors bring up the fact that MBR processes would not completely halt discharge of micropollutants and reckon that, although a promising technology, MBR processes still require optimization of design and operational conditions to overcome the incomplete removal of antibiotics. An overview of removal of pharmaceuticals with MBRs technology by Sipma and co-workers (2010) also supports this conclusion, while Larsen et al. (2004) also specified that MBR have high material costs and energy demands, albeit having the advantage of smaller space requirements and of increasing solids retention time.

Rejection of trace pollutants by ultrafiltration (UF), nanofiltration (NF) and/or reverse osmosis (RO) membrane systems have been showing good overall removal results (Li et al., 2004; Košutić et al., 2007; Snyder et al., 2007; Yoon et al., 2007; Koyuncu et al., 2008; Radjenović et al., 2008), but major drawbacks result from expensive membrane disposal and substitution, high energy and operation requirements and possible greater toxicity levels in the brine compared to the influent water (Snyder et al., 2007). Busetti and Heitz (2011) provides an example of the efficiency of a microfiltration-reverse osmosis treatment integrated in a full scale operational water reclamation plant in the removal of nitroimidaozle, sulfonamide, lincosamide and macrolide antibiotics detected in secondary treated effluents. The reported estimated membrane rejection was generally higher than 91%.

In recent years, the application of Advanced Oxidation Processes (AOPs) to treat wastewaters contaminated with components that have high chemical stability and/or low biodegradability, such as pesticides or pharmaceuticals, has been subject to intensive research. For this reason, the following section will deal entirely with AOPs.

1.4 Removal of antibiotics by Advanced Oxidation Processes

AOPs comprise different processes of generating the highly reactive and non-selective hydroxyl radicals (•OH). Malato et al. (2003) concisely enunciates that •OH radicals are the second strongest known oxidant after fluoride (E^o(•OH/H_2O) = 2.80 V/SHE), and that kinetic rate constants for most reactions fall in the order of 10^6 to 10^9 M^{-1} s^{-1}. The reactions through which they attack organic molecules can be hydrogen abstraction, electrophilic addition, electron transfer and also radical-radical reactions, citing Legrini et al. (1993) in the abovementioned work. A recent work by Wols and Hofman-Caris (2012) points out the very high •OH radical rate constants for a wide range of organic micropollutants, including antibiotics.

The classification of AOPs can be divided as follows: photochemical (UV/O_3, UV/H_2O_2, $UV/H_2O_2/O_3$), photocatalytic (TiO_2/UV, Photo-Fenton) or chemical oxidation processes (O_3, O_3/H_2O_2, H_2O_2/Fe^{2+}) (Poyatos et al., 2009). The characteristics and mechanisms of these processes will not be discussed here, as there are plenty of detailed studies regarding general and particular aspects of each technique or combination thereof (Andreozzi et al., 1999; Huber et al., 2003; Malato et al., 2003; Gogate and Pandit, 2004a; b; Pignatello et al., 2006; Poyatos et al., 2009).

Comprehensive reviews covering the application of AOPs to aqueous pharmaceuticals are also available (Ikehata et al., 2006; Dalrymple et al., 2007; Esplugas et al., 2007; Kanakaraju et al., 2013), as well as specific reviews dealing with antibiotic removal exclusively (Homem and Santos, 2011; Michael et al., 2013b; Oncu and Balcioglu, 2013). Fatta-Kassinos et al. (2011) published a pertinent review on the often neglected subject of the significance of the resulting transformation by-products. It compiles information concerning the identification of TPs formed during the application of natural photolytic and AOPs and the respective potential biological effects. It also presents a critical view on the discrepancies and differences between published experimental configurations for photo-driven (advanced oxidation) processes, which prevent an otherwise uniform comparison of data and information relevant to real environmental conditions.

Of special importance is the ability of AOPs to achieve the complete mineralization of this kind of pollutants, yielding CO_2, water and inorganic compounds, or at least a partial decomposition to more biodegradable and/or less harmful intermediates. The later would allow for a useful and cost efficient combination with biological processes (Marco et al., 1997; Schaar et al., 2010; Oller et al., 2011). Considering the current limitations of implementing these processes in existing WWTP (high flow rates, capital and reactant costs, catalyst separation step, for example), the combination of membrane processes with AOPs have also been proposed to

optimize wastewater treatment (Westerhoff et al., 2009; Senta et al., 2011; Liu et al., 2014). At last, with respect to high energetic costs of implementing UV lamp-based wastewater treatments (Rosenfeldt et al., 2006), the AOPs relying on solar irradiation, such as heterogeneous photocatalysis mediated by TiO_2/UV and the Photo-Fenton reaction, are considered the most promising and environmental friendly technologies (Muñoz et al., 2006).

The use of Compound Parabolic Collectors (CPCs) greatly enhances the efficiency of these solar photocatalytic processes as it increases the amount of incident solar UV photons, both direct and diffuse, that can be used to degrade target substances (Rodríguez et al., 2004; Colina-Márquez et al., 2010). Bandala and Estrada (2007) performed a comparative study between four types of solar collectors using oxalic acid and the pesticide carbaryl as model contaminants, employing TiO_2 as photocatalyst. Compound parabolic collector geometry demonstrated the highest turnover rate in the photocatalytic degradation of both target compounds, followed by V-shaped trough collector, parabolic concentrator and tubular collector.

An in-depth review put forth by Malato and co-workers (2009) expounds on the use of sunlight to produce $^{\bullet}OH$ radicals by means of these two solar-driven processes, describing the influence of fundamental parameters, the analytical and toxicological tools, the necessary hardware, photocatalyst enhancement techniques, treatment integration with other AOPs and/or biodegradation.

Both solar heterogeneous photocatalysis mediated by TiO_2/UV and solar Photo-Fenton process will be briefly addressed in the following sub-sections.

1.4.1 Solar TiO_2/UV photocatalysis

Heterogeneous photocatalysis using suspended TiO_2 is of special interest due to the chemical stability of the photocatalyst, low cost and ability of using the small percentage of the ultraviolet radiation coming from the sun.

Monteiro et al. (2014) described the mechanism as follows. The absorption by the the semiconductor (TiO_2) of incident photons of energy $h\upsilon$ matching or exceeding the semiconductor band-gap energy produces conduction-band electrons $e_{cb}^{-}(TiO_2)$ and valence-band holes $h_{vb}^{+}(TiO_2)$, i.e. electron-hole pairs (Eq. 1.01). Once at the surface of the semiconductor, the presence of as suitable acceptor (for e_{cb}^{-}) and donor (for h_{vb}^{+}) will avoid the near instantaneous and undesirable generated recombination (Linsebigler et al., 1995; Furube et al., 2001). Hydroxyl anions and water molecules adsorbed on TiO_2 surface act as electron donors, while molecular oxygen acts as electron acceptor, leading to the formation of hydroxyl ($^{\bullet}OH$) and superoxide ($O_2^{\bullet -}$) radicals (Peral and Ollis, 1992; Pelizzetti and

Minero, 1993; Augugliaro et al., 1999) (see eq. 1.02-1.04). When an organic molecule (RH) is adsorbed onto semiconductor surface, the reaction with hydroxyl radical occur, followed by structural breakdown into several intermediates until, eventually, total mineralization (see eq. 1.05) (Hoffmann et al., 1995; Kolen'ko et al., 2005). Due to their high oxidation potential, the photogenerated holes can also participate in the direct oxidation of the organic pollutants (eq. 1.06) (Cermenati et al., 1997; Benoit-Marquié et al., 2000). A Peroxide ($HOO^{\bullet}$) radical can also be generated from the protonation of $O_2^{\bullet -}$ radical and subsequently form hydrogen peroxide (see eq. 1.07-1.08).

$$TiO_2 + h\nu \longrightarrow e_{CB}^{-}(TiO_2) + h_{VB}^{+}(TiO_2) \quad (1.01)$$

$$h_{VB}^{+}(TiO_2) + H_2O_{ads} \longrightarrow {}^{\bullet}OH + H^{+} \quad (1.02)$$

$$h_{VB}^{+}(TiO_2) + OH_{ads}^{-} \longrightarrow {}^{\bullet}OH \quad (1.03)$$

$$e_{CB}^{-}(TiO_2) + O_{2(ads)} \longrightarrow O_{2(ads)}^{-\bullet} \quad (1.04)$$

$$HO^{\bullet} + RH \longrightarrow RH^{+\bullet} \longrightarrow R^{\bullet} + H^{+} \quad (1.05)$$

$$h_{VB}^{+}(TiO_2) + RH \longrightarrow RH^{+\bullet} \longrightarrow R^{\bullet} + H^{+} \quad (1.06)$$

$$O_2^{\bullet -} + H^{+} \longrightarrow HOO^{\bullet} \quad (1.07)$$

$$O_2^{\bullet -} + HOO^{\bullet} + H^{+} \longrightarrow H_2O_2 + O_2 \quad (10.8)$$

Table 1.2 summarizes the parameters and their influence on the photocatalytic rate kinetics, based on the abovementioned review by Malato et al. (2009).

Table 1.2. Fundamental TiO_2/UV photocatalytic parameters and respective effect on reaction rates. Adapted from Malato et al. (2009).

Parameter	**Influence or effect on reaction rates**
Initial pollutant concentration (C_0)	Most reactions follow pseudo-first order kinetics ($C = C_0 \times e^{-kt}$), so maximum efficiency would be attained at saturation level of the catalyst surface.
Catalyst load ([TiO_2])	Reaction rates increase with increasing catalyst load, up until a point in which, depending on reactor geometry and experimental conditions, additional catalyst particles block the penetration of incident UV light.
pH	Influences the pollutant adsorption onto the catalyst surface and the catalyst particles aggregation.
Temperature	Irrelevant influence in the range of 20 to 80 °C.
Irradiance	Only wavelengths up to 390 nm are useful (~ 5% solar spectrum). Reaction rate is proportional to the radiant flux (Φ), but high values should be avoided because electron-hole recombination is favored.
O_2 concentration	No mineralization is possible without O_2, while reaction rates increase with increasing dissolved oxygen concentration (up to a certain level).

1.4.2 Solar photo-Fenton process

Photo-Fenton comprises the combination of ferrous iron (Fe^{2+}) with hydrogen peroxide (H_2O_2) and (solar) UV-Vis radiation resulting in the production of two moles of $^{\bullet}OH$ per mole of hydrogen peroxide (Eq. 1.09 and 1.10), as simplified by Gogate and Pandit (2004b):

$$Fe^{2+} + H_2O_2 \rightarrow Fe^{3+} + {}^{\bullet}OH + HO^{-} \quad (1.09)$$

$$Fe(OH)^{2+} + h\upsilon \rightarrow Fe^{2+} + {}^{\bullet}OH \quad (1.10)$$

Pignatello et al. (2006) summarizes the reasons for the optimum operational pH value of the (photo-) Fenton process around 3 as follows: first, the solubility of Fe^{3+}-hydroxy complexes decreases for pH values above 3; second, $[Fe(OH)]^{2+}$, the most photoactive species (with absorption bands between 290 and 400 nm), reaches its maximum molar fraction around the aforementioned pH. Consequently, there is a limit in the application of this process in industrial scale due to the costs associated with pH corrections (initial acidification and final neutralization).

The formation of complexes between Fe (III) and carboxylate ions is pointed out as the most viable way to overcome this liability. In this way, the photo-Fenton process is improved by extending the solubility of iron to higher and more practical pH values, by presenting stronger radiation absorption at wavelengths until 580 nm and by increasing the quantum yield of Fe^{2+} production according to Eq. 1.11 (Jeong and Yoon, 2005; Pignatello et al., 2006).

$$Fe^{3+}(C_2O_4)_n^{(3-2n)} + h\upsilon \rightarrow Fe^{2+} + (n-1)C_2O_4^{2-} + C_2O_4^{2-\bullet} \quad (1.11)$$

Ferricarboxylate-mediated solar photo-Fenton has already been successfully applied to treat different wastewaters and specific pollutants, whereby carboxylate ions such as oxalate, citrate and EDDS (ethylenediamine-N, N'-disuccinic acid) were used to form complexes with Fe^{3+} (Silva et al., 2007; Prato-Garcia et al., 2009; Rodríguez et al., 2009; Huang et al., 2012; Monteagudo et al., 2012).

For a second time, the work by Malato and co-workers (2009) will be based upon to summarize the main photo-Fenton process parameters and their influence on photocatalytic rate kinetics (Table 1.3).

Table 1.3. Fundamental photo-Fenton process parameters and respective effect on reaction rates. Adapted from Malato et al. (2009).

Parameter	Influence or effect on reaction rates
pH	Controls the distribution of dissolved ferrous and ferric iron hydroxide species, which possess different molar absorption coefficients. Optimal pH ~ 2.8 avoids precipitation and maximizes quantum yields.
Iron concentration	Increasing iron concentration increases reaction rates. Relation is not proportional and levels off due to attenuation of incident radiation. Optimization needs to consider reactor geometry and inner filter effects.
Oxidant concentration	Equilibrium of H_2O_2 concentration must be found. Lower concentrations lead to a rate reduction of Fenton reaction, while higher lead to an unfavorable competition for $^{\bullet}OH$ radicals.
Temperature	Increasing temperature customarily increases reaction rates, up to the point where hydrogen peroxide is inefficiently consumed.
Irradiance	Useful radiation absorption over the UV/Vis spectrum, especially in the presence of carboxylate anions. Excess radiation favors parallel occurrence of thermal reactions. Optimization of optical pathlength greatly reduces amount of necessary photons.
Substrate concentration and characteristics	Higher concentrations require longer treatment times and are prone to cause inner filter effects. Released inorganic ions can interfere with the degradation process (e.g.: precipitation of iron by phosphate).

1.4.3 Application of solar AOPs towards antibiotic removal

In this sub-section. an overview of recently published research articles dealing with the application of solar-driven AOPs towards the removal of antibiotics from different aquatic media willis is presented, complemented with additional data in Table 14.

Zhao et al. (2013) substantiated that the degradation rates of Oxytetracycline (OTC) by photolysis and photocatalysis with nitrogen and fluorine doped TiO_2 film were greatly influenced by the solution pH, which determines the different speciation of OTC molecules. Five reaction pathways, including direct photolytic degradation were proposed, UV/Vis light-induced photocatalytic oxidation and reduction and visible light-induced self-photosensitized oxidation and reduction.

Reyes et al. (2006) studied the abatement efficiency of Tetracycline in aqueous suspensions of TiO_2 (0.5 g L^{-1}) with three different light sources (UV lamp, solarium device and UV-A lamp). Antibiotic removal, mineralization, biodegradability (only for the solarium device) and antibacterial activity were compared. Antibiotic half-life times obtained with each device were 10, 20 and 120 min, respectively. After 120 min, initial TOC depletion reached 90 % and 75 % under UV and solarium light sources, whereas it only reached 12% with the UV-A lamp. The Biological Oxygen Demand (BOD_5)/Chemical Oxygen Demand (COD) ratio increased from 0.45 to 0.85 after the same time using the solarium device. UV-A lamp treatment has also

shown to be the less effective in reducing antibacterial activity (only 15% reduction found after 120 min), as opposed to total deactivation reached after 55 and 70 min by solarium and the UV lamp. In another work of the same research group (Palominos et al., 2009), total Tetracycline degradation in aqueous solution was achieved in 15 minutes using different photocatalysts, TiO_2 (1.5 g L^{-1}, pH 8.7) and ZnO (1.0 g L^{-1}, pH 11), leading to different percentages of TOC removal after 60 min (70% against 100%, respectively).

Bautitz and Nogueira (2007) applied the Photo-Fenton process under black-light and solar irradiation was applied for the degradation of the same antibiotic (24 mg L^{-1}). The influences of iron source ($Fe(NO_3)_3$ or ferrioxalate, both present at 0.20 mmol L^{-1}), H_2O_2 concentration (1-10 mmol L^{-1}) and aquatic matrix (pure water, surface water and a WWTP effluent) were also studied. Results suggested that, under black-light irradiation, the use of $Fe(NO_3)_3$ is favored (full antibiotic degradation after 1 min), while under solar light, the use of ferrioxalate gives better results. However, no significant differences between iron sources were observed regarding TOC removal. Results are independent of H_2O_2 initial concentrations in the 1-5 mmol L^{-1} range, after which higher H_2O_2/Fe ratios hinder degradation. When using real WWTP effluent samples, black-light radiation was rather ineffective, as opposed to solar irradiation in the presence of ferrioxalate, which achieved total tetracycline degradation in 1.5 min.

Giraldo et al. (2010) optimized the catalyst load and pH for the degradation of 20 mg L^{-1} solutions of Oxolinic Acid using suspended TiO_2 in a lab-scale photocatalytic system. The optimal conditions, 1.0 g L^{-1} of TiO_2 and pH 7.5, eliminated both the antibiotic and antimicrobial activity on *E. coli*, and reduced initial DOC content by 47% after 30 min. Palominos et al. (2008) immobilized TiO_2 on sintered glass cylinders, requiring 60 min to decrease by one order of magnitude the initial 18 mg L^{-1} concentration of Oxolinic Acid. Full antibiotic removal was achieved after 120 min, with a 54% reduction of initial DOC. The remaining intermediates were refractory to further mineralization but did not inhibit bacterial growth.

Elmolla and Chaudhuri (2010) subjected a mixture of amoxicillin (AMX), ampicillin (AMP) and cloxacillin (CLX) antibiotics in distilled water to TiO_2 photocatalytic degradation coupled with the addition of H_2O_2, under UV-A irradiation. Initial experimental conditions were: antibiotic concentrations around 100 mg L^{-1} each, COD 520 mg L^{-1}, DOC 145 mg L^{-1} and a BOD_5/COD ratio near 0. Full antibiotic degradation was achieved after 30 min with a photocatalyst concentration of 1.0 g L^{-1}, pH 5 and 100 mg L^{-1} H_2O_2. After 300 min, COD and DOC removal was around 24% and 13%, respectively, with an increase of the BOD_5/COD ratio from 0.00 to near 0.10. Mineralization of sulfur and nitrogen contained in the antibiotic mixture required longer irradiation periods.

Klauson et al. (2010), reported a 80% conversion of 20 mg L^{-1} AMX (initial pH 6.0) using 1 g L^{-1} of TiO_2 after 2 hours of exposure to solar radiation in an evaporation dish batch reactor. Only 14 and 1.4% of the original sulfur and nitrogen contained in AMX were released, respectively. According to the reaction pathways proposed in the same study, some of the AMX photocatalytic by-products (identified via UPLC-ESI-MS analysis) still contain an intact β-lactamic ring structure, to which Dimitrakopoulou et al. (2012) attributed the residual antibacterial activity against a tested *enterococci* bacterial strain after TiO_2/UV-A photocatalysis reduced AMX concentrations below 5 mg L^{-1}.

Ay and Kargi (2010) and Ay and Kargi (2011) compared the advanced oxidation of pure AMX aqueous solutions by the Fenton and photo-Fenton treatment, respectively. The H_2O_2/Fe/AMX ratio was studied by means of a statistical experimental design. Optimized ratios for complete AMX removal were 255/25/105 mg L^{-1} and 100/40/105 mg L^{-1} for Fenton and photo-Fenton, respectively, but greater DOC removal was obtained in the second process (58%), compared to the first (38%).

Benitez et al. (2011) published an over ranging study on the removal of AMX simultaneously dissolved with three other pharmaceutical compounds in different water matrices, conducted by UV radiation alone, ozone, Fenton, Fenton-like and photo-Fenton systems, and combinations of UV radiation and ozone with H_2O_2, TiO_2, Fe (II) and Fe (III). The photo-driven processes resulted in higher oxidation rates in ultrapure water solutions, and were enhanced in the presence of any second oxidant, especially in the UV/TiO_2 and O_3/TiO_2 systems. Due to the presence of dissolved organic matter that competes for oxidant agent consumption, lower rates were achieved in natural waters and secondary effluents.

Trovó et al. (2011), using the photo-Fenton process under simulated solar radiation on pure solutions of AMX (C_0 = 50 mg L^{-1}), reported on the influence of iron species ($FeSO_4$ or Ferrioxalate (FeOx)), generated intermediary by-products and toxicity towards *Daphnia magna*. Both iron salts resulted in quick AMX removal (5 and 15 min for $FeSO_4$ and FeOx, respectively), but whereas oxalate always presented detrimental toxicity, the use of $FeSO_4$ decreased it from 65 to 5% after 90 min, after 53% of the original TOC was removed. After 240 min, the residual TOC no longer contained nitrogen, since 100% was released mainly as ammonium, whereas no information regarding sulphur content was given. Intermediary by-products identified by HPLC-ESI-TOF, which were responsible for the toxicity of the treatment until being reduced to short chain carboxylate anions, were influenced by the iron source.

The solar photocatalytic oxidation of Lincomycin in synthetic water, at pilot plant scale, studied in Augugliaro et al. (2005) followed pseudo-first order kinetics (initial concentrations = 10,

24,50 and 75 μM, TiO_2 = 0.2 g L^{-1}). The cumulative photonic energy for full antibiotic removal at each concentration was below 2 Einsteins, but full TOC removal depended on initial concentrations. Di Paola et al. (2006) treated 50, 20 and 10 mg L^{-1} solutions of the same substance with 0.4 g L^{-1} of TiO_2, in a Pyrex batch photo reactor illuminated with a 125 W medium pressure Hg lamp. Full antibiotic degradation was achieved after approximately 30, 45 and 75 min of illumination time, with correspondingly full TOC removal (except for the 50 mg L^{-1} solution) after 5, 8 and 10 h. The evolution of both organic and inorganic species formed during the photocatalytic degradation of the 20 mg L^{-1} solution was also followed.

Kaniou et al. (2005) reported on the heterogeneous photocatalytic degradation of 50 mg L^{-1} solutions of Sulfamethazine (SMT), using TiO_2 and ZnO (1 g L^{-1} each) as photocatalysts, under UV-A irradiation. After 60 min of light exposure, SMT was almost completely destroyed in the presence of ZnO (~92%), whereas with TiO_2, the reaction was slower (35% SMT remaining). The addition of H_2O_2 was found to increase the reaction by twofold (TiO_2), while a negative effect was observed with ZnO. DOC reduction after 4 h of illumination was similar for both catalysts (65% reduction). The desulfurization of the substrate was complete, while its nitrogen was released mainly in the form of nitrate and ammonium ions.

At a lab-scale solar apparatus, Abellán et al. (2007) treated a pure SMX solution (concentration = 100 mg L^{-1}) with 0.5 g L^{-1} of TiO_2. After 6 h of illumination, only 82% of SMX was removed, with only 23% of initial TOC removed. González et al. (2009), using 200 mg L^{-1} of SMX and applying the photo-Fenton (10 mg L^{-1} of Fe^{2+}, 300 mg L^{-1} of H_2O_2) process at lab-scale (BLB lamps), achieved full SMX degradation, with 30 % of initial TOC removed after 67 min of reaction. In a treatment of mixture of different contaminants by Klamerth et al. (2009), 100 μg L^{-1} of Sulfamethoxazole (SMX) were completely removed from demineralized water using both Solar photocatalysis (with 5 mg L^{-1} TiO2) and Solar Photo-Fenton (with 5 mg L^{-1} Fe at pH 2.8) in a solar pilot plant equipped with compound parabolic collectors, after 145 and 20 min, respectively. The later process was shown to be more effective both in Dissolved Organic Carbon removal and required reaction time (30 min against 145 min).

Trovó et al. (2013) obtained similar outcomes on the solar photo-Fenton treatment of 200 mg L^{-1} Chloramphenicol (CAP) aqueous solutions in a solar pilot plant equipped with CPCs, when compared to those obtained in lab-scale conditions (annular photoreactor with a 400 W high pressure mercury vapor lamp in the middle). At lab-scale, the optimized parameters for antibiotic, DOC, COD, toxicity and antibacterial activity removal were acidic pH (2.8 ~ 3.0), 10 mg L^{-1} of Fe^{2+} and a single addition of the near stoichiometric concentration of H_2O_2 (400 mg L^{-1}). In the solar pilot plant, CAP was already below the limit of quantification (1.0 mg L^{-1}) after 20 min of dark-Fenton, with a respective 10 and 37% decreased of initial DOC and COD

levels. After 60 min of solar radiation, these values were abated to 92 and 98%, respectively. Despite similar degradation efficiencies obtained between the two units, the solar pilot plant experiments required a lower dose of accumulated UV energy per liter of solution. The optical path of 2.92 cm of the CPC pilot plant photoreactors required only 5.3 kJ L^{-1} of UV radiation versus 31.7 kJ L^{-1} in the lab-scale reactor with 5.0 cm of optical path. Associated to the more favorable CPC configuration, was also the higher temperatures achieved under solar radiation (45 – 55 °C). However, the high temperatures also contributed to a higher consumption rate of H_2O_2 compared to lab-scale experiments, due to thermal decomposition of H_2O_2.

Michael and co-workers (2010) evaluated the key parameters of the solar photo-Fenton and solar TiO_2/UV for the chemical degradation of Ofloxacin (OFX) spiked in secondary treated domestic effluents, in a bench-scale solar simulator. Solar Fenton was more efficient than solar TiO_2, yielding complete OFX degradation and a 50% DOC reduction in 30 min of photocatalytic treatment. Toxicity profiles of generated OFX by-products along different photo-treatment periods towards *Daphnia magna* differed between the applied processes. A later study by the same authors (Michael et al., 2013a) investigated the removal of DOC in OFX-spiked matrices via the solar photo-Fenton carried out in a pilot-plant equipped with CPCs ($[Fe^{2+}]$ = 2 mg L^{-1} and pH_0 ~2.8). After 12 mg L^{-1} of H_2O_2 were consumed, DOC removal percentages were 78% in distilled water, 58% in surface water and 41 and 36% in simulated and real wastewater effluents, respectively. The different composition of the matrices regarding inorganic ions and dissolved organic matter not only clearly worked as inhibitors of the desired hydroxyl radical reactions, but also influenced the generation pathways of oxidation by-products, resulting in different toxicity profiles.

In lab-scale conditions, De la Cruz et al. (2012) demonstrated the feasibility of using photo-Fenton at near neutral, natural pH conditions on the removal of 32 selected micropollutants, including eight antibiotics of different classes, detected in an urban WWTP effluent after activated sludge treatment (real global quantity of micropollutants of 29 μg L^{-1}). UV-light emitting at 254 nm (UV_{254}) alone, Fenton and photo-Fenton under simulated sunlight were also tested, but the best results were achieved with photo-Fenton employing UV_{254} radiation, 50 mg L^{-1} of H_2O_2 with or without addition of iron (5 mg L^{-1} of Fe^{2+} added, or 1.48 mg L^{-1} of total iron already present). After 30 min of treatment, global global micropollutant removal percentages of 98 and 97% were achieved, respectively. The presence of dissolved organic matter (15.9 mg L^{-1} of DOC) did not present a significant shortcoming for the treatment.

In a solar pilot-plant equipped with CPCs, a similar study by Klamerth et al. (2013) compared the conventional photo-Fenton at pH = 3 with photo-Fenton modified with the presence of

complexing agents (humic acids, HA; Ethylenediamine-N,N'-disuccinic acid, EDDE) under the same conditions of the work by De la Cruz and co-workers ($[Fe^{2+}]$ = 5 mg L^{-1}, $[H_2O_2]_0$ = 50 mg L^{-1}), The tested urban WWTP effluents contained over 60 different micropollutants, including the antibiotics SMX, OFX, , Trimethoprim, Ciprofloxacin and Sulfapyridine, with ranging concentration from a new ng L^{-1} to tens of μg L^{-1}. In the three cases, over 95% of the contaminants were removed, with photo-Fenton at pH = 3 requiring less photo-treatment time (normalized illumination time, t_{30W}, = 50 min). The use of EDDS as a iron complexing agent was proved of great interest notwithstanding, since conventional photo-Fenton requires both acidification and neutralization steps, while the use of HA lowered the pH by the end of the reaction has the same drawback. EDDS not only did not lower the pH but is also a non-toxic and readily biodegradable substance, albeit being consumed during the process. EDDS required a comparable photo-treatment time (t_{30W}, = 63 min) and even consumed less $[H_2O_2]$ than the conventional photo-Fenton at pH = 3 (61 compared to 80 mg L^{-1}).

Table 1.4. Recent applications of solar-driven photocatalytic processes towards the removal of antibiotics from different aquatic media.

Antibiotics	Process	Operating conditions	Results	References
Oxytetracycline (OTC)	UV, UV/TiO_2	[OTC] = 5 - 40 mg L^{-1} Matrix: Ultrapure water NF-doped TiO_2 film pH = 2.0 - 11.0; Broadband light intensity: Visible: 0.399 mW cm^{-2}, Solar: 0.475 mW cm^{-2}; Radiation blocked below 420 nm.	OTC degradation largely influenced by the solution pH, which determines the different electric charge state of OTC species. With increasing pH, the light absorption of OTC exhibits red shift to the visible light while the degradation rate of OTC by photolysis under solar/visible light is significantly accelerated. Photocatalytic degradation suggests 5 pathways: direct photolytic degradation, UV/Vis light-induced photocatalytic oxidation and reduction, and visible light-induced OTC self-photosensitized oxidation and reduction.	Zhao et al. (2013)
Tetracycline (TC)	UV/TiO_2	[TC] = 40 mg L^{-1} Matrix: Deionized water [TiO_2] = 0.5 g L^{-1} Light intensity (360 nm): UV lamp: 1.210 mW cm^{-2} Solarium: 1.980 mW cm^{-2} UV-A lamp: 0.059 mW cm^{-2}	Antibiotic half-life: 10 (UV lamp), 20 (solarium) and 120 min (UV-A lamp) TOC removal after 120 min: 90%, 75%, 12%, respectively. BOD_5/COD ratio from 0.45 to 0.85 after 120 min (solarium device). Full antibacterial activity inhibition at 55 and 70 min (solarium, UV-lamp); only 15% reduction after 120 min (UV-A lamp),	Reyes et al. (2006)
Tetracycline (TC)	UV/TiO_2, UV/ZnO	[TC] = 20 mg L^{-1} Matrix: Deionized water [TiO_2] = 0.5 - 1.5 g L^{-1}; pH = 3 - 10 [ZnO] = 0.2 - 1.5 g L^{-1}; pH = 6 - 11 Light intensity (300–800 nm): Xe lamp: 250 W m^{-2}	Optimal oxidation conditions: [TiO_2] = 1.5 g L^{-1}, pH = 8.7; [ZnO] = 1.0 g L^{-1}; pH = 11. Complete antibiotic removal after 15 min with both photocatalysts. TOC removal after 60 min: 70 % (TiO_2), 100 % (ZnO). Full antibacterial activity inhibition at 30 min with TiO_2.	Palominos et al. (2009)
Tetracycline (TC)	Photo-Fenton	[TC] = 24 mg L^{-1} Matrix: Ultrapure water, Surface water (SW), Effluent from WWTP (WW) [FeOx], [$Fe(NO_3)_3$] = 0.20 mmol L^{-1} [H_2O_2] = 1 - 10 mmol L^{-1} pH = 2.5 Broadband light intensity: Black-light: 19 W m^{-2} Solar: 15 to 20 W m^{-2}	Black-light results: Complete TC degradation: 1-1.5 min ($Fe(NO_3)_3$), 8 min (FeOx). Similar residual TOC concentration after 60 min (4 mg L^{-1}). Similar efficiency in SW matrix, substantial loss of efficiency in WW matrix Solar light results: Complete antibiotic removal: 0.5 min/0.054 J cm^{-2} UV dose with FeOx against 3 min (0.270 J cm^{-2} UV dose) with $Fe(NO_3)_3$. Similar residual TOC concentration (2 mg L^{-1}) after 60 min/5.870 J cm^{-2} UV dose No interference of SW or WWTP matrices.	Bautitz and Nogueira (2007)

Table 1.4. (Continued)

Antibiotics	Process	Operating conditions	Results	References
Oxolinic Acid (OXA)	UV/TiO_2	[OXA] = 20 mg L^{-1} Matrix: Ultrapure water [TiO_2] = 0.2 - 1.5 g L^{-1}; pH = 7.5 - 11 Light intensity (max at 365 nm): Black light: 14 W m^{-2}	Optimal oxidation conditions: [TiO2] = 1.0 g L^{-1}, pH = 7.5 Complete antibiotic removal after 30 min. TOC and COD removal after 60 min: 50% Full antibacterial activity inhibition at 60 min. Initial toxicity (V. fischeri) reduced by ~70% after 60 min.	Giraldo et al. (2010)
	UV/TiO_2	[OXA] = 18 mg L^{-1} Matrix: Ultrapure water Immobilized TiO_2 in sintered glass cylinders pH = 9 Light intensity (max at 365 nm): Black light: 14 W m^{-2}	Complete antibiotic removal after 120 min. Similar COD removal profile. TOC removal after 100 min: 50% Average oxidation state (AOS): -1.5 (0 min), +2 (40 min), +3 (120 min) Full antibacterial activity inhibition at 60 min.	Palominos et al. (2008)
Mixture of Amoxicilin (AMX), Ampicillin (AMP), Cloxacillin (CLX)	UV/TiO_2	[AMX], [AMP], [CLX] ~100 mg L^{-1} Matrix: Deionized water [TiO_2] = 0.5 – 2.0 g L^{-1}; pH = 3 - 11 [H_2O_2] = 0 – 300 mg L^{-1} UVA lamp (365 nm) Nominal power: 6W	With [TiO2] = 1.0 g L^{-1}, pH = 11, [H_2O_2] = 0 mg L^{-1}, after 300 min: 70.9 % AMX, 91.4 % AMP, 100 % CLX removal 11.2 % COD and 3% DOC removal With [TiO2] = 1.0 g L^{-1}, pH = 5, [H_2O_2] = 100 mg L^{-1} Complete AMX and CLX removal after 20 mins Complete AMP removal after 30 min 26.3 % COD and 13.9% DOC removal after 300 min	Elmolla et al. (2010)
Amoxicillin (AMX)	UV/TiO_2	[AMX] = 1 -100 mg L^{-1} Matrix: Deionized water [TiO_2] = 1.0 g L^{-1} Carbon- and iron-doped titania pH = 3 - 9 Irradiance: UV-lamp (365 nm): 0.5 mW cm^{-2} Artificial daylight : 0.6 mW cm^{-2} Solar radiation: 16 mW cm^{-2}	UV-lamp results after 6 h: Best pH = 6.0; AMX conversion rates increase from 1 to 25 mg L^{-1}, decrease afterwards due to mass transfer limitation; COD removal between 10 and 40 %. Artificial daylight results after 6 h (AMX_0 = 25 mg L^{-1}, pH = 6.0): Regular TiO_2: ~80 % AMX removal Carbon-doped titania (37 at.% C, 200 °C): 30 % AMX removal Iron-doped titania (0.89 at.% Fe, 200 °C): 25 % AMX removal COD removal between 10 and 30 % After 2 h with solar radiation (AMX_0 = 25 mg L^{-1}, pH = 6.0): Regular TiO_2: > 80 % AMX removal Release of N: 1.5 % and of S: 14 % COD removal between 10 and 30 % Carbon-doped titania (37 at.% C, 200 °C): ~75 % AMX removal Iron-doped titania (2.2 at.% Fe, 200 °C): ~75 % AMX removal	Klauson et al. (2010)

Table 1.4. (Continued)

Antibiotics	Process	Operating conditions	Results	References
Amoxicillin (AMX)	UV/TiO_2	[AMX] = 2.5 -30 mg L^{-1} Matrix: Ultrapure water WWTP effluent [TiO_2] = 0.1 – 0.75 g L^{-1} pH = 5 or 7.5 UVA lamp (350 - 400 nm) Photon flux: 8×10^{-4} E L^{-1} min^{-1}	Effect of catalyst loading (g_{TiO2} L^{-1}) after 20 min (AMX_0 =10 mg L^{-1}, pH = 5.0): AMX removal: 100 %, except at 0.1 g L^{-1} (65 %) DOC removal: 43, 60, 65 and 70 % at 0.1, 0.25, 0.5 and 0.75 g_{TiO2} L^{-1}, respectively Effect of initial pH (AMX_0 = 10 mg L^{-1}, 0.5 g_{TiO2} L^{-1}): AMX removal after 25 min: 100 % with both pH; TOC removal after 90 min: 93 versus 75 % with pH = 5 and pH = 7.5, respectively. Effect of water matrix (AMX_0 = 10 mg L^{-1}, 0.5 g_{TiO2} L^{-1}, pH = 7.5): Ultrapure water: AMX removed after 25 min WWTP effluent: AMX removed after60 min Antibacterial properties: Depends on AMX concentration and the test bacteria in question; *Escherichia coli* and *Klebsiella pneumonia* are affected only by AMX, while *Enterococcus faecalis* is also partially affected by its reaction by-products	Dimitrikapoulou et al. (2012)
Amoxicillin (AMX)	Fenton	[AMX] = 10 -200 mg L^{-1} Matrix: Ultrapure water [Fe(II)] = 0 – 50 mg L^{-1} [H_2O_2] = 10 – 500 mg L^{-1} pH = 3.5	Optimized H_2O_2/Fe/AMX ratio: 255/25/105 mg L^{-1} AMX removal after 2.5 min: 100% TOC removal after 15 min: 37%	Ay and Kargi (2010)
Amoxicillin (AMX)	Photo-Fenton	[AMX] = 10 -200 mg L^{-1} Matrix: Ultrapure water [Fe(II)] = 0 – 50 mg L^{-1} [H_2O_2] = 10 – 500 mg L^{-1} pH = 3.5 UV lamp (254 nm): Light intensity: 4.98×10^{-6} E s^{-1}	Optimized H_2O_2/Fe/AMX ratio: 100/40/105 mg L^{-1} AMX removal after 2.5 min: 100% TOC removal after 60 min: 53%	Ay and Kargi (2011)

Table 1.4. (Continued)

Antibiotics	Process	Operating conditions	Results	References
Mixture of AMX with other pharmaceuticals	UV H_2O_2/Fe^{II}(/UV) H_2O_2/Fe^{III}(/UV) UV/H_2O_2 UV/TiO_2 O_3(+UV), O_3/H_2O_2(+UV) O_3/TiO_2(+UV)	[AMX] = 1 µM ~ 0.36 mg L^{-1} Matrix: Ultrapure water, Surface water Groundwater Effluents 1, 2 from WWTP pH = 3 (UV, Fenton-based trials) = 7 (reminder) pH = 8.1 (GW), 7.7 (SW), = 7.6 (WW1), 8.2 (WW2) [TiO2] = 0.001 g L^{-1} [Fe^{II}] and [Fe^{III}] = 10 µM [H_2O_2] = 10 µM O_3 flow rate: 16 mg h^{-1} UV lamp (254 nm) Light intensity: 1.81 × 10^{-6} E s^{-1}	Pseudo-first-order rates constants in UP (min^{-1}): pH = 3 UV: 0.109, H_2O_2/Fe^{II} = 0.117, H_2O_2/Fe^{III} = 0.028 UV/H_2O_2 = 0.237, UV/TiO_2 = 0.114, O_3 = 0.559 Fe^{II}/UV = 0.151, Fe^{III}/UV = 0.125 $H_2O_2/Fe^{II}/UV$ = 0.265, $H_2O_2/Fe^{III}/UV$ = 0.230 pH = 7 O_3 = 0.564, UV/O_3 = 1.172, O_3/H_2O_2 = 1.385, $O_3/H_2O_2/UV$ = 1.393, O_3/TiO_2 = 1.058, $O_3/TiO_2/UV$ = 1.203 Pseudo-first-order rates constants in real water matrices (min^{-1}): SW: UV: 0.041, UV/TiO_2 = 0.049, H_2O_2/Fe^{II} = 0.025, $H_2O_2/Fe^{II}/UV$ = 0.049 Gw: UV: 0.093, UV/TiO_2 = 0.102, H_2O_2/Fe^{II} = 0.037, $H_2O_2/Fe^{II}/UV$ = 0.095 WW1: O_3 = 0.498, O_3/H_2O_2 = 1.177 WW2: O_3 = 0.458, O_3/H_2O_2 = 1.059	Benitez et al. (2011)
Amoxicillin (AMX)	Photo-Fenton	[AMX] = 50 mg L^{-1} Matrix: Deionized water [FeOx], [$FeSO_4$] = 0.05 mM [H_2O_2] = 120 mg L^{-1} pH = 2.5-2.8 Light intensity (300–800 nm): Xe lamp: 250 W m^{-2}	FeOx results: Complete AMX removal after 5 min TOC removal after 240 min: 81 % 100% N release as ammonium after 240 min Inhibition towards: *V. fischeri:* maintained around 30% *D. magna*: between 70-95 % due to oxalate. Fe SO_4 results: Complete AMX removal after 15 min TOC removal after 240 min: 73 % 100% N release as ammonium after 240 min Inhibition towards: *V. fischeri:* maintained around 30% *D. magna*: 65 % (0 min), 5 % (90 min), 100 % (150 min), 45 % (240 min)	Trovó et al. (2011)

Table 1.4. (Continued)

Antibiotics	Process	Operating conditions	Results	References
Lincomycin (LCM)	UV/TiO_2	[LCM] = 10 – 75 μM (4 -30 mg L^{-1}) Matrix: Deionized water [TiO_2] = 0.2 g L^{-1} pH = 6.3 Solar light	Complete removal of LCM in every concentration value with less than 2 Einstein (cumulative photon energy). Full TOC removal depends on the initial concentration of LCM The presence of membrane reactors allowed catalyst separation and the operation in continuous mode, as the membranes rejection for LCM and its oxidation products was quite high.	Augugliaro et al. (2005)
Lincomycin (LCM)	UV/TiO_2	[LCM] = 10, 20 and 50 mg L^{-1} Matrix: Deionized water [TiO_2] = 0 and 0.4 g L^{-1} pH ranged between 5.6 – 6.5 Medium pressure Hg lamp (125 W): Photon flux: 10 mW cm^{-2}	[TiO_2] = 0 g L^{-1} results: LCM removal after 5 h: 70 (10 mg L^{-1}), 40 (20 mg L^{-1}) and 20 % (50 mg L^{-1}) No mineralization [TiO_2] = 0.4 g L^{-1} results: Complete LCM removal after: 0.5 (10 mg L^{-1}), 0.75 (20 mg L^{-1}) and 2 h (50 mg L^{-1}). Complete TOC removal after 5 (10 mg L^{-1}) and 8 h(20 mg L^{-1}) Nearly 95% TOC removal after 10 h (50 mg L^{-1}) Recovery of 70 % of sulfur as sulfate after 9 h Recovery of 75 % of N as ammonium and 25 % as nitrate	Di Paola et al. (2006)
Sulfamethazine (SMT)	UV/TiO_2, UV/ZnO	[SMT] = 50 mg L^{-1} Matrix: Deionized water [TiO_2] = [ZnO] = 1 g L^{-1} [H_2O_2] = 0 – 800 mg L^{-1} pH = 4.8 UVA lamp (max 366 nm): Photon flux: 2.02×10^{-4} E L^{-1} min^{-1}	Initial apparent photonic efficiencies (ξ) in SMT and TOC removal: TiO_2: 1.25 ± 0.08; 3.10 ± 0.08; 1.25 ± 0.08; ZnO: 2.15 ± 0.06; 3.58 ± 0.21; 1.25 ± 0.08; TiO_2 + 100 mg L^{-1} H_2O_2: 2.79 ± 0.08; 3.54 ± 0.07 ZnO + 100 mg L^{-1} H_2O_2: 1.02 ± 0.10; 2.47 ± 0.09	Kaniou et al. (2005).
Sulfamethoxazole (SMX)	UV/TiO_2	[SMS] = 100 mg L^{-1} Matrix: Ultrapure water [TiO_2] = 0 – 2.0 g L^{-1} pH = 2 – 11 Light intensity (300–800 nm): Xe lamp: 250 W m^{-2}	After 6 h with optimal oxidation conditions ([TiO2] = 0.5g L^{-1}, pH = 5): SMX removal: 82 %, TOC removal: 23 % Recovery of 40 % of sulfur as sulfate Recovery of 24 % of N as ammonium Slow increase of BOD_5/COD ratio from 0.0 to nearly 0.12, related to low decrease of the specific ultraviolet absorbance (aromaticity content).	Abellán et al. (2007)

Table 1.4. (Continued)

Antibiotics	Process	Operating conditions	Results	References
Sulfamethoxazole (SMX)	Photo-Fenton	[SMX] = 200 mg L^{-1} Matrix: Deionized water [Fe^{2+}] = 10 mg L^{-1} [H_2O_2] = 300 or 400 mg L^{-1} pH = 2.8 3 black-light blue lamps (8 W each)	Results with 300 mg L^{-1} of H_2O_2 after 67 min: Complete SMX removal, 30 % TOC removal Recovery of 26 % of N in the form of ammonium Final BOD_5/COD ratio of 0.18 Results with 400 mg L^{-1} of H_2O_2 after 88 min: Complete SMX removal, 53 % TOC removal Recovery of 31 % of N in the form of ammonium Final BOD_5/COD ratio 0.26 Both experiments presented neither inhibition towards activated sluge nor toxicity towards *V. fischeri*.	González et al. (2009)
Mixture of SMX with 8 other pharmaceutical compounds	UV/TiO_2 Photo-Fenton	[SMX] = 0.1 mg L^{-1} Matrix: Deionized water Freshwater (FW1) Freshwater w/o HCO_3 (FW2) [TiO_2] = 5 mg L^{-1} [Fe^{2+}] = 5 mg L^{-1} [H_2O_2] = 50 mg L^{-1} pH = 2.8, unadjusted Solar light	Irradiation time necessary to remove SMX DW: TiO_2: 145 min ($t_{30\ W}$) Photo-Fenton (pH = 2.8): 20 min ($t_{30\ W}$) Photo-Fenton (unadjusted pH): 13 min ($t_{30\ W}$) FW1: Photo-Fenton (unadjusted pH): 14 min ($t_{30\ W}$) FW2: Photo-Fenton (unadjusted pH): 50 min ($t_{30\ W}$)	Klamerth et al. (2009)
Chloramphenicol (CAP)	Photo-Fenton	[CAP] = 200 mg L^{-1} Matrix: Ultrapure water [Fe^{2+}] = 5 - 15 mg L^{-1} [H_2O_2] = 50 – 500 mg L^{-1} pH = 2.8 Photon flux of UVA lamp (400 W): 295-290 nm: 6.0×10-7 E s^{-1} 295-710 nm: 3.3×10-6 E s^{-1} Average UVA lamp irradiance: 1100 W m^{-2} Average solar UVA irradiance: 320-400 nm: 41.5 ± 1.2 W m^{-2}	Chosen conditions: [Fe^{2+}] = 10 mg L^{-1}, and [H_2O_2] = 400 mg L^{-1} (single addition). Results in lab-scale experiment after 60 min (Q_{UV} = 31.7 kJ L^{-1}): Complete CAP removal after 16 min TOC and COD removal: 90 and 93 %, respectively. AOS: from +0.48 to +3.39 H_2O_2 consumption rate: 6.7 mg L^{-1} min^{-1} Results in solar pilot-plant after 60 min (Q_{UV} = 5.3 kJ L^{-1}): Dark-Fenton removed 98% of CAP during mixing time. TOC and COD removal: 90 and 93 %, respectively. AOS: from +1.4 to +2.9 H_2O_2 consumption rate: 12.5 mg L^{-1} min^{-1}	Trovó et al. (2013)

Table 1.4. (Continued)

Antibiotics	Process	Operating conditions	Results	References
Ofloxacin (OFX)	UV/TiO_2 Photo-Fenton	[OFX] = 10 mg L^{-1} Matrix: Effluent from WWTP [TiO_2] = 0.25 - 4 g L^{-1} pH = 2, 8 and 10 [Fe^{2+}] = 1 - 5 mg L^{-1} [H_2O_2] = 1.357 – 8.142 mM (46 – 277 mg L^{-1}) pH = 2 – 4.5 Xenon lamp (1000 W): Irradiance: 273 W m^{-2}	Chosen Photo-Fenton conditions: [Fe^{2+}] = 5 mg L^{-1}, [H_2O_2] = 2.714 mM (92 mg L^{-1}) and pH = 3 Removal of OFX after 30 min: 100 % TOC removal after 120 min: 50 % Profile of toxicity towards *D. magna* (48h) at 0, 15, 30 60 and 120 min: 20, 40, 90, 90 and 50 % (respectively). Chosen TiO_2 conditions: [TiO_2] = 3 g L^{-1}, pH = 8 Removal of OFX after 120 min: 60 % TOC removal after 120 min: 10 % Profile of toxicity towards *D. magna* (48h) at 0, 15, 30 60 and 120 min: 10, 20, 20, 10 and 5 % (respectively).	Michael et al. (2010)
Ofloxacin (OFX)	Photo-Fenton	[OFX] = 10 mg L^{-1} Matrix: Demineralized water Simulated natural freshwater Simulated municipal wasteawater Real effluent from WWTP [Fe^{2+}] = 2 mg L^{-1} pH ~ 2.8 [H_2O_2] = 2.5 mg L^{-1} (dose addition after total consumption) Solar energy	Achieved TOC removal after the consumption of 12 mg L^{-1} of H_2O_2: Demineralized water: 78.1 % Simulated natural freshwater: 58,3 % Simulated municipal wastewater (SWW): 40.5 % Real effluent from WWTP (RE): 35.8 % Evaluation of toxicity towards *V. fischeri* (30 min): SWW: 33 % (0 min), 7 % (after 30 min of illumination) RE: 33 % (0 mg L^{-1} of H_2O_2), 64 % (12 mg L^{-1} of H_2O_2)	Michael et al. (2013)

Table 1.4. (Continued)

Antibiotics	Process	Operating conditions	Results						References
8 antibiotics, amongst 32 micropollutants, detected in real a secondary effluent	UV_{254}/H_2O_2, Photo-Fenton (UV_{254} or UV-VIS)	Σmicropollutants (ng L^{-1}) = 29.506, from which: [Azithromycin (ATM)] = 295, [Ciprofloxacin (CFX)] = 129 [Clarithromycin (CTM] = 518 [Metronidazole (MNZ)] = 456 [Norfloxacin (NFX)] = 27 [Ofloxacin (OFX)] = 41 [Sulfamethoxazole (SM)] = 578 [Trimethoprim (TMP)] = 131 Matrix: Effluent from WWTP [Fe^{2+}] = 5 mg L^{-1} (1.48 mg L^{-1} already present in the effluent) [H_2O_2] = 10 – 25, 50 mg L^{-1} Natural pH of the effluent (7.4) UVA lamp (254 nm): Photon flux: 1.5×10^{-6} E s^{-1} UV-VIS lamp (290 – 800 nm) Irradiance: 550 W m^{-2}		Removal % ([Fe^{2+}] = 5 mg L^{-1}, [H_2O_2] = 50 mg L^{-1}):						De la Cruz et al. (2012)
				UV_{254}/H_2O_2 (30 min)	Fenton (30 min)	P-F (UV_{254}) (30 min)	P-F (UV-VIS) (90 min)		
			ATM	100	23	23	32		
			CFX	100	60	60	100		
			CTM	100	10	10	15		
			MNZ	100	55	55	88		
			NFX	100	100	100	100		
			OFX	100	49	49	100		
			SMX	100	0	0	0		
			TMP	100	20	20	43		
4 antibiotics, amongst 62 micropollutants, detected in real secondary effluents	Photo-Fenton	Average detected concentrations (ng L^{-1}, n = 10): [Ciprofloxacin (CFX)] = 705 [Ofloxacin (OFX)] = 1082 [Sulfamethoxazole (SMX)] = 844 [Trimethoprim (TMP)] = 332 [Sulfapyridine (SPD)] = 241 Matrix: Effluents collected from WWTP [Fe^{2+}] = 5 mg L^{-1} [H_2O_2] kept at 50 mg L^{-1} pH = 3: classic photo-Fenton pH = 6.5: modified photo-Fenton with 10 mg L^{-1} Humic acids (HA) or 0.2 mM of EDDS Solar energy		Results of photo-Fenton experiments performed with:						Klamerth et al. (2013)
				pH = 3		Humic Acids		EDDS	
				Initial/residual concentration in ng L^{-1}					
			CFX	1045	0	178	0	192	0
			OFX	1303	0	1009	28	566	0
			SMX	1255	0	1588	52	1259	550
			TMP	160	0	454	0	596	0
			SPD	734	0	324	0	121	0

1.5 References

Directive 2000/60/EC of the European Parliament and of the Council of 23 October 2000, establishing a framework for Community action in the field of water policy European Comission, Official Journal of the European Communities, 2000.

Abellán, M.N., Bayarri, B., Giménez, J., Costa, J., 2007. Photocatalytic degradation of sulfamethoxazole in aqueous suspension of TiO_2. Appl. Catal., B 74, 233-241.

Adams, C., Wang, Y., Loftin, K., Meyer, M., 2002. Removal of antibiotics from surface and distilled water in conventional water treatment processes. J. Environ. Eng. 128, 253-260.

Alighardashi, A., Pandolfi, D., Potier, O., Pons, M.N., 2009. Acute sensitivity of activated sludge bacteria to erythromycin. J. Hazard. Mater. 172, 685-692.

Andreozzi, R., Caprio, V., Insola, A., Marotta, R., 1999. Advanced oxidation processes (AOP) for water purification and recovery. Catal. Today 53, 51-59.

Augugliaro, V., Coluccia, S., Loddo, V., Marchese, L., Martra, G., Palmisano, L., Schiavello, M., 1999. Photocatalytic oxidation of gaseous toluene on anatase TiO_2 catalyst: mechanistic aspects and FT-IR investigation. Appl Catal B-Environ 20, 15-27.

Augugliaro, V., García-López, E., Loddo, V., Malato-Rodríguez, S., Maldonado, I., Marcì, G., Molinari, R., Palmisano, L., 2005. Degradation of lincomycin in aqueous medium: Coupling of solar photocatalysis and membrane separation. Sol Energy 79, 402-408.

Ay, F., Kargi, F., 2010. Advanced oxidation of amoxicillin by Fenton's reagent treatment. J. Hazard. Mater. 179, 622-627.

Ay, F., Kargi, F., 2011. Effects of Reagent Concentrations on Advanced Oxidation of Amoxicillin by photo-Fenton Treatment. J. Environ. Eng. 137, 472-480.

Baguer, A.J., Jensen, J., Krogh, P.H., 2000. Effects of the antibiotics oxytetracycline and tylosin on soil fauna. Chemosphere 40, 751-757.

Bandala, E.R., Estrada, C., 2007. Comparison of solar collection geometries for application to photocatalytic degradation of organic contaminants. J. Sol. Energ.-T ASME 129, 22-26.

Baquero, F., Martínez, J.L., Cantón, R., 2008. Antibiotics and antibiotic resistance in water environments. Curr. Opin. Biotechnol. 19, 260-265.

Bautitz, I.R., Nogueira, R.F.P., 2007. Degradation of tetracycline by photo-Fenton process - Solar irradiation and matrix effects. J. Photochem. Photobiol. A: Chem. 187, 33-39.

Benitez, F.J., Acero, J.L., Real, F.J., Roldan, G., Casas, F., 2011. Comparison of different chemical oxidation treatments for the removal of selected pharmaceuticals in water matrices. Chem. Eng. J. 168, 1149-1156.

Benoit-Marquié, F., Wilkenhöner, U., Simon, V., Braun, A.M., Oliveros, E., Maurette, M.-T., 2000. VOC photodegradation at the gas–solid interface of a TiO_2 photocatalyst: Part I: 1-butanol and 1-butylamine. J Photochem. Photobiol. A 132, 225-232.

Boxall, A.B.A., Kolpin, D.W., Halling-Sørensen, B., Tolls, J., 2003. Are veterinary medicines causing environmental risks? Environ. Sci. Technol. 37.

Busetti, F., Heitz, A., 2011. Determination of human and veterinary antibiotics in indirect potable reuse systems. Int. J. Environ. Anal. Chem. 91, 989-1012.

Camacho-Muñoz, D., Martín, J., Santos, J.L., Aparicio, I., Alonso, E., 2012. Effectiveness of conventional and low-cost wastewater treatments in the removal of pharmaceutically active compounds. Water, Air, Soil Pollut. 223, 2611-2621.

Cars, O., Mölstad, S., Melander, A., 2001. Variation in antibiotic use in the European Union. Lancet 357, 1851-1853.

Cermenati, L., Pichat, P., Guillard, C., Albini, A., 1997. Probing the TiO_2 Photocatalytic Mechanisms in Water Purification by Use of Quinoline, Photo-Fenton Generated $OH^{\bullet}$ Radicals and Superoxide Dismutase. J. Phys. Chem. B 101, 2650-2658.

Chamberlain, E., Adams, C., 2006. Oxidation of sulfonamides, macrolides, and carbadox with free chlorine and monochloramine. Water Res. 40, 2517-2526.

Choi, K.J., Kim, S.G., Kim, S.H., 2008. Removal of antibiotics by coagulation and granular activated carbon filtration. J. Hazard. Mater. 151, 38-43.

Collier, A.C., 2007. Pharmaceutical contaminants in potable water: Potential concerns for pregnant women and children. EcoHealth 4, 164-171.

Cunningham, V.L., Buzby, M., Hutchinson, T., Mastrocco, F., Parke, N., Roden, N., 2006. Effects of human pharmaceuticals on aquatic life: Next steps. Environ. Sci. Technol. 40, 3456-3462.

Daghrir, R., Drogui, P., 2013. Tetracycline antibiotics in the environment: A review. Environ. Chem. Lett. 11, 209-227.

Dalrymple, O.K., Yeh, D.H., Trotz, M.A., 2007. Removing pharmaceuticals and endocrine-disrupting compounds from wastewater by photocatalysis. J. Chem. Technol. Biotechnol. 82, 121-134.

Dantas, G., Sommer, M.O.A., Oluwasegun, R.D., Church, G.M., 2008. Bacteria subsisting on antibiotics. Science 320, 100-103.

De la Cruz, N., Giménez, J., Esplugas, S., Grandjean, D., de Alencastro, L.F., Pulgarín, C., 2012. Degradation of 32 emergent contaminants by UV and neutral photo-fenton in domestic wastewater effluent previously treated by activated sludge. Water Res. 46, 1947-1957.

Di Paola, A., Addamo, M., Augugliaro, V., García-López, E., Loddo, V., Marcì, G., Palmisano, L., 2006. Photodegradation of lincomycin in aqueous solution. Int. J. Photoenergy 2006.

Dimitrakopoulou, D., Rethemiotaki, I., Frontistis, Z., Xekoukoulotakis, N.P., Venieri, D., Mantzavinos, D., 2012. Degradation, mineralization and antibiotic inactivation of amoxicillin by UV-A/TiO_2 photocatalysis. J. Environ. Manage. 98, 168-174.

Drillia, P., Dokianakis, S.N., Fountoulakis, M.S., Kornaros, M., Stamatelatou, K., Lyberatos, G., 2005. On the occasional biodegradation of pharmaceuticals in the activated sludge process: The example of the antibiotic sulfamethoxazole. J. Hazard. Mater. 122, 259-265.

Elmolla, E.S., Chaudhuri, M., 2010. Photocatalytic degradation of amoxicillin, ampicillin and cloxacillin antibiotics in aqueous solution using UV/TiO_2 and UV/H_2O_2/TiO_2 photocatalysis. Desalination 252, 46-52.

Esplugas, S., Bila, D.M., Krause, L.G.T., Dezotti, M., 2007. Ozonation and advanced oxidation technologies to remove endocrine disrupting chemicals (EDCs) and pharmaceuticals and personal care products (PPCPs) in water effluents. J. Hazard. Mater. 149, 631-642.

Fatta-Kassinos, D., Vasquez, M.I., Kümmerer, K., 2011. Transformation products of pharmaceuticals in surface waters and wastewater formed during photolysis and advanced oxidation processes - Degradation, elucidation of byproducts and assessment of their biological potency. Chemosphere 85, 693-709.

Fent, K., Weston, A.A., Caminada, D., 2006. Ecotoxicology of human pharmaceuticals. Aquat. Toxicol. 76, 122-159.

Furube, A., Asahi, T., Masuhara, H., Yamashita, H., Anpo, M., 2001. Direct observation of a picosecond charge separation process in photoexcited platinum-loaded TiO_2 particles by femtosecond diffuse reflectance spectroscopy. Chem. Phys. Lett. 336, 424-430.

García Galán, M.J., Díaz-Cruz, M.S., Barceló, D., 2012. Removal of sulfonamide antibiotics upon conventional activated sludge and advanced membrane bioreactor treatment. Anal. Bioanal. Chem. 404, 1505-1515.

Giraldo, A.L., Peñuela, G.A., Torres-Palma, R.A., Pino, N.J., Palominos, R.A., Mansilla, H.D., 2010. Degradation of the antibiotic oxolinic acid by photocatalysis with TiO_2 in suspension. Water Res. 44, 5158-5167.

Göbel, A., McArdell, C.S., Joss, A., Siegrist, H., Giger, W., 2007. Fate of sulfonamides, macrolides, and trimethoprim in different wastewater treatment technologies. Sci. Total Environ. 372, 361-371.

Gogate, P.R., Pandit, A.B., 2004a. A review of imperative technologies for wastewater treatment I: Oxidation technologies at ambient conditions. Adv. Environ. Res. 8, 501-551.

Gogate, P.R., Pandit, A.B., 2004b. A review of imperative technologies for wastewater treatment II: Hybrid methods. Adv. Environ. Res. 8, 553-597.

González, O., Esplugas, M., Sans, C., Torres, A., Esplugas, S., 2009. Performance of a Sequencing Batch Biofilm Reactor for the treatment of pre-oxidized Sulfamethoxazole solutions. Water Res. 43, 2149-2158.

Goossens, H., Ferech, M., Coenen, S., Stephens, P., Mittermayer, H., Metz, S., Markova, B., Andrasevic, A., Francetic, I., Bagatzouni, D., Vlcek, J., Monnet, D.L., Muller, A., Nielsen, A.A., Rootslane, L., Huovinen, P., Paakkari, P., Cavalié, P., Guillemot, D., Kern, W., Schroeder, H., Giamarellou, H., Antoniadou, A., Ternak, G., Benko, R., Kristinsson, K., Cunney, R., Oza, A., Raz, R., Cornaglia, G., Berzina, S., Valinteliene, R., Hemmer, R., Bruch, M., Borg, M., Zarb, P., Janknegt, R., Filius, M., Blix, H.S., Hryniewicz, W., Grzesiowski, P., Caldeira, L., Codita, I., Ratchina, S., Foltan, V., Tesar, T., Cizman, M., Campos, J., Lazaro, E., De Abajo, F., Cars, O., Skoog, G., Mölstad, S., Masiero, G., Unal, S., Davey, P., Ansari, F., 2007. Comparison of outpatient systemic antibacterial use in 2004 in the United States and 27 European countries. Clin. Infect. Dis. 44, 1091-1095.

Guerra, P., Kim, M., Shah, A., Alaee, M., Smyth, S.A., 2014. Occurrence and fate of antibiotic, analgesic/anti-inflammatory, and antifungal compounds in five wastewater treatment processes. Sci. Total Environ. 473-474, 235-243.

Halling-Sørensen, B., 2000. Algal toxicity of antibacterial agents used in intensive farming. Chemosphere 40, 731-739.

Halling-Sørensen, B., Nors Nielsen, S., Lanzky, P.F., Ingerslev, F., Holten Lützhøft, H.C., Jørgensen, S.E., 1998. Occurrence, fate and effects of pharmaceutical substances in the environment- A review. Chemosphere 36, 357-393.

Halling-Sørensen, B., Sengeløv, G., Tjørnelund, J., 2002. Toxicity of tetracyclines and tetracycline degradation products to environmentally relevant bacteria, including selected tetracycline-resistant bacteria. Arch. Environ. Contam. Toxicol. 42, 263-271.

Heberer, T., 2002. Tracking persistent pharmaceutical residues from municipal sewage to drinking water. Journal of Hydrology 266, 175-189.

Hektoen, H., Berge, J.A., Hormazabal, V., Yndestad, M., 1995. Persistence of antibacterial agents in marine sediments. Aquaculture 133, 175-184.

Hirsch, R., Ternes, T., Haberer, K., Kratz, K.L., 1999. Occurrence of antibiotics in the aquatic environment. Sci. Total Environ. 225, 109-118.

Hoffmann, M.R., Martin, S.T., Choi, W., Bahnemann, D.W., 1995. Environmental Applications of Semiconductor Photocatalysis. Chem. Rev. 95, 69-96.

Homem, V., Santos, L., 2011. Degradation and removal methods of antibiotics from aqueous matrices - A review. J. Environ. Manage. 92, 2304-2347.

Huang, W., Brigante, M., Wu, F., Hanna, K., Mailhot, G., 2012. Development of a new homogenous photo-Fenton process using Fe(III)-EDDS complexes. J. Photochem. Photobiol. A: Chem. 239, 17-23.

Huber, M.M., Canonica, S., Park, G.Y., Von Gunten, U., 2003. Oxidation of pharmaceuticals during ozonation and advanced oxidation processes. Environ. Sci. Technol. 37, 1016-1024.

Ikehata, K., Jodeiri Naghashkar, N., Gamal El-Din, M., 2006. Degradation of aqueous pharmaceuticals by ozonation and advanced oxidation processes: A review. Ozone Sci. Eng. 28, 353-414.

Ingerslev, F., Toräng, L., Loke, M.L., Halling-Sorensen, B., Nyholm, N., 2001. Primary biodegradation of veterinary antibiotics in aerobic and anaerobic surface water simulation systems. Chemosphere 44, 865-872.

Jeong, J., Yoon, J., 2005. pH effect on OH radical production in photo/ferrioxalate system. Water Res. 39, 2893-2900.

Jones, O.A.H., Lester, J.N., Voulvoulis, N., 2005a. Pharmaceuticals: A threat to drinking water? Trends Biotechnol. 23, 163-167.

Jones, O.A.H., Voulvoulis, N., Lester, J.N., 2005b. Human pharmaceuticals in wastewater treatment processes. Crit. Rev. Environ. Sci. Technol. 35, 401-427.

Kanakaraju, D., Glass, B.D., Oelgemöller, M., 2013. Titanium dioxide photocatalysis for pharmaceutical wastewater treatment. Environ. Chem. Lett. 12, 27-47.

Kaniou, S., Pitarakis, K., Barlagianni, I., Poulios, I., 2005. Photocatalytic oxidation of sulfamethazine. Chemosphere 60, 372-380.

Karthikeyan, K.G., Meyer, M.T., 2006. Occurrence of antibiotics in wastewater treatment facilities in Wisconsin, USA. Sci. Total Environ. 361, 196-207.

Kemper, N., 2008. Veterinary antibiotics in the aquatic and terrestrial environment. Ecol. Indicators 8, 1-13.

Kim, S., Eichhorn, P., Jensen, J.N., Weber, A.S., Aga, D.S., 2005. Removal of antibiotics in wastewater: Effect of hydraulic and solid retention times on the fate of tetracycline in the activated sludge process. Environ. Sci. Technol. 39, 5816-5823.

Klamerth, N., Malato, S., Agüera, A., Fernández-Alba, A., 2013. Photo-Fenton and modified photo-Fenton at neutral pH for the treatment of emerging contaminants in wastewater treatment plant effluents: A comparison. Water Res. 47, 833-840.

Klamerth, N., Miranda, N., Malato, S., Agüera, A., Fernández-Alba, A.R., Maldonado, M.I., Coronado, J.M., 2009. Degradation of emerging contaminants at low concentrations in MWTPs effluents with mild solar photo-Fenton and TiO_2. Catal. Today 144, 124-130.

Klauson, D., Babkina, J., Stepanova, K., Krichevskaya, M., Preis, S., 2010. Aqueous photocatalytic oxidation of amoxicillin. Catal. Today 151, 39-45.

Kolen'ko, Y.V., Kovnir, K.A., Gavrilov, A.I., Garshev, A.V., Meskin, P.E., Churagulov, B.R., Bouchard, M., Colbeau-Justin, C., Lebedev, O.I., Van Tendeloo, G., Yoshimura, M., 2005. Structural, Textural, and Electronic Properties of a Nanosized Mesoporous ZnxTi1-xO2-x Solid Solution Prepared by a Supercritical Drying Route. J. Phys. Chem. B 109, 20303-20309.

Kolpin, D.W., Furlong, E.T., Meyer, M.T., Thurman, E.M., Zaugg, S.D., Barber, L.B., Buxton, H.T., 2002. Pharmaceuticals, hormones, and other organic wastewater contaminants in U.S. streams, 1999-2000: A national reconnaissance. Environ. Sci. Technol. 36, 1202-1211.

Košutić, K., Dolar, D., Ašperger, D., Kunst, B., 2007. Removal of antibiotics from a model wastewater by RO/NF membranes. Sep. Purif. Technol. 53, 244-249.

Koyuncu, I., Arikan, O.A., Wiesner, M.R., Rice, C., 2008. Removal of hormones and antibiotics by nanofiltration membranes. J. Membr. Sci. 309, 94-101.

Kümmerer, K., 2001. Drugs in the environment: Emission of drugs, diagnostic aids and disinfectants into wastewater by hospitals in relation to other sources - A review. Chemosphere 45, 957-969.

Kümmerer, K., 2004. Resistance in the environment. J. Antimicrob. Chemother. 54, 311-320.

Kümmerer, K., 2009. Antibiotics in the aquatic environment - A review - Part I. Chemosphere 75, 417-434.

Kümmerer, K., Al-Ahmad, A., Mersch-Sundermann, V., 2000. Biodegradability of some antibiotics, elimination of the genotoxicity and affection of wastewater bacteria in a simple test. Chemosphere 40, 701-710.

Lamm, A., Gozlan, I., Rotstein, A., Avisar, D., 2009. Detection of amoxicillin-diketopiperazine-2', 5' in wastewater samples. J. Environ. Sci. Health A Tox. Hazard Subst. Environ. Eng. 44, 1512-1517.

Larsen, T.A., Lienert, J., Joss, A., Siegrist, H., 2004. How to avoid pharmaceuticals in the aquatic environment. J. Biotechnol. 113, 295-304.

Larsson, D.G.J., de Pedro, C., Paxeus, N., 2007. Effluent from drug manufactures contains extremely high levels of pharmaceuticals. J. Hazard. Mater. 148, 751-755.

Le-Minh, N., Khan, S.J., Drewes, J.E., Stuetz, R.M., 2010. Fate of antibiotics during municipal water recycling treatment processes. Water Res. 44, 4295-4323.

Le, T.X., Munekage, Y., 2004. Residues of selected antibiotics in water and mud from shrimp ponds in mangrove areas in Viet Nam. Mar. Pollut. Bull. 49, 922-929.

Li, B., Zhang, T., Xu, Z., Fang, H.H.P., 2009. Rapid analysis of 21 antibiotics of multiple classes in municipal wastewater using ultra performance liquid chromatography-tandem mass spectrometry. Anal. Chim. Acta 645, 64-72.

Li, D., Yang, M., Hu, J., Ren, L., Zhang, Y., Li, K., 2008a. Determination and fate of oxytetracycline and related compounds in oxytetracycline production wastewater and the receiving river. Environ. Toxicol. Chem. 27, 80-86.

Li, D., Yang, M., Hu, J., Zhang, Y., Chang, H., Jin, F., 2008b. Determination of penicillin G and its degradation products in a penicillin production wastewater treatment plant and the receiving river. Water Res. 42, 307-317.

Li, S.Z., Li, X.Y., Wang, D.Z., 2004. Membrane (RO-UF) filtration for antibiotic wastewater treatment and recovery of antibiotics. Sep. Purif. Technol. 34, 109-114.

Lin, A.Y.C., Yu, T.H., Lateef, S.K., 2009. Removal of pharmaceuticals in secondary wastewater treatment processes in Taiwan. J. Hazard. Mater. 167, 1163-1169.

Lindsey, M.E., Meyer, M., Thurman, E.M., 2001. Analysis of trace levels of sulfonamide and tetracycline antimicrobials in groundwater and surface water using solid-phase extraction and liquid chromatography/mass spectrometry. Anal. Chem. 73, 4640-4646.

Linsebigler, A.L., Lu, G., Yates, J., J. T., 1995. Photocatalysis on TiO_n Surfaces: Principles, Mechanisms, and Selected Results. Chem. Rev. 95, 735-758.

Liu, P., Zhang, H., Feng, Y., Yang, F., Zhang, J., 2014. Removal of trace antibiotics from wastewater: A systematic study of nanofiltration combined with ozone-based advanced oxidation processes. Chem. Eng. J. 240, 211-220.

Malato, S., Blanco, J., Vidal, A., Alarcón, D., Maldonado, M.I., Cáceres, J., Gernjak, W., 2003. Applied studies in solar photocatalytic detoxification: An overview. Sol Energy 75, 329-336.

Malato, S., Fernández-Ibáñez, P., Maldonado, M.I., Blanco, J., Gernjak, W., 2009. Decontamination and disinfection of water by solar photocatalysis: Recent overview and trends. Catal. Today 147, 1-59.

Marco, A., Esplugas, S., Saum, G., 1997. How and why combine chemical and biological processes for wastewater treatment. Water Sci. Technol. 35, 321-327.

Martinez, J.L., 2009. Environmental pollution by antibiotics and by antibiotic resistance determinants. Environ. Pollut. 157, 2893-2902.

McKeon, D.M., Calabrese, J.P., Bissonnette, G.K., 1995. Antibiotic resistant gram-negative bacteria in rural groundwater supplies. Water Res. 29, 1902-1908.

Michael, I., Hapeshi, E., Aceña, J., Perez, S., Petrović, M., Zapata, A., Barceló, D., Malato, S., Fatta-Kassinos, D., 2013a. Light-induced catalytic transformation of ofloxacin by solar Fenton in various water matrices at a pilot plant: Mineralization and characterization of major intermediate products. Sci. Total Environ. 461–462, 39-48.

Michael, I., Hapeshi, E., Michael, C., Fatta-Kassinos, D., 2010. Solar Fenton and solar TiO_2 catalytic treatment of ofloxacin in secondary treated effluents: Evaluation of operational and kinetic parameters. Water Res. 44, 5450-5462.

Michael, I., Rizzo, L., McArdell, C.S., Manaia, C.M., Merlin, C., Schwartz, T., Dagot, C., Fatta-Kassinos, D., 2013b. Urban wastewater treatment plants as hotspots for the release of antibiotics in the environment: A review. Water Res. 47, 957-995.

Miège, C., Choubert, J.M., Ribeiro, L., Eusèbe, M., Coquery, M., 2009. Fate of pharmaceuticals and personal care products in wastewater treatment plants - Conception of a database and first results. Environ. Pollut. 157, 1721-1726.

Mölstad, S., Lundborg, C.S., Karlsson, A.K., Cars, O., 2002. Antibiotic prescription rates vary markedly between 13 European countries. Scand. J. Infect. Dis. 34, 366-371.

Monteagudo, J.M., Durán, A., Corral, J.M., Carnicer, A., Frades, J.M., Alonso, M.A., 2012. Ferrioxalate-induced solar photo-Fenton system for the treatment of winery wastewaters. Chem. Eng. J. 181-182, 281-288.

Monteiro, R.A.R., Lopes, F.V.S., Silva, A.M.T., Ângelo, J., Silva, G.V., Mendes, A.M., Boaventura, R.A.R., Vilar, V.J.P., 2014. Are TiO_2-based exterior paints useful catalysts for gas-phase photooxidation processes? A case study on n-decane abatement for air detoxification. Appl. Catal., B 147, 988-999.

Morris, A.K., Masterton, R.G., 2002. Antibiotic resistance surveillance: Action for international studies. J. Antimicrob. Chemother. 49, 7-10.

Muñoz, I., Peral, J., Antonio Ayllón, J., Malato, S., Passarinho, P., Domènech, X., 2006. Life cycle assessment of a coupled solar photocatalytic-biological process for wastewater treatment. Water Res. 40, 3533-3540.

Oller, I., Malato, S., Sánchez-Pérez, J.A., 2011. Combination of Advanced Oxidation Processes and biological treatments for wastewater decontamination - A review. Sci. Total Environ. 409, 4141-4166.

Oncu, N.B., Balcioglu, I.A., 2013. Antimicrobial Contamination Removal from Environmentally Relevant Matrices: A Literature Review and a Comparison of Three Processes for Drinking Water Treatment. Ozone Sci. Eng. 35, 73-85.

Pailler, J.Y., Krein, A., Pfister, L., Hoffmann, L., Guignard, C., 2009. Solid phase extraction coupled to liquid chromatography-tandem mass spectrometry analysis of sulfonamides, tetracyclines, analgesics and hormones in surface water and wastewater in Luxembourg. Sci. Total Environ. 407, 4736-4743.

Palominos, R.A., Mondaca, M.A., Giraldo, A., Peñuela, G., Pérez-Moya, M., Mansilla, H.D., 2009. Photocatalytic oxidation of the antibiotic tetracycline on TiO_2 and ZnO suspensions. Catal. Today 144, 100-105.

Palominos, R.A., Mora, A., Mondaca, M.A., Pérez-Moya, M., Mansilla, H.D., 2008. Oxolinic acid photo-oxidation using immobilized TiO_2. J. Hazard. Mater. 158, 460-464.

Pelizzetti, E., Minero, C., 1993. Mechanism of the photo-oxidative degradation of organic pollutants over TiO_2 particles. Electrochim. Acta 38, 47-55.

Pena, A., Paulo, M., Silva, L.J.G., Seifrtová, M., Lino, C.M., Solich, P., 2010. Tetracycline antibiotics in hospital and municipal wastewaters: A pilot study in Portugal. Anal. Bioanal. Chem. 396, 2929-2936.

Peral, J., Ollis, D.F., 1992. Heterogeneous photocatalytic oxidation of gas-phase organics for air purification: Acetone, 1-butanol, butyraldehyde, formaldehyde, and m-xylene oxidation. J. Catal. 136, 554-565.

Pérez-Parada, A., Agüera, A., Gómez-Ramos, M.d.M., García-Reyes, J.F., Heinzen, H., Fernández-Alba, A.R., 2011. Behavior of amoxicillin in wastewater and river water: identification of its main transformation products by liquid chromatography/electrospray quadrupole time-of-flight mass spectrometry. Rapid Commun. Mass Spectrom. 25, 731-742.

Pignatello, J.J., Oliveros, E., MacKay, A., 2006. Advanced oxidation processes for organic contaminant destruction based on the fenton reaction and related chemistry. Crit. Rev. Environ. Sci. Technol. 36, 1-84.

Poyatos, J.M., Muñio, M.M., Almecija, M.C., Torres, J.C., Hontoria, E., Osorio, F., 2009. Advanced Oxidation Processes for Wastewater Treatment: State of the Art. Water, Air, Soil Pollut. 1-18.

Prato-Garcia, D., Vasquez-Medrano, R., Hernandez-Esparza, M., 2009. Solar photoassisted advanced oxidation of synthetic phenolic wastewaters using ferrioxalate complexes. Solar Energy 83, 306-315.

Radjenovic, J., Petrovic, M., Barceló, D., 2007. Analysis of pharmaceuticals in wastewater and removal using a membrane bioreactor. Anal. Bioanal. Chem. 387, 1365-1377.

Radjenović, J., Petrović, M., Barceló, D., 2009. Fate and distribution of pharmaceuticals in wastewater and sewage sludge of the conventional activated sludge (CAS) and advanced membrane bioreactor (MBR) treatment. Water Res. 43, 831-841.

Radjenović, J., Petrović, M., Ventura, F., Barceló, D., 2008. Rejection of pharmaceuticals in nanofiltration and reverse osmosis membrane drinking water treatment. Water Res. 42, 3601-3610.

Reyes, C., Fernández, J., Freer, J., Mondaca, M.A., Zaror, C., Malato, S., Mansilla, H.D., 2006. Degradation and inactivation of tetracycline by TiO_2 photocatalysis. J. Photochem. Photobiol. A: Chem. 184, 141-146.

Rivera-Utrilla, J., Gómez-Pacheco, C.V., Sánchez-Polo, M., López-Peñalver, J.J., Ocampo-Pérez, R., 2013a. Tetracycline removal from water by adsorption/bioadsorption on activated carbons and sludge-derived adsorbents. J. Environ. Manage. 131, 16-24.

Rivera-Utrilla, J., Prados-Joya, G., Sánchez-Polo, M., Ferro-García, M.A., Bautista-Toledo, I., 2009. Removal of nitroimidazole antibiotics from aqueous solution by adsorption/bioadsorption on activated carbon. J. Hazard. Mater. 170, 298-305.

Rivera-Utrilla, J., Sánchez-Polo, M., Ferro-García, M.Á., Prados-Joya, G., Ocampo-Pérez, R., 2013b. Pharmaceuticals as emerging contaminants and their removal from water. A review. Chemosphere 93, 1268-1287.

Rivera-Utrilla, J., Sánchez-Polo, M., Gómez-Serrano, V., Álvarez, P.M., Alvim-Ferraz, M.C.M., Dias, J.M., 2011. Activated carbon modifications to enhance its water treatment applications. An overview. J. Hazard. Mater. 187, 1-23.

Rizzo, L., Fiorentino, A., Anselmo, A., 2013. Advanced treatment of urban wastewater by UV radiation: Effect on antibiotics and antibiotic-resistant *E. coli* strains. Chemosphere 92, 171-176.

Roberts, P.H., Thomas, K.V., 2006. The occurrence of selected pharmaceuticals in wastewater effluent and surface waters of the lower Tyne catchment. Sci. Total Environ. 356, 143-153.

Rodríguez, E.M., Núñez, B., Fernández, G., Beltrán, F.J., 2009. Effects of some carboxylic acids on the Fe(III)/UVA photocatalytic oxidation of muconic acid in water. Appl. Catal., B 89, 214-222.

Rosenfeldt, E.J., Linden, K.G., Canonica, S., von Gunten, U., 2006. Comparison of the efficiency of ·OH radical formation during ozonation and the advanced oxidation processes O_3/H_2O_2 and UV/H_2O_2. Water Res. 40, 3695-3704.

Sarmah, A.K., Meyer, M.T., Boxall, A.B.A., 2006. A global perspective on the use, sales, exposure pathways, occurrence, fate and effects of veterinary antibiotics (VAs) in the environment. Chemosphere 65, 725-759.

Schaar, H., Clara, M., Gans, O., Kreuzinger, N., 2010. Micropollutant removal during biological wastewater treatment and a subsequent ozonation step. Environ. Pollut. 158, 1399-1404.

Seifrtová, M., Nováková, L., Lino, C., Pena, A., Solich, P., 2009. An overview of analytical methodologies for the determination of antibiotics in environmental waters. Anal. Chim. Acta 649, 158-179.

Senta, I., Matošić, M., Jakopović, H.K., Terzic, S., Ćurko, J., Mijatović, I., Ahel, M., 2011. Removal of antimicrobials using advanced wastewater treatment. J. Hazard. Mater. 192, 319-328.

Silva, M.R.A., Trovó, A.G., Nogueira, R.F.P., 2007. Degradation of the herbicide tebuthiuron using solar photo-Fenton process and ferric citrate complex at circumneutral pH. J. Photochem. Photobiol. A: Chem. 191, 187-192.

Sipma, J., Osuna, B., Collado, N., Monclús, H., Ferrero, G., Comas, J., Rodriguez-Roda, I., 2010. Comparison of removal of pharmaceuticals in MBR and activated sludge systems. Desalination 250, 653-659.

Snyder, S.A., Adham, S., Redding, A.M., Cannon, F.S., DeCarolis, J., Oppenheimer, J., Wert, E.C., Yoon, Y., 2007. Role of membranes and activated carbon in the removal of endocrine disruptors and pharmaceuticals. Desalination 202, 156-181.

Son, H.S., Ko, G., Zoh, K.D., 2009. Kinetics and mechanism of photolysis and TiO_2 photocatalysis of triclosan. J. Hazard. Mater. 166, 954-960.

Tambosi, J.L., de Sena, R.F., Favier, M., Gebhardt, W., José, H.J., Schröder, H.F., de Fatima Peralta Muniz Moreira, R., 2010. Removal of pharmaceutical compounds in membrane bioreactors (MBR) applying submerged membranes. Desalination 261, 148-156.

Thiele-Bruhn, S., 2003. Pharmaceutical antibiotic compounds in soils - A review. J. Plant Nutr. Soil Sci. 166, 145-167.

Trovó, A.G., de Paiva, V.A.B., Machado, A.E.H., de Oliveira, C.A., Santos, R.O., 2013. Degradation of the antibiotic chloramphenicol by photo-Fenton process at lab-scale and solar pilot plant: Kinetic, toxicity and inactivation assessment. Sol. Energy 97, 596-604.

Trovó, A.G., Pupo Nogueira, R.F., Agüera, A., Fernandez-Alba, A.R., Malato, S., 2011. Degradation of the antibiotic amoxicillin by photo-Fenton process - Chemical and toxicological assessment. Water Res. 45, 1394-1402.

Vaz-Moreira, I., Nunes, O.C., Manaia, C.M., 2011. Diversity and antibiotic resistance patterns of Sphingomonadaceae isolates from drinking water. Appl Environ Microbiol 77, 5697-5706.

Watkinson, A.J., Murby, E.J., Costanzo, S.D., 2007. Removal of antibiotics in conventional and advanced wastewater treatment: Implications for environmental discharge and wastewater recycling. Water Res. 41, 4164-4176.

Webb, S., Ternes, T., Gibert, M., Olejniczak, K., 2003. Indirect human exposure to pharmaceuticals via drinking water. Toxicol. Lett. 142, 157-167.

Westerhoff, P., Moon, H., Minakata, D., Crittenden, J., 2009. Oxidation of organics in retentates from reverse osmosis wastewater reuse facilities. Water Res. 43, 3992-3998.

Wilson, B.A., Smith, V.H., Denoyelles Jr, F., Larive, C.K., 2003. Effects of three pharmaceutical and personal care products on natural freshwater algal assemblages. Environ. Sci. Technol. 37, 1713-1719.

Wols, B.A., Hofman-Caris, C.H.M., 2012. Review of photochemical reaction constants of organic micropollutants required for UV advanced oxidation processes in water. Water Res. 46, 2815-2827.

Yoon, Y., Westerhoff, P., Snyder, S.A., Wert, E.C., Yoon, J., 2007. Removal of endocrine disrupting compounds and pharmaceuticals by nanofiltration and ultrafiltration membranes. Desalination 202, 16-23.

Zhao, C., Pelaez, M., Duan, X., Deng, H., O'Shea, K., Fatta-Kassinos, D., Dionysiou, D.D., 2013. Role of pH on photolytic and photocatalytic degradation of antibiotic oxytetracycline in aqueous solution under visible/solar light: Kinetics and mechanism studies. Appl. Catal., B 134–135, 83-92.

2 Materials and methods

This chapter contains an overview of all the chemicals and reagents used in this thesis, a detailed description of the experimental units used to perform all the photocatalytic trials and the corresponding experimental procedures. The employed analytical methods are also herein described.

2.1 Chemicals and Reagents

Oxytetracycline hydrochloride (OTC.HCl, CAS# 2058-46-0), Oxolinic acid (OXA, CAS# 14698-29-4) and Amoxicillin (AMX, CAS# 26787-78-0) were purchased from Sigma-Aldrich. Their molecular structure can be seen in Figure 2.1, while Table 2.1 presents a short summary of documented physico-chemical properties of the three compounds.

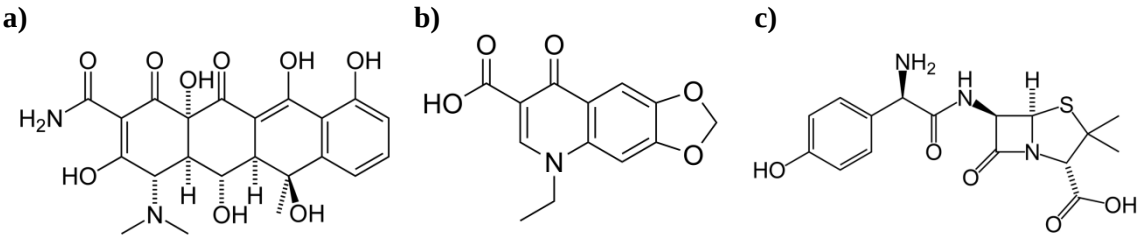

Figure 2.1. Molecular structures of **a)** OTC, **b)** OXA, **c)** AMX antibiotics.

Table 2.1. Physico-chemical properties of OTC, OXA and AMX antibiotics.

Property	OTC	OXA	AMX
Molecular formula[a]	$C_{22}H_{24}N_2O_9$ (.HCl)	$C_{13}H_{11}NO_5$	$C_{16}H_{19}N_3O_5S$
Molecular Weight (g mol^{-1})[a]	460.43 (496.89)	261.2	365.40
HPLC purity[a]	97 %	99 %	100 %
Specific gravity[b]	1.63	1.55	n.a.
Solubility (pH 7) - in water (20 °C)[b]	1000 mg L^{-1}	3.2 mg L^{-1}	3430 mg L^{-1}
Log K_{OW} at pH 7 (20 °C)[b]	-1.22	1.67	0.87
pK_{a1}	3.22[c]	6.92[d]	2.68[e]
pK_{a2}	7.46[c]	-	7.49[e]
pK_{a3}	8.94[c]	-	8.94[e]

n.a. – not available; [a]Certificate of analysis (Sigma-Aldrich); [b]VSDB (2013); [c]Qiang and Adams (2004): Ionic strength = 0 M; T = 23 °C ; [d]Jiménez-Lozano et al. (2002): Ionic strength = 0 M; T = 25 °C; [e]Andreozzi et al. (2005): Ionic strength = 0.1 M; T = 25 °C

Antibiotics were stored at 4 °C and solutions were prepared daily by weighting the appropriate mass, taking into consideration HPLC purity and molecular weight (as in the case of Oxytetracycline (OTC) against OTC.HCl). Solutions of OTC and AMX were easily prepared, whereas solutions of OXA, given its very limited solubility in neutral pH levels, required an initial pH adjustment. According to the Sigma-Aldrich product information sheet (Product number O0877), OXA solutions were prepared in 0.05 M NaOH (pH ~ 11), which required a subsequent neutralization step.

Heterogeneous photocatalytic experiments used Degussa P-25 (80 % anatase and 20 % rutile) Titanium Dioxide (TiO_2). Photo-Fenton experiments were performed using hydrogen peroxide (Quimitécnica, S.A., 50 % (w/v), 1.10 g cm^{-3}), iron (II) sulphate heptahydrate (Panreac),

iron (III) hexahydrate (Merck), oxalic acid dihydrate (VWR Prolabo, purity ≥ 98 %) and citric acid monohydrate (VWR; 100 %).

Ultrapure and deionized water necessary for analysis or antibiotic solutions were obtained using a millipore system (Direct-Q model) and reverse osmosis system (Panice®), respectively.

Pure or diluted solutions of sulfuric acid (Pronalab, 96 %, 1.84 g/cm^3) and sodium hydroxide (Merck) were used for pH adjustment.

NaCl, $MgSO_4.7H_2O$, $NaHCO_3$, KNO_3, NH_4Cl, $K_3PO_4.3H_2O$, D-Mannitol and NaN_3 were all analytical grade, while Humic acids were Alfa Aesar (CAS# 1415-93-6).

For HPLC-DAD analysis, gradient-grade acetonitrile and methanol were obtained from Merck, while oxalic acid dehydrate (100 %) was from VWR Prolabo.

2.2 Experimental units and procedure

2.2.1 SOLARBOX lab-scale photoreactor

2.2.1.1 *Description*

The first set of experiments described in Chapter 3 was performed in the Department of Chemical Engineering at the Faculty of Chemistry of the University of Barcelona.

The SOLARBOX lab-scale photocatalytic apparatus comprises: i) a solar radiation simulator (Solarbox, Co.fo.me.gra 220 V 50 Hz) ii) a tubular reactor (illuminated volume, V_i = 0.078 L, Schott-Duran type 3.3, Germany, cut-off at 280 nm, internal diameter 21.1 mm, length 223 mm and thickness 2.11 mm) in the axis of a parabolic mirror; iii) one glass vessel (capacity of 1.0 L) with a cooling jacket, coupled to a refrigerated thermostatic bath (Haake K10) to ensure a constant temperature during the experiment; iv) a magnetic stirrer (OVAN) to ensure complete homogenization of the solution inside the glass vessel; v) one peristaltic pump (Ismatec, model Ecoline VC-280 II) to promote the water recirculation between the photoreactor and the glass vessel; vi) pH meter (GLP 22).

All connections and pipes employed were made of Teflon and/or glass material to avoid losses by adsorption. A scheme and general views of the installation can be seen in Figure 2.2.

2.2.1.2 *Experimental procedure*

The stirred reservoir tank was filled with a 20 mg L^{-1} Oxytetracycline solution. The solution was continuously pumped through the Duran tubular reactor (illuminated volume, V_i = 0.078 L) placed at the bottom of the Solarbox, in the axis of a parabolic mirror, and recirculated to the reservoir tank at a flow rate of 0.65 L min^{-1} (illuminated time, t_i = 0.12 min; dark time, t_d = 1.42 min). Once the air of the system was purged and after some minutes of recirculation, a sample was taken. Then, TiO_2 was added to the reservoir tank and the resulting suspension was left recirculating in the dark for 60 minutes to achieve adsorption equilibrium. After that, the Solarbox was turned on and a Xe-OP lamp (Phillips 1 kW) placed inside started to irradiate the tubular reactor. Radiant power entering the reactor was determined to be 3.55 J s^{-1} (between 290 and 400 nm). It was calculated by uranyl oxalate actinometry (Kuhn et al., 2004) taking into account the transmittance of Duran glass, the reactor's geometry, the actinometric system quantum yield and the useful wavelengths for TiO_2. The temperature of the solution was kept at 25 ºC by controlling the temperature of the jacket in the reservoir tank through the ultra-thermostat bath. All samples were pre-filtrated through 0.2 μm Nylon VWR membrane filters

before analysis. Initial pH values were unbuffered and adjusted when needed with diluted phosphoric acid or sodium hydroxide solutions.

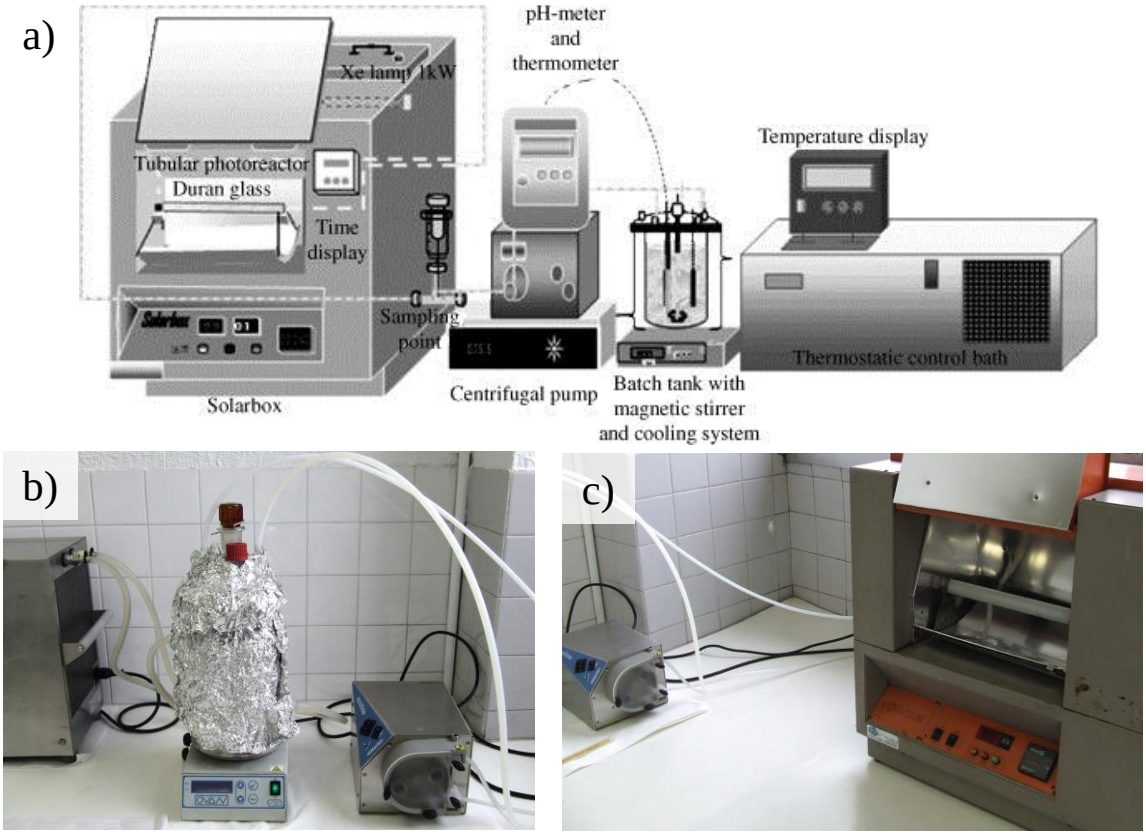

Figure 2.2. SOLARBOX lab-scale experimental set-up: **a)** schematic representation (adapted from Méndez-Arriaga et al. (2008)); **b)** and **c)** views of the thermostatic bath, reservoir tank, peristaltic pump, sunlight simulator and photoreactor equipped with a parabolic reflector

2.2.2 SUNTEST lab-scale photoreactor

2.2.2.1 *Description*

The lab-scale experiments described in Chapters 4, 5, 6 and 7 were performed at the Chemical Engineering Department of the Faculty of Engineering of the University of Porto (FEUP). The lab-scale photocatalytic apparatus (SUNTEST) comprises: i) a solar radiation simulator (ATLAS, model SUNTEST XLS+) with 1100 cm^2 of exposition area, a 1700 W air-cooled xenon arc lamp, a daylight filter and quartz filter with infrared (IR) coating; ii) a compound parabolic collector with 0.025 m^2 of illuminated area with electropolished anodized aluminium reflectors and borosilicate tube (Schott-Duran type 3.3, Germany, cut-off at 280 nm, internal diameter 46.4 mm, length 160 mm and thickness 1.8 mm); iii) one glass vessel (capacity of 1.5 L) with a cooling jacket, coupled to a refrigerated thermostatic bath (Lab. Companion, model RW-0525G) to ensure a constant temperature during the experiment; iv) a magnetic stirrer (Velp Scientifica, model ARE) to ensure complete homogenization of the solution inside the glass vessel; v) one peristaltic pump (Ismatec, model Ecoline VC-380 II, at a flow rate of 0.63 L min^{-1}) to promote the water recirculation between the photoreactor and the glass vessel; vi) pH and temperature meter (VWR sympHony SB90M5). V_i = 0.270 L; V_i/V_t = 0.23 (initial V_t of 1.2 L); t_i = 0.43 min; t_{dark} = 1.16 min. All the systems are connected using Teflon tubing. The photoreactor has two polypropylene caps with four equidistant inlets and outlets to ensure a better distribution of the feed stream throughout the reactor. A schematic representation of the SUNTEST installation can be seen in Figure 2.3.

2.2.2.2 *Experimental procedure*

In all the experiments, a solution of 1.2 L of 20 mg L^{-1} of OTC (4.34×10^{-5} M), OXA (7.66×10^{-5} M) or AMX (5.47×10^{-5} M), was added to the recirculation glass vessel and homogenized by stirring in darkness. The temperature set-point of the refrigerated thermostatic bath was controlled to keep the antibiotic solution at 25 °C. After 15 minutes, a sample was taken to confirm the initial antibiotic and DOC concentrations.

The experimental procedure then varied according to the employed photocatalytic processes: a) TiO_2/UV; b) Fe^{2+}/H_2O_2/UV-Vis and c) Fe^{3+}/Oxalate or Citrate/H_2O_2/UV-Vis.

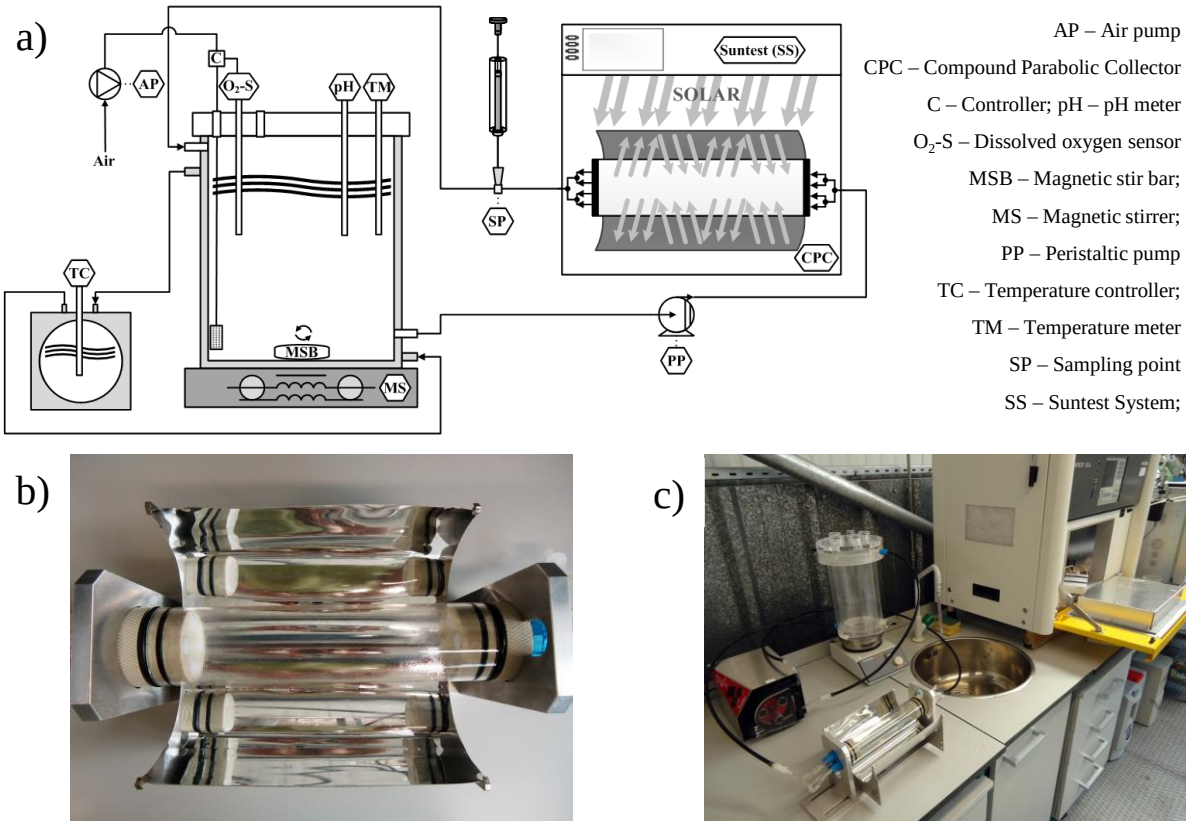

Figure 2.3. SUNTEST lab-scale experimental set-up: **a)** schematic representation; **b)** and **c)** views of the photoreactor equipped with a CPC, the peristaltic pump, the reservoir tank and the sunlight simulator

a) TiO_2/UV

In Chapters 4 and 5, experiments were performed to study the influence of individual inorganic ions and the formation of different reactive oxygen species (ROS), using selective scavengers, in the TiO_2/UV degradation of OTC, OXA and AMX. After the first sample was taken, the pH was adjusted (7.5) and the corresponding salt mass to achieve the desired concentration of each ion or ROS scavenger to be studied was added to the solution. Inorganic ion concentrations were adapted from Pouliquen et al. (2007) and based on the inorganic ion concentration ratio reported by Miralles-Cuevas et al. (2013), and were set as $[Cl^-] = [SO_4^{2-}] = [NO_3^-] = [NH_4^+] = PO_4^{3-}] = 1$ g L^{-1}; $[HCO_3^-] = 0.1$ g L^{-1}. The concentration of ROS scavengers were based on Hirakawa et al. (2004) and Raja et al. (2005): singlet oxygen: $[NaN_3] = 10$ mM; hydroxyl radical: [D-Mannitol] = 50 mM.

After 15 min, a sample was taken before the catalyst addition step ($[TiO_2] = 0.5$ g L^{-1}). After a period of 30 min to ensure adsorption equilibrium, another sample was taken and the solution was then pumped to the CPC unit before the SUNTEST was turned on. Irradiation was set as $I = 500$ W m^{-2}, which is equivalent to 44 W_{UV} m^{-2} measured in the wavelength range from 280 to 400 nm.

Samples were then taken at pre-defined times and were pre-filtrated through 0.45 μm Nylon VWR membrane filters before analysis to evaluate the photodegradation process.

In Chapter 7, the 0.2 g L^{-1} of TiO_2 were added to the supernatant obtained after AMX biodegradation (from EM, Buffer, NaCl or WW matrices, characteristics in Table 2.4), the pH was adjusted to 5.5 with sulfuric acid and the solution was left to homogenize in darkness for 30 minutes. A sample was taken before irradiation began to check initial AMX transformation products' (TPs) HPLC-UV areas and DOC concentration.

b) Fe^{2+}/H_2O_2/UV-Vis

In the Fe^{2+}/H_2O_2/UV-Vis experiments performed in Chapter 6, the initial pH was adjusted to 3.0, 4.0 or 5.0 with sulfuric acid and another sample was taken after 15 minutes. Iron (II) sulfate was added in order to achieve a concentration of 2 mg L^{-1} Fe (II). The solution was left to homogenize for 15 minutes, after which another sample was taken, and the initial iron concentration was also confirmed. The solution was then pumped to the CPC unit before the SUNTEST was turned on (I = 500 W m^{-2}). Immediately after irradiation began, the initial H_2O_2 dose was added, while the pH of the solution was left uncontrolled.

Samples were then taken during the experiments at pre-defined times and filtered through 0.45 μm Nylon VWR membrane filters before analysis to evaluate the photodegradation process. For HPLC analysis, samples were quenched with methanol to stop any further reactions, while DOC determination was performed without previous treatment since dark Fenton effects were negligible.

c) Fe^{3+}/Oxalate or Citrate/H_2O_2/UV-Vis

A similar procedure was followed in the Fe^{3+}/Oxalate/H_2O_2/UV-Vis and Fe^{3+}/Citrate/H_2O_2/UV-Vis experiments performed in Chapter 6, except for the addition of a 1:3 iron/oxalate molar ratio dose (extra DOC ~ 2.6 mg L^{-1}), or a 1:1 iron/citrate molar ratio dose (extra DOC ~ 4.3 mg L^{-1}), before the pH adjustment and Fe (III) chloride addition steps. In the Fe^{3+}/Oxalate/H_2O_2/UV-Vis experiments performed in Chapter 7, oxalic acid was first added to the supernatant obtained after AMX biodegradation (from NaCl or WW matrices) in a 1:3 (NaCl) or 1:9 (WW) iron/oxalate molar ratio dose and a sample was taken after 15 minutes. The pH was adjusted to 4.0 or 5.0 and iron (III) chloride was then added to achieve a concentration of 2 mg L^{-1} Fe (III).

In Chapter 6, the addition of inorganic ions ($[Cl^-] = [SO_4^{2-}] = [NO_3^-]$ = 1 g L^{-1}; $[HCO_3^-]$ = 0.1 g L^{-1}; values based on the inorganics concentration ratio of Miralles-Cuevas et al. (2013)) and natural organic matter (humic acids concentration based on Lindsey and Tarr (2000), extra [DOC] ~ 5 mg L^{-1}) to the initial OTC solution was also carried out.

To evaluate matrix effects in Chapter 6 and in AMX degradation, a concentration of 20 mg L^{-1} OTC or AMX were spiked into 1.2 L of wastewater treatment plant (WW: OTC and AMX) effluent or into a trout farm (TF: OTC only) effluent before the abovementioned steps. WW effluent was collected after secondary treatment in a urban WWTP (Northern Portugal), while TF effluent was collected in the outlet of a trout farm operated in open circuit regime (Northern Portugal), after final decantation. The main characteristics of the tested effluents are presented in Table 2.4.

The addition of H_2O_2 in all photo-Fenton experiments was based on the stoichiometric amount necessary to completely mineralize 20 mg L^{-1} of each antibiotic, according to Eq. 2.01, 2.02 and 2.03:

a) Oxytetracycline: 67 mg L^{-1} (2.3 mM) of H_2O_2.

$$C_{22}H_{24}N_2O_9 + 52H_2O_2 \rightarrow 22CO_2 + 63H_2O + 2HNO_3 \quad (2.01)$$

b) Oxolinic Acid: 46 mg L^{-1} (1.6 mM) of H_2O_2.

$$C_{13}H_{11}NO5 + 29H_2O_2 \rightarrow 13CO_2 + 34H_2O + HNO_3 \quad (2.02)$$

c) Amoxicillin: 76 mg L^{-1} (2.6 mM) of H_2O_2.

$$C_{16}H_{19}N_3O_5S + 47H_2O_2 \rightarrow 16CO_2 + 54H_2O + 3HNO_3 + H_2SO_4 \quad (2.03)$$

A control dosage strategy was followed in order to avoid excess H_2O_2 in solution (Klamerth et al., 2010). In this way, an initial 30 mg L^{-1} dose (~0.9 mM) was added in the beginning of every experiment, and supplementary 30 mg L^{-1} additions were performed when the H_2O_2 concentration approached 10 mg L^{-1} along the reactions (see sub-section 2.3.4).

2.2.3 Solar Pilot-plant equipped with CPCs

2.2.3.1 *Description*

The solar photocatalytic experiments were carried out in a CPC pilot plant installed at the roof of the Chemical Engineering Department of the Faculty of Engineering, University of Porto (FEUP), Portugal. The solar collector consists of a CPC unit (0.91 m^2) of four borosilicate (Duran) tubes (Schott–Duran type 3.3, Germany, cut-off at 280 nm, internal diameter 46.4 mm, length 1500 mm and width 1.8 mm) connected in series by polypropylene junctions, with their CPC mirrors in electropolished anodized aluminum, supported by a aluminum structure, oriented to south and tilted 41° (local latitude). The pilot plant has also two recirculation tanks (15 L and 20 L), two recirculation pumps (20 L min^{-1}), two flow rate meters, five polypropylene valves and an electric board for process control. The pilot plant was operated in two ways: using the total CPCs area (0.91 m^2) or using 0.455 m^2 of CPCs area individually, giving the possibility of performing two different experiments at the same time and under the same solar radiation conditions. The intensity of solar UV radiation is measured by a global UV radiometer (ACADUS 85-PLS) mounted on the pilot plant with the same inclination, which provides data in terms of incident W_{UV} m^{-2}. Temperature and pH were measured using a pH meter HANNA HI 4522. A schematic representation can be seen in Figure 2.4.

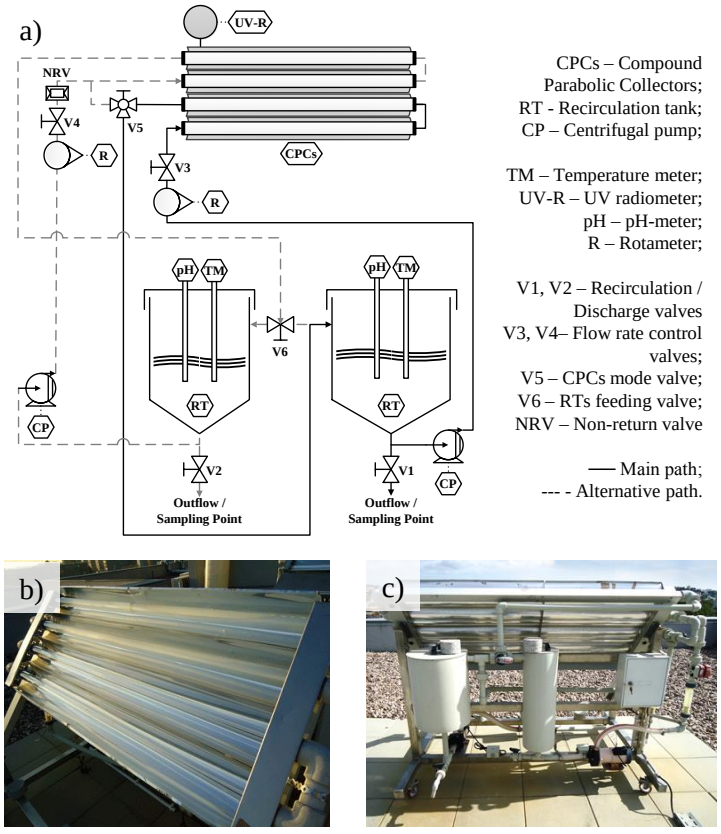

Figure 2.4. Solar pilot-plant experimental set-up: **a)** plant flowchart; **b)** front view; **c)** back view

Equation 2.04 allows the calculation of the accumulated UV energy ($Q_{UV,\,n}$, kJ L^{-1}) received on any surface in the same position with regard to the sun, per unit of volume of water inside the reactor, in the time interval Δt:

$$Q_{UV,n} = Q_{UV,n-1} + \Delta t_n \overline{UV}_{G,n} \frac{A_r}{1000 \times V_t}; \quad \Delta t_n = t_n - t_{n-1} \tag{2.04}$$

where t_n is the experimental time of each sample (s), V_t the total reactor volume (L), A_r the illuminated collector surface area (m^2) and $\overline{UV}_{G,n}$ the average solar ultraviolet radiation (W m^{-2}) measured during the period Δt_n (s).

2.2.3.2 *Experimental procedure*

In every photocatalytic experiment, the corresponding mass of antibiotic to obtain C_0 = 20 mg L^{-1} (OTC, OXA, or AMX) was dissolved in 15 L of deionized water added to the recirculation tank of the CPC unit (V_i = 5.1 L; V_i/V_t = 0.34; t_i = 0.25 min; t_{dark} = 0.50 min; A_{CPC} = 0.455 m^2) and homogenized by turbulent recirculation during 30 min in darkness. After this period, a sample was taken to confirm the initial antibiotic and DOC concentrations. The experimental procedure then varied according to the employed photocatalytic processes: a) TiO_2/UV; b) Fe^{3+}/Oxalate/H_2O_2/UV-Vis.

a) TiO_2/UV - In the experiment performed in Chapter 3, there was no initial pH adjustment (pH_0 = 4.4). In the experiments performed in Chapters 4 and 5, the initial pH of the solution was adjusted to 7.5 before the addition of 0.5 g L^{-1} of TiO_2. After 30 minutes another sample was taken before the CPCs were uncovered to start the experiments in order to evaluate the antibiotic(s) adsorption onto the catalyst surface. Throughout the reaction, samples were taken at pre-defined times to follow the photodegradation process. All samples were pre-filtrated through 0.45 μm Nylon VWR membrane filters before analysis and both temperature and pH were measured using a pH/conductivity meter HANNA HI 4522. To assess antibiotic photolytic degradation, the same methodology was used but in the absence of TiO_2.

b) Fe^{3+}/Oxalate/H_2O_2/UV-Vis - In the experiment performed in Chapter 6, oxalic acid was added to a solution of OTC (iron/oxalate molar ratio of 1:3), left to recirculate for 15 minutes, and a second sample was taken before the addition of iron (III) chloride (2 mg Fe (III) L^{-1}) and pH adjustment to 5.0. A third sample was taken after 15 minutes, and the initial iron concentration was confirmed. The CPCs were uncovered, the same initial H_2O_2 dose was added and the pH of the solution was left uncontrolled. Throughout the reaction, samples were taken at pre-defined times to follow the photodegradation process. All samples were pre-filtrated through 0.45 μm Nylon VWR membrane filters before analysis.

2.3 Analytical methods

2.3.1 High Performance Liquid Chromatography (HPLC)

High Performance Liquid Chromatography – Diode Array Detector (HPLC-DAD) was the selected method to determine the concentration of antibiotics in solution and to follow their degradation along the performed photolytic/photocatalytic experiments.

In the experiments performed with the Solarbox lab-scale photoreactor in Chapter 3, oxytetracycline concentration was measured by using Waters' HPLC apparatus (Photodiode array detector DAD 996, auto Sampler 717, controller 600) equipped with Millennium software. The reverse-phase column used was a Mediterranea Sea-18 (Technocroma, Spain) and the mobile phase was a 70:30 mixture of a buffered solution (H_2O:CH_3OH:H_3PO_4, 500:25:2) and Acetonitrile, isocratically delivered by a pump at a flow rate of 0.6 mL min^{-1}. Injection volume was 20 µL and the wavelength of the UV absorbance detector was fixed at 354 nm.

In the experiments performed with the Suntest lab-scale photoreactor and the solar pilot plant, the HPLC-DAD device was a Hitachi ELITE LaChrom (Merck-Hitach, Tokyo, Japan), equipped with a L-2130 pump, a L-2200 autosampler, L-2300 column oven and a L-2455 DAD and supplied with the software EZChrom Elite Version 3.2.1 (Agilent, 2005-2007)

In the experiments performed with the solar pilot plant in Chapter 3, the used reverse-phase (RP) column was a Superspher® RP-18 (4 µm) (Merck), operated at room temperature (25 °C). The mobile phase was also a 50:30:20 mixture of the buffered solution, acetonitrile and methanol, isocratically delivered at flow rate of 0.8 mL min^{-1}. Injection volume was 20 µL, and the wavelength of the UV absorbance detector was fixed at 354 nm.

Later on, a new reverse-phase column was acquired, a Purospher® RP-18e 125-4 (5 µm) (Merck). A method was developed for each antibiotic to maximize individual analysis, and the equipment was hereafter operated at gradient mode, at a flow rate of 0.8 mL min^{-1}, delivering an eluent consisted of a mixture of acetonitrile (mobile phase A), methanol (mobile phase B) and an aqueous solution of 0.01 M oxalic acid (mobile phase C, previously filtered through a 0.20 µm nylon filter and degassed). The injection volume was 20 µL and the wavelengths of the UV detector were set at 354 nm for OTC, 260 nm for OXA and 230 nm for AMX.

Table 2.2 presents the pump program for each antibiotic. Oxalic acid was used to reduce undesirable interactions between antibiotics and metal ion impurities (Delépée et al., 2000) and/or silanol group, as recommended in Oka et al. (2000).

Table 2.2. Pump program for HPLC gradient runs.

Time (min)	Mobile phase – A: B: C (%)								
	OTC			OXA			AMX		
0.0	10	10	10	20	10	70	10	5	80
3.0	15	10	15	25	10	65	15	5	75
5.0	20	10	20	30	10	60	20	5	70
7.0	10	10	10	20	10	70	10	5	80
14.0	10	10	10	20	10	70	10	5	80

The corresponding calibration curves of OTC, OXA and AMX were constructed with n = 5 concentration levels, ranging from 1.0 to 20 mg L^{-1}, using chromatographic peak areas as a function of their concentration, and limits of detection and quantification were also calculated. Table 2.3 presents a summary of the analytical parameters of the calibration curves for each antibiotic. The Limit of Quantification (LOQ) and Limit of Detection (LOD) values were obtained with the following calculations (adapted from Miller and Miller (1984)):

LOQ: $y_{LOQ} = a \times x_{LOQ} + b_b$, where $y_{LOQ} = b + 10 \times s_b$;

LOD: $y_{LOD} = a \times x_{LOD} + b_b$, where $y_{LOD} = b + 3 \times s_b$,

where a is the slope and s_b is the residual standard deviation of the intercept (b).

Table 2.3. Analytical parameters of working calibration curves of OTC, OXA and AMX antibiotics.

Antibiotic	λ (nm)	Regression equation parameters					
		Slope ($a \pm s_a$)	Intercept ($b \pm s_b$)	R^{2a}	s_a/a^b	LOQ[c]	LOD[d]
OTC	354	$162923 \pm 4\times10^2$	$-22762 \pm 5\times10^3$	0.999	0.265	0.33	0.10
OXA	260	$842813 \pm 2\times10^4$	$22548 \pm 2\times10^4$	0.999	0.281	0.29	0.09
AMX	230	$112963 \pm 4\times10^2$	$1681 \pm 4\times10^3$	0.999	0.311	0.38	0.11

[a]Correlation coefficient, [b]Relative standard deviation of a, [c, d]Limits of Quantification/Detection (mg L^{-1})

2.3.2 Dissolved Organic Carbon (DOC)

To assess the degree of mineralization of antibiotics in the photolytic/photocatalytic experiments, the dissolved organic carbon (DOC) was determined by means of a TC-TOC-TN analyzer, equipped with an ASI-V autosampler (Shimadzu, model TOC-VCSN) and provided with a NDIR detector. Calibrations were performed with standard solutions of potassium hydrogen phthalate (total carbon) and a mixture of sodium hydrogen carbonate/carbonate (inorganic carbon). Total nitrogen was measured in the same TC-TOC-TN analyzer coupled with a TNM-1 unit (Shimadzu, model TOC-VCSN) calibrated with standard solutions of potassium nitrate, through thermal decomposition and NO detection by chemiluminescence method.

2.3.3 Inorganic ions and low-molecular-weight carboxylate anions

Ion chromatography was used to monitor the release or formation of inorganic compounds and low-molecular-weight carboxylate anions (LMWCA) along the photocatalytic experiments, as well as to characterize the tested effluents used in chapter in Chapters 6 and 7.

Anions (chloride, nitrate, nitrite, phosphate, sulphate) and LMWCA (acetate, propionate, formate, pyruvate, valerate, malonate, maleate, oxalate, phthalate and citrate) were monitored with a Dionex ICS-2100 system, equipped with an AS 11-HC 4 × 250 mm column and a ASRS®300 4 mm suppressor. Cations (ammonium) were monitored with a Dionex DX-120 system, equipped with a CS12A 4 × 250 mm column and a CSRS®300 4 mm suppressor. Isocratic elution was performed using 30 mM NaOH/20 mM methane sulfonic acid, at a flow rate of 1.5 and 1.0 mL min^{-1}, for anion and cation analysis, respectively. The gradient program used for the quantification of LMWCA comprised a pre-run for 8 min with 1 mM NaOH, 20 min with 30 mM NaOH and 10 min with 60 mM NaOH, at a flow rate of 1.5 mL min^{-1}, using an eluent generator cartridge (Dionex, RFICTM). The chromatography software was Chromeleon client, version 6.80 DU10a (Dionex corporation, 1994-2010). In chapters 6 and 7, the same HPLC-DAD apparatus, using a Rezex™ ROA-Organic Acid H^+ (8 %), LC Column 300 × 7.8 mm), was also used to monitor oxalate, oxamate, tartronate, acetate, malonate, maleate and formate. The isocratic method used 0.005 N H_2SO_4 delivered at a flow rate of 0.5 mL min^{-1}. Run time was 50 min, injection volume 10 µL and the wavelength of the detector was set at 210 nm.

2.3.4 Hydrogen peroxide and dissolved iron concentration

Evaluation of H_2O_2 concentration during experiments was performed by the metavanadate method, based on the reaction of H_2O_2 with ammonium metavanadate in acidic medium, which results in the formation of a red-orange color peroxovanadium cation, with maximum absorbance at 450 nm (Nogueira et al., 2005). Dissolved iron concentration was determined by colorimetry with 1,10-phenantroline according to ISO 6332.

2.3.5 UV spectra and photometric measurements

The spectrophotometric measurements to obtain the antibiotics' UV absorption spectra were carried out with a UNICAM HEλIOS α spectrophotometer. The absorbance measurements to determine the concentration of dissolved iron and of H_2O_2 were carried out with a Spectroquant® Pharo 100 (Merck) spectrophotometer.

2.3.6 Ecotoxicity and Antimicrobial activity

In Chapter 3, ecotoxicity of the samples was measured as acute toxicity using the Microtox® test, where the inhibition percentage of the bioluminiscence of *Vibrio fischeri* after 15 min of contact time was determined. For intermediates identification, samples were analyzed using an electrospray/mass spectrometer (ion spray) ESI-MS, and a LC-MSD-TOF (2006) mass spectrometer.

The antimicrobial activity (AA) was assessed by the biomass yield of strains *Escherichia coli* DSM 1103 (Chapters 4, 5) and *Staphylococcus aureus* DSM 1104 (Chapter 5) grown for 24 h in filter sterilized phototreated samples. The samples were supplemented with 2 g L^{-1} yeast extract, and AA was measured by changes in optical density (λ = 610 nm) and normalized by that of a positive control grown in mineral medium B (Barreiros et al., 2003) supplemented with the same concentration of yeast extract. All the assays were performed in triplicate.In Chapter 6, the AA assays were carried out in 96-well microtiter plates using a Synergy HT Multi-Mode Microplate Reader (Biotek Instruments, USA) and *E. coli* DSM 1103 as test strain. Samples collected over time were supplemented with 2 g L^{-1} of yeast extract and inoculated with the test strain at an initial optical density at 610 nm of 0.08. Cultures were grown at 30 °C and 300 rpm for 20 h. Controls with different OTC concentrations (0 to 20 mg L^{-1}) were grown in parallel under the same conditions. Normalized biomass yield was obtained by dividing the biomass yield of the culture grown in the sample by the biomass yield obtained in the absence of OTC.

2.3.7 BOD_5 and COD analysis

In Chapter 3, biochemical oxygen demand at 5 days (BOD_5) determinations were carried out according to the Standard Methods (5120D) by means of the OxiTop® system, while for chemical oxygen demand (COD), the Standard Methods (5220D) procedures were followed (APHA, 1985).

2.4 Kinetic modelling

A pseudo-first-order mathematical model was fitted to the experimental data obtained from the kinetic studies by a non-linear regression method (software Fig.P for Windows from Fig.P Software Incorporated). The model parameters were obtained by minimizing the sum of the squared deviations between experimental and predicted values. Model goodness was evaluated through the calculation of relative standard deviations (σ_i), regression coefficients (R^2) and residual variance (S_R^2).

2.5 Matrix characterization

Table 2.4 presents the main characteristics of the four matrices in which AMX biodegradation trials were performed in chapter 8, as well as of the two effluents into which OTC was spiked in Chapter 6.

Table 2.4. Main characteristics of the used matrices (Chapter 7) and tested effluents (Chapter 6, 7).

Matrix	**pH**	**DOC / IC (mg L^{-1})**	**Average anion concentrations (g L^{-1})**		
			[PO_4^{3-}]	**[Cl^-]**	**[SO_4^{2-}]**
EM	7.2	421 / 4.24	2.56	0.34	0.38
Buffer	7.2	Residual	4.75		
NaCl	6.5	Residual		5.15	
WW	6.8	5.6 / 4.9	0.01	0.06	0.04
Effluent	**pH**	**DOC / IC (mg L^{-1})**	**Average anion concentrations (mg L^{-1})**		
			[PO_4^{3-}]	**[Cl^-]**	**[SO_4^{2-}]**
WW	6.5	5.5 / 5.1	13.5	61.5	42.9
TF	6.7	3.9 / 1.8	0.95		

2.6 References

Andreozzi, R., Canterino, M., Marotta, R., Paxeus, N., 2005. Antibiotic removal from wastewaters: The ozonation of amoxicillin. J. Hazard. Mater. 122, 243-250.

APHA, 1985. Standard Methods for the Examination of Water and Wastewater (sixteenth ed.). American Public Health Association/American Water Works Association/Water Pollution Control Federation, Washington DC, USA (1985).

Barreiros, L., Nogales, B., Manaia, C.M., Silva Ferreira, A.C., Pieper, D.H., Reis, M.A., Nunes, O.C., 2003. A novel pathway for mineralization of the thiocarbamate herbicide molinate by a defined bacterial mixed culture. Environ. Microbiol. 5, 944-953.

Delépée, R., Maume, D., Le Bizec, B., Pouliquen, H., 2000. Preliminary assays to elucidate the structure of oxytetracycline's degradation products in sediments: Determination of natural tetracyclines by high-performance liquid chromatography–fast atom bombardment mass spectrometry. J. Chrom. B Biomed. Sci. Appl. 748, 369-381.

Hirakawa, K., Mori, M., Yoshida, M., Oikawa, S., Kawanishi, S., 2004. Photo-irradiated titanium dioxide catalyzes site specific DNA damage via generation of hydrogen peroxide. Free Radical Res. 38, 439-447.

Jiménez-Lozano, E., Marqués, I., Barrón, D., Beltrán, J.L., Barbosa, J., 2002. Determination of p*K*a values of quinolones from mobility and spectroscopic data obtained by capillary electrophoresis and a diode array detector. Anal. Chim. Acta 464, 37-45.

Klamerth, N., Rizzo, L., Malato, S., Maldonado, M.I., Agüera, A., Fernández-Alba, A.R., 2010. Degradation of fifteen emerging contaminants at μg L^{-1} initial concentrations by mild solar photo-Fenton in MWTP effluents. Water Res. 44, 545-554.

Kuhn, H.J., Braslavsky, S.E., Schmidt, R., 2004. Chemical actinometry (IUPAC technical report). Pure Appl. Chem. 76, 2105-2146.

Lindsey, M.E., Tarr, M.A., 2000. Inhibition of hydroxyl radical reaction with aromatics by dissolved natural organic matter. Environ. Sci. Technol. 34, 444-449.

Méndez-Arriaga, F., Esplugas, S., Giménez, J., 2008. Photocatalytic degradation of non-steroidal anti-inflammatory drugs with TiO_2 and simulated solar irradiation. Water Res. 42, 585-594.

Miller, J.C., Miller, J.N., 1984. Statistics for Analytical Chemistry. Wiley, New York.

Miralles-Cuevas, S., Arqués, A., Maldonado, M.I., Sánchez-Pérez, J.A., Malato Rodríguez, S., 2013. Combined nanofiltration and photo-Fenton treatment of water containing micropollutants. Chem. Eng. J. 224, 89-95.

Nogueira, R.F.P., Oliveira, M.C., Paterlini, W.C., 2005. Simple and fast spectrophotometric determination of H_2O_2 in photo-Fenton reactions using metavanadate. Talanta 66, 86-91.

Oka, H., Ito, Y., Matsumoto, H., 2000. Chromatographic analysis of tetracycline antibiotics in foods. J. Chromatogr. A 882, 109-133.

Pouliquen, H., Delépée, R., Larhantec-Verdier, M., Morvan, M.L., Le Bris, H., 2007. Comparative hydrolysis and photolysis of four antibacterial agents (oxytetracycline oxolinic

acid, flumequine and florfenicol) in deionised water, freshwater and seawater under abiotic conditions. Aquaculture 262, 23-28.

Qiang, Z., Adams, C., 2004. Potentiometric determination of acid dissociation constants (p*K*a) for human and veterinary antibiotics. Water Res. 38, 2874-2890.

Raja, P., Bozzi, A., Mansilla, H., Kiwi, J., 2005. Evidence for superoxide-radical anion, singlet oxygen and OH-radical intervention during the degradation of the lignin model compound (3-methoxy-4-hydroxyphenylmethylcarbinol). J. Photochem. Photobiol. A: Chem. 169, 271-278.

VSDB, The Veterinary Substance Database, in, developed by the Agriculture & Environment Research Unit (AERU), University of Hertfordshire 2011-2013, 2013.

3 Photocatalytic degradation of oxytetracycline using TiO_2 under natural and simulated solar radiation

The main objective of the present study was to assess the photocatalytic degradation mediated by suspended TiO_2 of the antibiotic Oxytetracycline (OTC), under simulated solar irradiation. The influence of the photocatalyst concentration and initial pH was tested, and optimal parameters to remove OTC and enhance its mineralization were found to be 0.5 g L^{-1} of TiO_2 with no initial pH adjustment ($pH_0 \sim 4.4$). Under optimal conditions, biodegradability was enhanced, while its toxicity was decreased. A scheme of possible degradation pathways of OTC is presented. The same experiment performed in pilot-plant equipped with Compound Parabolic Collectors (CPCs), using natural solar radiation, demonstrates that CPC reactors were more effective in the usage of accumulated UV energy to completely degrade and almost completely mineralize OTC.

This Chapter is based on the research article "Pereira, J.H.O.S., Vilar, V.J.P., Borges, M.T., González, O., Esplugas, S., Boaventura, R.A.R. *Photocatalytic degradation of oxytetracycline using TiO_2 under natural and simulated solar radiation*. Sol. Energy (2011) 85, 2732-2740".

3.1 Introduction

The contamination of the environment by human and veterinary pharmaceuticals as a result of metabolic excretion, improper disposal and/or industrial waste has been subject to special attention over recent years (Halling-Sørensen et al., 1998). The main concern lies on their continual release and subsequent widespread presence in the environment because even at trace concentrations (ng L^{-1} to µg L^{-1}), these drugs present a whole spectrum of possible and still mostly unknown physiological effects on non-target species (Daughton and Ternes, 1999). Among these substances, antibiotics are worrisome due to the risk of aquatic toxicity and the development of resistant bacterial strains (Kemper, 2008; Kümmerer, 2009).

Conventional wastewater treatment plants (WWTPs) are not designed to remove antibiotics present at trace levels (Okuda et al., 2008; Miège et al., 2009). Different approaches to this problem may rely on source control measures or on the improvement of WWTPs with new end-of-pipe technologies (Larsen et al., 2004), including advanced treatments such as membrane filtration, activated carbon adsorption and Advanced Oxidation Processes (AOPs). AOPs are recommended when wastewater constituents, such as pesticides or pharmaceuticals, have a high chemical stability and/or low degradability. Considering the ability of AOPs to achieve the complete mineralization of pollutants to CO_2, water and inorganic compounds, or at least their partial oxidation to more biodegradable and/or less harmful intermediates, they allow a more useful and cost efficient combination with biological processes (Marco et al., 1997; Ikehata et al., 2006). AOPs comprise different processes that involve the generation of hydroxyl radicals ($^{\bullet}OH$), which are very reactive and non-selective, and can be divided in photochemical (UV/O_3, UV/H_2O_2), photocatalytic (TiO_2/UV, Photo-Fenton) or chemical oxidation processes (O_3, O_3/H_2O_2, H_2O_2/Fe^{2+}) (Gogate and Pandit, 2004a; b; Poyatos et al., 2009). These processes are rather costly and energy intensive (Rosenfeldt et al., 2006), therefore, research is being focused on the application of AOPs assisted by solar irradiation, such as heterogeneous photocatalysis and Photo-Fenton reaction (Bahnemann, 2004; Muñoz et al., 2005).

Oxytetracycline (OTC, Figure 3.1) is a widely used broad spectrum antibiotic, especially employed in veterinary medicine (Halling-Sørensen et al., 1998; Sarmah et al., 2006). Studies on OTC photolytic and ozonation degradation (Pouliquen et al., 2007; Jiao et al., 2008; Li et al., 2008; Zhao et al., 2009; Zhao et al., 2010) and on TiO_2-supported zeolites using UV sterilization lamps (Zhao and Deng, 2009; Zhao et al., 2009; Zhao et al., 2010) have been reported in the literature, but none, to the best of our knowledge, used both suspended TiO_2 and UV radiation in the solar range.

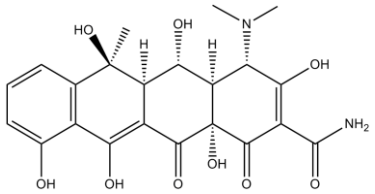

Figure 3.1. Molecular Structure of Oxytetracycline (OTC)

The main aim of the present work was to assess the heterogeneous photocatalytic degradation over TiO_2 of aqueous suspensions of Oxytetracycline with natural and simulated solar radiation. Firstly, at lab-scale, the influence of the catalyst load and initial pH was studied to determine the best conditions for OTC degradation and Total Organic Carbon (TOC) removal. After that, the evolution of biodegradability and ecotoxicity, as well as the main intermediary byproducts formation were also investigated. Finally, another experiment was conducted under the determined best conditions in a pilot plant equipped with CPCs, in order to compare the removal and mineralization of OTC with the lab-scale experiments, in terms of accumulated UV energy entering the reactor.

3.2 Materials and Methods

All the chemicals and reagents used in this work, the detailed description of the lab-scale and pilot-plant scale experimental units, along with the corresponding experimental procedures followed, and, finally, the employed analytical methods can be consulted in Chapter 2.

3.3 Results and discussion

3.3.1 Simulated solar radiation experiments

3.3.1.1 OTC photolysis

A photolytic degradation experiment was initially carried out to monitor the removal and mineralization of OTC without the addition of TiO_2, and to compare with a single photocatalytic experiment using 0.2 g L^{-1} of TiO_2. As can be seen in Figure 3.2 after 60 min of irradiation, only 36% of the initial antibiotic concentration was removed, in contrast to the nearly 95% obtained with suspended TiO_2. The negligible degree of photolytic mineralization observed after 180 min suggests that OTC molecules are merely degraded into more stable intermediary byproducts, as reported by Jiao and co-workers (Jiao et al., 2008), whereas with 0.2 g L^{-1} of TiO_2 almost 80% of TOC removal was achieved for the same reaction time. The variation of pH values in both reactions, also plotted in Figure 3.2, was found to be only of a slight increase. Taking that into consideration, in the following sections it was purposely not plotted, for it was also found to be nearly negligible in the realization of the experiments.

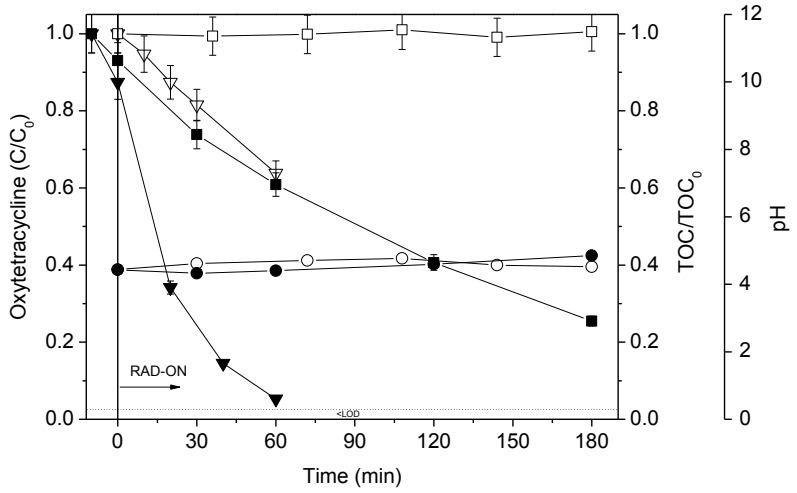

Figure 3.2. OTC (▽, ▼), TOC (□, ■) and pH (○, ●) monitoring under simulated solar photolysis (open symbols) and photocatalysis with 0.2 g L^{-1} TiO_2 (solid symbols).

3.3.1.2 *Influence of catalyst load*

Two more photocatalytic experiments using 0.1 and 0.5 g L^{-1} of TiO_2 were performed in order to optimize the TiO_2 concentration. No amounts higher than 0.5 g L^{-1} were tested as suggested by Malato and co-workers (2009) and Rodríguez and co-workers (2004) to ensure sufficient absorption of efficient photons and to avoid sedimentation and deposition of TiO_2 particles along the experimental circuit. Figure 3.3 clearly shows that a [TiO_2] = 0.5 g L^{-1} leads to the best antibiotic removal (>95% after only 35 min of irradiation) and mineralization (>90%

after 180 min of irradiation), whereas the other two concentrations tested show a very similar behaviour regarding mineralization and also an expected slower OTC removal rate for $[TiO_2] = 0.1$ g L^{-1}.

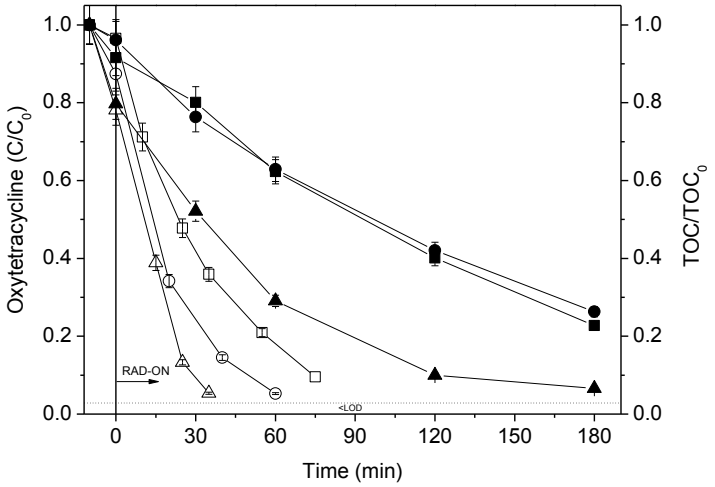

Figure 3.3. Removal profiles of OTC (open symbols) and TOC (solid symbols) under different catalyst loads (□, ■ - 0.1 g L^{-1} TiO_2; ○, ● - 0.2 g L^{-1} TiO_2; △, ▲ - 0.5 g L^{-1} TiO_2).

The increase in antibiotic adsorption over the catalyst surface when increasing the amounts of catalyst, as can be seen in the figure by the difference between C_0 and C before irradiation, may explain the more efficient photocatalytic degradation of both antibiotic and intermediary byproducts. From this point on, a TiO_2 concentration of 0.5 g L^{-1} was used in the rest of the photocatalytic experiments.

3.3.1.3 *Influence of initial pH*

OTC presents p*K*a values of 3.22, 7.46 and 8.94 and its photolytic and hydrolytic stability in deionized water is highly influenced by the initial pH level of the solution (Doi and Stoskopf, 2000; Loftin et al., 2008), becoming lower as pH values increase. Since TiO_2 has an amphoteric character, pH also influences its surface properties. It presents a zero charge point between pH 5.6 and 6.4 (Abellán et al., 2007), resulting in repulsive or attractive effects when catalyst and antibiotic show equal or different charges, respectively. Thus, pH is expected to play an important role in OTC photocatalytic experiments. As such, Figure 3.4 shows that as the initial pH value goes from acidic to basic, the irradiation time needed to achieve complete OTC removal decreases considerably, from nearly 45 min to little more than 10 min. On the contrary, it can be seen that basic pH levels are detrimental to OTC mineralization, showing contrasting results as pH values go up, especially for an initial pH of 11.

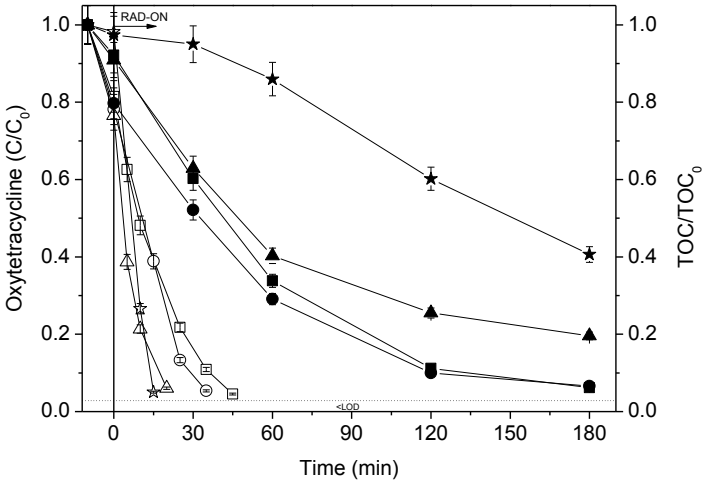

Figure 3.4. Removal profiles of OTC (open symbols) and TOC (closed symbols) with $[TiO_2]$ = 0.5 g L^{-1} and different initial pH values (□, ■ - pH = 3; ○, ● - free pH; △, ▲ - pH = 9; ☆, ★ - pH = 11).

Since both OTC and TiO_2 present negative charges from a pH higher than 9, adsorption of OTC on TiO_2 surface decreases due to the repulsive effect. However, negatively charged OTC molecules tend to facilitate OTC photolysis and, consequently, the formation of intermediary byproducts more recalcitrant to mineralization (Jiao et al., 2008), suggesting that photocatalysis plays a smaller role at such higher pH levels. As the experiment with no initial pH modification showed to be the best combination for both OTC removal and mineralization, the biodegradability and toxicity assessments and the solar experiment were carried out with $[TiO_2]$ = 0.5 g L^{-1} and free initial pH.

3.3.1.4 *Biodegradability and ecotoxicity assessment*

The biodegradability and toxicity of antibiotics are important parameters when considering coupling photocatalysis with a subsequent biological treatment as a strategy to reduce overall operation costs (Malato et al., 2003). Antibiotics are generally non-readily biodegradable (Kümmerer et al., 2000; Alexy et al., 2004) and available acute and even chronic toxicity tests vary widely in the evaluation of toxicity to environmentally relevant bacteria (Backhaus and Grimme, 1999; van der Grinten et al., 2010).

The biodegradability of the initial solution containing 20 mg L^{-1} of OTC, measured as BOD_5/COD, results to be very low (~0.05), as seen in Figure 3.5. During the photo-treatment period, the BOD_5/COD ratio steadily increases up to nearly 0.5 after 90 min of irradiation, suggesting that the photocatalytic degradation of OTC leads to the formation of more biodegradable intermediary byproducts.

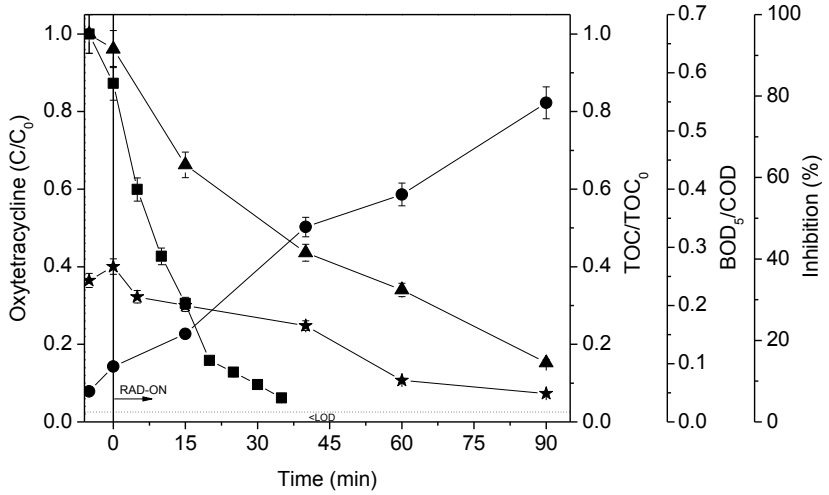

Figure 3.5. Evolution profiles of Biodegradability (●) and Inhibition percentage (★) under 0.5 g L^{-1} TiO_2 and free initial pH against OTC (■) and TOC (▲) removal profiles.

Acute toxicity evolution along the same photocatalytic experiment, calculated by the light emission inhibition percentage of the marine photobacteria *Vibrio fischeri* after 15 min of exposition (measured by Microtox®), is also shown in Figure 3.5. From an initial value of nearly 35%, the percentage of inhibition of the solution smoothly decreased during irradiation time, to finally reach a value of 7%. This result seems to be in accordance with the biodegradability enhancement achieved through this treatment, and possibly implies a lesser risk of more toxic intermediates formation during the OTC mineralization process, which could hinder a further biological treatment, if necessary (González et al., 2007).

Samples were also withdrawn to study the degradation byproducts formation via LC-MS in ESI (-) mode. Seven main intermediates were identified, and their molecular formulas and respective double bond equivalents, which represent the number of rings and double bonds of a molecule, are shown in Table 3.1. A LC-MS spectrum at 30 min of irradiation time is also presented in Figure 3.6.

Table 3.1. Elemental compositions and exact mass measurements of OTC and its degradation by-products ([TiO_2] = 0.5 g L^{-1}, free pH, Solarbox experiment), using HPLC-MS-ESI(-).

Molecule	Formula	m/z	Error (ppm)	DBE[a]
OTC	$C_{22}H_{24}N_2O_9$	460	-1.32	12
P1	$C_{22}H_{24}N_2O_{10}$	476	n / a	12
P2	$C_{22}H_{20}N_2O_9$	456	-1.55	14
P3	$C_{22}H_{20}N_2O_8$	440	-2.03	14
P4	$C_{21}H_{22}N_2O_7$	414	-1.27	12
P5	$C_{19}H_{15}NO_8$	385	-5.70	13
P6	$C_{19}H_{14}NO_7$	367	-0.34	14
P7	$C_{17}H_{11}O_8$	343	1.92	12

a – Double Bond Equivalent

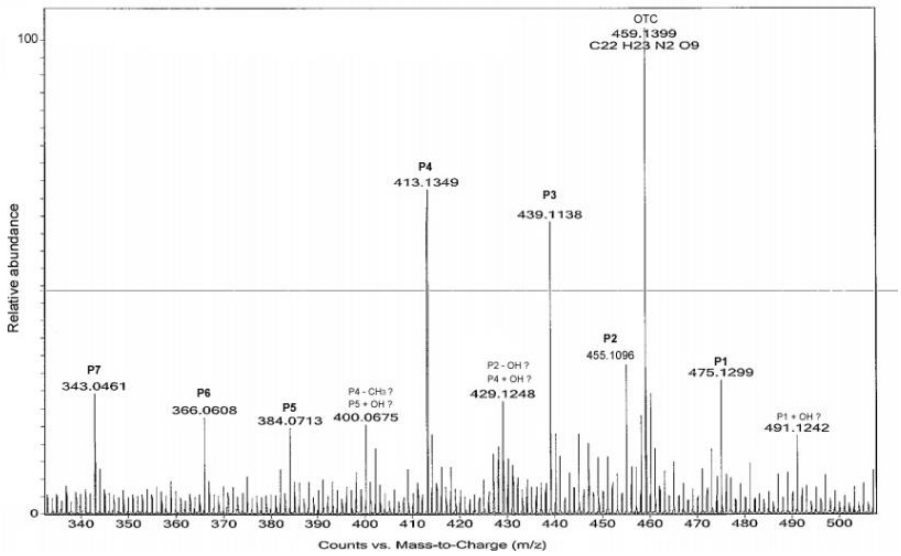

Figure 3.6. LC-MS-ESI (-) mass spectra of OTC and its degradation by-products at 30 minutes of irradiation ([TiO_2] = 0.5 g L-1, free pH, Solarbox experiment)

Figure 3.7 depicts the proposed photocatalytic degradation pathway. Intermediate P1 is consistent with the addition of ˙OH (16 mass units) to the aromatic ring 1 of OTC (molecular weight 460). Hydrogen abstraction at C5a and the oxidation of –OH at C5 (Jeong et al., 2010) possibly accounts for the formation of P3 (MW 440), which differs from P2 (MW 456) by the absence of the hydroxylation of ring 1. P4 (MW 414) stems from OTC via loss of N-methyl, water at C6 and hydroxyl group at C3. P5 (MW 385) shows the loss of N-methyl and amide groups as well as the addition of ˙OH to ring 1. A quinone is formed at ring 1 and the loss of -OH at C3 (P6. MW 367) leads to the final opening of the ring 4 to form P7 (MW 344) (Halling-Sørensen, 2001).

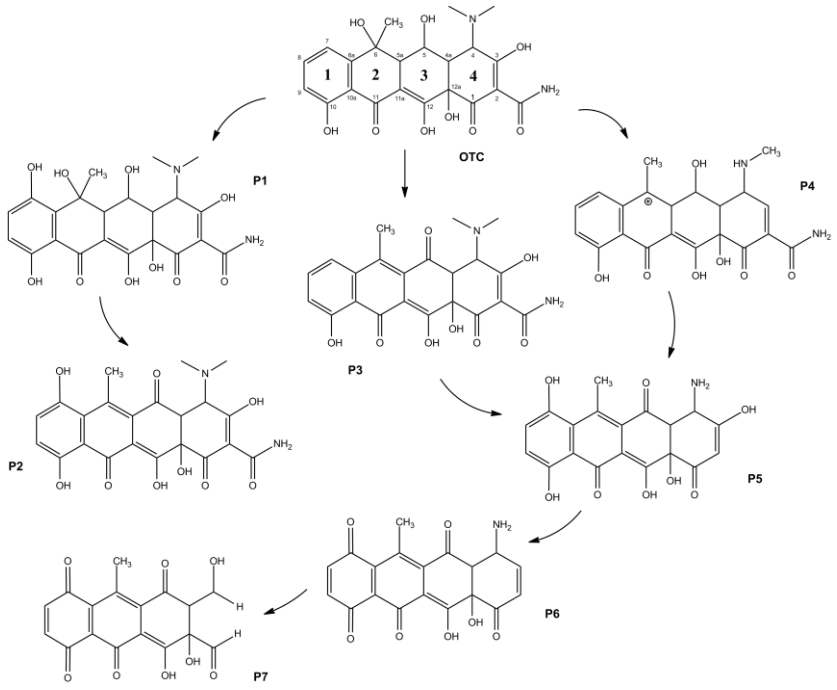

Figure 3.7. Proposed scheme of OTC degradation pathways ([TiO_2] = 0.5 g L^{-1}, free pH, Solarbox experiment)

3.3.2 Solar CPC pilot plant experiments

Using the same initial conditions ([OTC] = 20 mg L^{-1}, [TiO_2] = 0.5 g L^{-1} and free pH), a photolytic and photocatalytic set of experiments were carried out in the CPC pilot plant, during summer days. Both antibiotic degradation and mineralization are plotted in terms of accumulated UV energy ($Q_{UV,n}$ kJ L^{-1}) in Figure 3.8. Solar photocatalysis needed almost 10 times less energy (1.6 kJ L^{-1}) than solar photolysis (12 kJ L^{-1}) to completely remove OTC from solution. After 9 kJ L^{-1} of accumulated energy, 80% of mineralization was reached for solar photocatalysis and, as expected, almost negligible mineralization with solar photolysis. It must be taken into consideration that the CPC pilot plant has no means to maintain a constant temperature, and, in spite of the fact that it generally fails to play a significant role in the photocatalytic process (Malato et al., 2009), temperature of the aqueous solution during solar exposure may have influenced OTC removal/mineralization (Doi and Stoskopf, 2000). Although similar amounts of accumulated UV energy are expected for the same degrees of OTC degradation and mineralization when using natural and simulated solar radiation, our experiments show that this was not the case, as it can be seen in Figure 3.8, which also presents the Solarbox results under the same conditions, but expressed in terms of Q_{UV} (kJ L^{-1}).

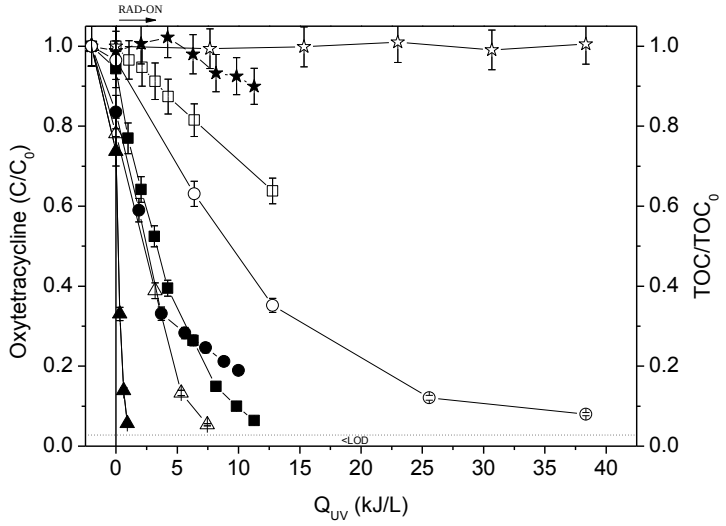

Figure 3.8. Removal profiles of OTC and TOC under simulated (□,☆) and real (■,★) solar photolysis and under simulated (△,○) and real (▲,●) solar photocatalysis with 0.5 g L^{-1} TiO_2 and free initial pH.

Hence, the kinetics of both photolytic and photocatalytic degradation of OTC for each experimental set-up were studied in order to compare their efficiency and are presented in Table 3.2. The fitting of the results showed that all reactions approximately followed pseudo-first order kinetics. The photolytic rate constants were calculated as 0.033 ± 0.001 L kJ^{-1} and 0.205 ± 0.005 L kJ^{-1}, for Solarbox and CPC experiments respectively, whereas photocalytic rate constants were 0.28 ± 0.03 L kJ^{-1} and 2.63 ± 0.03 L kJ^{-1}, for Solarbox and CPC experiments

respectively. The somewhat proportionally increase of rate constants from photolytic to photocatalytic experiments are relatively similar for both experimental set-ups, but the major difference lies on the increase of rate constants for each reaction from the Solarbox to the CPC experiments, corroborated with the initial rate of reactions, presented in Table 3.2

Table 3.2. Kinetic constant values for Solarbox and CPC photolysis and photocatalysis ([TiO_2] = 0.5 g L^{-1}, free pH) experiments.

Experiment	k (L kJ^{-1})[a]	r_0 (mg kJ^{-1})[b]	R^2	S_R^2 (mg^2 L^{-2})
Solarbox photolysis	0.033 ± 0.001	0.73 ± 0.02	0.995	0.069
CPC photolysis	0.205 ± 0.005	2.6 ± 0.2	0.999	0.083
Solarbox TiO_2	0.28 ± 0.03	4.3 ± 0.5	0.988	1.165
CPC TiO_2	2.63 ± 0.03	36.2 ± 0.4	0.999	0.009

a – pseudo-first order kinetic rate, b - initial reaction rate

The relationship between the amount of radiation that enters a reactor and the radiation absorbed by the catalyst is the most important difference between different scale/set-up experiments (Wiebe and Moore, 1977), and it depends on radiation source and its spectral distribution, catalyst and contaminant concentration, and, finally, reactor geometry. As most of these parameters are the same, or fairly equal between the two experimental setups used, despite both systems presenting different residence times and illuminated volume to total volume ratios, we may assume that the smaller diameter of the Solarbox reactor accounts significantly for this difference, as the light pathway length is much smaller, and so there are more photons failing to be absorbed by TiO_2 particles.

3.4 Conclusions

Simulated solar photocatalysis using suspended TiO_2 showed a good performance for the elimination of the antibiotic Oxytetracycline from aqueous solutions, not only enhancing its mineralization and biodegradability, but also decreasing its toxicity. OTC degradation conditions depend considerably on catalyst concentration and initial pH levels showed to be [TiO_2] = 0.5 g L^{-1} and free initial pH. OTC molecule degradation pathways were also proposed. The major difference between experiments using the best conditions in lab-scale using simulated solar radiation and in pilot plant scale using natural solar radiation regarded reactor geometry, demonstrating that CPC reactors were more effective in the usage of accumulated UV energy to completely degrade and almost completely mineralize OTC.

3.5 References

Abellán, M.N., Bayarri, B., Giménez, J., Costa, J., 2007. Photocatalytic degradation of sulfamethoxazole in aqueous suspension of TiO_2. Appl. Catal., B 74, 233-241.

Alexy, R., Kümpel, T., Kümmerer, K., 2004. Assessment of degradation of 18 antibiotics in the Closed Bottle Test. Chemosphere 57, 505-512.

Backhaus, T., Grimme, L.H., 1999. The toxicity of antibiotic agents to the luminescent bacterium *Vibrio fischeri*. Chemosphere 38, 3291-3301.

Bahnemann, D., 2004. Photocatalytic water treatment: Solar energy applications. Sol. Energy 77, 445-459.

Daughton, C.G., Ternes, T.A., 1999. Pharmaceuticals and personal care products in the environment: Agents of subtle change? Environ. Health Perspect. 107, 907-938.

Doi, A.M., Stoskopf, M.K., 2000. The kinetics of oxytetracycline degradation in deionized water under varying temperature, pH, light, substrate, and organic matter. J. Aquat. Anim. Health 12, 246-253.

Gogate, P.R., Pandit, A.B., 2004a. A review of imperative technologies for wastewater treatment I: Oxidation technologies at ambient conditions. Adv. Environ. Res. 8, 501-551.

Gogate, P.R., Pandit, A.B., 2004b. A review of imperative technologies for wastewater treatment II: Hybrid methods. Adv. Environ. Res. 8, 553-597.

González, O., Sans, C., Esplugas, S., 2007. Sulfamethoxazole abatement by photo-Fenton. Toxicity, inhibition and biodegradability assessment of intermediates. J. Hazard. Mater. 146, 459-464.

Halling-Sørensen, B., 2001. Inhibition of aerobic growth and nitrification of bacteria in sewage sludge by antibacterial agents. Arch. Environ. Contam. Toxicol. 40, 451-460.

Halling-Sørensen, B., Nors Nielsen, S., Lanzky, P.F., Ingerslev, F., Holten Lützhøft, H.C., Jørgensen, S.E., 1998. Occurrence, fate and effects of pharmaceutical substances in the environment - A review. Chemosphere 36, 357-393.

Ikehata, K., Jodeiri Naghashkar, N., Gamal El-Din, M., 2006. Degradation of aqueous pharmaceuticals by ozonation and advanced oxidation processes: A review. Ozone Sci. Eng. 28, 353-414.

Jeong, J., Song, W., Cooper, W.J., Jung, J., Greaves, J., 2010. Degradation of tetracycline antibiotics: Mechanisms and kinetic studies for advanced oxidation/reduction processes. Chemosphere 78, 533-540.

Jiao, S., Zheng, S., Yin, D., Wang, L., Chen, L., 2008. Aqueous oxytetracycline degradation and the toxicity change of degradation compounds in photoirradiation process. J. Environ. Sci. 20, 806-813.

Kemper, N., 2008. Veterinary antibiotics in the aquatic and terrestrial environment. Ecol. Indicators 8, 1-13.

Kümmerer, K., 2009. Antibiotics in the aquatic environment - A review - Part I. Chemosphere 75, 417-434.

Kümmerer, K., Al-Ahmad, A., Mersch-Sundermann, V., 2000. Biodegradability of some antibiotics, elimination of the genotoxicity and affection of wastewater bacteria in a simple test. Chemosphere 40, 701-710.

Larsen, T.A., Lienert, J., Joss, A., Siegrist, H., 2004. How to avoid pharmaceuticals in the aquatic environment. J. Biotechnol. 113, 295-304.

Li, K., Yediler, A., Yang, M., Schulte-Hostede, S., Wong, M.H., 2008. Ozonation of oxytetracycline and toxicological assessment of its oxidation by-products. Chemosphere 72, 473-478.

Loftin, K.A., Adams, C.D., Meyer, M.T., Surampalli, R., 2008. Effects of ionic strength, temperature, and pH on degradation of selected antibiotics. J. Environ. Qual. 37, 378-386.

Malato, S., Blanco, J., Vidal, A., Alarcón, D., Maldonado, M.I., Cáceres, J., Gernjak, W., 2003. Applied studies in solar photocatalytic detoxification: An overview. Solar Energy 75, 329-336.

Malato, S., Fernández-Ibáñez, P., Maldonado, M.I., Blanco, J., Gernjak, W., 2009. Decontamination and disinfection of water by solar photocatalysis: Recent overview and trends. Catal. Today 147, 1-59.

Marco, A., Esplugas, S., Saum, G., 1997. How and why combine chemical and biological processes for wastewater treatment. Water Sci. Technol. 35, 321-327.

Miège, C., Choubert, J.M., Ribeiro, L., Eusèbe, M., Coquery, M., 2009. Fate of pharmaceuticals and personal care products in wastewater treatment plants - Conception of a database and first results. Environ. Pollut. 157, 1721-1726.

Muñoz, I., Rieradevall, J., Torrades, F., Peral, J., Domènech, X., 2005. Environmental assessment of different solar driven advanced oxidation processes. Sol Energy 79, 369-375.

Okuda, T., Kobayashi, Y., Nagao, R., Yamashita, N., Tanaka, H., Tanaka, S., Fujii, S., Konishi, C., Houwa, I., 2008. Removal efficiency of 66 pharmaceuticals during wastewater treatment process in Japan Water Sci. Technol. 57, 65-71.

Pouliquen, H., Delépée, R., Larhantec-Verdier, M., Morvan, M.L., Le Bris, H., 2007. Comparative hydrolysis and photolysis of four antibacterial agents (oxytetracycline oxolinic acid, flumequine and florfenicol) in deionised water, freshwater and seawater under abiotic conditions. Aquaculture 262, 23-28.

Poyatos, J.M., Muñio, M.M., Almecija, M.C., Torres, J.C., Hontoria, E., Osorio, F., 2009. Advanced Oxidation Processes for Wastewater Treatment: State of the Art. Water, Air, Soil Pollut. 1-18.

Rodríguez, S.M., Gálvez, J.B., Rubio, M.I.M., Ibáñez, P.F., Padilla, D.A., Pereira, M.C., Mendes, J.F., De Oliveira, J.C., 2004. Engineering of solar photocatalytic collectors. Sol. Energy 77, 513-524.

Rosenfeldt, E.J., Linden, K.G., Canonica, S., von Gunten, U., 2006. Comparison of the efficiency of $^{\cdot}OH$ radical formation during ozonation and the advanced oxidation processes O_3/H_2O_2 and UV/H_2O_2. Water Res. 40, 3695-3704.

Sarmah, A.K., Meyer, M.T., Boxall, A.B.A., 2006. A global perspective on the use, sales, exposure pathways, occurrence, fate and effects of veterinary antibiotics (VAs) in the environment. Chemosphere 65, 725-759.

van der Grinten, E., Pikkemaat, M.G., van den Brandhof, E.J., Stroomberg, G.J., Kraak, M.H.S., 2010. Comparing the sensitivity of algal, cyanobacterial and bacterial bioassays to different groups of antibiotics. Chemosphere 80, 1-6.

Wiebe, J.A., Moore, D.E., 1977. Oxidation photosensitized by tetracyclines. J. Pharm. Sci. 66, 186-189.

Zhao, C., Deng, H., 2009. Removal of oxytetracycline in water by UV/Hydrophobic Zeolite loaded with TiO_2. J. Tongji Univ. 37, 1360-1365.

Zhao, C., Deng, H., Li, Y., Liu, Z., 2010. Photodegradation of oxytetracycline in aqueous by 5A and 13X loaded with TiO_2 under UV irradiation. J. Hazard. Mater. 176, 884-892.

Zhao, C., Deng, H.P., Shang, R., 2009. Removal of oxytetracycline in water by improved UV disinfection process. J Civ. Arch Env. Eng. 31, 152-156.

4 Insights into Solar TiO_2-Assisted Photocatalytic Oxidation of Two Antibiotics Employed in Aquatic Animal Production, Oxolinic acid and Oxytetracycline

In this study, solar driven, TiO_2-assisted heterogeneous photocatalytic experiments in a pilot-plant with compound parabolic collectors (CPCs) were carried out to study the degradation of two authorized veterinary antibiotics with particular relevance in finfish aquaculture, Oxolinic Acid (OXA) and Oxytetracycline (OTC), using pure solutions of individual or mixed antibiotics. Firstly, the influence of natural solar photolysis was assessed for each antibiotic. Secondly, photocatalytic degradation kinetic rate constants for individual and mixed antibiotics were compared, using a catalyst load of 0.5 g L^{-1} and an initial pH around 7.5. Thirdly, for individually photocatalytic-treated OXA and OTC in the same conditions, the growth inhibition of Escherichia coli DSM 1103 was followed, and the mineralization extent was assessed by the residual dissolved organic carbon (DOC), low-molecular-weight carboxylate anions and inorganic ions concentration. Finally, the effect of inorganic ions, such as chlorides, sulfates, nitrates, phosphates, ammonium and bicarbonates, on the photocatalytic degradation of individual solutions of OXA and OTC was also evaluated and the formation of different reactive oxygen species were probed using selective scavengers.

This Chapter is based on the research article "João H.O.S. Pereira, Ana C. Reis, Daniel Queirós, Maria T. Borges, Olga C. Nunes, Vítor J. P. Vilar, Rui A. R. Boaventura. *Insights into Solar TiO_2-Assisted Photocatalytic Oxidation of Two Antibiotics Employed in Aquatic Animal Production, Oxolinic acid and Oxytetracycline*. Sci Tot Environ (2013) 274-283".

4.1 Introduction

The resulting environmental contamination by the use of antibiotics in a wide range of human activities has been receiving special attention in recent years (Sarmah et al., 2006; Li et al., 2008; Verlicchi et al., 2010; Michael et al., 2013).

A particular case of major concern lies on the use of these substances as a means to control infectious diseases in animal production. Aquaculture, the controlled production of aquatic organisms, is an important food industry that represents a special situation as, in contrast to terrestrial farms, therapeutic agents are most often directly added to the water (Burka et al., 1997; Cabello, 2006; Noga, 2010). Freshwater or marine water finfish aquaculture practices encompass open or closed systems, and according to the suitability of each case, antibiotics may be administered by medicated feed pellets, bath treatments or individual injection (Rigos and Troisi, 2005). Individual injection of large amounts of fish is mostly impractical, while oral administration is considered the main route of fish medication (Samuelsen, 2006).

As most of these systems are interconnected with surrounding water bodies, continuous or intermittent wastewater discharges containing unconsumed food and animal faeces, may result in their contamination (Rico et al., 2012), contributing to the development of antibiotic (multi)resistant bacteria resistant strains of bacteria and potential drug accumulation and toxicity to aquatic fauna and flora (Sapkota et al., 2008; Buschmann et al., 2012; Henríquez-Núñez et al., 2012). In the particular case of bath treatments, recommended for recirculating aquaculture systems (due to biofilter bacteria drug sensitivity) or small sized facilities, fishes are moved to smaller containers (20 L, for instance (Samuelsen and Ervik, 2001)) and put directly in contact with antibiotic solution during the prescribed treatment time.

Antibiotic concentrations used may range from 10 to 200 mg L^{-1} (Samuelsen, 2006) and the resulting effluents are either commonly diluted until residues reach acceptable disposal levels or filtered through activated carbon treatment units (Aitcheson et al., 2000; 2001; Noga, 2010), which are not destructive methods. Therefore, alternative and proper means of disposal have to be proposed before safely discharging these effluents into surrounding aquatic systems.

The use of Advanced Oxidation Processes (AOPs) to degrade antibiotics has been showing promising results in recent years (Uslu and Balcioglu, 2008; González et al., 2009; Rozas et al., 2010). AOPs are characterized by the production of •OH radicals, which are very reactive and non-selective, leading to largely satisfactory results in the mineralization of pollutants to CO_2, water and inorganic compounds, or in their partial degradation to less harmful and/or more biodegradable compounds (Malato et al., 2009; Oller et al., 2011).

Heterogeneous photocatalysis using suspended TiO_2 is one AOP of special interest due to the chemical stability of the photocatalyst, low cost, and ability of using the small percentage of the ultraviolet radiation coming from the sun, which may also greatly reduce the operation costs. The use of Compound Parabolic Collectors (CPC) greatly enhances the efficiency of this process (Rodríguez et al., 2004; Colina-Márquez et al., 2010) as it increases the amount of incident photons that can be used to degrade target substances.

In this work, the degradation of Oxolinic Acid and Oxytetracycline (two of the most extensively used antibiotics in aquaculture (Rigos and Troisi, 2005; Alday-Sanz et al., 2012)), in aqueous solution, was studied, individually and in a mixture, using heterogeneous photocatalysis with suspended TiO_2 at pilot-plant scale under natural solar radiation. The antibiotics' UV normalized absorbance spectra, speciation diagrams as a function of pH and schemes of dissociation equilibrium are shown in Figure 4.1.

Despite the fact that some photocatalytic studies (optimization of process parameters such as catalyst load, pH, etc.) have already been made with these substances (Palominos et al., 2008; Giraldo et al., 2010; Zhao et al., 2010; Pereira et al., 2011), none so far has been carried out at this scale and in a situation of mutual presence, a relevant issue given the natural co-occurrence of different antibiotic residues whose relevance results from the natural occurrence and/or application of antibiotic mixtures (Avisar et al., 2010).

Moreover, for each individual antibiotic, the influence of natural solar photolysis was also assessed, the antibacterial activity followed, and the mineralization extent quantified (in terms of Dissolved Organic Carbon (DOC), low-molecular-weight carboxylate ions and inorganic ions present in the solutions). Furthermore, the influence of commonly occurring inorganic ions in fresh and marine fish farms waters, and of reactive oxygen species scavengers was also determined in a lab-scale CPC photoreactor using artificial sunlight.

The use of a figure-of-merit has been provided for the direct comparison of the solar energy efficiency of the photocatalytic process independent of the nature of the system (Bolton et al., 2001).

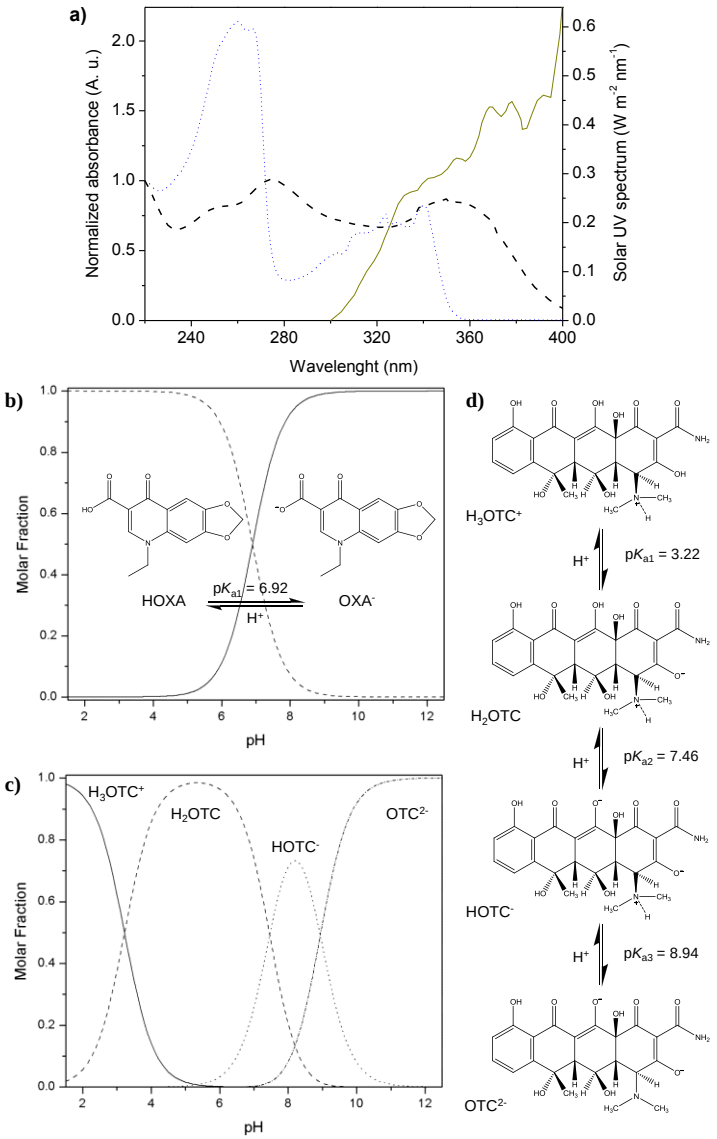

Figure 4.1. a) Normalized absorbance spectra of OXA (blue dotted line) and OTC (black dashed line) at pH = 7.5; solar UV spectrum (yellow solid line) adapted from Malato et al. (2002); **b)** OXA speciation diagram as a function of pH, including schematics of dissociation equilibrium (pK_a value from Jiménez-Lozano et al. (2002). Ionic strength = 0 M, T = 25°C); **c)** OTC speciation diagram as a function of pH and **d)** OTC dissociation equilibrium (pK_a values from Qiang and Adams (2004), Ionic strength = 0 M, T = 23°C).

4.2 Materials and Methods

All the chemicals and reagents used in this work, the detailed description of the lab-scale and pilot-plant scale experimental units, along with the corresponding experimental procedures followed, and, finally, the employed analytical methods can be consulted in Chapter 2.

4.3 Results and discussion

4.3.1 Solar photolytic and photocatalytic degradation of individual antibiotics

In order to assess the influence of the sun irradiance, a photolytic experiment was carried out for each antibiotic (C_0 = 20 mg L^{-1}), and compared with a single photocatalytic experiment using 0.5 g L^{-1} of TiO_2 in aqueous suspension. Figure 4.2 shows that the solar photolysis plays a lesser role in the removal of OXA (a) when comparing to OTC (b).

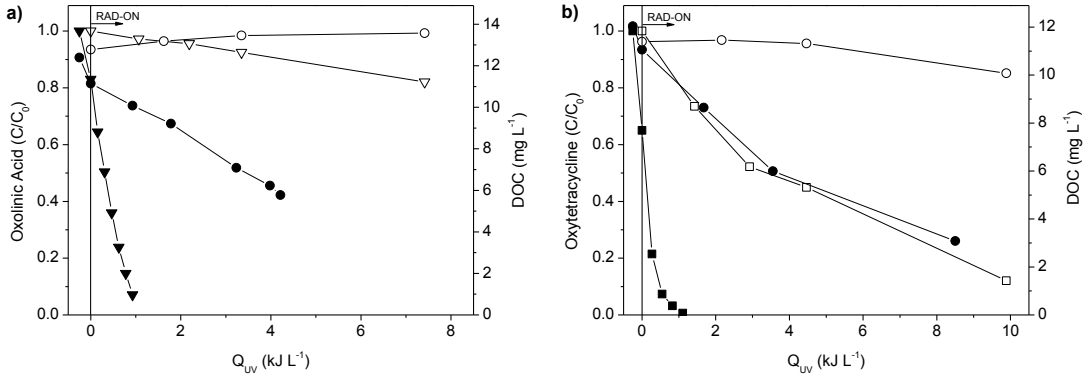

Figure 4.2. Solar photolysis (open symbols) and photocatalysis with 0.5 g L^{-1} of TiO_2 (solid symbols) of 20 mg L^{-1} OXA and OTC solutions at pH = 7.5: **a)** OXA concentration (▽,▼) and DOC (○, ●); **b)** OTC concentration (□, ■) and DOC (○,●).

It was necessary only nearly 10 kJ L^{-1} of accumulated UV energy to achieve 90% of OTC removal, whereas with 8.4 kJ_{UV} L^{-1} (Q_{UV}), only 18% of OTC removal was achieved. These results are in agreement with those reported in Pouliquen et al. (2007), where photolytic degradation of some antibiotics, including OXA and OTC, was studied with different water matrixes. Mineralization of both substances by photolysis was negligible, suggesting that the incident radiation on the reactor is only able to transform the parent compounds into more stable intermediary products, as proposed by other authors (Palominos et al., 2008; Pereira et al., 2011).

On the other hand, the photocatalytic experiments show that a very small and similar amount of Q_{UV}, around 1.0 kJ_{UV} L^{-1}, was enough to completely remove each antibiotic below the detection limit of the equipment (< 0.09 mg L^{-1}). Beyond that point, DOC content of the OXA solution underwent 53% of mineralization after 4.2 kJ_{UV} L^{-1}, while the remaining DOC in OTC solution decreased by 50% with just a slightly lower amount of Q_{UV}, 3.6 kJ L^{-1}.

Even considering the limitation in comparing situations in which different radiation sources or systems are used (Bayarri et al., 2007), Giraldo and co-workers (2010) were able to completely degrade 20 mg L^{-1} of OXA over 30 min under similar pH conditions (pH = 7.5), but with a double amount of TiO_2 (1.0 g L^{-1}) and using black light irradiation in a lab-scale photocatalytic

system, achieving a constant mineralization degree of 50%. For OTC, the results obtained are consistent with the findings of a previous study by Pereira and co-workers (2011), where a difference in the initial pH level (pH = 5.5) resulted in a slightly slower antibiotic abatement (100% after 1.8 kJ_{UV} L^{-1}) despite similar mineralization levels. According to Figure 4.1c, at a pH value of 5.5, the main OTC species present in solution is the zwitterionic H_2OTC, while at a pH value of 7.5, OTC is nearly equally distributed between zwitterionic H_2OTC and anionic $HOTC^-$ forms. Several studies have shown that the anionic forms of certain antibiotics are more susceptible to photochemical degradation (Boreen et al., 2004; Jiao et al., 2008; Zhao et al., 2013), which is very appropriate given environmentally-relevant pH values.

4.3.2 Solar photocatalytic degradation of a mixed OXA and OTC solution

The behavior of the photocatalytic degradation of an OXA and OTC mixture solution (C_0 = 20 mg L^{-1} each) is depicted in Figure 4.3. After 2.5 kJ_{UV} L^{-1}, both antibiotics concentrations were below the detection limit of the equipment (< 0.09 mg L^{-1}). Moreover, around 60% of the initial DOC content was mineralized after only 6 kJ of accumulated UV energy per liter of solution.

A pseudo-first order kinetic model was able to fit the obtained results for the antibiotic mixture. The results, presented in Table 4.1, show a photocatalytic pseudo-first-order kinetic rate constant for individual OTC of 4.03 ± 0.07 L kJ^{-1}, which was more than the double for OTC in the mixture (1.8 ± 0.2 L kJ^{-1}). For OXA, the values were very similar, 1.9 ± 0.1 L kJ^{-1} and 1.3 ± 0.1 L kJ^{-1}, respectively.

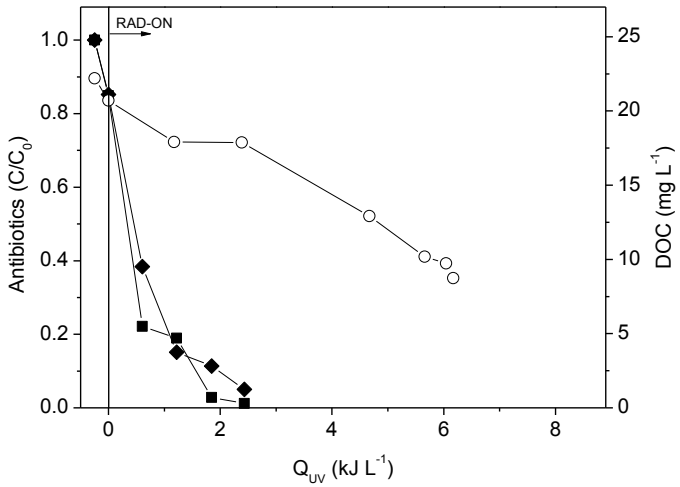

Figure 4.3. Removal profiles of OXA (◆) and OTC (■) concentrations and DOC (○) evolution in the combined antibiotic solar photocatalytic experiment with 0.5 g L^{-1} of TiO_2 and pH = 7.5 (C_0 = 20 mg L^{-1} each).

In spite of the fact that initial reaction rates for each antibiotic suffer a decrease when present in the mixture, possibly due to the competition for holes or hydroxyl radicals, the very nearly simultaneous disappearance of OXA and OTC demonstrates that the solar photocatalytic

process can be used as an effective method to remove and further mineralize these antibiotics simultaneously, as it may occur in situations where these antibiotics are used simultaneously due to their different modes of action against bacterial agents (Toral et al., 2011).

Table 4.1. Pseudo-first-order kinetic parameters for solar photocatalytic degradation experiments of OXA and OTC, [TiO_2] = 0.5 g L^{-1}; pH = 7.5.

Antibiotic	Experiment	*CPC pilot plant*			
		k (L kJ^{-1})[a]	r_0 (mg kJ^{-1})[b]	R^2	S_R^2 (mg^2 L^{-2})
OXA	C_0 = 20 mg L^{-1}	1.9 ± 0.1	33 ± 2	0.985	0.648
	C_0 = 40 mg L^{-1}	0.84 ± 0.06	18 ± 1	0.977	1.707
OTC	C_0 = 20 mg L^{-1}	4.03 ± 0.07	49.5 ± 0.8	0.999	0.009
	C_0 = 40 mg L^{-1}	2.21 ± 0.09	74 ± 3	0.996	0.594
MIX	OXA C_0 = 20 mg L^{-1}	1.3 ± 0.1	21 ± 1	0.995	0.181
	OTC C_0 = 20 mg L^{-1}	1.8 ± 0.3	29 ± 4	0.973	1.189

a – pseudo-first order kinetic rate, b - initial reaction rate

4.3.3 Detailed characterization of the antibiotics degradation

Experiments with individual antibiotics under the same initial conditions, but with a doubled antibiotic concentration (C_0 = 40 mg L^{-1}), were carried out for a more thorough understanding of the effectiveness of the solar photocatalytic degradation of OXA and OTC. The antibacterial activity of the treated solutions against *E. coli*, the formation of low-molecular-weight carboxylate anions (in terms of carbon content) and the release of inorganic ions (in terms of nitrogen content) were assessed during the phototreatment.

4.3.3.1 OXA experiment

In Figure 4.4, it can be clearly seen that the antibacterial activity against the tested organism was maintained as long as OXA remained in solution. Initially, *E. coli* was inhibited and growth was only slightly resumed when the antibiotic concentration was 1.69 mg L^{-1} (Q_{UV} = 4.6 kJ L^{-1}), which approaches the range of OXA its minimum inhibition concentration (MIC), as determined by Miller and co-workers (2005), 0.06–0.25 mg L^{-1}. After that, OXA was no longer detected ([OXA] < 0.09 mg L^{-1}) and the remaining degradation by-products no longer presented antibacterial activity. Up to this point, a negligible DOC removal was observed and 37% of the carbon content was attributed to low-molecular-weight carboxylate anions (mainly propionic acid).

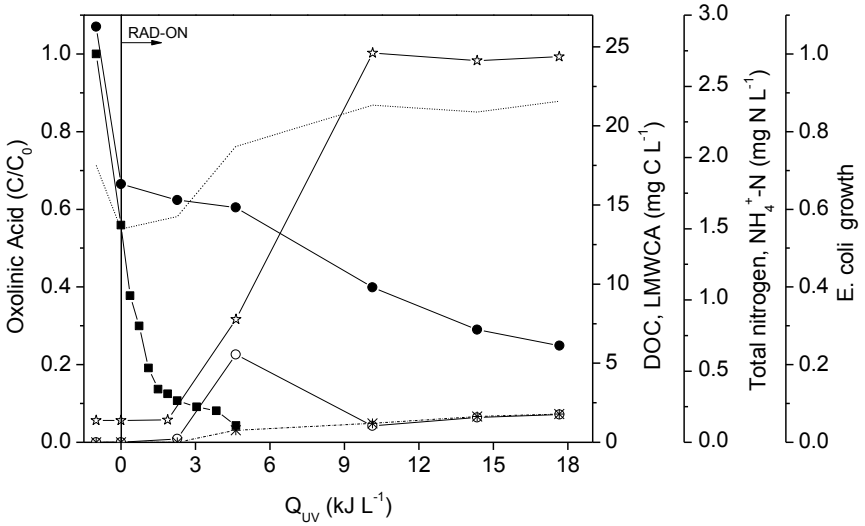

Figure 4.4. Evolution profiles of OXA concentration (■), DOC (●), sum of low-molecular-weight carboxylate anions as mg C L^{-1} (LMWCA - ○), total nitrogen (dotted line) and ammonium concentrations as mg N L^{-1} (∗) and Normalized *E. coli* growth (☆) under solar photocatalysis with 0.5 g L^{-1} of TiO_2, pH = 7.5 ($[OXA]_0$ = 40 mg L^{-1}).

After the disappearance of the antibiotic, a 73% mineralization was achieved after 17.7 kJ_{UV} L^{-1}, and 28% of the remaining carbon content consisted in formic, propionic, citric and acetic acids. Ion chromatography analysis showed that the nitrogen atom contained in each OXA molecule suffered a slow and steady release in the form of ammonium during the phototreatment time, achieving 10% of the stoichiometric quantity by the end of this process. The photocatalytic pseudo-first-order kinetic constant was found to decrease approximately by half, compared to the previous experiment with 20 mg L^{-1} OXA (Table 4.1).

4.3.3.2 OTC experiment

Regarding the 40 mg L^{-1} OTC experiment, it can be seen in Figure 4.5 that 2.0 kJ of accumulated UV energy per liter of solution were enough to lower the concentration of OTC by 98%, which falls near the lower OTC MIC range of 0.25-2 mg L^{-1} (Miller et al., 2005). Mineralization of the remaining degradation by-products, which thus no longer presented antibacterial activity as compared to the positive control test, proceeded henceforth and reached a degree of 81% by the end of the reaction. Simultaneously, the amount of detected carboxylic acids in solution began to increase steadily up to a peak of concentration around 8.5 kJ_{UV} L^{-1}, representing 72% of the remaining DOC, encompassing mainly maleic acid and smaller amounts of propionic, oxalic and acetic acids. Subsequently, their concentration decreased over the mineralization process, finally accounting for 46% of DOC present in the solution, mainly consisting of acetic acid (39% of DOC) and small amounts of maleic and oxalic acids.

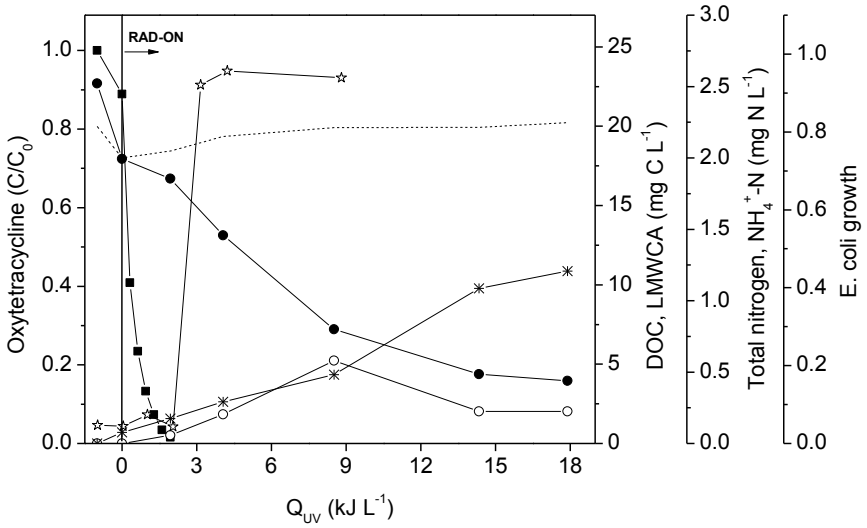

Figure 4.5. Evolution profiles of OTC concentration (■), DOC (●), sum of low-molecular-weight carboxylate anions as mg C L^{-1} (LMWCA - ○), total nitrogen concentration (dotted line), ammonium concentration as mg N L^{-1} (✳) and Normalized *E. coli* growth (☆) under solar photocatalysis with 0.5 g L^{-1} of TiO_2, pH = 7.5 ($[OTC]_0$ = 40 mg L^{-1}).

Contrasting to the case of OXA, the nitrogen contained in OTC molecule was converted to ammonium in a greater extent (55% of stoichiometric quantity). For both cases, no conversion to nitrite or nitrate was detected. As there was no decrease in the nitrogen content of the solution, as can be seen in the follow-up of total nitrogen in Figure 4.4 and Figure 4.5, either the nitrogen-containing species left remained adsorbed onto the catalyst surface, or an induction period in the expected release of ammonium occurred (Calza et al., 2005). It can also be speculated that the unmineralized nitrogen could also be present in oxamic acid molecules, a common oxidation by-product refractory to AOPs (Faria et al., 2008; Garcia-Segura and Brillas, 2011). The different results regarding mineralization of organic nitrogen under photocatalytic processes can be explained by distinct features such as the initial oxidation state of nitrogen or the structure of organic molecules (Calza et al., 2005). Similar mineral nitrogen yields were found for other TiO_2-assisted photocatalysis of antibiotics of the same class as those studied in this work. Sirtori and co-workers (2009), studying the solar photocatalytic treatment of Flumequine and Nalidixic acid (quinolones) in distilled water, reported a 5.2% conversion of N into nitrate and ammonium in the former, and the 9.4% of N conversion to nitrate and ammonia in the later, while Yahiat and co-workers (2011) reported a mineralization of 45% of the nitrogen contained in Tetracycline, released mainly as ammonium.

In the case of OTC, the photocatalytic pseudo-first-order kinetic constant was also found to decrease approximately by half, compared to the individual 20 mg L^{-1} OTC experiment (Table 4.1).

4.3.4 Effects of inorganic ions and scavengers on the photocatalytic efficiency

Inorganic ions have been found to affect photocatalytic oxidation of organic pollutants, depending on their nature, concentration, and on the pH of the solution. Effects may range from inhibition ($^{\bullet}OH$-scavenging effect, adsorption competition on the catalyst surface, for instance) to promotion (increasing the charge separation by accepting conduction band electrons) of photocatalytic kinetic rates (Abdullah, 1990; Guillard et al., 2005; Ahmed et al., 2011).

The results of the individual effect of 1 g L^{-1} of Cl^-, SO_4^{2-}, PO_4^{3-}, NO_3^-, NH_4^+ and 0.1 g L^{-1} HCO_3^- on the degradation of OXA and OTC at laboratory scale using 0.5 g L^{-1} TiO_2, over 30 and 60 min of simulated solar irradiation, respectively, are presented in Figure 4.6 (a) and (b):

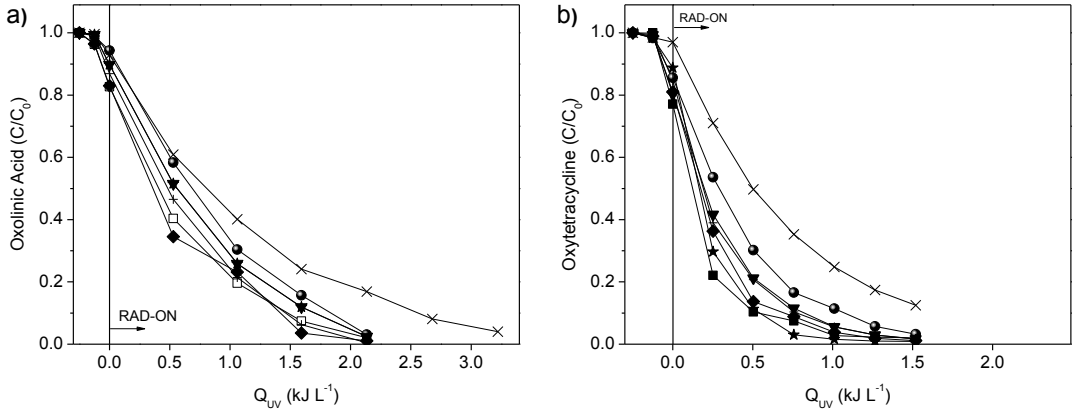

Figure 4.6. Removal profiles of **a)** OXA (□) and **b)** OTC (■), alone and in the presence of 1 g L^{-1} of Cl^- (+), SO_4^{2-} (●), NO_3^- ▼, NH_4^+ (♦), PO_4^{3-} (×), 0.1 g L^{-1} HCO_3^- (★) under simulated solar photocatalysis with 0.5 g L^{-1} TiO_2, pH = 7.5 ($[OXA]_0 = [OTC]_0 = 20$ mg L^{-1}).

The near 20% of each antibiotic dark adsorption on TiO_2, under the tested initial pH value of 7.5, may be accounted for as follows. According to Figure 4.1 (b) and (c), OXA is represented by approximately 60% of its deprotonated fraction (OXA^-) and 40% of its neutral fraction (OXA-H), whereas OTC is nearly evenly distributed in its zwitterion ($H_2OTC^{\pm}$) and neutral ($HOTC^-$) forms (Zhao et al., 2013). Thus, an electrostatic attraction between negatively charged TiO_2 particles (pH > pH_{PZC}, pH of Point of Zero Charge = 6.7 (Fernández-Ibáñez et al., 2003; Malato et al., 2009)) and the neutral fractions of both antibiotics may be favored. The negative effect of adsorption competition in the catalyst surface was found to be pronounced in the case of OTC, resulting in less favorable kinetic rates (Guillard et al., 2003) in the presence of each inorganic ion, as seen in Table 4.2.

On the other hand, overall OXA kinetic rates were slightly improved, even in the cases in which a decrease in adsorption occurred, which singles out the differences of inhibition or promotion effects according to the nature of the pollutants (Abdullah, 1990). Nevertheless, by the end of the respective photo-treatment period, the removal of OXA or OTC was only notably reduced in

the presence of PO_4^{3-}, which strongly adsorbs on the surface of TiO_2 (Chen et al., 2003) and whose negative charges results in a repulsion effect between TiO_2 and both antibiotics.

Table 4.2. Pseudo-first-order kinetic parameters simulated solar photocatalytic degradation experiments of OXA and OTC, alone or with (+) inorganic ions and scavengers; $[TiO_2] = 0.5$ g L^{-1}; pH = 7.5; ($[OXA]_0 = [OTC]_0 = 20$ mg L^{-1}).

Antibiotic	Experiment	*Lab-scale photoreactor (I = 44 W m^{-2})*			
		k (L kJ^{-1})[a]	r_0 (mg kJ^{-1})[b]	R^2	S_R^2 (mg^2 L^{-2})
OXA	individual	1.09 ± 0.07	18 ± 1	0.989	0.425
	+ 1.0 g L^{-1} Cl^-	1.33 ± 0.08	22 ± 1	0.995	0.285
	+ 1.0 g L^{-1} NO_3^-	1.29 ± 0.04	21.5 ± 0.7	0.998	0.068
	+ 1.0 g L^{-1} HCO_3^-	1.16 ± 0.03	20.7 ± 0.5	0.998	0.088
	+ 1.0 g L^{-1} SO_4^{2-}	1.04 ± 0.03	19.0 ± 0.5	0.998	0.121
	+ 1.0 g L^{-1} NH_4^+	1.5 ± 0.1	25 ± 2	0.985	0.696
	+ 1.0 g L^{-1} PO_4^{3-}	0.83 ± 0.02	14.9 ± 0.4	0.997	0.117
	+ 10 mM NaN_3	0.375 ± 0.008	6.7 ± 0.1	0.996	0.099
	+ 50 mM D-Mannitol	0.25 ± 0.03	4.2 ± 0.5	0.926	1.147
OTC	individual	4.3 ± 0.4	59 ± 6	0.993	0.293
	+ 1.0 g L^{-1} Cl^-	2.74 ± 0.08	44 ± 1	0.999	0.067
	+ 1.0 g L^{-1} NO_3^-	2.48 ± 0.02	36.1 ± 0.3	0.999	0.006
	+ 1.0 g L^{-1} HCO_3^-	4.11 ± 0.08	68 ± 1	0.999	0.022
	+ 1.0 g L^{-1} SO_4^{2-}	1.93 ± 0.03	32.0 ± 0.5	0.999	0.041
	+ 1.0 g L^{-1} NH_4^+	3.1 ± 0.1	47 ± 2	0.998	0.075
	+ 1.0 g L^{-1} PO_4^{3-}	1.25 ± 0.01	21.2 ± 0.1	0.999	0.006
	+ 10 mM NaN_3	0.97 ± 0.07	19 ± 1	0.969	1.551
	+ 50 mM D-Mannitol	0.59 ± 0.03	10.2 ±0.5	0.970	0.467

a – pseudo-first order kinetic rate, b - initial reaction rate

Selective scavengers D-Mannitol and sodium azide (NaN_3) were used to assess the role of reactive oxygen species, hydroxyl radical ($^{\bullet}OH$) and singlet oxygen ($^1O_2$), on the photocatalytic degradation of OXA and OTC under the same tested conditions. From the analysis of Figure 4.7 (a) and (b), it can be seen that, compared to the absence of reactive species scavengers, OXA and OTC degradation is mainly attributed to the $^{\bullet}OH$ attack, while $^1O_2$ plays a secondary, but non-negligible role in OXA and OTC self-sensitization under UV solar light. The remainder of the degradation may be explained by the participation of the abovementioned photolysis effect or by the participation of direct oxidation by photo-generated holes of molecules adsorbed on the catalyst surface (Giraldo et al., 2010; Zhao et al., 2013).

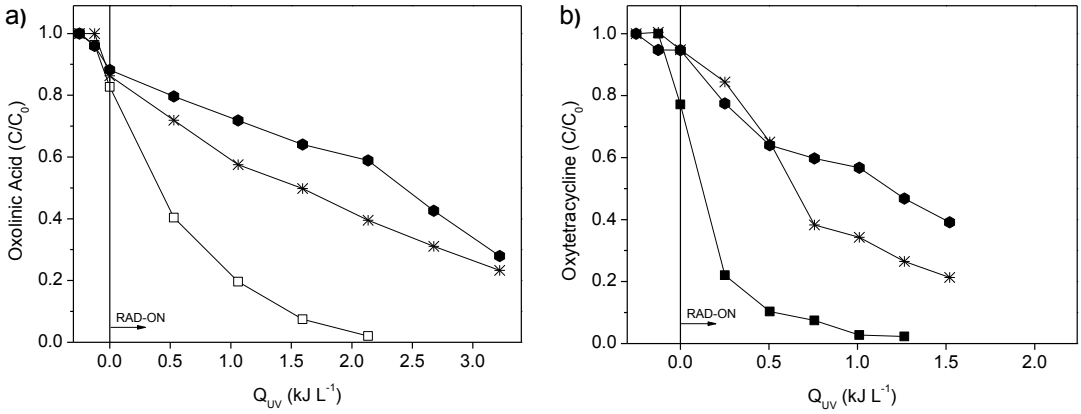

Figure 4.7. Removal profiles of **a)** OXA (□) and **b)** OTC (■), alone and in the presence of 10 mM NaN_3 (∗) and 50 mM D-mannitol (⬢) under simulated solar photocatalysis with 0.5 g L^{-1} TiO_2, pH = 7.5 ($[OXA]_0 = [OTC]_0 = 20$ mg L^{-1}).

4.3.5 Solar photocatalytic efficiency index

Valuable figures-of-merit have been recommended by the IUPAC to allow for a direct comparison between the electric- or solar- energy efficiency of different AOPs, independently of the nature of the used system. In the case of solar-based AOPs, where the cost of incident solar radiation is zero, the collector area is considered as the main capital cost. As the capital cost of the solar collectors are proportionally related to their area, it is suitable to use figures of merit based on the solar collector area. Therefore, for a low pollutant concentration range, the appropriate figure-of-merit is the collector area per order (A_{CO}) (Bolton et al., 2001).

A_{CO} is the collector area required to reduce the concentration of a contaminant (C) in polluted water in a unit of volume by one order of magnitude in a time (t_0 = 1 h) when the standardized incident solar irradiance (E_S^0) is 1000 W m^{-2}. The A_{CO} (m^2 m^{-3}-order), in batch operation, can be calculated from Eq. 3.01:

$$A_{CO} = \frac{A_r \times \overline{UV}_G \times t}{E_S^0 \times t_0 \times V_t \times \log\left(\frac{C}{C_0}\right)} \qquad (3.01)$$

where Ar is the illuminated collector surface area (m^2), $\overline{UV}_G$ is the average solar ultraviolet irradiance (W m^{-2}) over the period t of the treatment (h), V_t the total reactor volume (m^3), and C and C_0 are the final and initial antibiotic concentrations (mg L^{-1}, or mM in the case of the antibiotic mixture). This figure-of-merit is inversely proportional to fundamental efficiency factors, e.g., when A_{CO} values increase, there is a loss in the system efficiency. In the case of the two individual OXA photocatalytic experiments, at 20 and 40 mg L^{-1}, the A_{CO} index varied from 0.24 to 1.15 m^2 m^{-3}-order, respectively. Even though there was a near-5 fold decrease in

efficiency, it should be mentioned that $\overline{UV}_G$ values were nearly doubled between experiments (22.7 and 42.1 W m^{-2}, respectively) and so it was the necessary treatment time (0.5 and 1 h). In turn, the A_{CO} index for the two individual OTC photocatalytic experiments were 0.15 and 0.31 m^2 m^{-3}-order for the individual 20 and 40 mg L^{-1} experiments. The $\overline{UV}_G$ values were very similar (30.2 and 35.5 W m^{-2}, respectively), while the necessary time was doubled (0.33 and 0.5 h). In the combined antibiotic experiment, after adding up the OXA and OTC initial and final concentrations in terms of mM for the calculation of C_0 and C, the A_{CO} index was 0.49 m^2 m^{-3}-order ($\overline{UV}_G$ = 22.3 W m^{-2} and t = 1 h).

A similar A_{CO} index, 0.4 m^2 m^{-3}-order, was obtained by Sousa et al. (2013) in the TiO_2-assisted photocatalytic oxidation of the anxiolytic drug lorazepam with the same pilot-plant, but using only 0.2 g L^{-1} TiO_2. These results bring into consideration the viability of performing this treatment on these compounds (individually or mixed) on different times of the year without substantial conversion of efficiency losses.

4.4 Conclusions

Solar photocatalysis with TiO_2 was shown to be 100% efficient in the degradation of individual OXA and OTC solutions (C_0 = 20 mg L^{-1}) and mixtures, being necessary low amounts of accumulated UV energy per liter of solution (Q_{UV} ~ 1 kJ_{UV} L^{-1}), and also in the extensive mineralization of the remaining DOC content, as compared to solar photolysis alone. According to the pseudo-first-order kinetic rate constants, the individual removal of OTC fares better than that of OXA. Nevertheless, when both antibiotics are mixed, they disappear from solution quite simultaneously and reach a proper amount of mineralization shortly afterwards. Furthermore, within the operational conditions studied, the efficiency of the solar photocatalytic CPC reactor has shown to be consistent.

A detailed assessment of the antibacterial activity and formation of carboxylic acids and inorganic ions showed that after the point of complete antibiotic abatement, the remaining organics do not inhibit reference bacterial growth and consist largely of biodegradable substances.

Although the OXA and OTC degradation was mainly attributed to hydroxyl radicals, singlet oxygen also plays an important role in antibiotics self-photosensitization under UV/visible solar light. The presence of PO_4^{3-} considerably affects the photocatalytic efficiency and must be taken into consideration when applying TiO_2 photocatalysis in complex water matrixes (Raja et al., 2005), while other inorganic ions (Cl^-, SO_4^{2-}, NO_3^-, NH_4^+ and HCO_3^-) do not substantially hinder complete OXA and OTC removal.

This treatment could be proposed as a viable alternative to treat effluents resulting from high antibiotic-using activities such as bath treatments in fish farms. Effluents could be treated locally, requiring only short periods of solar exposure, and safely discharged after a proper catalyst recovery step.

4.5 References

Abdullah, M., 1990. Effects of common inorganic anions on rates of photocatalytic oxidation of organic carbon over illuminated titanium dioxide. J. Phys. Chem. 94, 6820-6825.

Ahmed, S., Rasul, M.G., Martens, W.N., Brown, R., Hashib, M.A., 2011. Advances in heterogeneous photocatalytic degradation of phenols and dyes in wastewater: A review. Water, Air, Soil Pollut. 215, 3-29.

Barreiros, L., Nogales, B., Manaia, C.M., Silva Ferreira, A.C., Pieper, D.H., Reis, M.A., Nunes, O.C., 2003. A novel pathway for mineralization of the thiocarbamate herbicide molinate by a defined bacterial mixed culture. Environ. Microbiol. 5, 944-953.

Bayarri, B., Abellán, M.N., Giménez, J., Esplugas, S., 2007. Study of the wavelength effect in the photolysis and heterogeneous photocatalysis. Catal. Today 129, 231-239.

Boaventura, R., Pedro, A.M., Coimbra, J., Lencastre, E., 1997. Trout farm effluents: Characterization and impact on the receiving streams. Environ. Pollut. 95, 379-387.

Bolton, J.R., Bircher, K.G., Tumas, W., Tolman, C.A., 2001. Figures-of-merit for the technical development and application of advanced oxidation technologies for both electric- and solar-driven systems. Pure Appl. Chem. 73, 627-637.

Boreen, A.L., Arnold, W.A., McNeill, K., 2004. Photochemical fate of sulfa drugs in then aquatic environment: Sulfa drugs containing five-membered heterocyclic groups. Environ. Sci. Technol. 38, 3933-3940.

Calza, P., Pelizzetti, E., Minero, C., 2005. The fate of organic nitrogen in photocatalysis: An overview. J. Appl. Electrochem. 35, 665-673.

Chen, F., Zhao, J., Hidaka, H., 2003. Adsorption factor and photocatalytic degradation of dye-constituent aromatics on the surface of TiO_2 in the presence of phosphate anions. Res. Chem. Intermed. 29, 733-748.

Colina-Márquez, J., MacHuca-Martínez, F., Puma, G.L., 2010. Radiation absorption and optimization of solar photocatalytic reactors for environmental applications. Environ. Sci. Technol. 44, 5112-5120.

Faria, P.C.C., Órfão, J.J.M., Pereira, M.F.R., 2008. Activated carbon catalytic ozonation of oxamic and oxalic acids. App. Cat. B: Environ. 79, 237-243.

Fernández-Ibáñez, P., Blanco, J., Malato, S., De Las Nieves, F.J., 2003. Application of the colloidal stability of TiO_2 particles for recovery and reuse in solar photocatalysis. Water Res. 37, 3180-3188.

Garcia-Segura, S., Brillas, E., 2011. Mineralization of the recalcitrant oxalic and oxamic acids by electrochemical advanced oxidation processes using a boron-doped diamond anode. Water Res. 45, 2975-2984.

Giraldo, A.L., Peñuela, G.A., Torres-Palma, R.A., Pino, N.J., Palominos, R.A., Mansilla, H.D., 2010. Degradation of the antibiotic oxolinic acid by photocatalysis with TiO_2 in suspension. Water Res. 44, 5158-5167.

Guillard, C., Lachheb, H., Houas, A., Ksibi, M., Elaloui, E., Herrmann, J.M., 2003. Influence of chemical structure of dyes, of pH and of inorganic salts on their photocatalytic degradation by

TiO_2 comparison of the efficiency of powder and supported TiO_2. J. Photochem. Photobiol. A: Chem. 158, 27-36.

Guillard, C., Puzenat, E., Lachheb, H., Houas, A., Herrmann, J.M., 2005. Why inorganic salts decrease the TiO_2 photocatalytic efficiency. Int. J. of Photoener 7, 1-9.

Han, S.K., Hwang, T.M., Yoon, Y., Kang, J.W., 2011. Evidence of singlet oxygen and hydroxyl radical formation in aqueous goethite suspension using spin-trapping electron paramagnetic resonance (EPR). Chemosphere 84, 1095-1101.

Hirakawa, K., Mori, M., Yoshida, M., Oikawa, S., Kawanishi, S., 2004. Photo-irradiated titanium dioxide catalyzes site specific DNA damage via generation of hydrogen peroxide. Free Radical Res. 38, 439-447.

Jiao, S., Zheng, S., Yin, D., Wang, L., Chen, L., 2008. Aqueous photolysis of tetracycline and toxicity of photolytic products to luminescent bacteria. Chemosphere 73, 377-382.

Jiménez-Lozano, E., Marqués, I., Barrón, D., Beltrán, J.L., Barbosa, J., 2002. Determination of p*K*a values of quinolones from mobility and spectroscopic data obtained by capillary electrophoresis and a diode array detector. Anal. Chim. Acta 464, 37-45.

Malato, S., Fernández-Ibáñez, P., Maldonado, M.I., Blanco, J., Gernjak, W., 2009. Decontamination and disinfection of water by solar photocatalysis: Recent overview and trends. Catal. Today 147, 1-59.

Miller, R.A., Walker, R.D., Carson, J., Coles, M., Coyne, R., Dalsgaard, I., Gieseker, C., Hsu, H.M., Mathers, J.J., Papapetropoulou, M., Petty, B., Teitzel, C., Reimschuessel, R., 2005. Standardization of a broth microdilution susceptibility testing method to determine minimum inhibitory concentrations of aquatic bacteria. Dis. Aquat. Org. 64, 211-222.

Miralles-Cuevas, S., Arqués, A., Maldonado, M.I., Sánchez-Pérez, J.A., Malato Rodríguez, S., 2013. Combined nanofiltration and photo-Fenton treatment of water containing micropollutants. Chem. Eng. J. 224, 89-95.

Oller, I., Malato, S., Sánchez-Pérez, J.A., 2011. Combination of Advanced Oxidation Processes and biological treatments for wastewater decontamination - A review. Sci. Tot. Environ. 409: 4141-4166.

Palominos, R.A., Mora, A., Mondaca, M.A., Pérez-Moya, M., Mansilla, H.D., 2008. Oxolinic acid photo-oxidation using immobilized TiO_2. J. Hazard. Mater. 158, 460-464.

Pereira, J.H.O.S., Vilar, V.J.P., Borges, M.T., González, O., Esplugas, S., Boaventura, R.A.R., 2011. Photocatalytic degradation of oxytetracycline using TiO_2 under natural and simulated solar radiation. Sol. Energy 85, 2732-2740.

Pouliquen, H., Delépée, R., Larhantec-Verdier, M., Morvan, M.L., Le Bris, H., 2007. Comparative hydrolysis and photolysis of four antibacterial agents (oxytetracycline oxolinic acid, flumequine and florfenicol) in deionised water, freshwater and seawater under abiotic conditions. Aquaculture 262, 23-28.

Qiang, Z., Adams, C., 2004. Potentiometric determination of acid dissociation constants (p*K*a) for human and veterinary antibiotics. Water Res. 38, 2874-2890.

Raja, P., Bozzi, A., Mansilla, H., Kiwi, J., 2005. Evidence for superoxide-radical anion, singlet oxygen and OH-radical intervention during the degradation of the lignin model compound (3-methoxy-4-hydroxyphenylmethylcarbinol). J. Photochem. Photobiol. A: Chem. 169, 271-278.

Sirtori, C., Zapata, A., Malato, S., Gernjak, W., Fernández-Alba, A.R., Agüera, A., 2009. Solar photocatalytic treatment of quinolones: Intermediates and toxicity evaluation. Photochemical and Photobiological Sciences 8, 644-651.

Soares, P.A., Silva, T.F.C.V., Manenti, D.R., Souza, S.M.A.G.U., Boaventura, R.A.R., Vilar, V.J.P., 2013. Insights into real cotton-textile dyeing wastewater treatment using solar advanced oxidation processes. Enviro. Sci. Pollut. Res. 1-14.

Sousa, M.A., Gonçalves, C., Pereira, J.H.O.S., Vilar, V.J.P., Boaventura, R.A.R., Alpendurada, M.F., 2013. Photolytic and TiO_2-assisted photocatalytic oxidation of the anxiolytic drug lorazepam (Lorenin® pills) under artificial UV light and natural sunlight: A comparative and comprehensive study. Sol. Energy 87, 219-228.

Toral, M.I., Orellana, S.L., Soto, C.A., Richter, P., 2011. Extraction and Determination of Oxytetracycline Hydrochloride and Oxolinic Acid in Fish Feed by Derivative Spectrophotometry of First Order. Food Anal. Method 1-8.

Yahiat, S., Fourcade, F., Brosillon, S., Amrane, A., 2011. Removal of antibiotics by an integrated process coupling photocatalysis and biological treatment - Case of tetracycline and tylosin. Int. Biodeterior. Biodegrad. 65, 997-1003.

Zhao, C., Pelaez, M., Duan, X., Deng, H., O'Shea, K., Fatta-Kassinos, D., Dionysiou, D.D., 2013. Role of pH on photolytic and photocatalytic degradation of antibiotic oxytetracycline in aqueous solution under visible/solar light: Kinetics and mechanism studies. App. Cat. B Environ. 134–135, 83-92.

5 Assessment of Solar Driven TiO_2-Assisted Photocatalysis Efficiency on Amoxicillin Degradation

The objective of this work was to evaluate the efficiency of a solar TiO_2-assisted photocatalytic process on Amoxicillin (AMX) degradation. Firstly, solar photolysis of AMX was compared with solar photocatalysis in a CPC pilot scale photoreactor. Another experiment was also carried out to accurately follow the antibacterial activity against Escherichia coli DSM 1103 and Staphylococcus aureus DSM 1104 and mineralization of AMX by tracing the contents of dissolved organic carbon (DOC), low-molecular-weight carboxylate anions and inorganic anions. Finally, the influence of individual inorganic ions on AMX photocatalytic degradation efficiency and the involvement of some reactive oxygen species were also assessed.

This Chapter is based on the research article "João H.O.S. Pereira, Ana C. Reis, Olga C. Nunes, Maria T. Borges, Vítor J. P. Vilar, Rui A. R. Boaventura. *Assessment of Solar Driven TiO_2-Assisted Photocatalysis Efficiency on Amoxicillin Degradation*. Environ Sci Pollut Res (2014) 21:1292-1303".

5.1 Introduction

The most widely used group of antibiotics in human medicine in Europe is the penicillin's, which have showed an increasing trend of prescription over the last decade (Versporten et al. 2011). In 2009 they represented 47% of total outpatient use, from which the use of amoxicillin (AMX) alone, or combined with β-lactamase inhibitors, represented 83.9% (Versporten et al. 2011). The combination of this high level of prescription and the fact that amoxicillin has a low metabolic rate in humans, leading to excretion rates of 80-90% (Hirsch et al. 1999), accounts for an ubiquitous presence of this pharmaceutical in domestic and hospital wastewaters (Andreozzi et al. 2004; Längin et al. 2009; Watkinson et al. 2009; Leung et al. 2012). Adding to the varying efficiencies reported for the removal of antibiotics in conventional wastewater treatment plants (WWTP), which were not specifically designed to remove them (Leung et al. 2012), amoxicillin, as well as other antibacterial drugs, are frequently found in rivers and other water bodies receiving treated WWTP effluents (Kasprzyk-Hordern et al. 2008).

Another source of antibiotic contamination may result from animal husbandry use, as is the case of fish farming activities (Lalumera et al. 2004; Rigos and Troisi 2005), where effluents resulting from bath immersion treatments using amoxicillin concentrations as high as 200 mg L^{-1} (Mitchell and Rodger 2011) require special consideration before disposal. These are often diluted in aquatic receiving bodies or often treated with non-destructive methods (Noga 2010). Despite the fact that some of these substances do not persist due to natural degradation processes (Jones et al. 2005), their continual release to the environment raises several concerns regarding their ecotoxicological potential to humans and animals (Kim and Aga 2007; Martinez 2009; Santos et al. 2010; Escher et al. 2011).

Several alternative treatments have been proposed in recent years to tackle this situation, which are summarized in the revision performed by Homem and Santos (2011) and Michael et al. (2013). Among them, Advanced Oxidation Processes (AOPs) comprise different processes of generating hydroxyl radicals ($^{\bullet}OH$), which are very reactive and not highly selective. AOPs can be divided in photochemical (UV, UV/O_3, UV/H_2O_2), photocatalytic (TiO_2/UV, Fe^{2+}/H_2O_2/UV-Vis) or chemical oxidation processes (O_3, O_3/H_2O_2, H_2O_2/Fe^{2+}) (Poyatos et al. 2009). Their operation for full chemical degradation can be rather costly, so research is being focused on the application of AOPs that rely on solar irradiation as the source of UV radiation (such as heterogeneous photocatalysis and photo-Fenton reaction) and the possible combination with a pre or post biological treatment step (Malato et al. 2009; Oller et al. 2011).

Although several bench-scale studies on different AOPs using simulated UV radiation applied to aqueous solutions of amoxicillin have been undertaken (Elmolla and Chaudhuri 2009; Rizzo et al. 2009; Elmolla and Chaudhuri 2010a, b, c, 2011; Dimitrakopoulou et al. 2012), only three report results from solar photo-Fenton (Trovó et al. 2008; Mavronikola et al. 2009) and solar TiO_2 (Klauson et al. 2010) processes. However, to the best of our knowledge, none so far have neither applied Compound Parabolic Collectors (CPC) as photoreactors, nor have studied the influence of the individual presence of common occurring inorganic ions on the degradation of amoxicillin in aqueous solution. Theoretical and experimental studies (Fernández et al. 2005; González et al. 2009; Vilar et al. 2009; Colina-Márquez et al. 2010) have shown that CPCs are highly efficient on collecting solar radiation, so they are considered the best choice for different solar photocatalytic processes (Malato et al. 2002).

Thus, the main objective of this work was to study the enhancement of the photocatalytic degradation of AMX in a CPC pilot-plant, promoted by the presence of suspended TiO_2 and natural sunlight, when compared with solar photolysis. AMX mineralization was assessed in terms of Dissolved Organic Carbon (DOC), low-molecular-weight carboxylate ions and inorganic ions present in the solution. The antibacterial activity was assessed at different phototreatment times and correlated with the AMX concentration. A figure-of-merit, collector area per order (A_{CO}), was employed for both photocatalytic experiments in order to assess the possible factors that may affect the facility's efficiency, such as average solar UV irradiance over time and/or the volume of water to be treated. The influence of some inorganic ions typically occurring in wastewaters in TiO_2-assisted photocatalytic efficiency was also determined in a lab-scale CPC photoreactor equipped with a solar radiation simulator. Moreover, the formation of different reactive species, hydroxyl radical and singlet oxygen were probed using selective scavengers.

5.2 Materials and Methods

All the chemicals and reagents used in this work, the detailed description of the lab-scale and pilot-plant scale experimental units, along with the corresponding experimental procedures followed, and, finally, the employed analytical methods can be consulted in Chapter 2.

5.3 Results and discussion

5.3.1 Pilot-scale AMX photolysis and photocatalysis

To rule out the influence of solar photolysis on the degradation of AMX (molecular structure and UV absorbance spectrum in Figure 5.1), an experiment with 20 mg L^{-1} in aqueous solution was carried out in the absence of TiO_2.

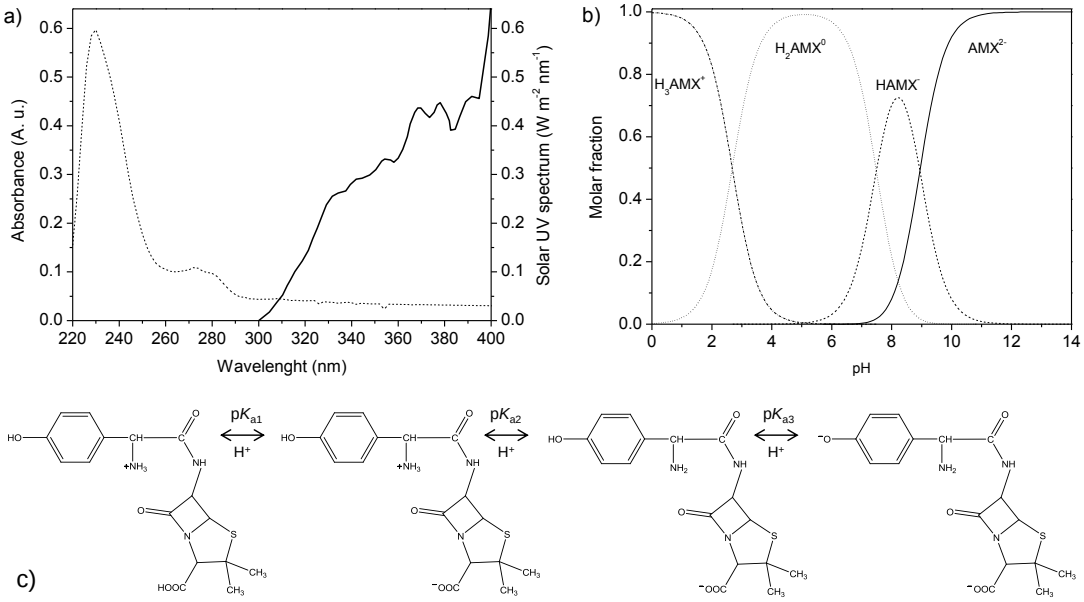

Figure 5.1. a) Amoxicillin UV absorbance spectrum (dashed line) and solar UV spectrum (solid line) adapted from Malato et al. (2002); **b)** Antibiotic speciation diagram as a function of pH and **c)** Schematics of dissociation equilibrium (pK_a values from Andreozzi et al. (2005); Ionic strength = 0.1 M, T = 25°C).

Figure 5.2 shows that direct photolysis was unable to considerably attack the molecules of the antibiotic and did not mineralize them in the given period of solar exposure (irradiation time (t_{ir}) = 215 min). This can be explained by the fact that the absorption of UV radiation, from the range of solar UV radiation that enters the reactor, by the AMX molecule is negligible, as seen by the very low-overlapping spectra in Figure 5.1a as highlighted in Rizzo et al. (2012). Xu and co-workers (2011) reported that direct photolysis in a solar simulator accounted for 6 to 21% of AMX loss in simulated natural waters, albeit for significantly higher exposure times (40 h) than the ones performed in this work (5 h of exposure, in average). The solar photocatalytic degradation of AMX was studied for a TiO_2 load of 0.5 g L^{-1} and pH = 7.5. After 3.1 kJ_{UV} of accumulated UV energy per liter of solution in the system (Figure 5.2; t_{ir} = 60 min), the AMX concentration was below the respective detection limit (0.11 mg L^{-1}). The kinetic results showed that the TiO_2-assisted photocatalytic process follows a pseudo-first order reaction, and the rate constant for AMX was calculated as 0.80 ± 0.02 L kJ_{UV}^{-1}, while the initial reaction rate (r_0) was 16.0 ± 0.3 mg kJ_{UV}^{-1} (Table 5.1).

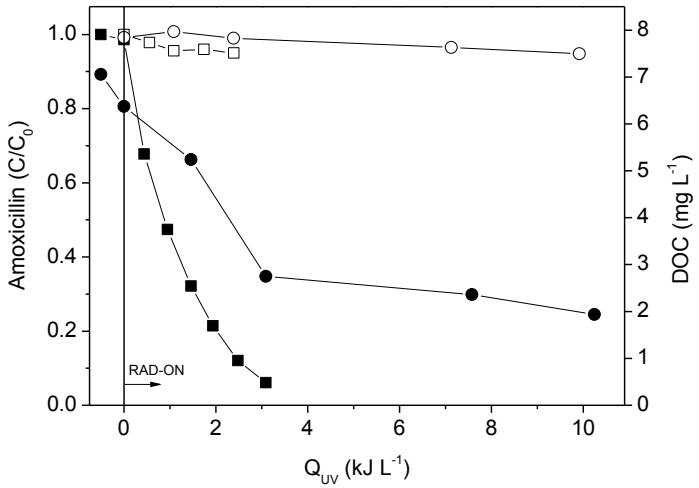

Figure 5.2. Solar photolysis (open symbols) and photocatalysis with 0.5 g L^{-1} of TiO_2 (solid symbols) of AMX solutions with 20 mg L^{-1} at pH = 7.5: dimensionless AMX concentration (□, ■) and DOC (○, ●).

In a previous work (Pereira et al. 2013), under the same experimental conditions, pseudo-first order kinetic rate constants five and two times higher were obtained for Oxytetracycline (OTC) and Oxolinic acid (OXA), respectively. It must be underlined that despite the difference between the molar concentrations used (0.087 mmol OTC L^{-1}, 0.109 mmol AMX L^{-1} and 0.153 mmol OXA L^{-1}) was not that high, the studied antibiotics present notable differences in terms of structure and functional groups, which may influence their adsorption properties onto the photocatalyst surface (Figueroa-Diva et al. 2010) and the susceptibility to solar UV radiation absorption and attack of the reactive oxidant species.

Table 5.1. Pseudo-first order kinetic constant values for AMX degradation under solar TiO_2-assisted photocatalytic system: [TiO_2] = 0.5 g L^{-1}; pH = 7.5.

Solar CPC pilot plant				
Experiment	***k* (L kJ^{-1})[a]**	***r_0* (mg kJ^{-1})[b]**	***R^2***	***S_R^2* (mg^2 L^{-2})**
AMX C_0 = 20 mg L^{-1}	0.80 ± 0.02	16.0 ± 0.3	0.998	0.071
AMX C_0 = 40 mg L^{-1}	0.43 ± 0.01	18.9 ± 0.4	0.998	0.331

a – pseudo-first order kinetic rate, b - initial reaction rate

5.3.2 Evaluation of the AMX mineralization

To better understand the effectiveness of the solar photocatalytic degradation of AMX, an experiment using an antibiotic concentration of 40 mg L^{-1} was carried out under the same initial conditions. As shown in Figure 5.3, AMX was almost fully degraded (residual concentration = 3.1 mg L^{-1}) after 4.6 kJ of accumulated UV energy per litre of solution (t_{ir} = 110 min), achieving a mineralization of 44%. 21% of the organic carbon in solution (according to the carboxylic

acids analyzed) is attributed to low-molecular-weight carboxylate anions, mainly formic, propionic and maleic acids. However, most of the other organic intermediates still contained sulfur and nitrogen, since only 17% of the total nitrogen in solution was detected in the form of ammonium ($[N_{AMX}]_t$ = 4.6 mg L^{-1}), and only 69% of the stoichiometric quantity of sulfate ($[S_{AMX}]_t$ = 1.75 mg L^{-1}) was already released. The TiO_2 solar photocatalysis was able to reduce the remaining DOC content to 29% of the original value after 11.7 kJ_{UV} L^{-1} sunlight exposure (t_i = 351 min). Seventy percent of the residual DOC content was in the form of low molecular weight carboxylate anions, mainly propionic and maleic acids, which is consistent with the decrease in the initial pH level down to around 6.40 in the same photo-treatment period.

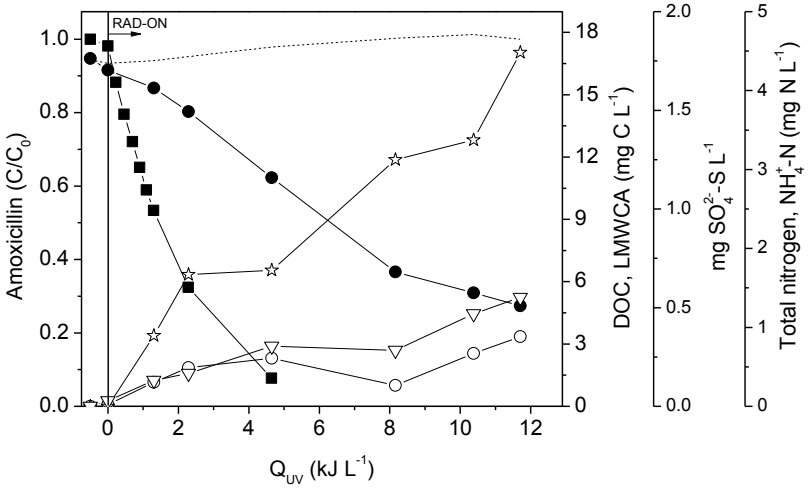

Figure 5.3. Solar photocatalysis ($[TiO_2]$ = 0.5 g L^{-1}) of AMX solution with 40 mg L^{-1}: dimensionless AMX concentration (■), DOC (●), sum of low-molecular-weight carboxylate anions as mg C L^{-1} (LMWCA, ○), sulfate as mg SO_4^{2-}-S L^{-1} (☆), Total nitrogen (--) and ammonium as mg N L^{-1} (▽).

The amount of sulfate detected at the end of the reaction corresponds to the stoichiometric conversion of sulfur contained in AMX to sulfate ion, showing that its complete mineralization occurred and that sulfur was not present in the remaining organic by-products. On the other hand, the on-going degradation of nitrogenated by-products was less effective during the same period, as only 30% of the initial nitrogen was converted to ammonium by the end of the process. No losses of nitrogen have been observed from the monitoring of total nitrogen, therefore the enduring nitrogen atoms are not present in nitrogenated organics adsorbed onto the surface of the catalyst. Lower levels of mineralization of sulfur and nitrogen contained in AMX have been reported by Klauson et al. (2010), releasing 14 and 1.4% respectively. Elmolla and Chaudhuri (2010b) reported the need of long irradiation times for the mineralization of sulfur contained in a mixture of Amoxicillin and two other β-lactam antibiotics in aqueous solution under UV-A/TiO_2/H_2O_2 photocatalysis.

Minimum inhibitory concentrations (MICs) are defined as the lowest concentration required to inhibit the visible growth of a microorganism in contrast to a positive control (Carson et al. 1995) and are used by diagnostic laboratories mainly to confirm resistance (Miller et al. 2005).

For the enterobacterial strain tested, AMX antibacterial activity with an accumulation of 4.6 kJ_{UV} L^{-1} (t_{ir} = 110 min) in the system was found to be considerably reduced when growth was compared to the control (Figure 5.4). Antibiotic concentration in this point, [AMX] = 3.1 mg L^{-1}, was slightly below the value reported by Andrews (2001) to be sufficient to inhibit *E. coli* growth (4 mg L^{-1}). Conversely, at the same point, *S. aureus* growth was still inconsequential, as the defined MIC value of 0.25 mg L^{-1}, reported in the same study (Andrews 2001), is considerably lower. When a Q_{UV} amount of 6.4 kJ_{UV} L^{-1} (t_{ir} = 150 min) was reached ([AMX] below the detection limit of the equipment, 0.11 mg L^{-1}), AMX antibacterial activity against *E. coli* was completely relieved, and some *S. aureus* growth occurred, though half of that of the positive control.

In a UV-A/TiO_2 photocatalysis experiment with 30 mg L^{-1} of AMX, Dimitrakopoulou et al. (2012) reported that antibacterial activity against two different bacterial strains belonging to the *Enterobacteriaceae* family, with broader MIC values than the strains used in this study, was inactivated when AMX concentration dropped below 25 mg L^{-1}. However, for a concentration below 5 mg L^{-1}, an *enterococci* bacterial strain studied by the same authors showed to be affected, especially by AMX intermediary by-products.

According to the reaction pathways proposed by Klauson et al. (2010), some of the AMX photocatalytic by-products (identified via UPLC-ESI-MS analysis) still contain an intact β-lactamic ring structure, which accounts for this residual antibacterial activity.

Consequently, in this work, an accumulated UV energy value of 7.7 kJ L^{-1} (t_{ir} = 180 min) is suggested to be enough to achieve the complete cleavage of the β-lactamic ring, as the solution no longer presented antibacterial activity against *S. aureus* (Figure 5.4), and no longer presents the risk of promoting antibiotic resistance among bacteria in the potential receiving water body.

Some works have reported the adsorption of penicillin antibiotics on non-illuminated iron and TiO_2 nanoparticles and the consequent breakdown of the the β-lactamic ring of the original compounds over different pH conditions (Ghauch et al. 2009; Peterson et al. 2012). However, in the photocatalytic experiments performed in this work no significant loss of AMX was seen in the period of time between the catalyst addition step and the beginning of the irradiation.

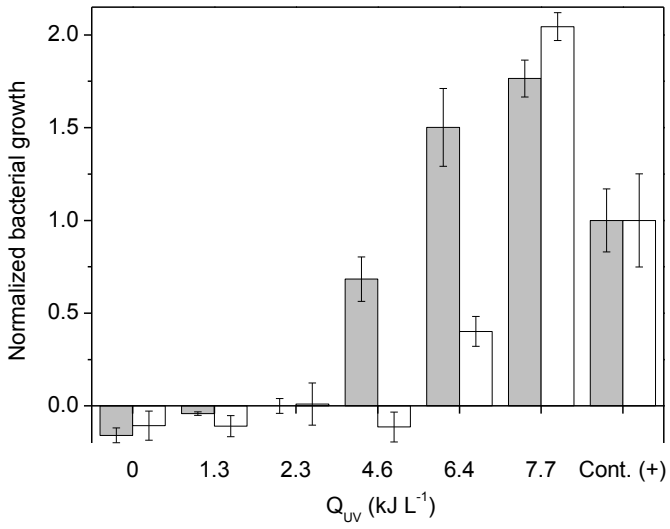

Figure 5.4. *Escherichia coli* (grey columns) and *Staphylococcus aureus* (white columns) normalized bacterial growth at different phototreatment times under solar photocatalysis with 0.5 g L^{-1} of TiO_2 at pH 7.5 ($[AMX]_0$ = 40 mg L^{-1}), compared to the respective positive control, Cont. (+).

The photocatalytic pseudo-first-order kinetic constant for AMX was found to be 0.43 ± 0.01 L kJ_{UV}^{-1}, approximately half of the kinetic constant obtained in the first experiment (20 mg L^{-1} AMX) (Table 5.1). As the initial dark adsorption of AMX onto the photocatalyst surface was minimal and very similar in both experiments, the calculated initial reaction rate was in this case 18.9 ± 0.4 kJ_{UV}^{-1}.

5.3.3 Influence of inorganic ions and scavengers

Inorganic ions, such as those present in various types of wastewaters, have been found to inconsistently affect the rates of photocatalytic oxidation of organic pollutants (Abdullah 1990; Ahmed et al. 2010). Figure 5.5a presents the individual effect of Cl^-, SO_4^{2-}, PO_4^{3-}, NO_3^- and NH_4^+ (1 g L^{-1}) and HCO_3^- (0.1 g L^{-1}) on the photocatalytic (0.5 g L^{-1} TiO_2) degradation of AMX (20 mg L^{-1}) after an endpoint of 60 min of simulated solar irradiation in the lab-scale photoreactor. Guillard et al. (2005) have shown that the decrease in efficiency of TiO_2 photocatalysis in the presence of inorganic ions at neutral pH conditions is mainly caused by the formation of an inorganic layer at the catalyst surface, inhibiting the contaminant adsorption. Under the tested pH value, and according to Figure 5.1b and c, the AMX species in solution may present overall neutral (48.5% as H_2AMX) or negative charges (49.7% as $HAMX^-$), and the surface of TiO_2 particles is neutral and negatively charged (76% as -TiOH and 24% as $-TiO^-$; pH > pH_{PZC}, pH of Point of Zero Charge = 6.7) (Fernández-Ibáñez et al. 2003; Malato et al. 2009). According to Dimitrakopoulou et al. (2012), this does not favor an electrostatic attraction between AMX and TiO_2, and leads to the minimal amount of antibiotic adsorption in the dark, as it can be seen in Figure 5.5 a.

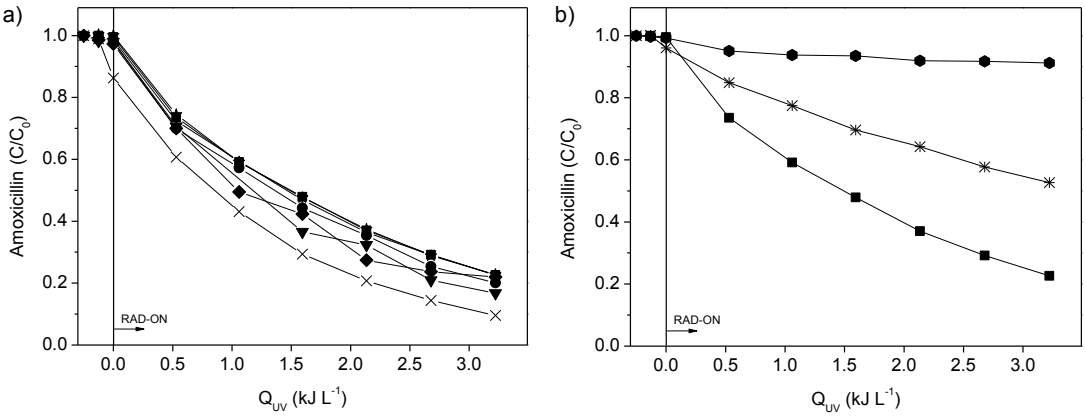

Figure 5.5. Removal profiles of 20 mg L^{-1} of AMX alone (■) and **a)** in the presence of 1 g L^{-1} of Cl^- (+), SO_4^{2-} (●), NO_3^- (▼), NH_4^+ (◆), PO_4^{3-} (×), 0.1 g L^{-1} HCO_3^- (★) and **b)** in the presence of 10 mM NaN_3 (✳) and 50 mM D-mannitol (⬢) under simulated solar photocatalysis with 0.5 g L^{-1} TiO_2 and pH = 7.5.

Consequently, the aforementioned effect of the presence of most inorganic ions did not substantially affect the AMX photocatalytic kinetic rates (Table 5.1). The only considerable exception is the case of PO_4^{3-}, whose presence not only promoted the initial dark adsorption of AMX onto the catalyst surface, but consequently enhanced the oxidation rate of AMX compared to its absence (Figure 5.5a). Chen et al. (2003) have reported a similar phenomenon of increased adsorption of certain dye-constituent aromatics on the surface of TiO_2 in the presence of phosphate anions. The negatively charged phosphate anions strongly adsorbed onto the TiO_2 surface may favor not only the adsorption of AMX species bearing a positive (Chen et al. 2003) or neutral (Guillard et al. 2003) charge on the $–NH_2$ group, but also the formation of free hydroxyl radicals via the enhancement of the separation of the photogenerated hole and electron facilitated by an inner-sphere surface complex, as suggested by Zhao and co-workers (2008). The same authors thus concluded that phosphate modification accelerates the degradation of pollutants either more prone to hydroxyl radical attack or with weak adsorption on pure TiO_2 particles.

To evaluate the role of reactive species, such as hydroxyl radical ($^{\bullet}OH$) and singlet oxygen ($^1O_2$), in the AMX photocatalytic degradation, selective scavengers D-Mannitol and sodium azide (NaN_3), respectively, were used. The insignificant photocatalytic degradation of the antibiotic during the phototreatment period in the presence of D-Mannitol (Figure 5.5b and Table 5.2), purports the role of $^{\bullet}OH$ radicals as the major responsible for AMX degradation, which is in agreement with the results presented by Song et al. (2008). However, according to Figure 5.5 b, the $^1O_2$ reactive species also plays an important role in AMX self-photosensitization under UV/visible solar light, as reported by Zhao et al. (2013).

Table 5.2. Pseudo-first order kinetic constant values for AMX degradation, alone or with (+) inorganic ions and scavengers, under simulated solar TiO_2-assisted photocatalytic systems: [TiO2] = 0.5 g L^{-1}; pH = 7.5.

	Lab-scale Photoreactor (I = 44 W_{UV} m^{-2})				
	Experiment	***k* (L kJ^{-1})[a]**	***r_0* (mg kJ^{-1})[b]**	***R^2***	***S_R^2* (mg^2 L^{-2})**
AMX	individual	0.47 ± 0.01	8.4 ± 0.2	0.996	0.108
	+ 1.0 g L^{-1} Cl^-	0.47 ± 0.01	8.3 ± 0.2	0.997	0.119
	+ 1.0 g L^{-1} NO_3^-	0.57 ± 0.02	10.5 ± 0.4	0.996	0.171
	+ 0.1 g L^{-1} HCO_3^-	0.47 ± 0.01	8.9 ± 0.2	0.997	0.095
	+ 1.0 g L^{-1} SO_4^{2-}	0.50 ± 0.01	9 ± 2	0.993	0.167
	+ 1.0 g L^{-1} NH_4^+	0.55 ± 0.03	10.3 ± 0.6	0.985	0.513
	+ 1.0 g L^{-1} PO_4^{3-}	0.669 ± 0.004	10.76 ± 0.06	0.999	0.005
	+ 10 mM NaN_3	0.193 ± 0.004	3.52 ± 0.01	0.831	0.09
	+ 50 mM D-Mannitol	0.032 ± 0.004	0.59 ± 0.07	0.831	0.09

a – pseudo-first order kinetic rate, b - initial reaction rate

5.3.4 Solar photocatalytic efficiency index

In the case of AOPs based on free solar radiation, the main capital cost is proportionally related to the area of the collectors. As such, it is suitable to use a figure-of-merit based on the solar collector area recommended by the IUPAC to allow for a direct comparison between the solar-energy efficiency of different AOPs, independently of the nature of the used system. Therefore, for a low pollutant concentration range, the appropriate figure-of-merit is the collector area per order (A_{CO}) (Bolton et al. 2001). A_{CO} is the collector area required to reduce the concentration of a contaminant (C) in polluted water in a unit of volume by one order of magnitude in a time (t_0 = 1 h) when the standardized incident solar irradiance (E_S^0) is 1000 W m^{-2}. The A_{CO} (m^2 m^{-3}-order), in batch operation, can be calculated from Eq. 5.01:

$$A_{CO} = \frac{A_r \cdot \overline{UV}_G \cdot t}{E_S^0 \cdot t_0 \cdot V_t \cdot \log\left(\frac{C}{C_0}\right)} \qquad (5.01)$$

where Ar is the illuminated collector surface area (m^2), $\overline{UV}_G$ is the average solar ultraviolet irradiance (W m^{-2}, as measured in the 300-400 nm range, the useful UV wavelength range for solar photocatalysis with TiO_2) over the period t of the treatment (h), V_t the total reactor volume (m^3), and C and C_0 are the final and initial antibiotic concentrations (mg L^{-1}). This figure-of-merit indicates a loss in the system efficiency when A_{CO} values increase, in an inverse proportion. As previously mentioned, CPC geometry has been shown to be highly efficient when applied to solar photocatalytic treatments.

This remark has been emphasized by Bandala and Estrada (2007), when they compared the same figure-of-merit using different solar reactors (which use direct and diffuse UV irradiation).

Within this study, for the two different initial antibiotic concentrations, 20 and 40 mg L^{-1}, 0.85 ($\overline{UV}_G$ = 25.2 W m^{-2}) and 1.65 ($\overline{UV}_G$ = 32.18 W m^{-2}) hours were required to achieve a decrease of the initial AMX concentrations in one order of magnitude, resulting in an A_{CO} index of 0.65 to 1.21 m^2 m^{-3}-order, respectively. It should be mentioned that the 30% solar UV irradiance increase between experiments (given that these were performed in different days), was compensated by a decrease of the useful solar exposure time needed to reduce the AMX concentration by an order of magnitude. Therefore, according to the results obtained, there is no substantial conversion efficiency loss in the studied antibiotic concentration range. As expected, a 2 fold increase of pollutant concentration only doubled the A_{CO} index. A similar system efficiency was obtained by Sousa et al. (2013) in the solar photocatalytic oxidation of the anxiolytic drug lorazepam using the same pilot-plant but mediated by only 0.2 g L^{-1} TiO_2 (A_{CO} index = 0.4 m^2 m^{-3}-order).

5.4 Conclusions

The use of CPC photoreactors for solar UV photons capture was shown to be effective for the TiO_2-assisted photocatalytic ([TiO_2] = 0.5 g L^{-1}) degradation of the antibiotic Amoxicillin in aqueous solutions at neutral pH conditions (7.5).

Solar UV radiation alone was unable to attack the antibiotic molecules during the same photo-treatment period. The TiO_2 solar photocatalysis was able to reduce the antibiotic concentration from 40 to 3.1 mg L^{-1} after 4.6 kJ of UV accumulated energy per litre of solution, leading to a considerable reduction of the antibacterial activity. At the end of the phototreatment period (11.7 kJ L^{-1} of UV energy accumulated in the system), 71% mineralization was achieved, being seventy percent of the residual DOC content in the form of low molecular weight carboxylate anions, mainly propionic and maleic acids.

Even though the amount of sulfate detected at the end of the reaction corresponds to the stoichiometric conversion of sulfur contained in AMX, only 30% of the initial nitrogen was converted to ammonium, showing that the mineralization of nitrogenated by-products was less effective during the phototreatment period.

Although the AMX degradation was mainly attributed to hydroxyl radicals, singlet oxygen also plays an important role in AMX self-photosensitization under UV/visible solar light. Screenings of individual inorganic ions effects have shown that the presence of phosphates at the studied pH level enhance AMX photocatalytic oxidation, while the presence of other inorganic ions (Cl^-, SO_4^{2-}, NO_3^-, NH_4^+ and HCO_3^-) did not considerably alter the reaction rate.

The results obtained build on the potential for developing future treatments for wastewaters of various origins containing high concentrations of AMX with relatively short periods of solar irradiance, allowing their subsequent safe discharge due to the elimination of the risk of antibiotic resistance promotion.

5.5 References

Abdullah, M., 1990. Effects of common inorganic anions on rates of photocatalytic oxidation of organic carbon over illuminated titanium dioxide. J. Phys. Chem. 94, 6820-6825.

Ahmed, S., Rasul, M.G., Martens, W.N., Brown, R., Hashib, M.A., 2011. Advances in heterogeneous photocatalytic degradation of phenols and dyes in wastewater: A review. Water, Air, Soil Pollut. 215, 3-29.

Barreiros, L., Nogales, B., Manaia, C.M., Silva Ferreira, A.C., Pieper, D.H., Reis, M.A., Nunes, O.C., 2003. A novel pathway for mineralization of the thiocarbamate herbicide molinate by a defined bacterial mixed culture. Environ. Microbiol. 5, 944-953.

Bayarri, B., Abellán, M.N., Giménez, J., Esplugas, S., 2007. Study of the wavelength effect in the photolysis and heterogeneous photocatalysis. Catal. Today 129, 231-239.

Boaventura, R., Pedro, A.M., Coimbra, J., Lencastre, E., 1997. Trout farm effluents: Characterization and impact on the receiving streams. Environ. Pollut. 95, 379-387.

Bolton, J.R., Bircher, K.G., Tumas, W., Tolman, C.A., 2001. Figures-of-merit for the technical development and application of advanced oxidation technologies for both electric- and solar-driven systems. Pure Appl. Chem. 73, 627-637.

Boreen, A.L., Arnold, W.A., McNeill, K., 2004. Photochemical fate of sulfa drugs in then aquatic environment: Sulfa drugs containing five-membered heterocyclic groups. Environ. Sci. Technol. 38, 3933-3940.

Calza, P., Pelizzetti, E., Minero, C., 2005. The fate of organic nitrogen in photocatalysis: An overview. J. Appl. Electrochem. 35, 665-673.

Chen, F., Zhao, J., Hidaka, H., 2003. Adsorption factor and photocatalytic degradation of dye-constituent aromatics on the surface of TiO_2 in the presence of phosphate anions. Res. Chem. Intermed. 29, 733-748.

Colina-Márquez, J., MacHuca-Martínez, F., Puma, G.L., 2010. Radiation absorption and optimization of solar photocatalytic reactors for environmental applications. Environ. Sci. Technol. 44, 5112-5120.

Faria, P.C.C., Órfão, J.J.M., Pereira, M.F.R., 2008. Activated carbon catalytic ozonation of oxamic and oxalic acids. App. Cat. B Environ. 79, 237-243.

Fernández-Ibáñez, P., Blanco, J., Malato, S., De Las Nieves, F.J., 2003. Application of the colloidal stability of TiO_2 particles for recovery and reuse in solar photocatalysis. Water Res. 37, 3180-3188.

Fernández, P., Blanco, J., Sichel, C., Malato, S., 2005. Water disinfection by solar photocatalysis using compound parabolic collectors. Catal. Today 101, 345-352.

Garcia-Segura, S., Brillas, E., 2011. Mineralization of the recalcitrant oxalic and oxamic acids by electrochemical advanced oxidation processes using a boron-doped diamond anode. Water Res. 45, 2975-2984.

Giraldo, A.L., Peñuela, G.A., Torres-Palma, R.A., Pino, N.J., Palominos, R.A., Mansilla, H.D., 2010. Degradation of the antibiotic oxolinic acid by photocatalysis with TiO_2 in suspension. Water Res. 44, 5158-5167.

González, O., Sans, C., Esplugas, S., Malato, S. 2009. Application of solar advanced oxidation processes to the degradation of the antibiotic sulfamethoxazole. Photochem. Photobiol Sci. 8, 1032-1039

Guillard, C., Lachheb, H., Houas, A., Ksibi, M., Elaloui, E., Herrmann, J.M., 2003. Influence of chemical structure of dyes, of pH and of inorganic salts on their photocatalytic degradation by TiO_2 comparison of the efficiency of powder and supported TiO_2. J. Photochem. Photobiol. A: Chem. 158, 27-36.

Guillard, C., Puzenat, E., Lachheb, H., Houas, A., Herrmann, J.M., 2005. Why inorganic salts decrease the TiO_2 photocatalytic efficiency. Int. J. Photoener. 7, 1-9.

Han, S.K., Hwang, T.M., Yoon, Y., Kang, J.W., 2011. Evidence of singlet oxygen and hydroxyl radical formation in aqueous goethite suspension using spin-trapping electron paramagnetic resonance (EPR). Chemosphere 84, 1095-1101.

Hirakawa, K., Mori, M., Yoshida, M., Oikawa, S., Kawanishi, S., 2004. Photo-irradiated titanium dioxide catalyzes site specific DNA damage via generation of hydrogen peroxide. Free Radical Res. 38, 439-447.

Jiao, S., Zheng, S., Yin, D., Wang, L., Chen, L., 2008. Aqueous photolysis of tetracycline and toxicity of photolytic products to luminescent bacteria. Chemosphere 73, 377-382.

Jiménez-Lozano, E., Marqués, I., Barrón, D., Beltrán, J.L., Barbosa, J., 2002. Determination of p*K*a values of quinolones from mobility and spectroscopic data obtained by capillary electrophoresis and a diode array detector. Anal. Chim. Acta 464, 37-45.

Malato, S., Blanco J., Vidal, A., Richter, C., 2002. Photocatalysis with solar energy at a pilot-plant scale: An overview. App. Cat. B: Environ. 37, 1-15.

Malato, S., Fernández-Ibáñez, P., Maldonado, M.I., Blanco, J., Gernjak, W., 2009. Decontamination and disinfection of water by solar photocatalysis: Recent overview and trends. Catal. Today 147, 1-59.

Miller, R.A., Walker, R.D., Carson, J., Coles, M., Coyne, R., Dalsgaard, I., Gieseker, C., Hsu, H.M., Mathers, J.J., Papapetropoulou, M., Petty, B., Teitzel, C., Reimschuessel, R., 2005. Standardization of a broth microdilution susceptibility testing method to determine minimum inhibitory concentrations of aquatic bacteria. Dis. Aquat. Org. 64, 211-222.

Miralles-Cuevas, S., Arqués, A., Maldonado, M.I., Sánchez-Pérez, J.A., Malato Rodríguez, S., 2012. Combined nanofiltration and photo-Fenton treatment of water containing micropollutants. Chem. Eng. J.

Palominos, R.A., Mora, A., Mondaca, M.A., Pérez-Moya, M., Mansilla, H.D., 2008. Oxolinic acid photo-oxidation using immobilized TiO_2. J. Hazard. Mater. 158, 460-464.

Pereira, J.H.O.S., Vilar, V.J.P., Borges, M.T., González, O., Esplugas, S., Boaventura, R.A.R., 2011. Photocatalytic degradation of oxytetracycline using TiO_2 under natural and simulated solar radiation. Sol. Energy 85, 2732-2740.

Pouliquen, H., Delépée, R., Larhantec-Verdier, M., Morvan, M.L., Le Bris, H., 2007. Comparative hydrolysis and photolysis of four antibacterial agents (oxytetracycline oxolinic acid, flumequine and florfenicol) in deionised water, freshwater and seawater under abiotic conditions. Aquaculture 262, 23-28.

Qiang, Z., Adams, C., 2004. Potentiometric determination of acid dissociation constants (p*K*a) for human and veterinary antibiotics. Water Res. 38, 2874-2890.

Raja, P., Bozzi, A., Mansilla, H., Kiwi, J., 2005. Evidence for superoxide-radical anion, singlet oxygen and OH-radical intervention during the degradation of the lignin model compound (3-methoxy-4-hydroxyphenylmethylcarbinol). J. Photochem. Photobiol. A: Chem. 169, 271-278.

Sirtori, C., Zapata, A., Malato, S., Gernjak, W., Fernández-Alba, A.R., Agüera, A., 2009. Solar photocatalytic treatment of quinolones: Intermediates and toxicity evaluation. Photochem. Photobiol. Sci. 8, 644-651.

Soares, P.A., Silva, T.F.C.V., Manenti, D.R., Souza, S.M.A.G.U., Boaventura, R.A.R., Vilar, V.J.P., 2013. Insights into real cotton-textile dyeing wastewater treatment using solar advanced oxidation processes. Environ. Sci. Pollut. R.1-14.

Sousa, M.A., Gonçalves, C., Pereira, J.H.O.S., Vilar, V.J.P., Boaventura, R.A.R., Alpendurada, M.F., 2013. Photolytic and TiO_2-assisted photocatalytic oxidation of the anxiolytic drug lorazepam (Lorenin® pills) under artificial UV light and natural sunlight: A comparative and comprehensive study. Sol. Energy 87, 219-228.

Toral, M.I., Orellana, S.L., Soto, C.A., Richter, P., 2011. Extraction and Determination of Oxytetracycline Hydrochloride and Oxolinic Acid in Fish Feed by Derivative Spectrophotometry of First Order. Food Anal. Method 1-8.

Vilar, V.J.P., Gomes, A.I.E., Ramos, V.M., Maldonado, M.I., Boaventura, R.A.R. 2009. Solar photocatalysis of a recalcitrant coloured effluent from a wastewater treatment plant. Photochem. Photobiol. Sci. 8, 691-698.

Yahiat, S., Fourcade, F., Brosillon, S., Amrane, A., 2011. Removal of antibiotics by an integrated process coupling photocatalysis and biological treatment - Case of tetracycline and tylosin. Int. Biodeterior. Biodegrad. 65, 997-1003.

Zhao, C., Pelaez, M., Duan, X., Deng, H., O'Shea, K., Fatta-Kassinos, D., Dionysiou, D.D., 2013. Role of pH on photolytic and photocatalytic degradation of antibiotic oxytetracycline in aqueous solution under visible/solar light: Kinetics and mechanism studies. App. Cat. B Environ. 134–135, 83-92.

6 Process Intensification at Near Neutral pH of a Homogeneous Photo-Fenton Reaction Using Ferricarboxylate Complexes: Application to Oxytetracycline Degradation

This work demonstrates the application at near neutral pH of the photo-Fenton process mediated by ferricarboxylates on the treatment of aqueous solutions containing the antibiotic Oxytetracycline (OTC) under solar irradiation. The formation of a Fe:OTC complex after Fe^{2+} oxidation to Fe^{3+}, in the presence of H_2O_2, showed the inconvenience of using the conventional Fe^{2+}/H_2O_2/UV-Vis process at near neutral pH levels, as the Fe:OTC complex is retained in the filter. To overcome this, a Fe^{3+}/Oxalate or Fe^{3+}/Citrate/H_2O_2/UV-Vis process was proposed. Process efficiency was evaluated for different variables such as Fe^{3+} concentration, pH, temperature and irradiance, using a compound parabolic collector (CPC) photoreactor at lab-scale under simulated solar radiation. Reaction rates were compared in the presence of different inorganic anions and humic acids, and in two different real wastewater matrixes.

This Chapter is based on the research article "João H.O.S. Pereira, Daniel B. Queirós, Ana C. Reis, Olga C. Nunes , Maria T. Borges, Rui A. R. Boaventura, Vítor J. P. Vilar. *Process Enhancement at Near Neutral pH of a Homogeneous Photo-Fenton Reaction Using Ferricarboxylate Complexes: Application to Oxytetracycline Degradation*. Chem Eng J (2014) 253, 217-228".

6.1 Introduction

Antibiotics are a special group of pharmaceuticals used to control infection diseases in human and veterinary medicine. Residual concentration have been detected in various environmental compartments worldwide due to the fact that a large percentage of the consumed antibiotics are not completely metabolized (and thus are excreted as active substances) and that conventional wastewater treatment methods fail to completely remove them from solution (Kümmerer, 2009; Loos et al., 2009; Watkinson et al., 2009; Verlicchi et al., 2010).

Even though direct cause and effect relationships are still to be established, it is widely recognized that antibiotic pollution contibutes to antibiotic resistance dissemination (Escher et al., 2011; Tamminen et al., 2011; Manaia et al., 2012). Thus, research in recent years has been focused on alternative ways to prevent the contamination of water supplies by this kind of pollutants. Urban wastewater treatment plants (WWTP) are one of its major sources (Michael et al., 2013), but highly-contaminated effluents resulting from fish farming activities may also be a special case to be considered (Rigos et al., 2006).

Advanced oxidation processes (AOPs), a class of treatments involving different ways of generating the highly reactive and non-selective hydroxyl radical ($^{\bullet}OH$) and other reactive oxygen species (Gogate and Pandit, 2004a; b), have been considered for the removal of these substances, especially those involving catalysis and solar irradiation such as the photo-Fenton process (Malato et al., 2009; Homem and Santos, 2011). Photo-Fenton comprises the combination of ferrous iron (Fe^{2+}) with hydrogen peroxide (H_2O_2) and (solar) UV-Vis radiation resulting in the production of two moles of $^{\bullet}OH$ per mole of hydrogen peroxide (Eq. 6.01 and 6.02), as simplified by Gogate and Pandit (2004b):

$$Fe^{2+} + H_2O_2 \rightarrow Fe^{3+} + {}^{\bullet}OH + HO^{-} \quad (6.01)$$

$$Fe(OH)^{2+} + h\upsilon \rightarrow Fe^{2+} + {}^{\bullet}OH \quad (6.02)$$

Pignatello et al. (2006) summarizes the reasons for the optimum operational pH value of the (photo-) Fenton process around 3 as follows: first, the solubility of Fe^{3+}-hydroxy complexes decreases for pH values above 3; second, $[Fe(OH)]^{2+}$, the most photoactive species (with absorption bands between 290 and 400 nm), reaches its maximum molar fraction around the aforementioned pH. As a consequence, there is a limited viability of applying this process in industrial scale due to the costs associated with pH corrections (initial acidification and final neutralization).

Antibiotics are also known to form stable complexes with metallic cations (Albert, 1953; Ghandour et al., 1992). This cation:antibiotic interaction results in different physical properties which are environmentally relevant in many ways. Several works have reported, for instance, on the enhanced (Ogunniran et al., 2007) or decreased (Mikelens and Levinson, 1978) antibacterial properties, negative effects on soil microbial community (Kong et al., 2006), on the sorption and mobility behaviour in soils and aquatic sediments (Jones et al., 2005; Figueroa-Diva et al., 2010; Lalonde et al., 2012), or even Fe-Mn binary oxide oxidation and adsorption (Liu et al., 2012).

Pertinent to the photo-Fenton process is the formation of complexes between antibiotics and Fe (II) and Fe (III) for two reasons. It not only decreases degradation efficiencies (due to a lower iron availability to react with hydrogen peroxide (Batista and Nogueira, 2012)), but it may also lead to mistaken readings in analytical equipments (e.g., different retention times in HPLC chromatograms and/or different UV absorption spectra (Gu and Karthikeyan, 2005)), thereby to incorrectly calculated reaction rates.

However, this can be overcome by recurring to the complexation of Fe (III) with carboxylate ions, which also improves the photo-Fenton process by extending the solubility of iron to higher and more practical pH values, by presenting stronger radiation absorption at wavelengths until 580 nm and by increasing the quantum yield of Fe^{2+} production according to Eq. 6.03 (Jeong and Yoon, 2005; Pignatello et al., 2006; Malato et al., 2009).

$$Fe^{3+}\left(C_2O_4\right)_n^{(3-2n)} + h\upsilon \rightarrow Fe^{2+} + (n-1)C_2O_4^{2-} + C_2O_4^{2-\bullet} \qquad (6.03)$$

Ferricarboxylate-mediated solar photo-Fenton has already been successfully applied to treat different wastewaters and specific pollutants, whereby carboxylate ions such as oxalate, citrate and EDDS (ethylenediamine-N, N'-disuccinic acid) were used to form complexes with Fe^{3+} (Silva et al., 2007; Prato-Garcia et al., 2009; Rodríguez et al., 2009; Huang et al., 2012; Monteagudo et al., 2012).

Considering the current limitations of implementing these processes in existing WWTP (high flow rates, capital and reactant costs, removal of excess iron to comply with discharge limits, for example), the combination of membrane processes with AOPs have been recently proposed (Westerhoff et al., 2009). Miralles-Cuevas et al. (2013), for instance, have shown that mild solar photo-Fenton is best applied to higher micropollutants loads found in nanofiltration concentrates (up to the mg L^{-1} range), thus minimizing their disposal impact.

In this context, the aim of this work was thus the process intensification at near neutral pH conditions of a homogeneous solar photo-Fenton reaction through the use of ferricarboxylates complexes applied to the removal of Oxytetracycline in aqueous solutions.

Experiments at lab-scale using a CPC photoreactor under simulated solar radiation were performed to i) compare the conventional Fe^{2+}/H_2O_2/UV-Vis with the Fe^{3+}/Oxalate or Fe^{3+}/Citrate/H_2O_2/UV-Vis systems, ii) choose the optimum dissolved Fe (III) concentration (iron/oxalate molar ratio of 1:3) and also iii) the initial working pH level.

The influence of temperature, irradiance, and the presence of humic acids and of some commonly occuring inorganic ions in several types of wastewaters was also assessed. Matrix effects were studied by spiking OTC in two different media, a WWTP effluent after secondary treatment and a real troutfarm effluent.

Experiments in a solar pilot-scale plant equipped with CPCs were also carried out to evaluate the performance of the reaction under natural solar radiation conditions, the abatement of OTC, antibacterial activity and the composition of the remaining dissolved organic carbon in terms of low-molecular-weight carboxylate ions.

6.2 Materials and Methods

All the chemicals and reagents used in this work, the detailed description of the lab-scale and pilot-plant scale experimental units, along with the corresponding experimental procedures followed, and, finally, the employed analytical methods can be consulted in Chapter 2.

6.3 Results and discussion

In all experiments, a working OTC (molecular structure, UV absorbance spectrum and speciation diagram as a function of pH shown in Figure 6.1) concentration of 20 mg L^{-1} has been chosen bearing in mind the available analytical equipment and also the possibility of applying the processes under study in the decontamination of concentrates resulting from membrane separation processes, or from effluents resulting from bath immersion treatments using high antibiotic concentrations (Noga, 2010), as mentioned above.

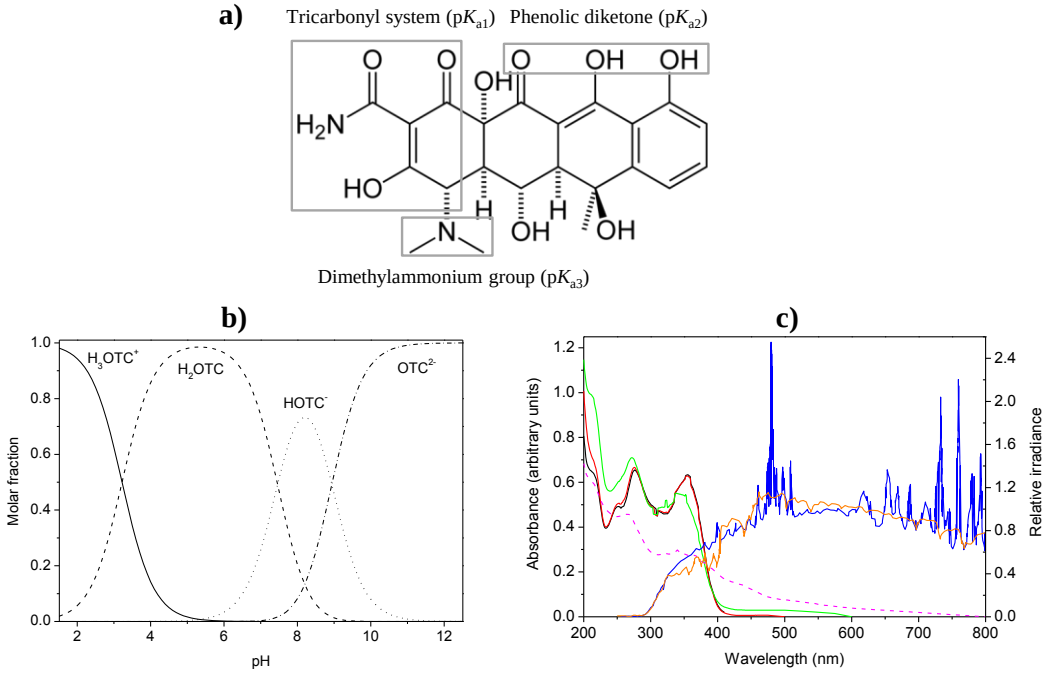

Figure 6.1. a) Structural formula and **b)** dissociation equilibrium diagram of OTC (pK_{a1} = 3.6, pK_{a2} = 7.58, pK_{a3} = 9.03, Ionic strength = 0 M, T = 23 °C (Qiang and Adams, 2004)); **c)** Absorption spectra of 20 mg L^{-1} OTC: OTC alone (——); OTC + 9.5 mg L^{-1} oxalic acid (——); OTC + 9.5 mg L^{-1} oxalic acid + 2 mg L^{-1} Fe^{3+} (——); OTC + 2 mg L^{-1} Fe^{3+} (– – –); solar spectrum (——); xenon lamp spectrum (——).

6.3.1 Conventional Fe^{2+}/H_2O_2/UV-Vis reaction

In a previous work it was reported the effect of solar and simulated solar photolysis on OTC degradation, which can be expected from the relative overlapping of the UV absorbance spectrum of OTC with both solar and xenon lamp spectra, as seen in Figure 6.1c (Pereira et al., 2013). Pseudo-first order kinetics, for instance, was found to be one order of magnitude lower in the case of solar photolysis of OTC (0.205 ± 0.005 L kJ^{-1}) when compared to solar photocatalysis mediated by 0.5 g L^{-1} of TiO_2 (2.63 ± 0.03 L kJ^{-1}) as reported by Pereira et al. (2011). Slow antibiotic degradation and lack of proper mineralization has brought up the need of exploring more effective oxidative methods.

The results of the conventional Fe^{2+}/H_2O_2/UV-Vis degradation of OTC under different initial pH values (3.0, 4.0 and 5.0), carried out in a lab-scale photoreactor equipped with a CPC, are shown in Figure 6.2. The concentration of Fe (II) was 2 mg L^{-1}, which is the total iron discharge limit into any water body, according to the Portuguese legislation (Decree-Law n.º 236/98) while H_2O_2 concentration was kept between 10 and 30 mg L^{-1} (total addition around 2 mM).

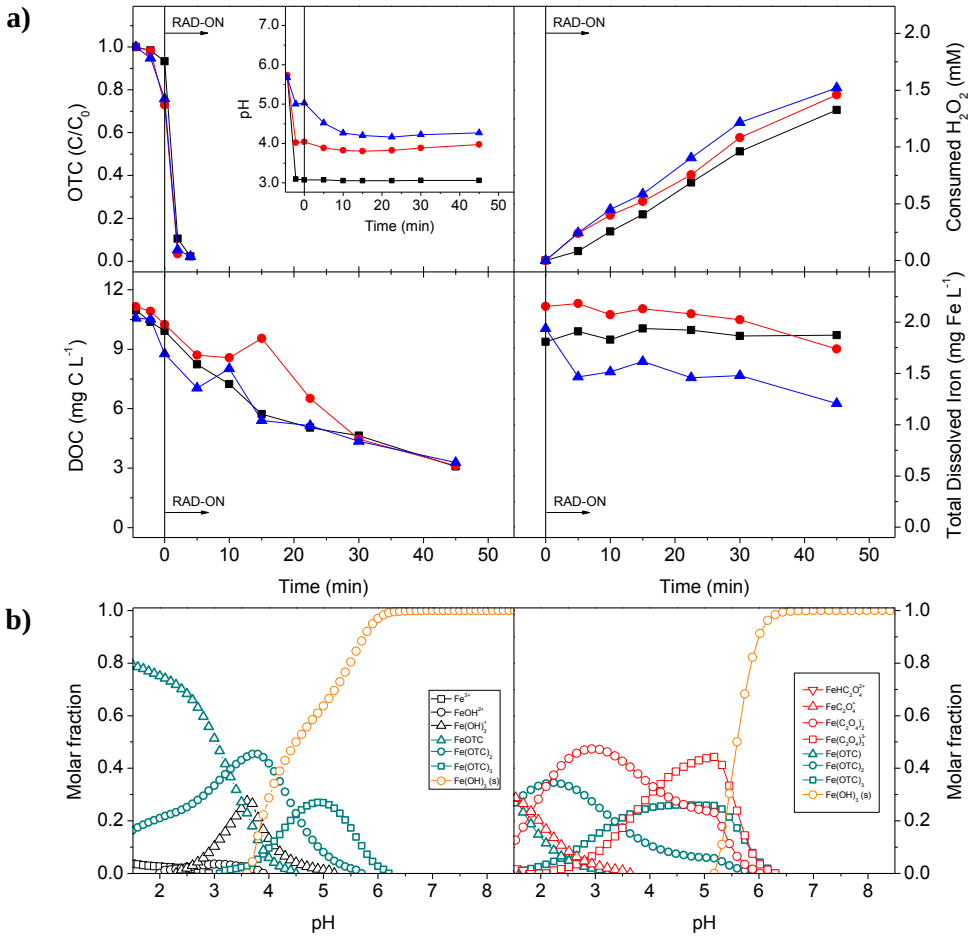

Figure 6.2. a) Effect of initial pH (■ - pH = 3.0; ● - pH = 4.0; ▲ - pH = 5.0) on the degradation of OTC (C_0 = 20 mg L^{-1}) using conventional solar photo-Fenton process mediated by 2 mg L^{-1} Fe (II). Follow-up of OTC degradation, DOC removal, H_2O_2 consumption, total dissolved iron and pH. Process parameters: T = 25 °C, I = 44 W_{UV} m^{-2}, total added H_2O_2 = 90 mg L^{-1}; **b)** Speciation diagrams for iron (III) as a function of pH in a solution containing 20 mg L^{-1} of OTC and 3.58 × 10^{-2} mM (2 mg L^{-1}) of Fe (III) without accounting (left) or accounting (right) for 1.07 × 10^{-1} mM (9.5 mg L^{-1}) oxalic acid. Ionic strength = 4 mM. The speciation software MINEQL+ was used to calculate the data.

In the three experiments performed, after the first addition of H_2O_2, the concentration of OTC approached LOQ levels approximately after 4 min of illumination (0.22 kJ_{UV} L^{-1}). The DOC levels slowly decreased down to near 30% of their initial values by the end of the photo-treatment period (45 min, 2.7 kJ_{UV} L^{-1}), while an average of 1.5 mM of H_2O_2 was consumed. Overall similar results were obtained by Bautitz and Nogueira (2007), who applied photo-Fenton mediated by iron (III) nitrate and potassium ferrioxalate at pH = 2.5 under black-light and solar irradiation to study the degradation of Tetracycline. In the present study, the only differences between the three experiments performed lie in the behaviour of the solution pH and in total dissolved iron concentration in the pH_0 = 5.0 experiment.

According to the OTC speciation diagram Figure 6.1b for pH values between 3.0 and 5.0, the molar fraction of zwitterionic OTC (H_2OTC) increases from 0.5 to nearly 1.0. Figueroa and Mackay (2005) and Gu and Karthikeyan (2005) reported that the expected initial decrease in the concentrations of OTC and DOC with increasing pH after the iron salt addition step is a consequence of the interaction between Fe (II) hydrous oxides and deprotonated OTC species.

Taking into consideration Eq. 6.01, after the Fe (II) oxidation step to Fe (III), the rapid decay of the antibiotic may be explained by the formation of stable complexes between OTC and Fe (III), which, according to the abovementioned authors, strongly interferes with HPLC measurements and may induce in erroneous kinetic calculations. Overall stability constants of the Fe (II)-OTC and Fe (III)-OTC complexes of 10.4 and 22.0, respectively, reported by Albert (1953), support this conclusion.

A survey of the available literature concerning Fe-OTC complex formation has shown a lack of agreement regarding the role of the different OTC species and the functional groups of the molecule in the stepwise formation of the 1:1, 1:2 and 1:3 metal-antibiotic complexes as a function of pH. Nevertheless, for clarification purposes, the complex formation between OTC and Fe (III) has been attempted using the equilibrium computer program MINEQL+ (Schecher and McAvoy, 2003).

To simplify the speciation diagram, only the zwitterionic OTC species was considered to interact with Fe (III), since it is the dominant species in the pH range used throughout this study (Figure 6.1b). Individual stability constants for 1:1 (log β_1 = 9.1), 1:2 (log β_2 = 7.08) and 1:3 (log β_3 = 5.08) iron-OTC complexes were also those used by Albert (1953) (Albert, 1953). Together with the default Fe (III) equilibrium reactions present in the software, the following equilibrium reactions (Eq. 6.05 to 6.07) were considered:

$$H_3OTC^{+} \leftrightarrow H_2OTC + H^{+} \quad (6.04)$$

$$Fe^{3+} + H_2OTC \leftrightarrow FeH_2OTC^{3+} \quad (6.05)$$

$$Fe^{3+} + 2(H_2OTC) \leftrightarrow Fe(H_2OTC)_2^{3+} \quad (6.06)$$

$$Fe^{3+} + 3(H_2OTC) \leftrightarrow Fe(H_2OTC)_3^{3+} \quad (6.07)$$

As seen in Figure 6.2b (left), a large fraction of Fe (III) would be expected to form complexes with the antibiotic. Bench-scale tests confirmed that by increasing the pH from 3.0 towards 5.0 of solutions containing only 2 mg L^{-1} Fe (III) and 20 mg L^{-1} of OTC, the original concentration of OTC not only gradually decreases but it also differs from filtered and non-filtered samples (data not shown). The same phenomenon occurs with DOC. As such, the

complete removal of OTC from solution by the conventional photo-Fenton reaction with increasing initial pH values could not be directly attributed. Zhou et al. (2012) also reported on the photo-reduction of Fe (III) in the Fe-OTC complexes, which is expected given the broad range of its UV-Vis spectrum (Figure 6.1c), leading to the oxidation of the OTC organic ligand (Chen et al., 2008). The low apparent quantum yield of the Fe (III)-Tetracycline complex photolysis, even at its highest UV absorbance peak (0.098, λ = 254 nm, pH = 3), adds to the decrease in H_2O_2 decomposition by the Fenton reaction and in the overall efficiency of the photo-Fenton process.

Silva et al. (2010) have demonstrated how the addition of organic ligands such as oxalate or citrate displaces the herbicide tebuthiuron (TBH) from the non-photoactive Fe (III)-TBH complex, improving the degradation process of TBH via the photo-Fenton reaction. In this way, we have introduced the following oxalate and iron-oxalate equilibrium reactions (Eq. 6.08 to 6.13) in MINEQL+ in order to calculate the formation of complexes between 2 mg Fe (III) L^{-1} with both 20 mg L^{-1} OTC and 9.5 mg L^{-1} oxalate (1:3 iron/oxalate ratio) present in solution. Dissociation constants of the oxalate and ferrioxalate species were those reported by Panias et al. (1996), corrected for 4 mM ionic strength using the Davies equation.

$$H_2C_2O_4 \leftrightarrow HC_2O_4^- + H^+ \quad (6.08)$$

$$HC_2O_4^- \leftrightarrow C_2O_4^{2-} + H^+ \quad (6.09)$$

$$Fe^{3+} + HC_2O_4^- \leftrightarrow FeHC_2O_4^{2+} \quad (6.10)$$

$$Fe^{3+} + C_2O_4^{2-} \leftrightarrow FeC_2O_4^+ \quad (6.11)$$

$$FeC_2O_4^+ + C_2O_4^{2-} \leftrightarrow Fe(C_2O_4)_2^- \quad (6.12)$$

$$Fe(C_2O_4)_2^- + C_2O_4^{2-} \leftrightarrow Fe(C_2O_4)_3^{3-} \quad (6.13)$$

Figure 6.2b (right) shows that the added oxalate clearly competes with OTC for the available Fe (III) in the pH range of interest. In the presence of oxalate, the concentration of OTC can also be properly followed by HPLC-DAD, which allows for a proper kinetic study. Taking this and the objective of operating this process at neutral pH values into consideration, the ability of carboxylates to improve the photo-Fenton process was henceforth studied.

6.3.2 Fe^{3+}/Carboxylate/H_2O_2/UV-Vis OTC degradation reactions

6.3.2.1 Influence of iron concentration

Figure 6.3a presents the OTC degradation efficiency by the photo-Fenton reaction using low iron concentrations in the threshold of the abovementioned iron discharge limit (1.0, 2.0 and 5.0

mg L^{-1}), with an iron/oxalate molar ratio of 1:3, without initial pH adjustment. The degradation profiles of OTC were very similar for all tested Fe (III) concentrations and the calculated pseudo-first order kinetic rate constants are presented in Table 6.1.

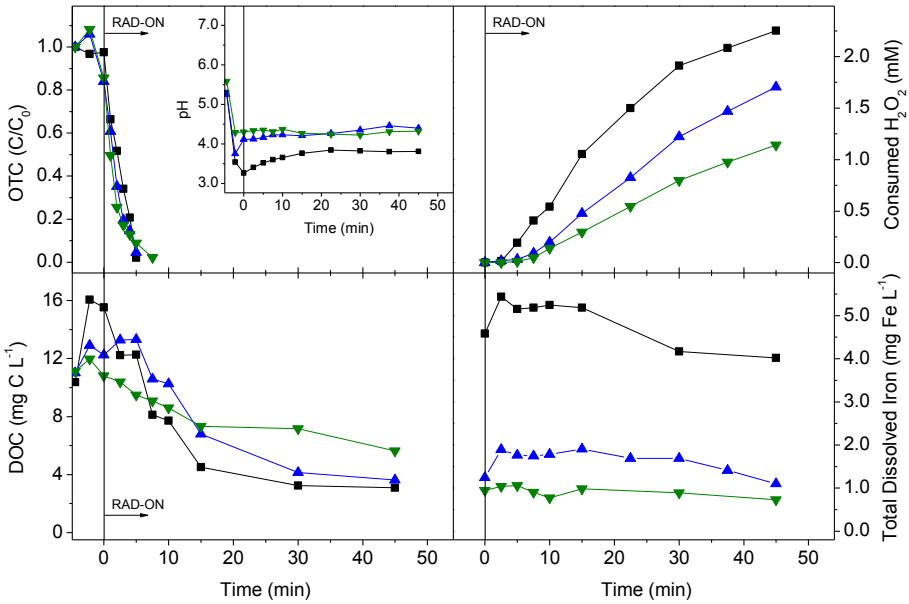

Figure 6.3. Effect of Fe (III) concentration (▼ – 1.0 mg L^{-1}; ▲ – 2.0 mg L^{-1}; ■ – 5.0 mg L^{-1}) on the degradation of OTC (C_0 = 20 mg L^{-1}) using solar photo-Fenton process mediated by ferrioxalate (1:3 iron/oxalate molar ratio). Follow-up of OTC degradation, DOC removal, H_2O_2 consumption, total dissolved iron and pH. Process parameters: T = 25 °C, I = 44 W_{UV} m^{-2}, initial pH unadjusted and total added H_2O_2 = 90 mg L^{-1}

A clear increase of reaction rates occurs with increasing iron amounts, but even with the lowest concentration tested, 1 mg L^{-1}, OTC was no longer detected (LOD = 0.10 mg L^{-1}) after 10 min of reaction (~0.6 kJ_{UV} L^{-1}). By the end of the photo-treatment period (45 min, 2.75 kJ_{UV} L^{-1}), 80% mineralization was achieved with both 2 and 5 mg L^{-1} of Fe (III), although a higher H_2O_2 consumption occurred with the highest Fe (III) concentration. In contrast, for 1 mg L^{-1} of Fe (III) only ~50% mineralization was achieved, with less H_2O_2 consumed than for the other Fe (III) concentrations. A direct relationship between the increases in hydroxyl radical formation and the initial Fe dosage is expected according to Eq. 6.01. The avoidance of the need of an iron removal step at the end of the treatment, associated with a satisfying mineralization degree, has shown 2 mg L^{-1} to be the concentration that represented the working option for photo-Fenton treatment with Fe (III)-oxalate complex.

The pseudo-first order kinetic rate constant of the 2 mg L^{-1} experiment, 8.6 ± 0.5 L kJ^{-1}, was the double of the rate constant reported in our previous work regarding the solar photocatalytic degradation of OTC in the presence of 0.5 g L^{-1} TiO_2 at a neutral pH, carried out with the same experimental installation, 4.3 ± 0.4 L kJ^{-1} (Pereira et al., 2013).

Table 6.1. Pseudo-first-order kinetic parameters for the Fe^{3+}/Oxalate/H_2O_2/UV-Vis process on the degradation of OTC (C_0 = 20 mg L^{-1}). Iron/oxalate molar ratio: 1:3. Overall conditions: total added H_2O_2 = 90 ppm; T = 25 °C; I = 44 W_{UV} m^{-2}.

Influence of iron concentration (unadjusted pH)			
Experiment	***k* (L kJ^{-1})[a]**	***R*²**	**S_R^2 (mg² L^{-2})**
[Fe^{3+}] = 1 mg L^{-1}	7.6 ± 0.4	0.993	0.207
[Fe^{3+}] = 2 mg L^{-1}	8.6 ± 0.5	0.988	2.111
[Fe^{3+}] = 5 mg L^{-1}	15.8 ± 0.8	0.994	1.076
Influence of initial pH ([Fe^{3+}] = 2 mg L^{-1})			
Experiment	***k* (L kJ^{-1})[a]**	***R*²**	**S_R^2 (mg² L^{-2})**
pH_0 ~ 4.0	8.6 ± 0.5	0.988	2.111
pH_0 = 5.0	6.3 ± 0.2	0.990	0.065
pH_0 = 6.0	2.3 ± 0.1	0.990	0.146
Influence of Temperature and Irradiance ([Fe^{3+}] = 2 mg L^{-1}, pH_0 = 5.0)			
Experiment	***k* (L kJ^{-1})[a]**	***R*²**	**S_R^2 (mg² L^{-2})**
T = 12 °C	3.4 ± 0.2	0.989	0.107
T = 35 °C	15.1 ± 0.6	0.998	0.012
I = 37 W_{UV} m^{-2}	7.5 ± 0.4	0.994	0.111
I = 24 W_{UV} m^{-2}	18 ± 2	0.987	0.513
Influence of Inorganic Ions and Humic Acids ([Fe^{3+}] = 2 mg L^{-1}, pH_0 = 5.0)			
Experiment	***k* (L kJ^{-1})[a]**	***R*²**	**S_R^2 (mg² L^{-2})**
+ 1.0 g L^{-1} Cl^-	5.8 ± 0.4	0.971	0.823
+ 1.0 g L^{-1} SO_4^{2-}	9.3 ± 0.9	0.974	0.541
+ 0.1 g L^{-1} HCO_3^-	7.9 ± 0.5	0.997	0.126
+ 1.0 g L^{-1} NO_3^-	7.2 ± 0.3	0.999	0.083
+ 5.0 mg C L^{-1} HA	5.3 ± 0.2	0.998	0.066
Influence of the matrix ([Fe^{3+}] = 2 mg L^{-1})			
Experiment	***k* (L kJ^{-1})[a]**	***R*²**	**S_R^2 (mg² L^{-2})**
WW effluent, pH_0 = 4.0	3.7 ± 0.3	0.991	0.417
WW effluent, pH_0 = 5.0	1.5 ± 0.2	0.964	0.799
TF effluent, pH_0 = 4.0	9.59 ± 0.04	0.999	0.001
TF effluent, pH_0 = 5.0	5.6 ± 0.4	0.997	0.277

a – pseudo-first order kinetic rate constant

6.3.2.2 Influence of initial solution pH

After the previous experiments, the effect of the initial solution pH value was studied in order to find the highest possible working pH without compromising the reaction efficiency. The results, presented in Figure 6.4a, show that with unadjusted initial pH (~4.1), pH = 5.0 and pH = 6.0, OTC was no longer detected after 5, 10 and 15 min of illumination time (0.3, 0.6 and 0.9 kJ L^{-1} of accumulated UV energy, respectively). By the same order, DOC concentration was reduced

by 75, 51 and 37% of its initial value after 45 min of reaction (2.78 kJ_{UV} L^{-1}). Despite the decreasing mineralization efficiency with increasing pH, there was not much difference between H_2O_2 consumption profiles.

First of all, it must be noted that after the oxalate and iron addition steps and consequent pH adjustment, the initial concentration of OTC still decreases with increasing pH. Examining the pH range between 4 and 6 in the attempted iron speciation diagram (Figure 6.2b, right), the sum of the fractions of oxalate and OTC iron complexes remain somewhat constant, while the formation of an iron solid phase (Ferrihydrite, $Fe(OH)_3$ (s)) is expected to form and rapidly increase after pH 5. Given the variation in both $Fe(C_2O_4)_2^+$ and $Fe(C_2O_4)_3^{3-}$ fractions, as well as in 1:2 and 1:3 Fe-OTC complexes, the observed phenomenon could be attributed either to a diminishing strength in complexing iron by $Fe(C_2O_4)_3^{3-}$ in favor of the 1:3 Fe-OTC complex, or to the slow formation of amorphous $Fe(OH)_3$, confirmed by the lower initial dissolved iron concentration measured in the experiments at pH 5.0 and 6.0 (Figure 6.4a). As soon as irradiation started, a competition phenomenon between both ligands (oxalate and OTC) to form complexes with iron occurs, as seen by the erratic behaviour of DOC.

A comparison with unfiltered DOC samples (data not shown) showed that in some sample points DOC is again retained in the filter. After hydroxyl radical attack of the original antibiotic molecule, some of the degradation products seems to retain iron (III)-chelating properties, whereby being retained in the filter at higher pH levels. However, after very low OTC concentrations, more iron is able to be chelated by oxalate, as a small increase in total dissolved iron concentration shows at 15 min. After this period, filtered and unfiltered DOC was found to be the same, so proper mineralization corresponds well with the marked increase in H_2O_2 consumption and possibly with the decarboxylation of ferrioxalate complexes, since iron levels begin to drop as well.

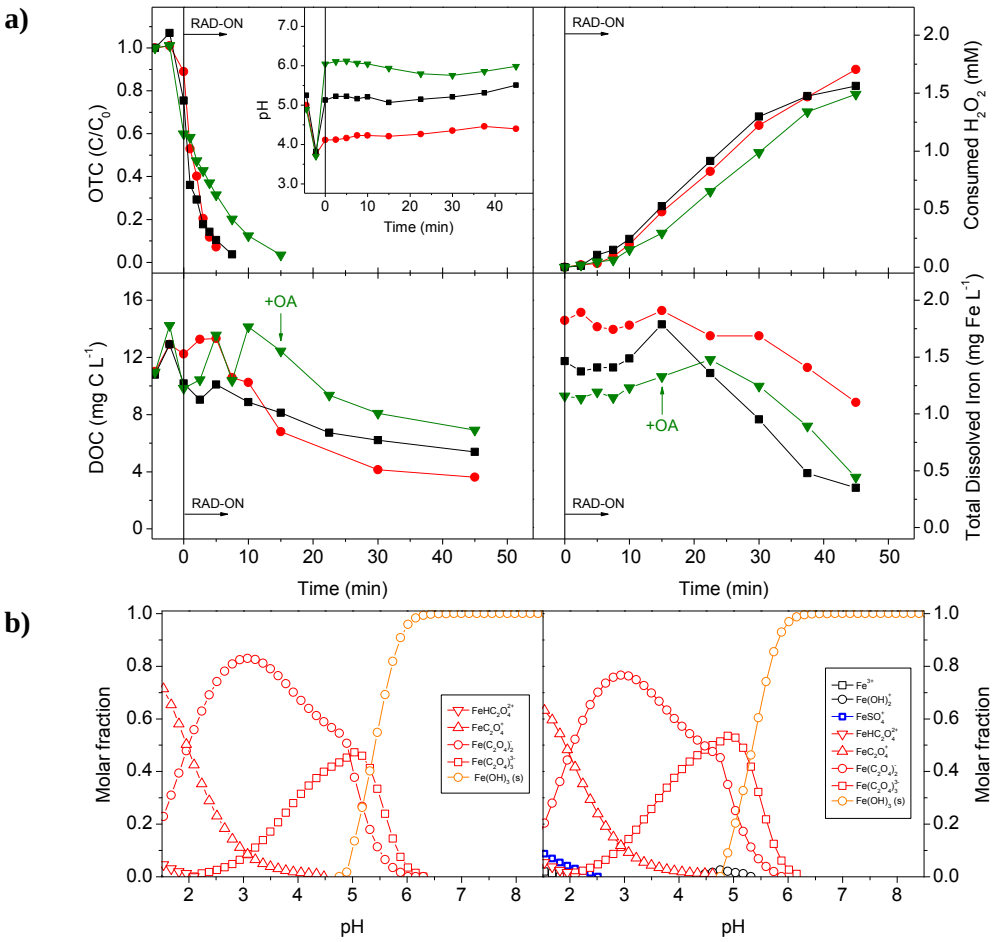

Figure 6.4. a) Effect of initial pH (● – pH_0 ~ 4.0; ■ - pH_0 = 5.0; ▼ - pH_0 = 6.0) on the degradation of OTC (C_0 = 20 mg L^{-1}) using solar photo-Fenton process mediated by 2 mg L^{-1} iron (III) and a 1:3 iron/oxalate molar ratio. Follow-up of OTC degradation, DOC removal, H_2O_2 consumption, total dissolved iron and pH. Process parameters: T = 25 °C, I = 44 W_{UV} m^{-2} and total added H_2O_2 = 90 mg L^{-1}.**b)** Speciation diagram for iron (III) as a function of pH in a solution containing 1.07 × 10^{-1} mM (9.5 mg L^{-1}) oxalic acid and 3.58 × 10^{-2} mM (2 mg L^{-1}) of Fe (III) without accounting (left) or accounting (right) for 10 mM (1 g L^{-1}) SO_4^{2-}. Ionic strength = 4 mM (left), Ionic strength = 30 mM (right). The speciation software MINEQL+ was used to calculate the data.

Furthermore, to counter the lower amount of total dissolved iron along the pH = 6.0 experiment, an extra dose of oxalic acid was added after this same point. Although indeed iron concentration increased, it quickly began to drop, with no considerable increase in the mineralization rate.

Regarding the influence of pH in the photochemistry itself, the role of the speciation of the main Fe (III)-oxalate complexes must be underlined. Faust and Zepp (1993) reported values of 1.0 and 0.6 at 436 nm for the two most photo-active Fe (III)-oxalate species, $Fe(C_2O_4)_2^-$ and $Fe(C_2O_4)_3^{3-}$, respectively. Recently, Weller et al. (2013) also determined individual quantum yields for $Fe(C_2O_4)_2^-$ as 1.17 (366 nm) and 1.40 (436 nm), and for $Fe(C_2O_4)_3^{3-}$ as 0.91 (366 nm) and 1.00 (436 nm). A speciation diagram discarding the Fe-OTC species, previously included for expository purposes only, has been calculated in the same manner (Figure 6.4b, left). Cumulatively, $Fe(C_2O_4)_2^-$ and $Fe(C_2O_4)_3^{3-}$ are the main iron species in the studied pH range, albeit with changing proportions over pH. It can be observed that the fraction of $Fe(C_2O_4)_2^-$ lowers smoothly from 0.7 down to less than 0.1, whereas the fraction of $Fe(C_2O_4)_3^{3-}$ evolves

from near 0.3, to a maximum of approximately 0.5 at pH = 5.0, and finally gets to less than 0.1 at pH = 6.0. Hence, by pH = 6.0, total iron precipitation would be expected. However, this precipitation occurs slowly, and Fe (III) may not be in equilibrium with the solid phase (Balmer and Sulzberger, 1999), so some oxalate is still expected to be found in solution, which may help to explain the decrease in the initial dissolved iron concentration shown at the maximum pH level tested.

The decreasing reaction rate constants at pH ~ 4.1, pH = 5.0 and pH = 6.0 experiments, 8.6 ± 0.5, 6.3 ± 0.2 and 2.3 ± 0.1 L^{-1} kJ, respectively, appear to reflect this relationship between the molar fractions of the referred iron-oxalate complexes and their respective quantum yields (Table 6.1). Considering these results, the working pH of 5.0 was chosen for the subsequent set of experiments, since no extra dosage of oxalic acid was needed to obtain a satisfactory 49 % mineralization of the initial DOC content, OTC was no longer detected after 10 min of illumination time (Q_{UV} = 0.6 kJ L^{-1}), and the final pH value of the solution approached the legal lower discharge pH value of 6.0 (Decree-Law n.º 236/98).

Before proceeding, two more experiments were performed: Fe^{3+}/Citrate/H_2O_2/UV-Vis system with 2 mg L^{-1} of Fe (III) and 1:1 iron/citrate molar ratio to compare the results with the previous unadjusted and adjusted initial pH = 5.0 Fe^{3+}/Oxalate/H_2O_2/UV-Vis reactions.

It can be seen in Figure 6.5a that for both initial pH values, the concentration of OTC after the citrate and ferric iron addition steps sharply decreases after only a minute of illumination time (Q_{UV} = 0.07 kJ L^{-1}). The residual amount (~12 % of $[OTC]_0$ in both cases) is slowly degraded until OTC is no longer detected after 5.0 and 7.5 min of reaction (0.3 and 0.4 kJ_{UV} L^{-1}) for unadjusted pH_0 and controlled pH_0 = 5.0, respectively. In the same order, the respective DOC content was reduced to 31 and 54% of its initial value by the end of the illumination periods, while an average of 1.49 mM of H_2O_2 was consumed.

The Fe^{3+}/Citrate/H_2O_2/UV-Vis system presented remarkably higher reaction rate constants with unadjusted and adjusted initial pH = 5.0, k = 23 ± 3 L kJ^{-1} and k = 23 ± 4 L kJ^{-1}, respectively. The speciation diagrams obtained with the MINEQL® software (Figure 6.5b) present significantly higher fractions of Fe (III) chelated with Citrate in the pH range of interest, compared with Oxalate. However, after the very quick initial OTC decay, total antibiotic removal seems to be hindered by the competitive effect of the progressive formation of not only intermediary byproducts resulting from OTC oxidation, but also from intermediates resulting from the ferricitrate decarboxylation (Rodríguez et al., 2009).

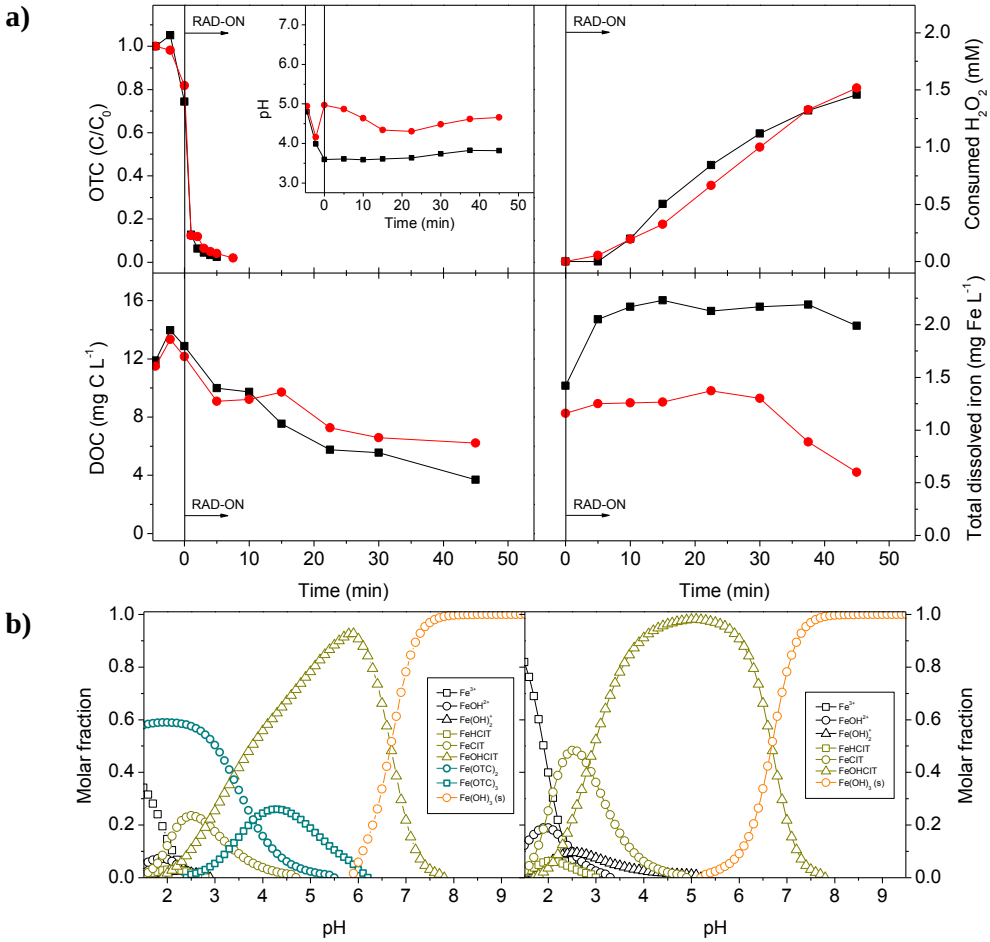

Figure 6.5. a) Effect of initial pH (■ - pH_0 ~ 3.6, ● – pH_0 = 5.0) on the degradation of OTC (C_0 = 20 mg L^{-1}) using solar photo-Fenton process mediated by 2 mg L^{-1} iron (III) and a 1:1 iron/citrate molar ratio. Follow-up of OTC degradation, DOC removal, H_2O_2 consumption, total dissolved iron and pH. Process parameters: T = 25 °C, I = 44 W_{UV} m^{-2} and total added H_2O_2 = 90 mg L^{-1}. **b)** Speciation diagram for iron (III) as a function of pH in a solution containing 3.58×10^{-2} mM (6.8 mg L^{-1}) citric acid and 3.58×10^{-2} mM (2 mg L^{-1}) of Fe (III), accounting (left) or not accounting (right) with 20 mg L^{-1} of OTC. Ionic strength = 4 mM. The speciation software MINEQL+ was used to calculate the data.

Feng et al. (2012) reported good Tetracycline (0-40 μM) photodegradation results at near neutral pH values using Fe (III)-citrate with substantially higher iron/citrate molar ratios (from 1:10 up to 1:30). Nevertheless, this would imply a significant addition of extra dissolved carbon, in the order of dozens of mg C L^{-1}. As a result, no further experiments with the Fe^{3+}/Citrate/H_2O_2/UV-Vis system were considered.

6.3.2.3 Influence of temperature and irradiance

When using photocatalytic systems under realistic conditions (solar pilot plants, for instance), special consideration must be given to two important process parameters, temperature and irradiance (Rodríguez et al., 2009; Zapata et al., 2009). There is a natural variability in solar irradiance depending on time of day, season of the year, atmospheric conditions, and even latitude, while the process usually takes place at ambient temperature (thus also depending on some of the abovementioned factors). In this way, further Fe^{3+}/Oxalate/H_2O_2/UV-Vis

experiments were performed under the chosen iron concentration, 2 mg L^{-1} of Fe (III), an iron/oxalate molar ratio of 1:3, and initial pH adjusted to 5.0, to screen the effects of different temperature and irradiance values on the decontamination of OTC in the lab-scale photoreactor.

Two typical water temperature values commonly achieved in summer and winter conditions in our CPC pilot-plant installation were tested, 12 and 35°C (Figure 6.6), and compared to the default set temperature (25 °C). The lower reaction rate constant achieved with 12 °C (3.4 ± 0.2 L kJ^{-1}) and the higher with 35 °C (15.1 ± 0.6 L kJ^{-1}), while OTC was no longer quantifiable after 10 and 3 min, respectively, reflect a positive role of temperature in the photo-Fenton process.

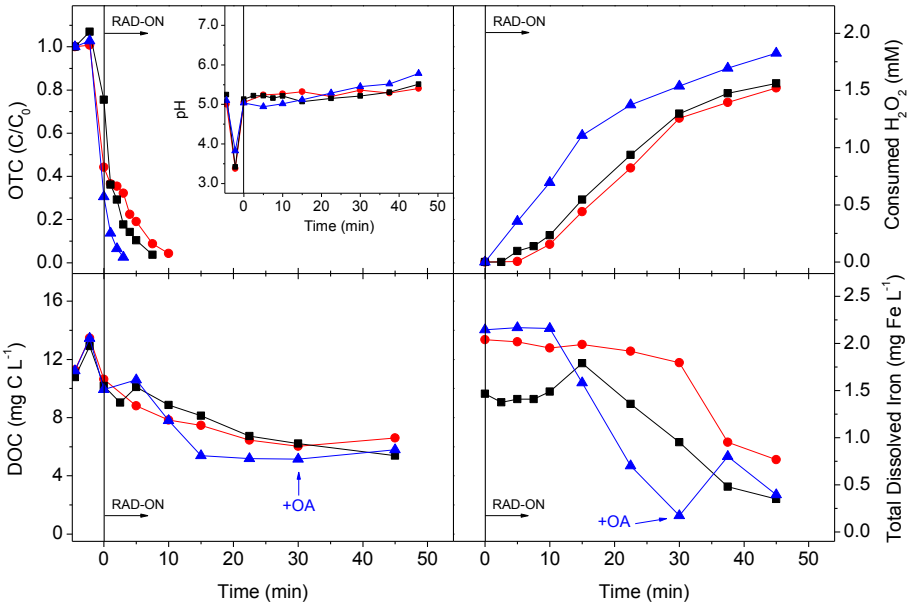

Figure 6.6. Degradation of OTC (C_0 = 20 mg L^{-1}) using solar photo-Fenton process mediated by 2 mg L^{-1} iron (III) and a 1:3 iron/oxalate molar ratio. Follow-up of OTC degradation, DOC removal, H_2O_2 consumption, total dissolved iron and pH. Process parameters: pH_0 = 5.0 and total added H_2O_2 = 90 mg L^{-1}. Effect of: **a)** Initial temperature (● – T = 12 °C; ■ - T = 25 °C; ▲ – T = 35 °C), I = 44 W_{UV} m^{-2}.

The quantum yield of ferrioxalate is independent of temperature (Nicodem and Aquilera, 1983), but higher temperatures promote the regeneration rate of ferrous iron from ferric iron, thereby increasing hydroxyl radical production (Pignatello et al., 2006), which, in this case, seems to be analogous to a likely faster consumption of oxalic acid (there is a steeper reduction in the DOC content) reflected in the earlier and more accentuated decrease in total dissolved iron concentration. Higher temperatures were not tested, because they may promote an inefficient H_2O_2 decomposition into H_2O and O_2 (Monteagudo et al., 2013).

Lower irradiances, 24 and 37 W_{UV} m^{-2}, on the other hand, did not result in major differences compared to the default value (I = 44 W_{UV} m^{-2}), regarding the required illumination time to fully degrade OTC, nor in H_2O_2 consumption rates (Figure 6.7).

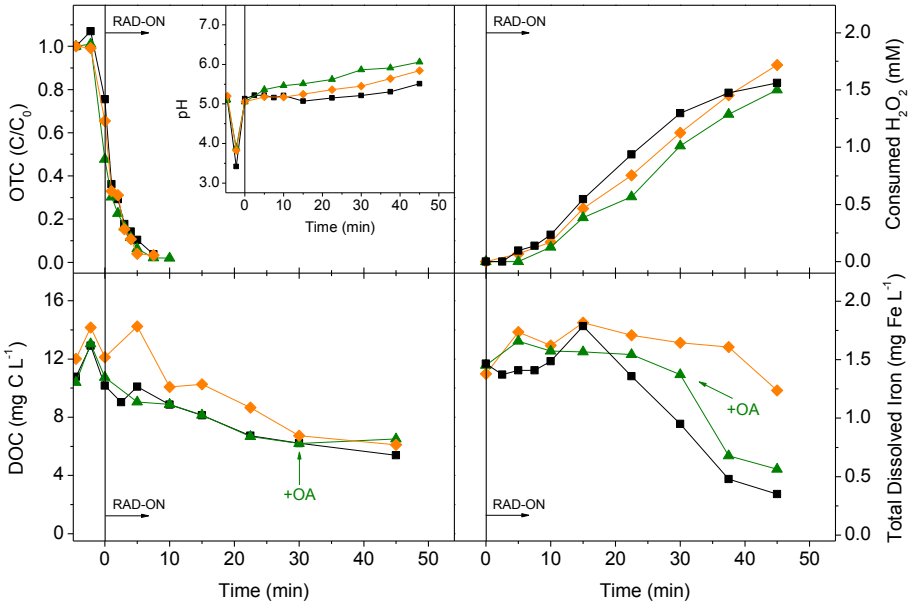

Figure 6.7. Degradation of OTC (C_0 = 20 mg L^{-1}) using solar photo-Fenton process mediated by 2 mg L^{-1} iron (III) and a 1:3 iron/oxalate molar ratio. Follow-up of OTC degradation, DOC removal, H_2O_2 consumption, total dissolved iron and pH. Process parameters: pH_0 = 5.0 and total added H_2O_2 = 90 mg L^{-1}. Effect of radiation intensity (♦ - I = 24.7 W_{UV} m^{-2}; ▲ – I = 37 W_{UV} m^{-2}; ■ - I = 44 W_{UV} m^{-2}), T = 25 °C.

Taking these results into consideration, the environmental/natural variation of these two parameters do not substantially affects the process efficiency, since the illumination time required for antibiotic disappearance and the achieved mineralization levels were otherwise similar under the conditions assayed.

6.3.2.4 Influence of inorganic anions and humic acids

Keeping in mind the perspective of applying the proposed process to treat concentrated micropollutants in retentates originating from membrane processes operation, the retention of other constituents which may affect the photo-Fenton process also needs to be considered (Martínez et al., 2013).

Inorganic anions, for instance, can concentrate up to the order of the hundreds of milligrams (Miralles-Cuevas et al., 2013), and may affect the process by i) complex formation with Fe (II) and Fe (III), ii) hydroxyl radicals scavenging and formation of less reactive inorganic radicals and iii) oxidation reactions involving these inorganic radicals (De Laat et al., 2004). The presence of dissolved natural organic matter, such as humic acids (HA), may also hamper the removal process since it may bind the micropollutants themselves (Gu et al., 2007), attenuate incoming radiation (Bautitz and Nogueira, 2007), act as a hydroxyl radical sink and finally, although their binding with iron may increase its solubility, it alters its redox cycle and changes the formation rate of hydroxyl radicals (Lindsey and Tarr, 2000).

For these reasons, a set of experiments was performed with 1 g L^{-1} of Cl^-, SO_4^{2-}, NO_3^-, 0.1 g L^{-1} of HCO_3^- and 5 mg C L^{-1} of HA to assess the individual effect of each interfering species in the degradation of OTC under the chosen conditions (Figure 6.8).

The required illumination time to bring the concentration of OTC under LOD levels only marginally increased in all experiments, except in the case of HA, which was longest. Likewise, HA was the only interfering species whose effect on the mineralization process was noteworthy, since initial DOC was only reduced by 35% against an average of 41% reduction compared to the other interfering species, and 46% in their absence, after 40 min of illumination time (Q_{UV} = 2.3 kJ L^{-1}). The overall consumption profiles of H_2O_2 reflected well these differences in mineralization degrees.

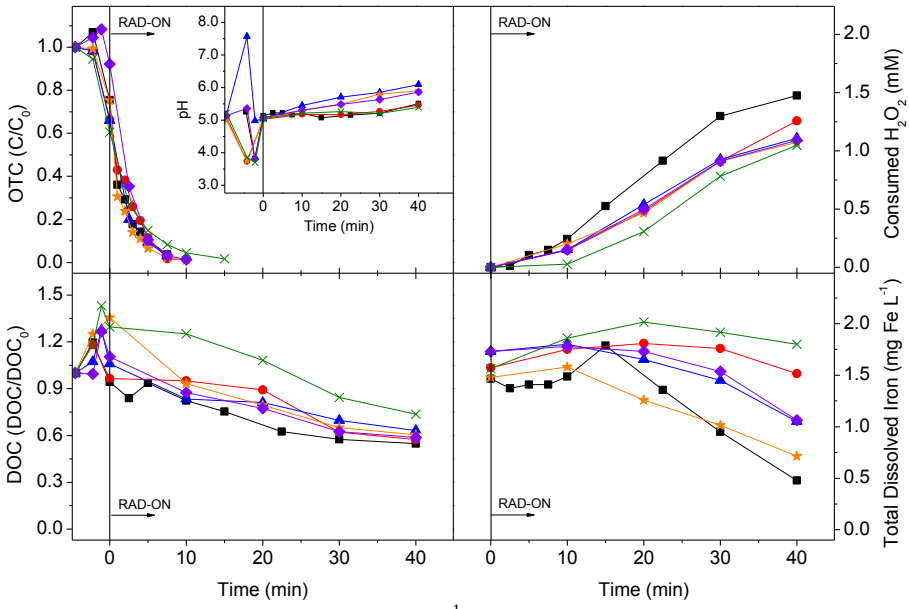

Figure 6.8. Follow-up of OTC degradation (C_0 = 20 mg L^{-1}), DOC removal, H_2O_2 consumption, total dissolved iron and pH in the absence (■) and in the presence of 1 g L^{-1} of Cl^- (●), SO_4^{2-} (★), NO_3^- (♦), 0.1 g L^{-1} of HCO_3^- (▲), 5 mg C L^{-1} of HA (×) using the solar photo-Fenton process mediated by 2 mg L^{-1} iron (III) and a 1:3 iron/oxalate molar ratio. Process parameters: pH_0 = 5.0, T = 25 °C, I = 44 W_{UV} m^{-2} and total added H_2O_2 = 90 mg L^{-1}.

This apparent weak impact in the reaction efficiency in the presence of iron-complexing species such as Cl^- or SO_4^{2-} could be also explained recurring to the study of the speciation of iron in solution via the MINEQL+ software. The equilibrium constants of ferrioxalate complexes are much higher than those of both Fe-Cl and Fe-SO_4 complexes (Truong et al., 2004), and thus it can be seen in Figure 6.4b that, for instance, the introduction of 1 g L^{-1} of SO_4^{2-} when plotting the iron complexes in solution (with the respective ionic strength correction, 30 mM) only alters the distribution of the $Fe(C_2O_4)_2^-$ complex in favor of $Fe(C_2O_4)_3^{3-}$, whereas none of the Fe-SO_4 complexes is shown to be formed at the pH range of interest.

6.3.2.5 *Influence of the matrix*

After assessing the potential influence of individual common wastewater components on the Fe^{3+}/Oxalate/H_2O_2/UV-Vis process, two different effluents were spiked with OTC (C_0 = 20 mg L^{-1}) to complementarily study the influence of real matrixes. Even though pH_0 = 5.0 was set beforehand as the chosen pH to study the process efficiency, experiments were also performed with pH_0= 4.0 in each media. This was due to the fact that after the oxalate and iron (III) addition steps, the pH of the TF effluent lowered to the same unadjusted pH of the DW solution, around 4.0. On the other hand, given composition of WW medium (Table 6.2), additional pH adjustment with acid was required, but it also helped to lower some of the initial inorganic carbon.

Table 6.2. Main characteristics of the tested effluents, before the OTC-spike step.

Effluent	pH	DOC / IC (mg L^{-1})	Average anion concentrations (mg L^{-1})		
			$[PO_4^{3-}]$	$[Cl^-]$	$[SO_4^{2-}]$
WW	6.46	5.5 / 5.1	13.5	61.5	42.9
TF	6.70	3.9 / 1.8	0.95		

The results comparing the efficiency of the process carried out in deionized water (DW), domestic wastewater (WW) and trout farm (TF) effluents are thus presented in Figure 6.9a. With pH_0 = 4.0, OTC was no longer detected after 10 min of illumination in WW effluent (Q_{UV} = 0.7 kJ L^{-1}), and after 6 min in TF effluent (Q_{UV} = 0.4 kJ L^{-1}). Required illumination times were higher in pH_0 = 5.0: 20 min in WW effluent (Q_{UV} = 1.4 kJ L^{-1}), and 10 min in TF effluent (Q_{UV} = 0.7 kJ L^{-1}).

The distribution of the iron (III) species in both media (Figure 6.9b) seems to explain the similar kinetic degradation rates achieved with TF effluent, and the worse with WW (Table 6.1). At pH_0 = 4.0, some fraction of iron (III) in the form of the mineral Strengite ($FePO_4.2H_2O$ (s)) is already expected to be found in WW, while in TF medium results, there is a relatively higher proportion of the more photo-active $Fe(C_2O_4)_2^-$ complex compared to that in DW (Figure 6.4b). The proportion of $FePO_4.2H_2O$ (s) at pH_0 = 5.0 in both effluents clearly reflects the lower OTC kinetic degradation rates, especially in the case of WW effluent.

Also to be considered is the abovementioned effect of the additional DOC/NOM content of both effluents in the overall process efficiency. Compared to the DW experiments, for instance, less H_2O_2 was consumed by the end of the photo-treatment period (45 min of illumination, Q_{UV} = 3.3 kJ L^{-1}), which may also reflect the lesser reduction in DOC content comparing with DW experiments at both tested pH values. Accounting for each effluent's initial DOC values, DOC reduction in WW effluent was of 39 and 31% for pH_0 = 4.0 and 5.0, respectively, whereas in TF effluent it was 56 and 49%, in the same order.

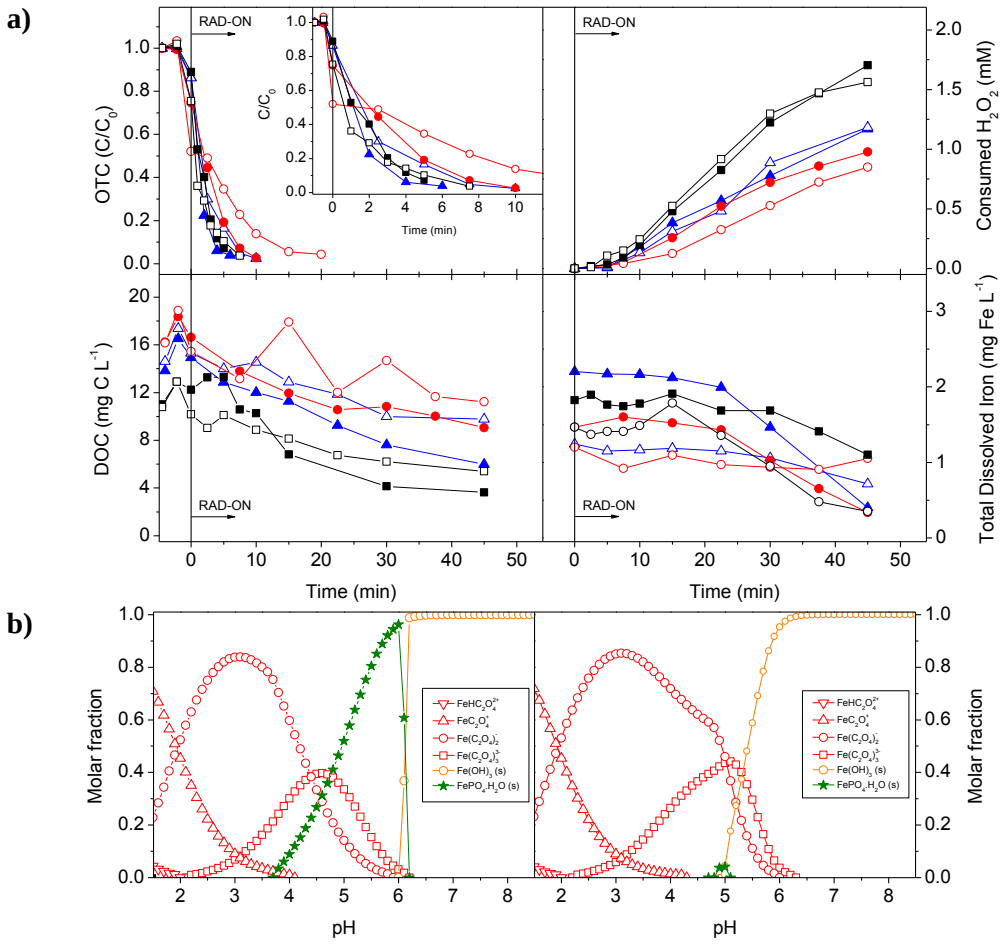

Figure 6.9. a) Effect of the matrix on OTC degradation (C_0 = 20 mg L^{-1}), DOC removal, H_2O_2 consumption and total dissolved iron using the solar photo-Fenton process mediated by 2 mg L^{-1} iron (III) and a 1:3 iron/oxalate molar ratio, performed at pH_0 = 4.0 (closed symbols) and pH_0 = 5.0 (open symbols). Matrixes: DW (■, □), TF (▲, △) WW (●, ○). Process parameters: T = 25 °C, I = 44 W_{UV} m^{-2} and total added H_2O_2 = 90 mg L^{-1}; **b)** Speciation diagram for iron (III) as a function of pH in WW (left) and TF (right) effluents, solution containing 1.07 × 10^{-1} mM (9.5 mg L^{-1}) oxalic acid and 3.58 × 10^{-2} mM (2 mg L^{-1}) of Fe (III). Ionic strength = 3 mM. The speciation software MINEQL+ was used to calculate the data.

6.3.3 Solar pilot-plant experiment

An experiment was also carried out in the CPC pilot-plant (Figure 6.10a) to compare the degradation of OTC by the Fe^{3+}/Oxalate/H_2O_2/UV-Vis system under real solar radiation conditions using the best conditions determined in the lab-scale experiments ([Fe (III) = 2 mg L^{-1}, 1:3 iron/oxalate molar ratio, pH_0 = 5.0, T = 25 °C, I = 44 W_{UV} m^{-2} and total added H_2O_2 = 90 mg L^{-1}).

To further increase the knowledge about the degradation efficiency, samples were also taken to follow-up the concentration of low-molecular-weight carboxylate anions (LMWCA, in terms of carbon content; individual concentrations in Figure 6.10b) and to monitor the antibacterial activity of the treated solution against *E. coli* (Figure 6.10c) along the reaction.

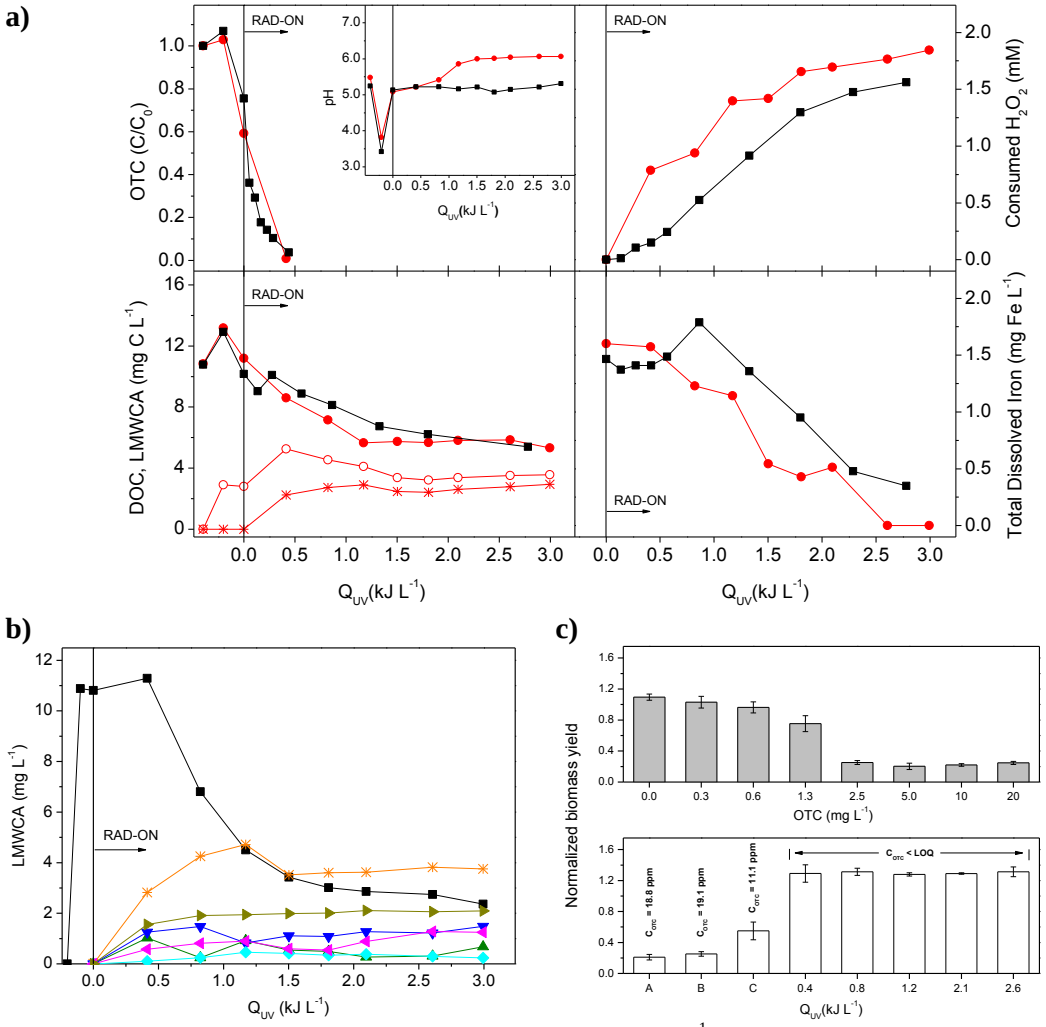

Figure 6.10. a) Evolution profiles of OTC degradation (C_0 = 20 mg L^{-1}), DOC removal, H_2O_2 consumption, total dissolved iron and pH using the solar photo-Fenton process mediated by 2 mg L^{-1} iron (III) and a 1:3 iron/oxalate molar ratio, performed in the lab-scale photoreactor (■) and in the pilot-plant (●). The sum of LMWCA in the pilot-plant experiment is shown with (○) and without (✳) initial oxalate concentration. Common process parameters: pH_0 = 5.0 and total added H_2O_2 = 90 mg L^{-1}. Lab-scale experiment process parameters: T = 25 °C, I = 44 W_{UV} m^{-2}; pilot-plant average process parameters: $\overline{T}$ = 26 °C, $\overline{UV}_G$ = 16 W_{UV} m^{-2}; **b)** Evolution profiles of detected low-molecular-weigth carboxylate anions during the solar pilot-plant experiment: oxalate (■), oxamate (✳) tartronate (▲), acetate (▼), malonate (♦), maleate (◄) and formate (►); **c)** Normalized biomass yield of *E. coli* DSM 1103 grown in the presence of different concentrations of OTC standards (upper, grey bars), and in the presence of samples taken at different photo-treatment periods (lower, white bars) of the experiment performed in the pilot-plant. Values represent means and standard deviation (n = 3). A – OTC only, B – OTC and added oxalic acid, C – OTC and added oxalic acid and Fe (III).

After the same amount of accumulated energy per litre of solution recorded in the lab-scale experiment (Q_{UV} = 0.41 kJ L^{-1}), OTC was no longer detected (Figure 6.10a). At the same time, the remaining organic matter no longer exhibited antibacterial activity (Figure 6.10c). A similar behavior was reported in a previous work (Pereira et al., 2013), where a solution containing 40 mg L^{-1} of OTC, treated with 0.5 g L^{-1} of TiO_2 in the same pilot-plant, lost its antibacterial activity against *E. coli* when OTC was nearly depleted after 2.0 kJ_{UV} of accumulated UV energy per liter of solution. Even though there was higher consumption of H_2O_2 along the same illumination period, the mineralization profile matches quite well with the one of the lab-scale experiment, achieving a final reduction of 51% of the initial DOC. The profile of the sum of

LMWCA (plotted in mg C L^{-1}) can also be seen in Figure 6.10b, where at Q_{UV} = 0.0 kJ_{UV} L^{-1} only oxalate was present after the addition of the 3:1 molar ratio to 2 mg L^{-1} of Fe (III) dose. After illumination started, and until Q_{UV} = 0.41 kJ_{UV} L^{-1}, the period when OTC was mostly degraded, there was a quick conversion of DOC into carboxylic acids. At this point, 61% of DOC consisted in still undepleted oxalate and in oxamate, tartronate, acetate, maleate and formate in smaller quantities. Afterwards, oxalic acid began to slowly deplete (corresponding well with the progressive decrease in the concentration of total dissolved iron), and until Q_{UV} = 1.17 kJ_{UV} L^{-1} a peak of 72.5% of DOC in the form of LMWCA was achieved, equivalent to the point where the mineralization process began to slow down, achieving the abovementioned final DOC level, from which 67.2% is in the form of low concentrations of oxalate, oxamate, tartronate, acetate, malonate, maleate and formate anions.

The hampering of the mineralization process along the illumination time parallels well with the decay of oxalate and the formation of the detected carboxylates. Some are generally quite stable in solution, such as acetate and formate (Franch et al., 2004), others are recalcitrant to hydroxyl radical attack (Garcia-Segura and Brillas, 2011), such as oxamate, while others, though being able to form Fe (III)-complexes as well, have lower or non-existent quantum yields of Fe (II) formation, such as malonate (Rodríguez et al., 2009).

Regarding the fate of the nitrogen atoms present in the original 20 mg L^{-1} OTC solution (around 1.2 mg N L^{-1}), 60% of the original N content is in the detected oxamate by the end of the photo-treatment period. The remaining N content could not be quantified by the ion chromatography.

6.4 Conclusions

In this work, it was shown how the highly photo-active ferricarboxylate complexes successfully promotes the photo-Fenton reaction in a lab-scale apparatus simulating solar radiation, equipped with a CPC photo-reactor, to remove the antibiotic Oxytetracycline from aqueous solution at near-neutral pH values.

The oxalic acid in a 1:3 iron/oxalate molar ratio with the aim of forming iron/oxalate complexes showed to be better than citric acid in a 1:1 iron/citrate molar ratio in deterring the inconvenient formation of Fe:OTC complexes, which undermine OTC analytical detection and hamper the regeneration of Fe (III) into Fe (II).

Good antibiotic and DOC removals were achieved using the maximum allowed iron concentration in treated effluents (2 mg L^{-1} of Fe (III)), oxalic acid in a 1:3 iron/oxalate molar ratio, and the initial pH of 5.0, requiring overall low accumulated UV energy per liter of solution.

Furthermore, it was shown that these operating conditions are not remarkably affected by temperature, irradiance and presence of individual possible interfering species such as Cl^-, SO_4^{2-}, NO_3^- and HCO_3^-, while the presence of dissolved organic matter (humic acids) affected more the reaction. By contrast, experiments performed in a domestic WWTP effluent showed slower OTC removal kinetics and lower DOC reduction mainly due to the precipitation of $FePO_4$. However, in a less complex effluent from the outlet of a trout farm it was shown that without the pH adjustment step, similar results were achieved, compared with deionized water experiments.

An experiment carried out in a CPC pilot-plant under real solar radiation compared well with the lab-scale photoreactor using simulated solar radiation. The treated solution loses antibacterial activity against *E. coli* as soon as OTC is degraded, and the remaining DOC is quickly converted to low-molecular-weight carboxylate anions. Although these are mostly recalcitrant to further mineralization by hydroxyl radical attack, they are easily biodegradable. Not only their final percentage in terms of DOC is quite high, but also, with the depletion of oxalic acid, the final pH achieved by the end of the treatment also meets the minimum discharge limit, reducing the need of relevant post-phototreatment steps.

6.5 References

Decree-Law n.º 236/98. 1st of August 1998. Diário da República - I Série-A, Portugal, pp. 3676-3722.

Albert, A., 1953. Avidity of Terramycin and Aureomycin for Metallic Cations. Nature 172, 201-201.

Balmer, M.E., Sulzberger, B., 1999. Atrazine degradation in irradiated iron/oxalate systems: Effects of pH and oxalate. Environ. Sci. Technol. 33, 2418-2424.

Batista, A.P.S., Nogueira, R.F.P., 2012. Parameters affecting sulfonamide photo-Fenton degradation - Iron complexation and substituent group. J. Photochem. Photobiol. A: Chem. 232, 8-13.

Bautitz, I.R., Nogueira, R.F.P., 2007. Degradation of tetracycline by photo-Fenton process - Solar irradiation and matrix effects. J. Photochem. Photobiol. A: Chem. 187, 33-39.

Chen, Y., Hu, C., Qu, J., Yang, M., 2008. Photodegradation of tetracycline and formation of reactive oxygen species in aqueous tetracycline solution under simulated sunlight irradiation. J. Photochem. Photobiol. A: Chem. 197, 81-87.

De Laat, J., Truong Le, G., Legube, B., 2004. A comparative study of the effects of chloride, sulfate and nitrate ions on the rates of decomposition of H_2O_2 and organic compounds by Fe(II)/H_2O_2 and Fe(III)/H_2O_2. Chemosphere 55, 715-723.

Escher, B.I., Baumgartner, R., Koller, M., Treyer, K., Lienert, J., McArdell, C.S., 2011. Environmental toxicology and risk assessment of pharmaceuticals from hospital wastewater. Water Res. 45, 75-92.

Faust, B.C., Zepp, R.G., 1993. Photochemistry of aqueous iron(III)-polycarboxylate complexes: Roles in the chemistry of atmospheric and surface waters. Environ. Sci. Technol. 27, 2517-2522.

Feng, X., Wang, Z., Chen, Y., Tao, T., Wu, F., 2012. Multivariate-Parameter Optimization for Photodegradation of Tetracycline by Fe(III)-Citrate Complexes at Near-Neutral pH. J. Environ. Eng. 138, 873-879.

Figueroa-Diva, R.A., Vasudevan, D., MacKay, A.A., 2010. Trends in soil sorption coefficients within common antimicrobial families. Chemosphere 79, 786-793.

Figueroa, R.A., Mackay, A.A., 2005. Sorption of oxytetracycline to iron oxides and iron oxide-rich soils. Environ. Sci. Technol. 39, 6664-6671.

Franch, M.I., Ayllón, J.A., Peral, J., Domènech, X., 2004. Fe(III) photocatalyzed degradation of low chain carboxylic acids: implications of the iron salt. Appl. Catal., B 50, 89-99.

Garcia-Segura, S., Brillas, E., 2011. Mineralization of the recalcitrant oxalic and oxamic acids by electrochemical advanced oxidation processes using a boron-doped diamond anode. Water Res. 45, 2975-2984.

Ghandour, M.A., Azab, H.A., Hassan, A., Ali, A.M., 1992. Potentiometric studies on the complexes of tetracycline (TC) and oxytetracyclin (OTC) with some metal ions. Monatsh. Chem. Chem. Mon. 123, 51-58.

Gogate, P.R., Pandit, A.B., 2004a. A review of imperative technologies for wastewater treatment I: Oxidation technologies at ambient conditions. Adv. Environ. Res. 8, 501-551.

Gogate, P.R., Pandit, A.B., 2004b. A review of imperative technologies for wastewater treatment II: Hybrid methods. Adv. Environ. Res. 8, 553-597.

Gu, C., Karthikeyan, K.G., 2005. Interaction of tetracycline with aluminum and iron hydrous oxides. Environ. Sci. Technol. 39, 2660-2667.

Gu, C., Karthikeyan, K.G., Sibley, S.D., Pedersen, J.A., 2007. Complexation of the antibiotic tetracycline with humic acid. Chemosphere 66, 1494-1501.

Homem, V., Santos, L., 2011. Degradation and removal methods of antibiotics from aqueous matrices - A review. J. Environ. Manage. 92, 2304-2347.

Huang, W., Brigante, M., Wu, F., Hanna, K., Mailhot, G., 2012. Development of a new homogenous photo-Fenton process using Fe(III)-EDDS complexes. J. Photochem. Photobiol. A: Chem. 239, 17-23.

Jeong, J., Yoon, J., 2005. pH effect on OH radical production in photo/ferrioxalate system. Water Res. 39, 2893-2900.

Jones, A.D., Bruland, G.L., Agrawal, S.G., Vasudevan, D., 2005. Factors influencing the sorption of oxytetracycline to soils. Environ. Toxicol. Chem. 24, 761-770.

Kong, W.D., Zhu, Y.G., Fu, B.J., Marschner, P., He, J.Z., 2006. The veterinary antibiotic oxytetracycline and Cu influence functional diversity of the soil microbial community. Environ. Pollut. 143, 129-137.

Kümmerer, K., 2009. The presence of pharmaceuticals in the environment due to human use - present knowledge and future challenges. J. Environ. Manage. 90, 2354-2366.

Lalonde, B.A., Ernst, W., Greenwood, L., 2012. Measurement of oxytetracycline and emamectin benzoate in freshwater sediments downstream of land based aquaculture facilities in the Atlantic Region of Canada. Bull. Environ. Contam. Toxicol. 89, 547-550.

Lindsey, M.E., Tarr, M.A., 2000. Inhibition of hydroxyl radical reaction with aromatics by dissolved natural organic matter. Environ. Sci. Technol. 34, 444-449.

Liu, H., Yang, Y., Kang, J., Fan, M., Qu, J., 2012. Removal of tetracycline from water by Fe-Mn binary oxide. J. Environ. Sci. 24, 242-247.

Loos, R., Gawlik, B.M., Locoro, G., Rimaviciute, E., Contini, S., Bidoglio, G., 2009. EU-wide survey of polar organic persistent pollutants in European river waters. Environ. Pollut. 157, 561-568.

Malato, S., Fernández-Ibáñez, P., Maldonado, M.I., Blanco, J., Gernjak, W., 2009. Decontamination and disinfection of water by solar photocatalysis: Recent overview and trends. Catal. Today 147, 1-59.

Manaia, C.M., Vaz-Moreira, I., Nunes, O.C., 2012. Antibiotic Resistance in Waste Water and Suface Water and Human Health Implications. in: D. Barceló (Ed.) Emerging Organic Contaminants and Human Health. Springer-Verlag Berling and Heidelberg GmbH & Co. KG, pp. 173-212.

Martínez, F., López-Muñoz, M.J., Aguado, J., Melero, J.A., Arsuaga, J., Sotto, A., Molina, R., Segura, Y., Pariente, M.I., Revilla, A., Cerro, L., Carenas, G., 2013. Coupling membrane separation and photocatalytic oxidation processes for the degradation of pharmaceutical pollutants. Water Res. 47, 5647-5658.

Michael, I., Rizzo, L., McArdell, C.S., Manaia, C.M., Merlin, C., Schwartz, T., Dagot, C., Fatta-Kassinos, D., 2013. Urban wastewater treatment plants as hotspots for the release of antibiotics in the environment: A review. Water Res. 47, 957-995.

Mikelens, P., Levinson, W., 1978. Nucleic-acid binding by tetracycline·metal ion complexes. Bioinor. Chem. 9, 421-429.

Miralles-Cuevas, S., Arqués, A., Maldonado, M.I., Sánchez-Pérez, J.A., Malato Rodríguez, S., 2013. Combined nanofiltration and photo-Fenton treatment of water containing micropollutants. Chem. Eng. J. 224, 89-95.

Monteagudo, J.M., Durán, A., Corral, J.M., Carnicer, A., Frades, J.M., Alonso, M.A., 2012. Ferrioxalate-induced solar photo-Fenton system for the treatment of winery wastewaters. Chem. Eng. J. 181-182, 281-288.

Monteagudo, J.M., Durán, A., Culebradas, R., San Martín, I., Carnicer, A., 2013. Optimization of pharmaceutical wastewater treatment by solar/ferrioxalate photo-catalysis. J. Environ. Manage. 128, 210-219.

Nicodem, D.E., Aquilera, O.M.V., 1983. Standardization of the potassium ferrioxalate actinometer over the temperature range 5 – 80 °C. J. Photochem. 21, 189-193.

Noga, E.J., 2010. Fish Disease: Diagnosis and Treatment, Second Edition. Second ed., Wiley-Blackwell.

Ogunniran, K.O., Tella, A.C., Alensela, M., Yakubu, M.T., 2007. Synthesis, physical properties, antimicrobial potentials of some antibiotics complexed with transition metals and their effects on alkaline phosphatase activities of selected rat tissues. Afr. J. Biotechnol. 6, 1202-1208.

Panias, D., Taxiarchou, M., Douni, I., Paspaliaris, I., Kontopoulos, A., 1996. Thermodynamic analysis of the reactions of iron oxides: Dissolution in oxalic acid. Can. Metall. Q. 35, 363-373.

Pereira, J.H.O.S., Reis, A.C., Queirós, D., Nunes, O.C., Borges, M.T., Vilar, V.P., Boaventura, R.A.R., 2013. Insights into solar TiO_2-assisted photocatalytic oxidation of two antibiotics employed in aquatic animal production, oxolinic acid and oxytetracycline. Sci. Total Environ. 463-464, 274-283.

Pereira, J.H.O.S., Vilar, V.J.P., Borges, M.T., González, O., Esplugas, S., Boaventura, R.A.R., 2011. Photocatalytic degradation of oxytetracycline using TiO_2 under natural and simulated solar radiation. Sol. Energy 85, 2732-2740.

Pignatello, J.J., Oliveros, E., MacKay, A., 2006. Advanced oxidation processes for organic contaminant destruction based on the fenton reaction and related chemistry. Crit. Rev. Environ. Sci. Technol. 36, 1-84.

Prato-Garcia, D., Vasquez-Medrano, R., Hernandez-Esparza, M., 2009. Solar photoassisted advanced oxidation of synthetic phenolic wastewaters using ferrioxalate complexes. Sol. Energy 83, 306-315.

Qiang, Z., Adams, C., 2004. Potentiometric determination of acid dissociation constants (pKa) for human and veterinary antibiotics. Water Res. 38, 2874-2890.

Rigos, G., Nengas, I., Alexis, M., 2006. Oxytetracycline (OTC) uptake following bath treatment in gilthead sea bream (*Sparus aurata*). Aquaculture 261, 1151-1155.

Rodríguez, E.M., Núñez, B., Fernández, G., Beltrán, F.J., 2009. Effects of some carboxylic acids on the Fe(III)/UVA photocatalytic oxidation of muconic acid in water. Appl. Catal., B 89, 214-222.

Schecher, W.D., McAvoy, D.C., MINEQL+: A Chemical Equilibrium Modeling System, Version 4.5 for Windows. Environmental Research Software, Hallowell, Maine, 2003.

Silva, M.R.A., Trovó, A.G., Nogueira, R.F.P., 2007. Degradation of the herbicide tebuthiuron using solar photo-Fenton process and ferric citrate complex at circumneutral pH. J. Photochem. Photobiol. A: Chem. 191, 187-192.

Silva, M.R.A., Vilegas, W., Zanoni, M.V.B., Pupo Nogueira, R.F., 2010. Photo-Fenton degradation of the herbicide tebuthiuron under solar irradiation: Iron complexation and initial intermediates. Water Res. 44, 3745-3753.

Tamminen, M., Karkman, A., Lõhmus, A., Muziasari, W.I., Takasu, H., Wada, S., Suzuki, S., Virta, M., 2011. Tetracycline resistance genes persist at aquaculture farms in the absence of selection pressure. Environ. Sci. Technol. 45, 386-391.

Truong, G.L., Laat, J.D., Legube, B., 2004. Effects of chloride and sulfate on the rate of oxidation of ferrous ion by H_2O_2. Water Res. 38, 2384-2394.

Verlicchi, P., Galletti, A., Petrovic, M., Barceló, D., 2010. Hospital effluents as a source of emerging pollutants: An overview of micropollutants and sustainable treatment options. J. Hydrol. 389, 416-428.

Watkinson, A.J., Murby, E.J., Kolpin, D.W., Costanzo, S.D., 2009. The occurrence of antibiotics in an urban watershed: From wastewater to drinking water. Sci. Total Environ. 407, 2711-2723.

Weller, C., Horn, S., Herrmann, H., 2013. Effects of Fe(III)-concentration, speciation, excitation-wavelength and light intensity on the quantum yield of iron(III)-oxalato complex photolysis. J. Photochem. Photobiol. A: Chem. 255, 41-49.

Westerhoff, P., Moon, H., Minakata, D., Crittenden, J., 2009. Oxidation of organics in retentates from reverse osmosis wastewater reuse facilities. Water Res. 43, 3992-3998.

Zapata, A., Oller, I., Bizani, E., Sánchez-Pérez, J.A., Maldonado, M.I., Malato, S., 2009. Evaluation of operational parameters involved in solar photo-Fenton degradation of a commercial pesticide mixture. Catal. Today 144, 94-99.

Zhou, D., Wang, J., Hou, L., Xu, J., Zhao, Y., Photochemistry of Fe(III)-tetracycline complexes in aqueous solution under UV irradiation. Guilin, Guangxi, 2012, pp. 608-611.

7 Biodegradation of Amoxicillin by a Mixed Culture and Oxidation of Metabolic By-products by Solar Photocatalysis

This Chapter studies the feasibility of using a multistage treatment system for amoxicillin (AMX) spiked solutions combining: i) a biological treatment process using an enriched culture to metabolize AMX, with ii) a solar photocatalytic system to achieve the removal of the metabolized transformation products (TPs) identified via LC-MS, recalcitrant to further biological degradation. Firstly, a mixed culture (MC) was obtained through the enrichment of an activated sludge sample collected in an urban wastewater treatment plant (WWTP). Secondly, different aqueous matrices spiked with AMX were treated with the MC and the metabolic transformation products were identified. Thirdly, the efficiency of two solar assisted photocatalytic processes (TiO_2/UV or Fe^{3+}/Oxalate/H_2O_2/UV-Vis) was assessed in the degradation of the obtained TPs using a lab-scale prototype equipped with a compound parabolic collector (CPC).

This Chapter is based on the research article "João H.O.S. Pereira, Ana C. Reis, Vera Homem, José A. Silva, Arminda Alves, Maria T. Borges, Rui A. R. Boaventura, Vítor J. P. Vilar, Olga C. Nunes. Solar Photocatalytic Oxidation of Recalcitrant Natural Metabolic By-products of Amoxicillin Biodegradation" (2014). Submitted . Ana C. Reis is the co-author of this work.

7.1 Introduction

In the last decades, the use of antibiotic has evolved from preventing and treating human and veterinary infections to other applications in diverse areas, such as agriculture, aquaculture and animal husbandry (Kümmerer, 2009). To this date, β-lactams remain one of the most important and prescribed group of antibiotics (Bailon-Perez et al., 2008), with amoxicillin (AMX) as one of most relevant of its class. Amoxicillin is a broad-spectrum and semi-synthetic penicillin, mainly (80-90%) excreted in unchanged form due to its low metabolism in the organism (Hirsch et al., 1999).

Conventional wastewater treatment technologies are unable to achieve complete antibiotic removal. Watkinson et al. (2007) found a maximum concentration of 280 ng L^{-1} in raw sewage and 30 ng L^{-1} in the final effluent of a conventional wastewater treatment plant (WWTP) in Brisbane (Australia); while Andreozzi et al. (2004) reported a maximum concentration of 120 ng L^{-1} in a WWTP effluent in Palermo (Italy). Christian et al. (2003) reported AMX concentrations below 10 ng L^{-1} in only 4 of 32 samples taken in 16 river banks in North Rhine-Westphalia (Germany). Consequently, part of this antibiotic reaches the environment in the active form. Despite of the fact that antibiotics such as AMX present low persistence and concentration in water matrices, this is compensated by their intensive use and continuous discharge into the environment (Petrović et al., 2003; Kemper, 2008). Deshpande et al. (2004) suggest that the infrequent detection of AMX in the environment could be explained by low efficiency and sensitivity of extraction and detection methods, combined with the highly reactive β-lactam ring, which is broken under a wide range of environmental conditions (e.g. low or high pH, high temperature and by β-lactamase action).

Amoxicillin has low toxicity and, for that reason, direct effects in the environment are highly unlikely (Kemper, 2008). Nevertheless, indirect effects, such as propagation of β lactam resistant bacteria (Schwartz et al., 2003) and the impact of metabolites are more pressing concerns. Several studies reported an increasing proportion of β-lactam resistant organisms after wastewater treatment (Zhang et al., 2009; Łuczkiewicz et al., 2010; Novo and Manaia, 2010; Merlin et al., 2011; Mokracka et al., 2012; Rizzo et al., 2013). Possible causes include the rearrangement of the bacterial populations, whereby antibiotic susceptible bacteria are outcompeted, and horizontal gene transfer, whereby antibiotic resistance genetic determinants are transferred into susceptible organisms (Figueira et al., 2011). It is also known that metabolized penicillins lose their antimicrobial properties, albeit retaining allergenic properties that can cause, to some extent, adverse reactions in sensitive individuals (Torres et al., 2010).

A high content of these transformation products has also been detected in the environment (Li et al., 2008; Lamm et al., 2009; Pérez-Parada et al., 2011).

Given the aforementioned detrimental effects, the development of treatment methods able to remove antibiotic residues and their by-products is henceforth an environmental priority. With this in mind, advanced oxidation processes (AOPs) are known as highly efficient methods to treat otherwise recalcitrant organic pollutants. They are characterized by different ways of generating the highly reactive and non-selective hydroxyl radical ($^{\bullet}OH$) and other reactive oxygen species (Gogate and Pandit, 2004b; a). As a way of reducing operating costs, recent research has been focusing on the combination of AOPs able to use solar radiation as the source of UV photons, such as TiO_2/UV and the photo-Fenton process, with biological oxidation systems as a pre- or post-treatment stage (González et al., 2008; Elmolla and Chaudhuri, 2011; Oller et al., 2011).

Our research groups have previously dealt with each of these processes separately. Barreiros et al. (2003) and Lopes et al. (2013) successfully isolated bacteria commonly found in contaminated sites and applied them, *in situ*, for the biodegradation of an organic pollutant. Additionally, Pereira et al. (2013a) and Pereira et al. (2013b) reported on the removal of antibiotics such as Amoxicillin, Oxytetracycline and Oxolinic Acid from aqueous solutions by solar TiO_2-assisted photocatalysis using a pilot-plant equipped with compound parabolic collectors (CPCs). Although Amoxicillin has been previously subject to several degradation studies via various AOPs (Mavronikola et al., 2009; Homem et al., 2010; Ay and Kargi, 2011; Trovó et al., 2011; Dimitrakopoulou et al., 2012), none has focused on the removal of common transformation products resulting from the slow transformation that the parent compound undergoes in aquatic environments (Nägele and Moritz, 2005; Längin et al., 2009; Gozlan et al., 2013).

In this way, the aim of this study was to evaluate a multistage treatment for AMX-spiked solutions combining: i) a biological treatment step to metabolize the AMX molecule, with ii) a solar photocatalytic system to achieve the mineralization of the transformation products (TPs), recalcitrant to further biological removal. Firstly, a mixed culture (MC) was obtained through the enrichment of an activated sludge sample collected in an urban WWTP treating urban wastewater in order to optimize AMX biotransformation. Secondly, different aqueous matrices spiked with AMX were treated with the MC and the metabolic transformation products were identified. Thirdly, the efficiency of the photocatalytic step was assessed in the removal of the metabolized TPs in a lab-scale photoreactor prototype equipped with a compound parabolic collector (CPC). The two proposed solar AOPs are the well-known photocatalytic system

mediated by TiO_2 (TiO_2/UV) and a modification of the conventional photo-Fenton process in order to work with near-neutral pH levels, the Fe^{3+}/Oxalate/H_2O_2/UV-Vis system.

7.2 Materials and methods

7.2.1 Reagents

Amoxicillin (MW: 365.4, CAS# 26787-78-0, HPLC-UV chromatogram and MS/MS spectrum in Figure 7.1a and b, respectively) was purchased from Sigma-Aldrich. HPLC grade methanol was from Prolabo, H_3PO_4 (85% p.a.), KH_2PO_4 and $(NH_4)_2SO_4$ from Merck (analytical grade) and yeast extract (YE) from Fisher Scientific. For the LC-MS analysis, methanol hypergrade for LC-MS (LiChrosolv®) from Merck, water LC-MS Chromasolv® and formic acid (98% p.a.) from Fluka were used. Syringe filters with 0.2 μm nylon membranes were purchased from Whatman and 0.45 μm nylon filter membranes from Supelco. Titanium dioxide used in photocatalytic experiments was Degussa P25 (80% anatase and 20% rutile). Photo-Fenton experiments were performed using hydrogen peroxide (Quimitécnica, S.A., 50% (w/v), 1.10 g cm^{-3}), iron (III) chloride hexahydrate (Merck) and oxalic acid dihydrate (VWR Prolabo, purity 98%). Sulfuric acid (Pronalab, 96%, 1.84 g cm^{-3}) and sodium hydroxide (Merck) were used for pH adjustment.

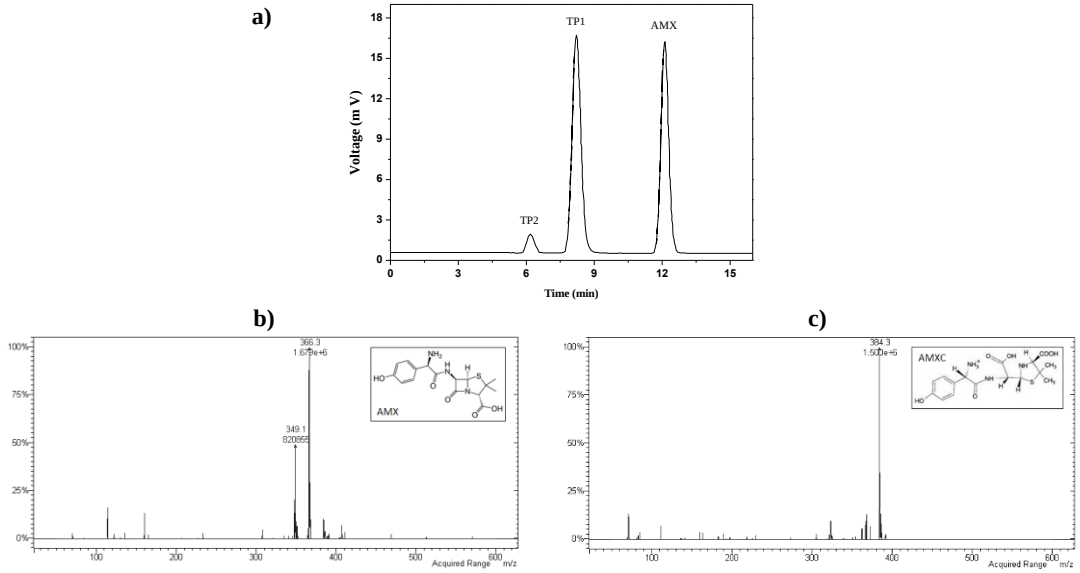

Figure 7.1. a) Chromatograms obtained by HPLC-UV/Vis analysis at 230 nm. Retention times of the compounds are: AMX: 12.1 min; TP1: 8.2 min and TP2: 6.9 min; **b)** MS/MS spectrum of Amoxicillin [m/z = 366]; **c)** MS/MS of Amoxicilloic acid [m/z = 384].

7.2.2 Microbial growth media and conditions

Mineral medium B (Barreiros et al., 2003) was used as microbial growth medium, supplemented with 0.53 g L^{-1} $(NH_4)_2SO_4$ and 1 g L^{-1} yeast extract (YE) as nitrogen and carbon sources,

respectively. This medium (pH = 7.2), hereafter designated as enrichment medium (EM), was supplemented with 0.01 to 0.03 g L^{-1} of AMX. Antibiotic stock solutions were prepared weekly in distilled water at a final concentration of 2 g L^{-1} and kept at -20°C prior to use. Incubation was carried out in the dark at 30°C and constant stirring at 120 rpm.

7.2.3 Culture enrichment

A sample from the aerobic activated sludge biological reactor collected in an urban WWTP (Northern Portugal) was diluted 2-fold in EM initially spiked with 0.01 g L^{-1} AMX. The enrichment culture was successively transferred to fresh medium with increasing AMX content, up to 0.03 g L^{-1}, and with initial cell densities corresponding to 0.02 g L^{-1} dry weight. Transferences were performed for 24 weeks at intervals of 1 to 15 d. The final culture obtained was named mixed culture (MC).

7.2.4 Bacteria isolation and identification

The MC referred above was serially diluted in sterile saline solution (0.85%, w/v), spread on Plate Count Agar (PCA) supplemented with AMX (0.03 g L^{-1}) and incubated at 30 °C for 48 hours. Individual colonies with distinct morphologies were purified by subculturing on the same medium. Isolates were identified by 16S rRNA sequence analysis. Amplification of the gene was performed by PCR using universal primers 27F (5'- AGAGTTTGATCMTGGCTCAG-3') and 1492R (5'-TACCTTGTTACGACTT-3') (Lane, 1991). Nucleotide sequences were compared to those available in public databases using Eztaxon library (Chun et al., 2007). Resting cells assays were carried out in phosphate buffer (50 mM, pH 7.2) with each distinct isolate to determine their role in AMX degradation.

7.2.5 Combined treatment process

Different matrices were tested in order to optimize the combined treatment process. The matrices consisted in EM, saline solution (NaCl, 0.85%, w/v), phosphate buffer (Buffer; 50 mM, pH 7.2), and wastewater (WW) collected after secondary wastewater treatment in an urban WWTP (in Northern Portugal). The main characteristics of each medium are presented in Table 7.1.

The high initial AMX concentration, 0.02 g L^{-1}, was chosen to properly follow the formation and depletion of the TPs by HPLC-UV/Vis analysis.

Table 7.1. Main characteristics of the used aqueous matrices before MC inoculation.

Matrix	pH	DOC / IC	Ionic strength	Average anion concentrations (g L^{-1})		
		(mg L^{-1})	(M)	[PO_4^{3-}]	[Cl^-]	[SO_4^{2-}]
EM	7.2	421 / 4.24	0.039	2.56	0.34	0.38
Buffer	7.2	Residual	0.050	4.75		
NaCl	6.5	Residual	0.145		5.15	
WW	6.8	5.6 / 4.9	0.003	0.014	0.062	0.043

7.2.5.1 Biological treatment

The biological treatment step was carried out in a batch system using a 5 L Erlenmeyer flask, containing 1.2 L of the test matrix spiked with 0.02 g L^{-1} of AMX, in parallel with a control flask to monitor abiotic degradation.

Inoculum was previously obtained by growing the MC in EM spiked with 0.02 g L^{-1} AMX. Cells were harvested at the late exponential phase, washed twice and resuspended in sterile saline solution (0.85%, w/v). Given the inability of cells to grow in the absence of macro- and micronutrients, decreasing complexity of the tested matrices demanded increasing initial biomass concentration.

For the experiments carried out in EM, 0.03 g L^{-1} of cell dry weight was used, in phosphate buffer, 0.11 g L^{-1}, and for both saline solution and real wastewater, 0.26 g L^{-1}. MC cells were separated from the respective medium by centrifugation at 26,000 × g when AMX was found in residual concentrations (0.57 to 1.97 g L^{-1}). This premature stop in the biological step was necessary because AMX degradation continues to be carried out in the supernatant due to active β-lactamases excreted by the MC members. As expected, for the experiments in Buffer, NaCl and WW matrices, no bacterial growth was observed, and AMX degradation followed zero order kinetics. The degradation rate was obtained by simple linear regression, as expressed by Eq. 7.01:

$$S = S_0 - kt \tag{7.01}$$

where S represents the substrate content at time t (mg L^{-1}), S_0 the substrate content at $t = 0$, t the time (h) and k the degradation rate (h^{-1}). The half-life ($t_{1/2}$) and the specific degradation rate constants (k_s) were calculated as follows (Eq. 7.02 and 7.03):

$$t_{1/2} = \frac{S_0}{2k} \tag{7.02}$$

$$k_s = \frac{k}{X} \quad (7.03)$$

where X represents the biomass content in cell dry weight (mg L^{-1}).

7.2.5.2 Solar Photocatalytic treatment

In all experiments, 1.1 L (V_t) of the resulting supernatant from the biological treatment step was transferred into the recirculation glass vessel of the lab-scale photoreactor provided with a sunlight simulator, wherein the TiO_2/UV or the Fe^{3+}/Oxalate/H_2O_2/UV-Vis processes were performed in order to assess their efficiency in the degradation and mineralization of the AMX metabolic by-products. The pH was not controlled in any of the reactions, in both AOP systems.

The description of the lab-scale photoreactor apparatus and the detailed experimental procedure, and the respective analytical procedures can be consulted in Chapter 2.

7.2.6 Analytical procedures

AMX concentration and transformation products (TPs) areas were obtained by HPLC, in a system equipped with an UV-Vis detector (Knauer), operating at 230 nm and using a 5 μm Superspher 100 RP-18e (125 x 4 mm) column from Merck. For the mobile phase, a mixture of 96% (v/v) KH_2PO_4 buffer (50 mM) and methanol acidified at pH 3 with ortophosphoric acid was used at 1 mL min^{-1}. Retention time for AMX was 11.8 ± 0.2 min. TP1, TP2, TP3 and TP4 were detected at 8.3 ± 0.2, 6.80 ± 0.09, 4.10 ± 0.03 and 2.70 ± 0.01 min, respectively.

Identification of the TPs was performed using a Varian LC-MS system (Lake Forest, USA), constituted by a ProStar 210 Binary Solvent Delivery Module and a 500-MS LC Ion Trap Mass Spectrometer, equipped with an electrospray ionization source (ESI). Data was acquired and processed by Varian MS Workstation Version 6.9 software. A Pursuit XRs Ultra C18 column (100 mm x 2.0 mm i.d., particle size: 2.8 μm), in combination with a MetaGuard column Pursuit® C18 (10 mm x 2.0 mm i.d., particle size: 5 μm) were purchased from Varian (Lake Forest, USA). The mobile phase was composed of ≈ 6% water with 0.1% formic acid and 4% methanol, running in isocratic mode at a flow rate of 0.2 mL min^{-1}. The injection volume was 10 μL. The mass spectrometer had an electrospray interface operated in positive mode using: capillary voltage, 69.0 V; shield voltage, 600 V; needle voltage, 3453 V; RF loading, 90%; drying gas pressure, 15 psi; drying gas temperature, 250 ºC; nebulizing gas pressure, 50 psi; multiplier offset, 300 V; MS scan range, 50-600 m/z.

Cell growth was measured by optical density (OD_{610}) using a UV/Vis Unicam Heλios spectrophotometer and by dry weight using a calibration curve. The later was obtained by

filtering cell suspensions through 0.45 μm membranes (Advantec), dried at 70°C until constant weight.

Growth inhibition assays were carried out in 96-well microtiter plates using a Synergy HT Multi-Mode Microplate Reader (Biotek Instruments, USA) in order to test the toxicity of treated samples. *Escherichia coli* (DSM 1103) and *Staphylococcus aureus* (DSM 1104) were used as test strains. Minimum inhibitory concentrations (MIC) for each strain were 4.0 and 0.25 mg AMX L^{-1}, respectively (Andrews, 2001). Each plate, in addition to the treated samples, contained both negative and positive controls (inoculated media with and without 0.02 g L^{-1} AMX, respectively), and blanks (cell-free media). All wells were supplemented with 2 g L^{-1} YE and the plates were then incubated at 30 °C, continuously shaken for 20 h, with absorbance measurements at 610 nm every 30 min. Each sample was tested in triplicate and a zero-order kinetic model was used to fit the experimental data, being the specific growth rate (h^{-1}) normalized by that of the positive control. Comparison of means was made by a one-way ANOVA test using R software (R Development Core Team, 2013).

7.3 Results and discussion

7.3.1 Characterization of the mixed culture (MC)

A mixed culture (MC) able to degrade AMX was obtained after enrichment of activated sludge with this antibiotic. MC was able to grow unimpaired up to 0.45 g L^{-1} AMX in the presence of 1 g L^{-1} YE. However, no growth was observed when AMX acted as a sole carbon source (data not shown).

The spread plate method revealed the presence 33 different morphotypes, which were affiliated to 6 distinct genera (Table 7.2). The majority of these organisms belongs to the phylum *Proteobacteria*, commonly known to degrade a great variety of organic pollutants (Esplugas et al., 2013). Within this group a great percentage of isolates was closely related to *Citrobacter freundii*, followed *by Stenotrophomonas acidaminiphila* and *Shingobacterium multivorium*. When individually tested in phosphate buffer (0.05 M, pH = 7.2, 0.035 g L^{-1} AMX), resting cells of all strains were able to degrade AMX, albeit at different rates. The overall specific degradation rate of the MC (0.11 g_{AMX} $g_{biomass}^{-1}$ h^{-1}) closely corresponded to that of *C. freundii* (0.09 g_{AMX} $g_{biomass}^{-1}$ h^{-1}). Other isolates exhibited either slower (*Elizabethkingia meningoseptica*, 0.03 g_{AMX} $g_{biomass}^{-1}$ h^{-1}), or higher (*Stenotrophomonas nitritireducens*, 2.95 g_{AMX} $gbiomass^{-1}$ h^{-1}) degradation rates.

The isolated strains have been described previously as carriers of different β-lactam resistance genes (Literacka et al., 2004; Vaz-Moreira et al., 2011; Henriques et al., 2012). Thus, the MC is expected to produce more than one type of β-lactamases. Jacoby (2009) has detected AmpC β-lactamase genes in *C.freundii* isolates. Experimental data supports this hypothesis since these isolates present a board range of resistance to β-lactam antibiotics but were susceptible to carbapenems, corresponding to the resistance profile reported for carriers of the AmpC gene (Barlow and Hall, 2002). Furthermore, no significant differences were observed between the specific degradation rates of *C.freundii* and the MC ($p > 0.05$). For that reason, AmpC may be the main responsible for AMX hydrolysis in our culture. Other isolated strains such as *E. meningoseptica*, *Stenotrophomonas sp*. and *Pseudomonas sp.* may also contribute to AMX depletion, since they have been reported to possess metallo-β-lactamases (Galleni et al., 2001), which are able to degrade most β-lactam antibiotics including carbapenems (Walsh et al., 2005). These enzymes may possess substantially different affinities with the AMX molecule, resulting in significant differences in degradation rates.

Table 7.2. Identification of bacterial strains recovered from the AMX-enriched culture (MC).

Phylum / Class	Species	Type strain	GenBank accession no.	No. of isolates	16S rRNA gene sequence similarity
Proteobacteria/ Gammaproteobacteria	*Citrobacter freundii*	ATCC8090	ANAV01000046	13	99.9 ± 0.0
Bacteroidetes/ Sphingobacteriia	*Sphingobacterium multivorum*	IAM14316	AB100738	5	99.8 ± 0.4
Proteobacteria/ Gammaproteobacteria	*Stenotrophomonas acidaminiphila*	AMX19	AF273080	5	99.5 ± 0.5
Bacteroidetes/ Flavobacteriia	*Elizabethkingia meningoseptica*	ATCC13253	ASAN01000081	4	99.7 ± 0.2
Proteobacteria/ Gammaproteobacteria	*Pseudomonas guariconensis*	PCAVU11	HF674459	4	99.9 ± 0.0
Proteobacteria/ Gammaproteobacteria	*Stenotrophomonas nitritireducens*	L2	AJ012229	1	99.9
Proteobacteria/ Alphaproteobacteria	*Sphingomonas molluscorum*	KMM3882	AB248285	1	99.8

As the MC was originated from an activated sludge, this attests well the widespread resistance to β-lactam antibiotics in WWTP (Szczepanowski et al., 2009; Vaz-Moreira et al., 2011; Igbinosa and Okoh, 2012). Given a mixed culture is a better surrogate of activated sludge than pure bacterial cultures, MC was further used in the combined treatment.

7.3.2 Combined treatment for AMX removal

7.3.2.1 Biological degradation step performance

In all tested matrices, the degradation of AMX occurred concomitantly with the accumulation of two distinct TPs, detected by HPLC analysis (TP1 and TP2, HPLC-UV/Vis chromatograms in Figure 7.1a). Further analysis by LC-MS/MS allowed their identification as the stereoisomers (5*S*) and (5*R*) of amoxicilloic acid ($[C_{16}H_{21}N_3O_6S+H]^+$, m/z = 384, Figure 7.1c). According to Davis et al. (1991) and Deshpande (2004) the hydrolysis of penicillins renders the formation of 5*R*-penicilloic acids, which slowly epimerizes to the 5*S* configuration, since the carbon atom between nitrogen and sulphur in the thiazolidine ring is chiral. The 5*R*-epimer has also been reported as the main β-lactam metabolite found in urine (Testa and Mayer, 2006).

Both TP1 and 2 were found to be resistant to further hydrolysis (data not shown), which can occur due to their increased stability or to the consequential lack of regeneration of the enzyme

(Davis et al 1991). Their formation is a product of the hydrolysis of the highly reactive β-lactam ring and results in the total loss of antimicrobial activity (Deshpande et al. (2004), Nägele and Moritz (2005)). Furthermore, Ghauch et al. (2009) and Längin et al. (2009) have also detected the production of amoxilloic acid, product of TP1 and 2 decarboxylation. Nevertheless, this compound was never detected during the biodegradation assays.

For the combined treatment assays, the endpoint of the biological step was set between 90 and 95% of AMX depletion (Table 7.3). AMX hydrolysis by the MC followed a zero-order kinetic model, except in the assay carried out in EM. In this particular case, the presence of YE resulted in increasing biomass content over time, with the degradation following first-order kinetics, not allowing a direct comparison with the experiments carried out in other matrices.

Table 7.3. Zero-order kinetic parameters for AMX depletion by the MC in different aqueous matrices. $[AMX]_0$ = 0.02 g L^{-1}; Incubation T = 30 °C; Continuous shaking at 120 rpm; V_0 = 1.2 L. All experiments were performed at near-neutral pH.

Matrix	Incubation time (h)	Biomass content (mg L^{-1})	Specific degradation rate (g_{AMX} $g_{biomass}^{-1}$ h^{-1})	Half-life ($t_{1/2}$, h)
EM	3.7	26 ± 3	n.d.	n.d.
Buffer	3.2	112 ± 1	0.10 ± 0.01	0.9 ± 0.1
NaCl	4.8	(26 ± 1)×10	0.03 ± 0.01	1.5 ± 0.3
WW	3.8	(21 ± 4)×10	0.13 ± 0.07	0.5 ± 0.2

n.d. - not determined. Values represent means ± standard deviation.

AMX biodegradation was significantly faster (p < 0.05) in Buffer and WW than in the NaCl matrix, as assessed by the obtained specific degradation rates (k_S). These differences can be explained by the distinct chemical composition and pH values of each matrix. Ohsuka et al. (1995) has reported on the pH-dependence of AmpC β-lactamases of *C.freundii*, which may present less activity in slightly acidic media. Buffer and WW matrices displayed similar specific degradation rates (p > 0.05). Since WW has lower pH and ionic strength values, this could indicate the presence of unknown organic and inorganic compounds that provide favorable conditions for AMX hydrolysis. The high standard deviation observed for the WW experiments may be explained by variations in its chemical and microbiological composition. Abiotic degradation of the parent compound in the cell-free matrix was negligible for all experiments (data not shown). By the end of the biological step, the liquid phase no longer presented antibacterial activity towards *E. coli*, whereas growth inhibition of *S. aureus* was greatly reduced, as seen in the example of one of the photo-Fenton experiments performed in NaCl in Figure 7.2.

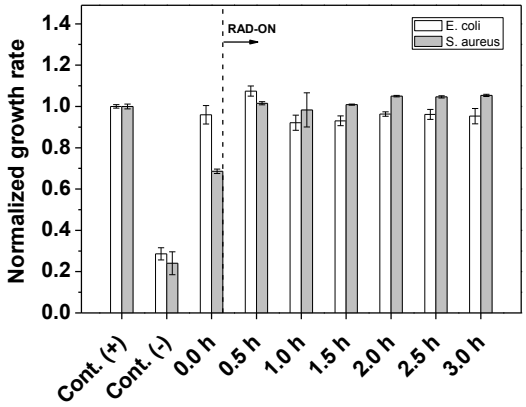

Figure 7.2. Normalized growth rate in samples taken in the Bio-photo-Fenton combined process in NaCl matrix, at pH_0 = 5.0. Values represent means and standard deviation (*n* = 3). Control (-) and Time 0.0 h are representative of the beginning and the end of the biological step. Time 0.5 h and onwards represent the photo-treatment period.

DOC content remained constant, except in the EM experiments, where the consumption of YE by the mixed culture led to a 25% decrease in the initial carbon content. Mineralization by means of biological treatment alone is expected to be slow, due to abovementioned factors. The same recalcitrant behavior of TP1/TP2 was observed with the MC, which could not remove these products even after 46 d of incubation (data not shown). Längin et al. (2009) reported a 75% DOC reduction only after 14 d in the Zahn-Wellens test, and no visible mineralization in the Closed Bottle Test. Similar results were also reported by Alexy et al. (2004). Accordingly, TP1/TP2 were detected in relatively high concentrations by Gozlan et al. (2013) after the secondary treatment in a WWTP, while Pérez-Parada et al. (2011) estimated that only an average of 55% of the initial content of these products is removed by conventional wastewater treatment.

These results highlight the need of complementing AMX biodegradation with the proposed photocatalytic methods for the removal of the resulting transformation products.

7.3.2.2 TiO_2/UV photocatalysis step performance

For the TiO_2/UV photocatalytic experiments, the catalyst concentration was chosen in accordance to Rodríguez et al. (2004), wherein 0.2 g L^{-1} was considered to be the optimal concentration when working with the CPC unit described in this work (internal diameter 46.4 mm).

The pH value of the matrices remained constant throughout the previous step, and in preliminary experiments, the pH was kept unchanged. However, the removal of TP1/TP2 was remarkably slow (data not shown), with no apparent mineralization, despite of the fact that measured inorganic carbon levels were not relevant. To the best of our knowledge, no information regarding the pK_a constants of TP1/TP2 is available, thus not allowing any direct

conclusion regarding the role of electrostatic attraction between TiO_2 particles and TP1/TP2 molecules. For that reason, all the matrices were acidified (5.5) prior to photocatalytic treatment to take advantage of the positive effect of increased catalyst surface when smaller TiO_2 particle size is favoured under pH values lower than the Point of Zero Charge of Degussa P25 (pH_{PZC} = 6.7 (Malato et al., 2009)), as recommended by Li et al. (2010).

Figure 7.3a and b presents the results of the application the TiO_2/UV system in the removal of TP1/TP2. The NaCl solution was the most favourable matrix, as TP1 and TP2 were no longer detected after 90 min of illumination (Q_{UV} = 5.3 kJ L^{-1}); the Buffer matrix followed, requiring 180 min of illumination (Q_{UV} = 10.9 kJ L^{-1}). However, a third unidentified TP (TP3) accumulated in all matrices, and a forth in WW (TP4), albeit transiently.

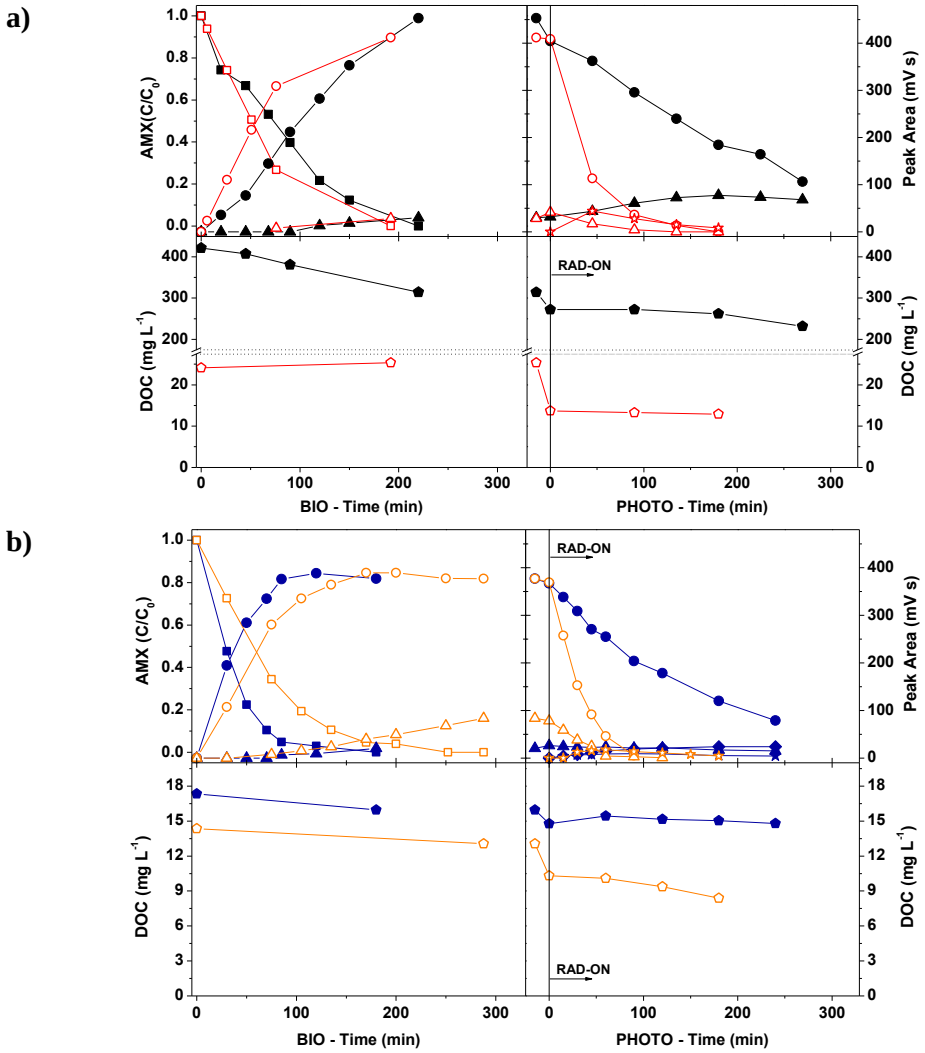

Figure 7.3. Follow-up of the Bio-TiO_2 combined process on the degradation of AMX (square), its resulting transformation products (TP1 - circle; TP2 - triangle; TP3 – star; TP4 - diamond) and DOC (pentagon), using: **a)** EM (black symbols) or Buffer (red symbols); **b)** WW (blue symbols) or Cl (orange symbols). $[AMX]_0$ = 20 mg L^{-1}, Photocatalytic process parameters: $[TiO_2]$ = 0.2 g L^{-1}, pH_0 = 5.5, T = 25 °C, I = 44 W_{UV} m^{-2}.

Differences in matrices complexity in EM and WW experiments seem to account for the inability of completely removing TP1/TP2 under similar photo-treatment periods.

The pronounced amount of organic matter compared to the simpler matrices may have not only competed with the catalyst for absorption of incident UV radiation, but also with the TP1/TP2 attack by the generated •OH radicals. Controls were performed in the absence of light and no considerable effects were found.

No notable reduction in the initial DOC content was achieved after 180 min of illumination. The high concentrations of Cl^- (NaCl) and PO_4^{3-} (Buffer) of each matrix may explain this, probably due to competitive adsorption onto TiO_2 surface, to their •OH radical scavenger effect and formation of less reactive inorganic radicals, as suggested by Guillard et al. (2005) and De Laat et al. (2004) . The exception was the NaCl experiment, which saw a 35 % DOC reduction after 180 min, when compared to the initial value before the catalyst addition step.

7.3.2.3 *Photo-Fenton step performance*

Given the apparent unsuitability of using the TiO_2/UV system with the most realistic matrix (WW), the Fe^{3+}/Oxalate/H_2O_2/UV-Vis system was tested as an alternative suited to near-neutral pH levels. Beforehand, some considerations about this treatment must be made. The conventional photo-Fenton process, as simplified by Gogate and Pandit (2004b), comprises the combination of ferrous iron (Fe^{2+}) with hydrogen peroxide (H_2O_2) and (solar) UV-Vis radiation resulting in the production of two moles of •OH per mole of hydrogen peroxide (Eq. 7.05 and 7.06):

$$Fe^{2+} + H_2O_2 \rightarrow Fe^{3+} + {}^{\bullet}OH + HO^- \quad (7.05)$$

$$Fe(OH)^{2+} + h\upsilon \rightarrow Fe^{2+} + {}^{\bullet}OH \quad (7.06)$$

The solubility of Fe^{3+}-hydroxy complexes, especially considering the molar fraction of the most photoactive species, $[Fe(OH)]^{2+}$ (with absorption bands between 290 and 400 nm), is very limited for pH values above 3 (Pignatello et al., 2006), which would demand additional costs of initial acidification and final neutralization of the solution. However, this can be overcome by means of the formation of Fe(III)-carboxylate complexes, which are able to extend the solubility of iron to near neutral pH working conditions. At the same time, these complexes present stronger radiation absorption at wavelengths up to 580 nm and can increase the quantum yield of Fe^{2+} production according to Eq. 7.07 (Jeong and Yoon, 2005; Pignatello et al., 2006):

$$Fe^{3+}(C_2O_4)_n^{(3-2n)} + h\upsilon \rightarrow Fe^{2+} + (n-1)C_2O_4^{2-} + C_2O_4^{2-\bullet} \quad (7.07)$$

For this reason, the Fe(III)-oxalate complex was chosen, as the quantum yield of its two most photo-active species, $Fe(C_2O_4)_2^-$ and $Fe(C_2O_4)_3^{3-}$, were reported by Faust and Zepp (1993) as being 1.0 and 0.6 (436 nm), respectively. The working pH of the consequent experiments was

decided according to the distribution of these species in solution. In view of that, MINEQL+ software was used to study the distribution of the Fe (III) complexes as a function of pH. The presence of inorganic ions such as PO_4^{3-}, SO_4^{2-} and Cl^- in the different matrices (Table 7.1), which can compete with oxalate for available iron, thus hindering the process performance (De Laat et al., 2004), was also considered. The following oxalate and iron-oxalate equilibrium reactions were introduced in MINEQL+ (Eq. 7.08 to 7.13), with dissociation constants (Panias et al., 1996) corrected using the Davies equation for the approximate ionic strength of the corresponding matrix:

$$H_2C_2O_4 \leftrightarrow HC_2O_4^- + H^+ \quad (7.08)$$

$$HC_2O_4^- \leftrightarrow C_2O_4^{2-} + H^+ \quad (7.09)$$

$$Fe^{3+} + HC_2O_4^- \leftrightarrow FeHC_2O_4^{2+} \quad (7.10)$$

$$Fe^{3+} + C_2O_4^{2-} \leftrightarrow FeC_2O_4^+ \quad (7.11)$$

$$FeC_2O_4^+ + C_2O_4^{2-} \leftrightarrow Fe\left(C_2O_4\right)_2^- \quad (7.12)$$

$$Fe\left(C_2O_4\right)_2^- + C_2O_4^{2-} \leftrightarrow Fe\left(C_2O_4\right)_3^{3-} \quad (7.13)$$

Notwithstanding the use of the iron(III)-oxalate complexes, the solubility/concentration of iron (III) would be highly limited by the high phosphate content of the Buffer and EM media, which would result in the immediate precipitation of the mineral Strengite ($FePO_4.2H_2O$). Additionally, the amount of organic carbon of the EM matrix would also be highly deleterious. For these reasons, photo-Fenton experiments were not performed in these two matrices.

Figure 7.4a and b shows the calculated iron speciation diagrams according to the molar concentration of each known component (Table 7.1) for NaCl and WW, respectively, in the absence (left) or in the presence (right) of oxalate. Initially, a 1:3 Fe(III)-oxalate molar ratio was considered to ensure the formation of the three photo-active complexes. The respective inorganic anion content of NaCl and WW was not expected to interfere in the formation of the Fe(III)-oxalate complexes. Despite this, WW experiments eventually required a higher iron/oxalate molar ratio dose (1:9), than NaCl matrix (1:3), resulting in remarkably different profiles. In experiments performed with the initial 1:3 iron/oxalate molar ratio dose (data not shown), the added oxalate was not sufficient to keep a satisfactory Fe(III) concentration in solution along reaction time, due to the probable binding of iron to natural dissolved organic matter contained in the WW matrix (Lindsey and Tarr, 2000).

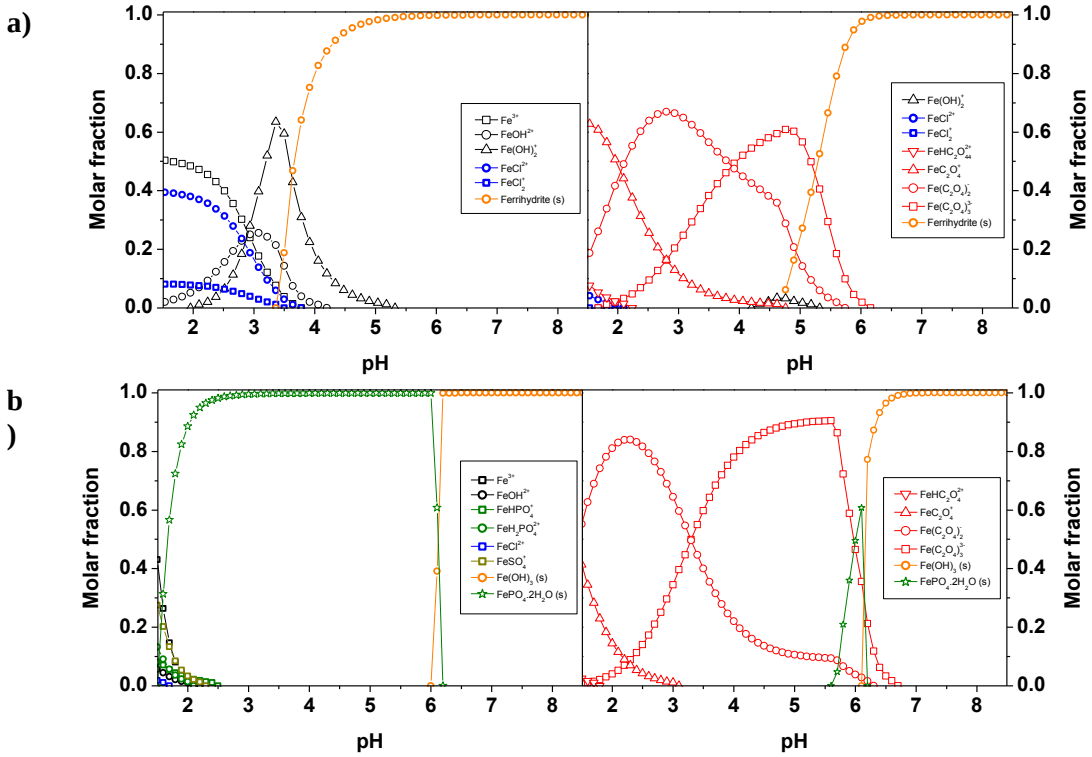

Figure 7.4. Speciation diagrams for iron(III) species as a function of pH in: **a)** NaCl matrix: without accounting (left) or accounting (right) for 1.07×10^{-1} mM (9.5 mg L^{-1}) oxalic acid; [Fe (III)] = 3.58×10^{-2} mM (2 mg L^{-1}), Ionic strength = 0.15 M; and **b)** WW matrix: without accounting (left) or accounting (right) for 3.22×10^{-1} mM (29 mg L^{-1}) oxalic acid. [Fe (III)] = 3.58×10^{-2} mM (2 mg L^{-1}). Ionic strength = 3.3 mM. The speciation software MINEQL+ was used to calculate the data.

Ultimately, Fe^{3+}/Oxalate/H_2O_2/UV-Vis experiments were performed in NaCl and WW under two initial pH values, 4 and 5, as both $Fe(C_2O_4)_2^-$ and $Fe(C_2O_4)_3^{3-}$ are prominent in this pH range. Higher pH values were not considered due to the fact that in NaCl matrix the Ferrihydrite ($Fe(OH)_3$ (s)) fraction is shown to quickly rise near pH = 5.0, and becomes dominant at pH = 6.0 (Figure 7.4a), while in WW matrix, iron is expected to precipitate in the form of Strengite ($FePO_4.2H_2O$) after pH = 5.5, and as Ferrihydrite ($Fe(OH)_3$ (s)) after pH = 6.0 (Figure 7.4b).

The results on TP1/TP2 removal from NaCl and WW matrix can be seen in Figure 7.5a and b (right), respectively. Compared to the TiO_2/UV system, TP1/TP2 removal was clearly improved, in both matrices and respective pH_0 values. In both pH_0 = 4.0 experiments, TP1/TP2 were no longer detected after 20 min of illumination (Q_{UV} = 1.3 kJ L^{-1}), while the pH_0 = 5.0 experiments required a longer period of illumination, 40 minutes (Q_{UV} = 2.6 kJ L^{-1}). In WW experiments, a third unidentified TP (TP3) appeared at 10 min of illumination, but it was no longer detected after 60 min (Q_{UV} = 4.0 kJ L^{-1}). Control experiments performed in darkness did not show significant TP1/TP2 removal in the same period.

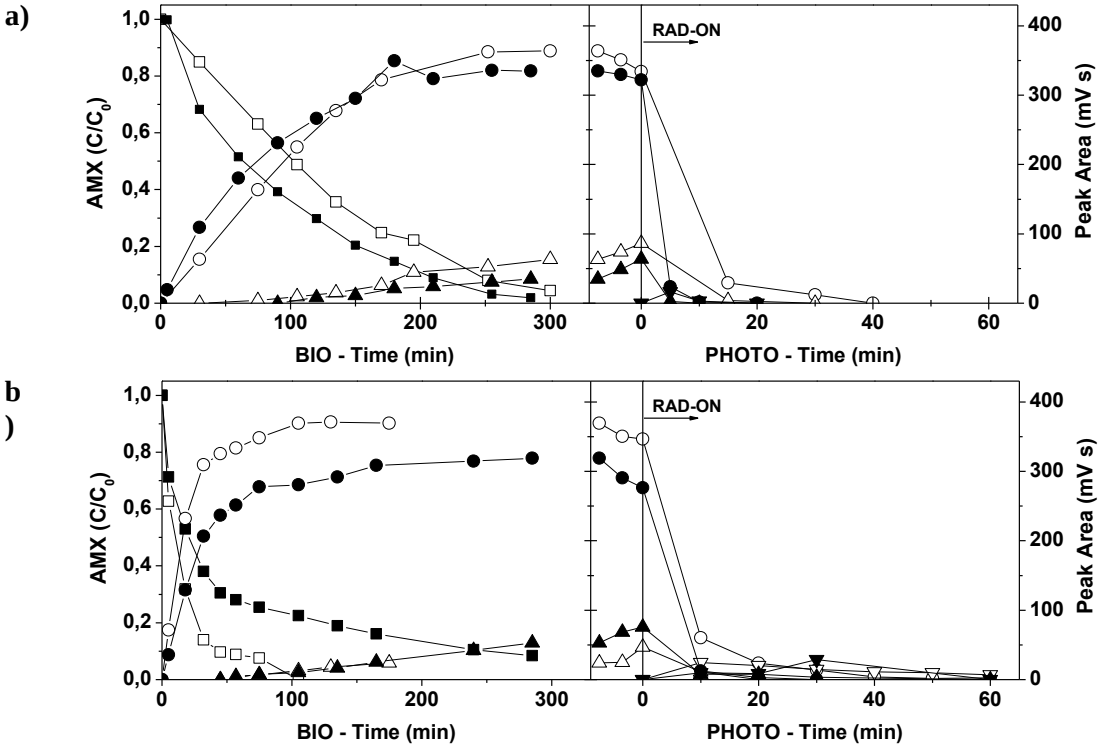

Figure 7.5. Evolution profiles of AMX (square) and its transformation products (TP1 - circle; TP2 - triangle; TP3 - diamond) during the Bio-Fe^{3+}/Oxalate/H_2O_2/UV-Vis combined process performed in **a)** NaCl matrix, and **b)** WW matrix. The pH in the photocatalytic step was adjusted to 4.0 (closed symbols) or to 5.0 (open symbols).

The general influence of pH on the experiments may be explained with the distribution of the abovementioned Fe (III)-oxalate species. Even considering the differences in their relative proportion over pH due to different iron/oxalate molar ratio doses, the fraction of most photo_active species, $Fe(C_2O_4)_2^-$, tends to be higher around pH = 4.0, compared to pH = 5.0. The higher consumption of H_2O_2 seems to attest to this fact.

The process details for both matrices can be consulted in Figure 7.6 a and b. By the end of the first 30 min of illumination (Q_{UV} = 1.9 kJ L^{-1}), an overall steady decrease can be seen in total soluble iron concentration. This corresponded well with the concomitant ongoing depletion of oxalate, apparent in HPLC analysis of low-molecular-weight carboxylate anions (LMWCA). With dwindling amounts of oxalate in solution, the distribution of iron (III) species seen in the right side of Figure 7.4 a and b would progress into what can be seen in the left side of the same Figure.

Up until this point in both NaCl matrix experiments, nevertheless, reduction of DOC exceeded the oxalate depletion, and an average of 45% of the remaining DOC was already in the form of tartronate, oxamate, malonate, glycolate, formate and acetate, besides a lower amount of oxalate itself. In both WW experiments, on the other hand, DOC decreased along with the oxalate depletion, with vestigial amounts of other LMWCA.

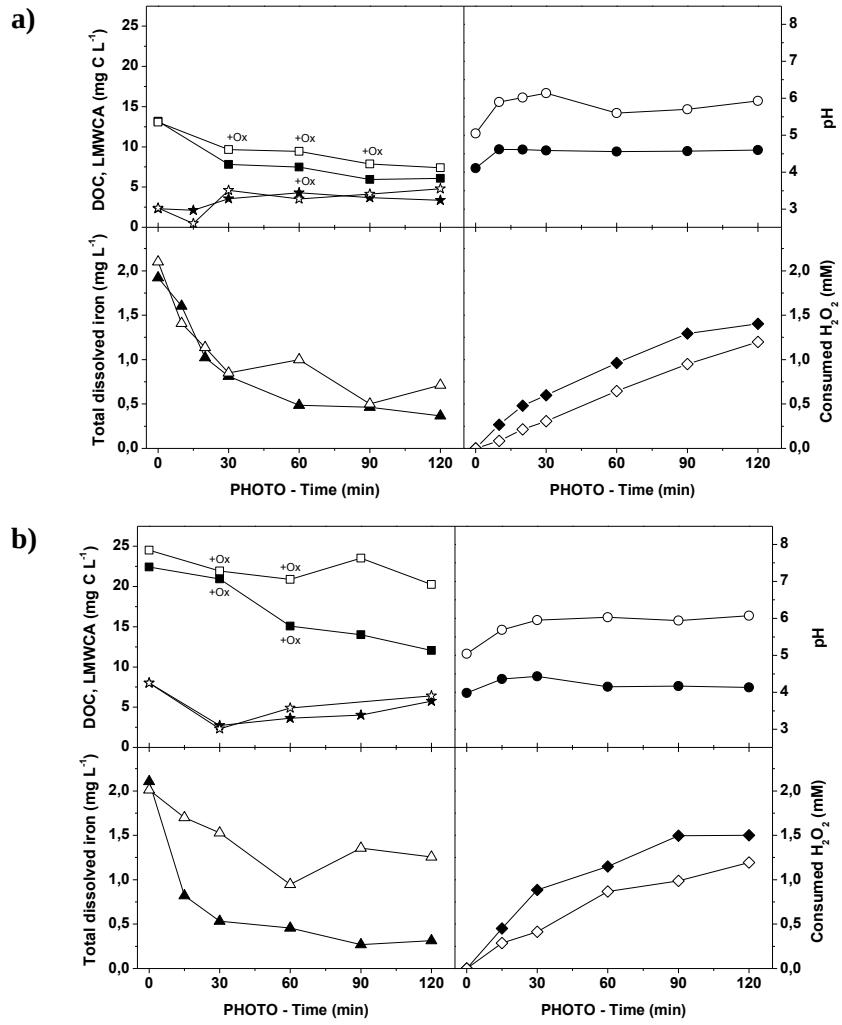

Figure 7.6. Follow-up of DOC removal (square), sum of LMWCA (star), pH (circle), total dissolved iron (triangle) and H_2O_2 consumption (diamond) during the photocatalytic stage of the Bio--Fe^{3+}/Oxalate/H_2O_2/UV-Vis combined process performed in: **a)** NaCl matrix, and **b)** WW matrix, at pH = 4.0 (closed symbols) or pH = 5.0 (open symbols). Process parameters: [Fe (III)] = 2 mg L^{-1}, initial 1:3 (NaCl) or 1:9 (WW) iron/oxalate molar ratio, total added H_2O_2 = 90 mg L^{-1}, T = 25°C, I = 44 W_{UV} m^{-2}. +Ox represents extra additions of oxalic acid.

Given the abovementioned fact that, in each matrix and tested pH_0 level, complete, or near complete TP1/TP2 removal occurred by 40 min of illumination, the process was extended with additional dosages of oxalate (marked as +Ox in Figure 7.6 a and b), in order to keep iron in solution and see the effects on the remaining DOC content. Notwithstanding the added carbon with each oxalate addition, and the apparent levelling of DOC content in both NaCl and WW experiments, depletion of oxalate was quick between additions. After 120 min of illumination (Q_{UV} = 8.3 kJ L^{-1}) in NaCl experiments, an average of 55% of the final DOC content was in the form of LMWCA. In WW medium, only the pH_0 = 4.0 experiment benefited with the additional oxalate, as it can be seen in the progressive decrease of DOC content and its final 48% amount in the form of LMWCA, compared to 28% in the case of pH_0 = 5.0. Altogether, initial DOC concentration in the NaCl matrix was reduced by 54% (pH_0 = 4.0) and 51% (pH_0 = 5.0), while in the WW matrix it was reduced by 48% (pH_0 = 4.0) and 21% (pH_0 = 5.0).

7.4 Conclusions

In this work, a mixed culture able to degrade the antibiotic Amoxicillin in different matrices was successfully obtained and characterized. Highest AMX specific degradation rates were obtained in Buffer and WW. The resulting TPs were identified as stereoisomers of amoxicillin penicilloic acid (AMXC), and did not show antibacterial activity. However, they resisted further bacterial action, which brought up the need of a further, more efficient treatment. In this way, a complementary photocatalytic oxidation step was proposed to enhance AMXC degradation in a lab-scale apparatus simulating solar radiation, equipped with a CPC photo-reactor. The first process proposed was a photocatalytic system promoted by 0.2 g L^{-1} of TiO_2 (TiO_2/UV), carried out at pH_0 = 5.5. In NaCl and Buffer, the respective TP1/TP2 peaks were no longer detected after 90 (Q_{UV} = 5.3 kJ L^{-1}) and 180 (Q_{UV} = 10.9 kJ L^{-1}) min of illumination. In the most complex matrices (EM and WW), however, TPs were still present by the end of the irradiance period. None of the TiO_2/UV experiments showed considerable DOC removal by the end of photocatalytic step (maximum of ~ 35% initial DOC content in NaCl solution after 180 min).

The second process proposed was the photo-Fenton reaction enhanced by the Fe(III)-oxalate complex (Fe^{3+}/Oxalate/H_2O_2/UV-Vis), carried out using 2 mg Fe(III) L^{-1}, an 1:3 (NaCl) or 1:9 (WW) iron/oxalate molar ratio and a total H_2O_2 addition of 90 mg L^{-1}. Based on the distribution of the two most photo-active species, $Fe(C_2O_4)_2^-$ and $Fe(C_2O_4)_3^{3-}$, experiments with NaCl and WW were performed under two initial pH values, 4.0 and 5.0. Substantially lower amounts of accumulated UV energy per litre of solution were required to remove TP1/TP2, compared to the TiO_2/UV experiments. With both pH_0 = 4.0 experiments, 20 min (Q_{UV} = 1.3 kJ L^{-1}) were necessary, while with pH_0 = 5.0 experiments, 40 min (Q_{UV} = 2.6 kJ L^{-1}) sufficed to remove TP1 and TP2. Regardless of the need of supplementary oxalate additions to extend the process beyond TP1/TP2 removal, the remaining carbon content was either converted to easily biodegradable low-molecular-weight carboxylate anions or removed in higher proportions after 120 min (Q_{UV} = 8.3 kJ L^{-1}). The Fe^{3+}/Oxalate/H_2O_2/UV-Vis system should thus be preferred for this kind of treatment, even at near neutral pH levels.

Generally speaking, research concerning treatment methods to remove pharmaceuticals such as antibiotics from effluents mainly focuses on the parent compounds. Nevertheless, importance must also be given to naturally occurring by-products, which can also present environmental risks by themselves. In this way, combined treatments, such as the one proposed in this work, should be further developed for safe effluent discharge.

7.5 References

Alexy, R., Kümpel, T., Kümmerer, K., 2004. Assessment of degradation of 18 antibiotics in the Closed Bottle Test. Chemosphere 57, 505-512.

Andreozzi, R., Caprio, V., Ciniglia, C., de Champdoré, M., Lo Giudice, R., Marotta, R., Zuccato, E., 2004. Antibiotics in the Environment: Occurrence in Italian STPs, Fate, and Preliminary Assessment on Algal Toxicity of Amoxicillin. Env. Sci. & Techn. 38, 6832-6838.

Andrews, J.M., 2001. Determination of minimum inhibitory concentrations. J. Antimicrob. Chemother. 48, 5-16.

Ay, F., Kargi, F., 2011. Effects of Reagent Concentrations on Advanced Oxidation of Amoxicillin by photo-Fenton Treatment. J. Environ. Eng. 137, 472-480.

Bailon-Perez, M.I., Garcia-Campana, A.M., Cruces-Blanco, C., del Olmo Iruela, M., 2008. Trace determination of beta-lactam antibiotics in environmental aqueous samples using off-line and on-line preconcentration in capillary electrophoresis. J. Chromatogr. A 1185, 273-280.

Barreiros, L., Nogales, B., Manaia, C.M., Ferreira, A.C.S., Pieper, D.H., Reis, M.A., Nunes, O.C., 2003. A novel pathway for mineralization of the thiocarbamate herbicide molinate by a defined bacterial mixed culture. Environ. Microbiol. 5, 944-953.

Christian, T., Schneider, R.J., Farber, H.A., Skutlarek, D., Meyer, M.T., Goldbach, H.E., 2003. Determination of antibiotic residues in manure, soil, and surface waters. Acta Hydroch. Hydrob. 31, 36-44.

Chun, J., Lee, J.H., Jung, Y., Kim, M., Kim, S., Kim, B.K., Lim, Y.W., 2007. EzTaxon: a web-based tool for the identification of prokaryotes based on 16S ribosomal RNA gene sequences. Int. J. Syst. Evol. Micr. 57, 2259-2261. INT J SYST EVOL MICR

Davis, A.M., Jones, M., Page, M.I., 1991. Thiazolidine ring opening in penicillin derivatives. Part 1. Imine formation. J. Chem. Soc. Perkin Trans. 2 1219-1223.

De Laat, J., Truong Le, G., Legube, B., 2004. A comparative study of the effects of chloride, sulfate and nitrate ions on the rates of decomposition of H_2O_2 and organic compounds by Fe(II)/H_2O_2 and Fe(III)/H_2O_2. Chemosphere 55, 715-723.

Deshpande, A.D., Baheti, K.G., Chatterjee, N.R., 2004. Degradation of beta-lactam antibiotics. Curr. Sci. India 87, 1684-1695.

Dimitrakopoulou, D., Rethemiotaki, I., Frontistis, Z., Xekoukoulotakis, N.P., Venieri, D., Mantzavinos, D., 2012. Degradation, mineralization and antibiotic inactivation of amoxicillin by UV-A/TiO_2 photocatalysis. J. of Environ. Manage. 98, 168-174.

Elmolla, E.S., Chaudhuri, M., 2011. Combined photo-Fenton–SBR process for antibiotic wastewater treatment. J. Hazard. Mater. 192, 1418-1426.

Esplugas, M., Gonzalez, O., Sans, C., 2013. Bacterial community characterization of a sequencing batch reactor treating pre-ozonized sulfamethoxazole in water. Environ. Technol. 34, 1583-1591.

Faust, B.C., Zepp, R.G., 1993. Photochemistry of aqueous iron(III)-polycarboxylate complexes: Roles in the chemistry of atmospheric and surface waters. Env. Sci. Technol. 27, 2517-2522.

Figueira, V., Vaz-Moreira, I., Silva, M., Manaia, C.M., 2011. Diversity and antibiotic resistance of *Aeromonas spp*. in drinking and waste water treatment plants. Water. Res. 45, 5599-5611.

Galleni, M., Lamotte-Brasseur, J., Rossolini, G.M., Spencer, J., Dideberg, O., Frere, J.M., 2001. Standard numbering scheme for class B beta-lactamases. Antimicrob. Agents Chemother. 45, 660-663.

Ghauch, A., Tuqan, A., Assi, H.A., 2009. Antibiotic removal from water: Elimination of amoxicillin and ampicillin by microscale and nanoscale iron particles. Environ. Pollut. 157, 1626-1635.

Gogate, P.R., Pandit, A.B., 2004a. A review of imperative technologies for wastewater treatment I: Oxidation technologies at ambient conditions. Adv. Environ Res 8, 501-551.

Gogate, P.R., Pandit, A.B., 2004b. A review of imperative technologies for wastewater treatment II: Hybrid methods. Adv. Environ Res 8, 553-597.

González, O., Esplugas, M., Sans, C., Esplugas, S., 2008. Biodegradation of photo-fenton pre-treated solutions of sulfamethoxazole by aerobic communities. Molecular biology techniques applied to the determination of existing strains. J. Adv. Oxid. Technol 11, 238-245.

Gozlan, I., Rotstein, A., Avisar, D., 2013. Amoxicillin-degradation products formed under controlled environmental conditions: Identification and determination in the aquatic environment. Chemosphere 91, 985-992.

Guillard, C., Puzenat, E., Lachheb, H., Houas, A., Herrmann, J.M., 2005. Why inorganic salts decrease the TiO_2 photocatalytic efficiency. Int. J. Photoener. 7, 1-9.

Henriques, I.S., Araujo, S., Azevedo, J.S., Alves, M.S., Chouchani, C., Pereira, A., Correia, A., 2012. Prevalence and diversity of carbapenem-resistant bacteria in untreated drinking water in Portugal. Microbial drug resistance (Larchmont, N.Y.) 18, 531-537.

Hirsch, R., Ternes, T., Haberer, K., Kratz, K.L., 1999. Occurrence of antibiotics in the aquatic environment. Sci. Total Environ. 225, 109-118.

Homem, V., Alves, A., Santos, L., 2010. Amoxicillin degradation at ppb levels by Fenton's oxidation using design of experiments. Sci. Tot. Environ. 408, 6272-6280.

Igbinosa, I.H., Okoh, A.I., 2012. Antibiotic susceptibility profile of *Aeromonas* species isolated from wastewater treatment plant. Sci. World J. 2012, 764563.

Jacoby, G.A., 2009. AmpC beta-lactamases. Clin. Microbiol. Rev. 22, 161-182, Table of Contents.

Jeong, J., Yoon, J., 2005. pH effect on $^{\bullet}OH$ radical production in photo/ferrioxalate system. Water Res. 39, 2893-2900.

Kemper, N., 2008. Veterinary antibiotics in the aquatic and terrestrial environment. Ecol. Indic. 8, 1-13.

Kümmerer, K., 2009. Antibiotics in the aquatic environment - A review - Part I. Chemosphere 75, 417-434.

Lamm, A., Gozlan, I., Rotstein, A., Avisar, D., 2009. Detection of amoxicillin-diketopiperazine-2', 5' in wastewater samples. J. Environ. Sci. Health A Tox. Hazard. Subst. Environ. Eng. 44, 1512-1517.

Lane, D.J., 1991. 16S/23S rRNA sequencing. Wiley, New York.

Längin, A., Alexy, R., König, A., Kümmerer, K., 2009. Deactivation and transformation products in biodegradability testing of ß-lactams amoxicillin and piperacillin. Chemosphere 75, 347-354.

Li, D., Yang, M., Hu, J., Zhang, Y., Chang, H., Jin, F., 2008. Determination of penicillin G and its degradation products in a penicillin production wastewater treatment plant and the receiving river. Water Res. 42, 307-317.

Li, G., Lv, L., Fan, H., Ma, J., Li, Y., Wan, Y., Zhao, X.S., 2010. Effect of the agglomeration of TiO_2 nanoparticles on their photocatalytic performance in the aqueous phase. *J. Colloid Interface* Sci. 348, 342-347.

Lindsey, M.E., Tarr, M.A., 2000. Inhibition of Hydroxyl Radical Reaction with Aromatics by Dissolved Natural Organic Matter. Environ. Sci. Technol. 34, 444-449.

Literacka, E., Empel, J., Baraniak, A., Sadowy, E., Hryniewicz, W., Gniadkowski, M., 2004. Four variants of the *Citrobacter freundii* AmpC-Type cephalosporinases, including novel enzymes CMY-14 and CMY-15, in a *Proteus mirabilis* clone widespread in Poland. Antimicrob. Agents Chemother. 48, 4136-4143.

Lopes, A.R., Danko, A.S., Manaia, C.M., Nunes, O.C., 2013. Molinate biodegradation in soils: natural attenuation versus bioaugmentation. Appl. Microbiol. Biotechnol. 97, 2691-2700.

Łuczkiewicz, A., Jankowska, K., Fudala-Książek, S., Olańczuk-Neyman, K., 2010. Antimicrobial resistance of fecal indicators in municipal wastewater treatment plant. Water Res. 44, 5089-5097.

Malato, S., Fernández-Ibáñez, P., Maldonado, M.I., Blanco, J., Gernjak, W., 2009. Decontamination and disinfection of water by solar photocatalysis: Recent overview and trends. Cat. Today 147, 1-59.

Mavronikola, C., Demetriou, M., Hapeshi, E., Partassides, D., Michael, C., Mantzavinos, D., Kassinos, D., 2009. Mineralisation of the antibiotic amoxicillin in pure and surface waters by artificial UVA- and sunlight-induced fenton oxidation. J. Chem. Technol. Biotechnol. 84, 1211-1217.

Merlin, C., Bonot, S., Courtois, S., Block, J.-C., 2011. Persistence and dissemination of the multiple-antibiotic-resistance plasmid pB10 in the microbial communities of wastewater sludge microcosms. Water Res 45, 2897-2905.

Mokracka, J., Koczura, R., Kaznowski, A., 2012. Multiresistant *Enterobacteriaceae* with class 1 and class 2 integrons in a municipal wastewater treatment plant. Water Res 46, 3353-3363.

Nägele, E., Moritz, R., 2005. Structure Elucidation of Degradation Products of the Antibiotic Amoxicillin with Ion Trap MSn and Accurate Mass Determination by ESI TOF. J. Am. Soc. Mass Spectrom. 16, 1670-1676.

Novo, A., Manaia, C.M., 2010. Factors influencing antibiotic resistance burden in municipal wastewater treatment plants. Appl. Microbiol. Biotechnol. 87, 1157-1166.

Ohsuka, S., Arakawa, Y., Horii, T., Ito, H., Ohta, M., 1995. Effect of pH on activities of novel beta-lactamases and beta-lactamase inhibitors against these beta-lactamases. Antimicrob. Agents Chemother. 39, 1856-1858.

Oller, I., Malato, S., Sánchez-Pérez, J.A., 2011. Combination of Advanced Oxidation Processes and biological treatments for wastewater decontamination - A review. Sci. Tot. Environ. 409, 4141-4166.

Panias, D., Taxiarchou, M., Douni, I., Paspaliaris, I., Kontopoulos, A., 1996. Thermodynamic analysis of the reactions of iron oxides: Dissolution in oxalic acid. Can. Metall. Quart. 35, 363-373.

Pereira, J.H.O.S., Reis, A.C., Nunes, O.C., Borges, M.T., Vilar, V.J.P., Boaventura, R.A.R., 2013a. Assessment of solar driven TiO_2-assisted photocatalysis efficiency on amoxicillin degradation. Environ. Sci. Pollut. Res. 1-12.

Pereira, J.H.O.S., Reis, A.C., Queirós, D., Nunes, O.C., Borges, M.T., Vilar, V.P., Boaventura, R.A.R., 2013b. Insights into solar TiO_2-assisted photocatalytic oxidation of two antibiotics employed in aquatic animal production, oxolinic acid and oxytetracycline. Sci. Tot. Environ. 463-464, 274-283.

Pérez-Parada, A., Agüera, A., Gómez-Ramos, M.d.M., García-Reyes, J.F., Heinzen, H., Fernández-Alba, A.R., 2011. Behavior of amoxicillin in wastewater and river water: identification of its main transformation products by liquid chromatography/electrospray quadrupole time-of-flight mass spectrometry. Rapid Commun. Mass Sp. 25, 731-742.

Petrović, M., Gonzalez, S., Barceló, D., 2003. Analysis and removal of emerging contaminants in wastewater and drinking water. TrAC Trend. Anal. Chem. 22, 685-696.

Pignatello, J.J., Oliveros, E., MacKay, A., 2006. Advanced oxidation processes for organic contaminant destruction based on the fenton reaction and related chemistry. Crit. Rev. Env. Sci. Tehcnol. 36, 1-84.

R Development Core Team, R: A language and environment for statistical computing. R Foundation for Statistical Computing, Vienna, Austria, 2013.

Rizzo, L., Manaia, C., Merlin, C., Schwartz, T., Dagot, C., Ploy, M.C., Michael, I., Fatta-Kassinos, D., 2013. Urban wastewater treatment plants as hotspots for antibiotic resistant bacteria and genes spread into the environment: A review. Sci. Tot. Env. 447, 345-360.

Rodríguez, S.M., Gálvez, J.B., Rubio, M.I.M., Ibáñez, P.F., Padilla, D.A., Pereira, M.C., Mendes, J.F., De Oliveira, J.C., 2004. Engineering of solar photocatalytic collectors. Sol. Energy 77, 513-524.

Schwartz, T., Kohnen, W., Jansen, B., Obst, U., 2003. Detection of antibiotic-resistant bacteria and their resistance genes in wastewater, surface water, and drinking water biofilms. FEMS Microbiol. Ecol. 43, 325-335.

Szczepanowski, R., Linke, B., Krahn, I., Gartemann, K.H., Gutzkow, T., Eichler, W., Puhler, A., Schluter, A., 2009. Detection of 140 clinically relevant antibiotic-resistance genes in the plasmid metagenome of wastewater treatment plant bacteria showing reduced susceptibility to selected antibiotics. Microbiology (Reading, Engl.) 155, 2306-2319.

Testa, B., Mayer, J.M., 2006. The Hydrolysis of Lactams. in: Hydrolysis in Drug and Prodrug Metabolism. Verlag Helv. Chim. Acta, pp. 163-234.

Torres, M.J., Ariza, A., Fernandez, J., Moreno, E., Laguna, J.J., Montanez, M.I., Ruiz-Sanchez, A.J., Blanca, M., 2010. Role of minor determinants of amoxicillin in the diagnosis of immediate allergic reactions to amoxicillin. Allergy 65, 590-596.

Trovó, A.G., Pupo Nogueira, R.F., Agüera, A., Fernandez-Alba, A.R., Malato, S., 2011. Degradation of the antibiotic amoxicillin by photo-Fenton process - Chemical and toxicological assessment. Water. Res. 45, 1394-1402.

Vaz-Moreira, I., Nunes, O.C., Manaia, C.M., 2011. Diversity and antibiotic resistance patterns of *Sphingomonadaceae* isolates from drinking water. Appl. Envirom. Microbiol. 77, 5697-5706.

Walsh, T.R., Toleman, M.A., Poirel, L., Nordmann, P., 2005. Metallo-beta-lactamases: the quiet before the storm? Clin. Microbiol. Rev. 18, 306-325.

Watkinson, A.J., Murby, E.J., Costanzo, S.D., 2007. Removal of antibiotics in conventional and advanced wastewater treatment: Implications for environmental discharge and wastewater recycling. Water. Res. 41, 4164-4176.

Zhang, Y., Marrs, C.F., Simon, C., Xi, C., 2009. Wastewater treatment contributes to selective increase of antibiotic resistance among *Acinetobacter spp*. Sci. Tot. Environ. 407, 3702-3706

8 Main conclusions and future work

This final Chapter presents a recollection of the most pertinent results and conclusions stated in the previous Chapters, complemented with some recommendations for future work.

8.1 Main conclusions

The main goal of this thesis was to study the detoxification of three selected antibiotics, Oxytetracycline (OTC), Oxolinic acid (OXA) and Amoxicillin (AMX) in aqueous solutions, by means of two solar-driven photocatalytic processes, TiO_2/UV and photo-Fenton. Both processes were performed in lab- and pilot-scale experimental units equipped with Compound Parabolic Collectors (CPCs). The process efficiency was mainly based on measurements of antibiotic concentration by HPLC-DAD, dissolved organic carbon (DOC), accumulated UV energy per liter of solution (Q_{UV}) and pH value; ion chromatography analysis of inorganic ions released by the original antibiotic molecules and low-molecular-weight carboxylate anions (LMWCA); antibacterial activity against tested bacterial strains; dissolved iron concentration and hydrogen peroxide consumption by colorimetric measurement (photo-Fenton process). Initial antibiotic concentration values were 20 mg L^{-1}, except in the solar TiO_2/UV experiments performed in Chapters 4 and 5, where 40 mg L^{-1} were necessary to accurately follow inorganic ion release and formation of LWMCA by ion chromatography analysis.

8.1.1 Solar photolysis

Solar photolytic experiments were performed in Chapters 3, 4 and 5 in order to assess the influence of incident solar radiation by itself in the degradation of individual antibiotic solutions. Different outcomes were achieved, matching well with the overlapping degree of each antibiotic UV absorbance spectrum with the spectrum of incident solar UV inside the photo-reactor. OTC, followed by OXA, was the most susceptible compound to solar photolytic degradation, whereas AMX concentrations were unaffected in the tested photo-treatment period. Mineralization was absent in all cases, showing that that the incident radiation is only able to transform the susceptible parent compounds into more stable intermediary products.

8.1.2 TiO_2/UV system

In Chapter 3, preliminary lab-scale testing of the TiO_2/UV system in a Solarbox device allowed for the study of the influence of the catalyst load (P25 Degussa TiO_2) and solution pH to treat 20 mg L^{-1} OTC solutions. With the optimal conditions, 0.5 g L^{-1} of TiO_2 with no initial pH adjustment (pH ~ 4.4), 100% of OTC was removed after 40 min of irradiance (Q_{UV} = 7.5 kJ_{UV} L^{-1}) and over 90% of initial DOC after 180 min (Q_{UV} = 38.3 kJ_{UV} L^{-1}). An improvement in biodegradability was shown by the increase of the BOD_5/COD ratio from almost 0 to nearly 0.5, while Inhibition Percentage of bioluminescence of *Vibro fischeri* after 15 min of exposition measured by Microtox® decreased significantly from 35 % down to 7 %.

Based on the degradation by-products identified by Liquid Chromatography – Mass Spectrometry (LC-MS), an OTC degradation mechanism was proposed. The same conditions applied in the solar pilot plant demonstrated how the reactor size and geometry differed in the amount of necessary UV dose to obtain similar OTC and DOC removal results (100% OTC and almost 80% DOC removal with Q_{UV} values of 1.8 kJ_{UV} L^{-1} and 11.3 kJ_{UV} L^{-1}, respectively), since the photoreactor inside the Solarbox had smaller diameter and a less efficient parabolic mirror to reflect diffuse radiation than the CPC photoreactors.

In Chapters 4 and 5, the operation conditions were fixed at 0.5 g L^{-1} of TiO_2 and at more environmentally relevant pH_0 = 7.5. The results of the solar photocatalytic degradation of 20 mg L^{-1} individual solutions of OTC, OXA and AMX followed pseudo-first order kinetics. The highest rate constant was presented by OTC, 4.03 ± 0.07 L kJ_{UV}^{-1}, followed by OXA, 1.9 ± 0.1 L kJ_{UV}^{-1}, and AMX, 0.80 ± 0.02 L kJ_{UV}^{-1}. After very small and similar amounts of Q_{UV}, around 1.0 kJ_{UV} L^{-1}, OXA and OTC were removed below detection limit levels, while AMX required a 3.1 kJ_{UV} L^{-1}. Beyond that point, the initial DOC content in the OTC solution decreased 74% (Q_{UV} = 8.5 kJ_{UV} L^{-1}), in the OXA solution by 53% (Q_{UV}= 4.2 kJ_{UV} L^{-1}), and in the AMX solution by 73% (Q_{UV} = 10.2 kJ_{UV} L^{-1}). The efficiency of antibiotic degradation and respective DOC removal could be accounted for by the abovementioned differences in molecule susceptibility to solar photolysis attack, by the different molecular structural properties, that influence $^{\bullet}OH$ attack, and by the antibiotic speciation as a function of pH. Despite of the nearly halved decrease in the rate constants of OTC and OXA in a mixture of the same concentration of these compounds, the overall results of the TiO_2/UV system proved worthwhile in situations where both antibiotics could be present simultaneously.

In lab-scale conditions, the antibiotic speciation helped to explain the notably negative (OTC and OXA) and positive (AMX) effects of the presence of phosphates on degradation rate constants, when compared to other tested inorganic ions. Phosphate strongly adsorbs onto the catalyst surface, and its negative charges exerted a repulsion effect of the zwitterionic/anionic OTC and OXA. This accounted for the deleterious effect on the degradation rates of both antibiotics, since their adsorption degree onto the catalyst surface was affected. In contrast, an attraction effect occurred in the case of AMX, since initial antibiotic adsorption onto TiO_2 was otherwise inexistent. In the presence of selective reactive oxygen species scavengers, the role of $^{\bullet}OH$ radicals attack of the three antibiotic were highlighted.

Individually treated OTC, OXA and AMX solutions (C_0 = 40 mg L^{-1}) ceased to inhibit growth of tested bacterial strains when the amount of accumulated UV energy was enough to lower their concentrations below minimum bacterial inhibitory levels. By the end of the respective photo-treatment periods, a high percentage of remaining DOC content was in the form of easily

biodegradable LMWCA, recalcitrant to further •OH attack, but otherwise favoring a possible integration with biological treatment, if necessary. The original nitrogen content in OTC, OXA and AMX molecules was incompletely released as ammonium, in different oxidation degrees, but 100% desulfurization of AMX by-products was achieved.

A figure-of-merit based on the solar collector area recommended by the IUPAC, collector area per order (A_{CO}), allowed for a direct comparison between the overall solar-energy efficiency of the TiO_2/UV system applied to the individual treatment of 20 and 40 mg L^{-1} solutions of OTC, OXA and AMX. For C_0 = 20 mg L^{-1}, the obtained A_{CO} values for OTC, OXA and AMX were 0.15, 0.24 and 0.85 m^2 m^{-3}-order, while A_{CO} values for C_0 = 40 mg L^{-1}, they were 0.31, 1.15 and 1.65 m^2 m^{-3}-order in the same order. This figure-of-merit indicates a loss in the system efficiency when A_{CO} values increase, in an inverse proportion, and reflected well the contrasting results between increasing amounts of the same antibiotic and between the different antibiotic degradation.

8.1.3 Photo-Fenton process

As far as the author is concerned, no studies are available regarding the application of the photo-Fenton process to OTC, so a detailed study was performed with this antibiotic. Due to the limited solubility of OXA under pH values lower than 7.5, it was chosen not to perform any photo-Fenton experiments with this antibiotic.

In Chapter 6, the application of the conventional Fe^{2+}/H_2O_2/UV-Vis process at near neutral pH levels to treat 20 mg L^{-1} solutions of OTC resulted problematic, since after Fe^{2+} oxidation to Fe^{3+} in the presence of H_2O_2, a highly stable Fe(III)-OTC complex is formed. Bench-scale tests confirmed that by increasing the pH from 3.0 towards 5.0 of solutions containing only 2 mg L^{-1} Fe (III) and 20 mg L^{-1} of OTC, the original concentration of OTC not only gradually decreases, but it also differs from filtered and non-filtered samples. To overcome this, a Fe^{3+}/Oxalate or Fe^{3+}/Citrate/H_2O_2/UV-Vis process was proposed. The high tendency of Fe (III) to form complexes with carboxylate ions, avoids the formation of ferric-OTC complexes and allowed for proper OTC detection along reaction times. Low iron (III) concentrations were tested in order to comply with legal discharge limits.

The oxalic acid used in a 1:3 iron/oxalate molar ratio with the aim of forming iron/oxalate complexes showed to perform better than citric acid in a 1:1 iron/citrate molar ratio in deterring the inconvenient formation of Fe:OTC complexes along the reaction. The most photo-active species, $Fe(C_2O_4)_2^-$ and $Fe(C_2O_4)_3^{3-}$, are the main soluble iron species in the pH range of 4 to 6, albeit with changing proportions over pH. By modelling the iron (III)-species distribution as a

function of pH, it was found that from pH = 4.0 onwards, the fraction of $Fe(C_2O_4)_2^-$ lowers smoothly from 0.7 down to less than 0.1, whereas the fraction of $Fe(C_2O_4)_3^{3-}$ evolves from near 0.3, to a maximum of approximately 0.5 at pH = 5.0. By pH = 6.0, iron precipitation in the form of the mineral Ferrihydrite is expected, as seen also by the less than 2 mg L^{-1} total dissolved iron concentration available in a pH_0 = 6.0 experiment

Optimal process parameters were thus [Fe (III)] = 2 mg L^{-1}, pH_0 = 5.0 and the iron/oxalate molar ratio of 1:3, with a total addition of 90 mg L^{-1} of H_2O_2. Under these conditions, the photocatalytic rate constant was 6.3 ± 0.2 L kJ_{UV}^{-1}, OTC was no longer detected after 10 min of illumination time (Q_{UV} = 0.6 kJ_{UV} L^{-1}), while 49% of the initial DOC content was removed after only 45 min (Q_{UV} = 2.78 kJ_{UV} L^{-1}). These results are in accordance to the general higher efficiency of the photo-Fenton process when compared to the TiO_2/UV system.

It was shown that under these operating conditions, OTC degradation is neither remarkably affected by temperature and irradiance, nor by the individual presence of possible interfering species such as Cl^-, SO_4^{2-}, NO_3^- and HCO_3^-, while the presence of dissolved organic matter (humic acids) negatively affected the reaction. To evaluate the effect of more complex matrices, experiments performed with an urban WWTP effluent showed slower OTC removal kinetics and lower DOC reduction mainly due to the precipitation of $FePO_4$. However, in a less complex effluent from the outlet of a trout farm it was shown that without the pH adjustment step, similar results were achieved, compared with the deionized water control experiments.

Under solar pilot plant conditions, it was shown that the antibacterial activity of the solution is also consequently lost after the quick OTC removal from solution (Q_{UV} = 0.4 kJ_{UV} L^{-1}). Until Q_{UV} = 1.2 kJ_{UV} L^{-1}, a peak of 72.5% of the DOC content in the form of LMWCA was achieved, equivalent to the point where the mineralization process began to slow down, in parallel with the decay of available oxalate and the presence of said detected carboxylates. The final pH achieved by the end of the treatment meets the minimum legal discharge limit, and so this system seems to reduce the need of relevant post-phototreatment steps. The lab-scale unit design was ultimately shown to be practical to compare the process efficiency between simulated and real solar radiation experiments.

Given the higher antibiotic degradation kinetics, the lower UV energy doses required to achieve a high level of DOC content in the form of LMWCA, and since the concentration of iron (III) used is the maximum allowable discharge limit imposed by Portuguese legislation, the application of Fe^{3+}/Oxalate/H_2O_2/UV-Vis system was shown to be more viable than the TiO_2/UV system.

Regarding AMX, some authors have already applied the photo-Fenton process to this antibiotic, as was referred to in Chapter 5. Nevertheless, some experiments were performed in order to compare removal efficiency between both antibiotics and between both the photo-Fenton process and the TiO_2/UV system, under similar conditions as those optimized with OTC in Chapter 6.

AMX experiments were initially performed in the lab-scale photocatalytic apparatus under two initial pH values (unadjusted (~ 4.0) and 5.0), [Fe (III)] = 2 mg L^{-1}, 1:3 iron/oxalate molar ration and a total addition of 90 mg L^{-1} of H_2O_2. Results showed that in the pH_0 = 4.0 experiment, AMX was no longer detected after only 0.7 kJ_{UV} L^{-1}, a Q_{UV} value significantly lower than the 3.1 kJ_{UV} L^{-1} required in the solar TiO_2/UV experiment. However, by this amount of accumulated UV energy per solution, the TiO_2/UV system had already decreased the initial DOC of the solution by 61%, whereas with 4.5 kJ_{UV} L^{-1}, the Fe^{3+}/Oxalate/H_2O_2/UV-Vis process only decreased it by 56%. The process performance with pH_0 = 5.0 fared worse, as the concentration of AMX was only reduced by 77% by 1.4 kJ_{UV} L^{-1}. Such loss of efficiency could be explained by the concomitantly quick rise of the solution pH up to values near 6.0, which translated into the near absence of $Fe(C_2O_4)_2^-$ and $Fe(C_2O_4)_3^{3-}$, according to the distribution of iron(III)-species as a function of pH previously mentioned. Alternatively, the same experiment was repeated with punctual additions of diluted sulphuric acid in order to control the pH level under a maximum of 5.5. This resulted in complete AMX degradation after 1.2 kJ_{UV} L^{-1}, although only 28% of the initial DOC was removed.

The same strategy was followed to test the effect of the matrix by spiking AMX into the same urban WWTP effluent used in Chapter 6. Given the level of dissolved phosphates, the initial iron/oxalate molar ratio was increased to 1:6 to try to ensure a favorable proportion of ferricarboxylate species in solution. AMX was no longer detected after a similar Q_{UV} value, 1.4 kJ_{UV} L^{-1}, but then the original DOC content of the effluent, around 7 mg L^{-1}, and the formation of the mineral Strengite ($FePO_4.2H_2O$ (s)) after oxalate depletion, completely hampered the mineralization process.

8.1.4 Combined treatment of AMX solutions

The objective of Chapter 7 was the development of an alternative multistage treatment combining the biological degradation of AMX by means of an enriched culture with a solar photocatalytic system.

A mixed bacterial culture (MC) able to degrade AMX in different matrices (Enrichment Media, EM; Buffer, NaCl and Wastewater, WW) was successfully obtained and characterized. The

majority of these organisms belong to the phylum *Proteobacteria*, commonly known to degrade a great variety of organic pollutants. Within this group a great percentage of isolates was closely related to *Citrobacter freundii*, followed by *Stenotrophomonas sp.* and *Shingobacterium multivorium*. The overall specific degradation rate of the MC (0.11 g_{AMX} $g_{biomass}^{-1}$ h^{-1}) closely corresponded to that of *C. freundii* (0.09 g_{AMX} $g_{biomass}^{-1}$ h^{-1}). The isolated strains have been described previously as carriers of different β-lactamases, enzymes which are able to degrade most β-lactam antibiotics.

In all tested matrices, the degradation of AMX occurred concomitantly with the accumulation of two distinct TPs, which were identified as stereoisomers (5*S*) and (5*R*) of amoxicillin penicilloic acid (AMXC). Their formation is a product of the hydrolysis of the highly reactive β-lactam ring of AMX and results in the total loss of antimicrobial activity. However, they resisted additional bacterial action, which brought up the need of a further, more efficient treatment, since these compounds may also pose ecotoxicological risks.

In this way, a complementary photocatalytic oxidation step was proposed to enhance AMXC degradation in the lab-scale apparatus simulating solar radiation.

The first process proposed was a TiO_2/UV system promoted by 0.2 g L^{-1} of TiO_2 carried out at pH_0 = 5.5. In NaCl and Buffer, the respective TP1/TP2 peaks were no longer detected after 90 (Q_{UV} = 5.3 kJ_{UV} L^{-1}) and 180 (Q_{UV} = 10.9 kJ_{UV} L^{-1}) min of illumination. In the most complex matrices (EM and WW), however, TPs were still present by the end of the irradiance period. None of the TiO_2/UV experiments showed considerable DOC removal by the end of photocatalytic step.

The second process proposed was the Fe^{3+}/Oxalate/H_2O_2/UV-Vis system, carried out using 2 mg Fe(III) L^{-1}, an 1:3 (NaCl) or 1:9 (WW) iron/oxalate molar ratio, uncontrolled pH, and a total H_2O_2 addition of 90 mg L^{-1}. Based on the distribution of the two most photo-active species, $Fe(C_2O_4)_2^-$ and $Fe(C_2O_4)_3^{3-}$, experiments with NaCl and WW were performed under two initial pH values, 4.0 and 5.0.

Substantially lower amounts of accumulated UV energy per litre of solution were required to remove TP1/TP2, compared to the TiO_2/UV experiments. Both pH_0 = 4.0 experiments required only 20 min (Q_{UV} = 1.3 kJ_{UV} L^{-1}), while with pH_0 = 5.0 experiments, 40 min (Q_{UV} = 2.6 kJ_{UV} L^{-1}) were needed to remove TP1 and TP2. Regardless of the need of supplementary oxalate additions to extend the process beyond TP1/TP2 removal, the remaining carbon content was either converted to easily biodegradable low-molecular-weight carboxylate anions or removed in higher proportions after 120 min (Q_{UV} = 8.3 kJ_{UV} L^{-1}).

8.2 Recommendations for future work

The use of novel photocatalysts with high activity and visible light response properties would greatly improve the TiO_2/UV system, and despite their demonstrated efficiency on the treatment of the tested antibiotics, it would be interesting to work with an immobilized catalyst in order to avoid the rather limiting catalyst separation step. The same strategy could be applied to the photo-Fenton process, in order to overcome the restrictions of working with high pH levels. Moreover, both photocatalytic techniques could be also greatly benefitted by a complementary integration with Electrochemical Advanced Oxidation Processes, considering their capacity for *in situ* generation of H_2O_2.

To improve the photo-Fenton process, different iron-carboxylate molar ratios should be optimized, whereas the photo-activity and iron-chelating properties of other organic ligands should be tested.

Considering the high percentage of remaining DOC in the form of low-molecular-weight carboxylate, the biodegradability and ecotoxicity towards different test organisms of the photo-treated solutions would greatly build up on the obtained results.

Given the prompt unavailability of LC-MS analysis along the realization of this work, studies using more realistic antibiotic concentrations would be greatly complementary. Likewise with the identification of the intermediary by-products generated under the performed photo-Fenton conditions.

Further matrix effects should be studied besides testing with antibiotic-spiked effluents. Concentrates obtained after advanced membrane treatment of antibiotic-contaminated wastewater are of special interest.

The combined treatment still requires further optimization concerning the mineralization of the remaining DOC. Nevertheless, it brings into attention that research on treating pharmaceuticals such as antibiotics from effluents should also focus on naturally occurring antibiotic by-products.

The development of photocatalytic membranes (separation function/photocatalytic activity) would enhance its antifouling properties and at the same time would leads to membrane concentrates with lower organic loads.

Finally, process intensification could be accomplished through the use of Microreactors/Static Mixers, and through breakthrough optical system designs for sunlight capture (non-imaging optics techniques) and for photoreactors using artificial light (CFD tool).